MAX-PLANCK-INSTITUT
FÜR HERZ- UND LUNGENFORSCHUNG

JUSTUS-LIEBIG-
UNIVERSITÄT
GIESSEN

Functional Characterization of RBPMS-Positive Ribonucleoprotein Granules in Cardiomyocytes

INAUGURAL DISSERTATION

zur Erlangung des Doktorgrades der Naturwissenschaften

– Doctor rerum naturalium –

(Dr. rer. nat.)

Angefertigt am Max-Planck-Institut für Herz- und Lungenforschung, Bad Nauheim

Vorgelegt dem Fachbereich für Biologie und Chemie (FB 08)

der Justus-Liebig-Universität Giessen

Eingereicht von

M.Sc. Yvonne Eibach

Giessen, 2025

Prüfer

Erstgutachter: Prof. Dr. Dr. Thomas Braun

Zweitgutachter: PD Dr. habil. Oliver Rossbach

Weitere Prüfer: Prof. Dr. Sandra Hake, Prof. Dr. Andreas Krueger

Datum der Disputation: 10.03.2026

Eidesstattliche Erklärung

Ich erkläre: Ich habe die vorgelegte Dissertation selbständig, ohne unerlaubte fremde Hilfe und nur mit den Hilfen angefertigt, die ich in der Dissertation angegeben habe. Alle Textstellen, die wörtlich oder sinngemäß aus veröffentlichten oder nicht veröffentlichten Schriften entnommen sind, und alle Angaben, die auf mündlichen Auskünften beruhen, sind als solche kenntlich gemacht. Bei den von mir durchgeführten und in der Dissertation erwähnten Untersuchungen habe ich die Grundsätze guter wissenschaftlicher Praxis, wie sie in der „Satzung der Justus-Liebig-Universität Gießen zur Sicherung guter wissenschaftlicher Praxis“ niedergelegt sind, eingehalten.

Gießen, den _____

Yvonne Eibach

Publications

Eibach Y, Kreher S, Poetsch MS, Kho AL, Gaertner U, Clemen CS, Schröder R, Guo K, Milting H, Meder B, Potente M, Richter M, Schneider A, Meiners S, Gautel M, Braun T. The deubiquitinase USP5 prevents accumulation of protein aggregates in cardiomyocytes. Science Advances. 2025 Jan 24;11(4):eado3852.
doi: 10.1126/sciadv.ado3852

Lin S, Dieterich C, Britto-Borges T, Günther S, Kreher S, **Eibach Y**, Kuenne C, Schneider A, Braun T. Rbpms2 prevents major cardiac defects in cardiomyocyte-specific Rbpms-deficient mice. Developmental Cell. 2025.
doi: 10.1016/j.devcel.2025.06.013

"Science is fun. Science is curiosity. We all have natural curiosity. Science is the process of investigating. Its posing questions and coming up with a method. Its delving in."

Sally Ride

Table of Contents

List of Figures

List of Tables

Summary

RNA-Binding Protein with Multiple Splicing (RBPMS) is a member of the RNA-binding protein family and localizes to both the nucleus and cytoplasm. In addition to its function in transcriptional co-regulation, RBPMS may also play a role in the cytoplasm for regulation of mRNA stability, transport and recruitment into cytoplasmic granules. Although aberrant RNA processing and dysregulated ribonucleoprotein assemblies are known to contribute to the pathogenesis of neurodegenerative diseases, the composition of RNPs and their (patho)physiological roles in the cardiovascular system remain poorly understood. In this study, I investigated the role of RBPMS in regulating RNP assemblies and their dynamics in response to cardiovascular stress.

I developed an optimized protocol for APEX2-mediated proximity labeling in murine HL-1 cardiomyocytes. The approach enabled high-resolution mapping of the cardiac stress granule proteome, revealing a previously uncharacterized complexity and tissue-specific adaptation in SG composition. Interestingly, proximity interactions between SG components in unstressed cells point to pre-assembly mechanisms facilitating rapid SG formation during stress. Interactome analysis of GFP-tagged RBPMSA and RBPMSB isoforms identified key partners involved in DNA damage response and phase separation. Additionally, RBPMSB was found to interact with mitochondrial proteins, potentially linking phase-separated compartments and cellular organelles in stress responses. Upon doxorubicin-induced DNA damage, RBPMS initially translocates to SGs in the cytoplasm and subsequently forms nuclear puncta, coinciding with chromatin reorganization. These observations suggest that RBPMS contributes to both acute and long-term stress adaptation, potentially modulating DDR and chromatin phase transitions.

Importantly, doxorubicin-induced genotoxic stress alters the abundance and localization of RBPMS isoforms, disrupts splicing factor dynamics, and impairs mitochondrial biogenesis, collectively contributing to cardiotoxicity. The identification of age-dependent differences in alternative splicing regulation further highlights the complexity of the cardiac stress response. The interplay between RBPMS, splicing factors, and SGs emerged as a critical determinant of cardiomyocyte survival and function under stress.

Taken together, my findings establish RBPMS as a regulator of RNP assembly and cellular stress responses in cardiovascular disease, highlighting its potential as a therapeutic target and providing a foundation for further investigation into its role in DNA damage response and stress-related cardiac pathologies.

Zusammenfassung

RNA-Binding Protein with Multiple Splicing (RBPMS) ist ein Mitglied der Familie der RNA-bindenden Proteine, das sowohl im Zellkern als auch im Zytoplasma lokalisiert ist. Neben seiner Funktion als Ko-Regulator der Transkription spielt RBMPS wahrscheinlich auch eine Rolle bei der Regulation der zytoplasmatischen mRNA-Stabilität, dem Transport sowie der Rekrutierung in zytoplasmatische Granula. Obwohl bekannt ist, dass fehlerhafte RNA-Prozessierung und eine Dysregulation von Ribonukleoprotein-Komplexen zur Pathogenese neurodegenerativer Erkrankungen beitragen, sind ihre Zusammensetzung und (patho)physiologischen Funktionen im kardiovaskulären System bislang weitgehend unerforscht. Meine Untersuchungen konzentrierten sich daher auf die Rolle von RBPMS bei der Regulation von RNP-Komplexen und deren Dynamik in der kardiovaskulären Stressantwort.

Erstmals wurde ein optimiertes Protokoll für APEX2-vermittelte Proximitätsmarkierung von Proteinen in murinen HL-1-Kardiomyozyten etabliert, das eine hochauflösende Kartierung des Stressgranula-Proteoms ermöglicht. Dieser Ansatz erlaubte die detaillierte Charakterisierung bislang unbekannter SG-Komponenten sowie deren gewebespezifische Anpassung im Herzen. Interessanterweise deuten proximale Interaktionen zwischen SG-Komponenten in nicht gestressten Zellen auf eine Präassemblierung einzelner Komponenten hin, die eine schnelle SG-Bildung während Stress begünstigen. Die Interaktomanalyse von GFP-fusionierten RBPMSA- und RBPMSB-Isoformen identifizierte Interaktionspartner, die an der DNA-Schadensantwort und an Prozessen der Phasentrennung beteiligt sind. Zudem konnte eine Interaktion von RBPMSB mit mitochondrialen Proteinen nachgewiesen werden, was auf eine funktionelle Verbindung zwischen phasengetrennten subzellulären Kompartimenten und zellulären Organellen in der Stressantwort hindeutet. Nach Doxorubicin-induzierter DNA-Schädigung wird RBPMS zunächst in SGs integriert, bildet aber auch nukleäre Kondensate, die mit einer Chromatinreorganisation einhergehen. Diese Beobachtungen legen nahe, dass RBPMS sowohl an der akuten als auch an der langfristigen Stressadaptation beteiligt ist und möglicherweise die DNA-Schadensantwort sowie Chromatin-Phasentransitionen moduliert.

Besonders hervorzuheben ist, dass Doxorubicin-induzierter genotoxischer Stress sowohl die Expression als auch die subzelluläre Lokalisation der RBPMS-Isoformen verändert, die Dynamik von Spleißfaktoren beeinflusst und die mitochondriale Biogenese beeinträchtigt - Faktoren, die in ihrer Gesamtheit zur Kardiotoxizität beitragen. Die altersabhängige Regulation alternativen Spleißens verdeutlicht zudem die komplexe Natur der kardialen Stressanpassung. Das Zusammenspiel zwischen RBPMS, Spleißfaktoren und SGs erwies sich als entscheidender Faktor für das Überleben und die Funktion von Kardiomyozyten unter Stress.

Die Ergebnisse dieser Studie etablieren RBPMS als Regulator von RNP-Komplexen und zellulären Stressantworten im Herzen und unterstreichen das Potenzial als therapeutisches Target. Meine Arbeiten werden als Grundlage für weitere Untersuchungen dienen, um die Rolle von RBPMS in der DNA-Schadensantwort und stressassoziierten kardialen Pathologien zu klären.

1. Introduction

The conventional view of cellular organization is based on the lipid bilayer membrane, which engulfs classic organelles including the nucleus, mitochondria, and endoplasmic reticulum, introducing a selective barrier defined by their composition. This compartmentalization allows the organization of complex biochemical reactions in space and time (Hyman et al., 2014; Shorter, 2016). Subcellular organization of macromolecules is essential for vital cellular processes such as homeostasis, cell division and development. However, recent progresses in cell biology necessitate a reassessment of this established model. In particular, the discovery of biomolecular condensates is challenging the understanding of cellular organization (Mullard, 2019).

1.1 Membraneless organelles

Eukaryotic cells contain many membrane-bound organelles, which establish a network of distinct microenvironments with diverse physiochemical properties. In addition to these, cells harbor various membraneless organelles (MLOs), which exhibit liquid-like properties and exist as distinct phases separated from the surrounding medium and are often referred to as granules or biomolecular condensates (Brangwynne et al., 2015). These structures constitute a distinct type of intracellular compartment that has recently received increased attention and are known to play critical roles in cellular organization and function (Hyman et al., 2014). MLOs possess a mesoscopic size and display diverse shapes, consisting of distinct protein compositions and typically containing nucleic acids, such as RNA and/or DNA. In contrast to membrane-surrounded organelles, these structures are highly dynamic, enabling them to respond rapidly to environmental changes and thereby regulate biochemical reactions in a spatiotemporal manner. Some of them are constitutively present, while others appear in response to stressors. These organelles are present in both the nucleoplasm and cytoplasm, and they arise through liquid-liquid phase separation (LLPS). Unlike traditional organelles, they lack a surrounding membrane and are formed via dynamic assembly of biomolecules within the cell. In this context, multivalent weak macromolecular interactions between proteins and/or nucleic acids promotes phase separation by exceeding a threshold concentration (Harmon et al., 2017).

The first membraneless compartment identified in cells was the nucleolus, observed within the nucleus of neuronal cells in the 1830s (Pederson, 2011). Since the initial discovery, many biomolecular condensates have been uncovered in the nucleus and cytoplasm of almost all eukaryotic cells. The MLOs encompass a range of ribonucleoprotein (RNP) granules, including stress granules (SGs), processing bodies (P-bodies), germ granules, and neuronal RNA granules in the cytoplasm as well as paraspeckles (PSs), nuclear speckles and Cajal bodies within the nucleus (Figure 1). These organelles can be classified based on their spatial

localization within the cell, their molecular composition, and their specific biological functions. Proteins that undergo LLPS are characterized by the presence of low-complexity, intrinsically disordered regions (IDRs) that mediate intermolecular interactions. IDRs drive the formation of biomolecular condensates by engaging in weak, multivalent interactions between amino acid residues. These interactions allow intrinsically disordered proteins (IDPs) to undergo liquid–liquid phase separation, concentrating into liquid-like droplets or condensates. (Harmon et al., 2017; Wang et al., 2018). Proteins that primarily drive phase transitions are termed scaffolds, whereas other components incorporated into the condensates are classified as clients (Banani et al., 2017; Posey et al., 2018).

Figure 1 Schematic overview of membraneless organelles in a eukaryotic cell.
Membraneless biomolecular condensates distributed across the nucleus and cytoplasm of eukaryotic cells. Membraneless organelles (MLOs) highlighted in this study are shown in color; all other MLOs are depicted in grey. Processing bodies (P-bodies) are ubiquitously present across cell types under normal conditions, paraspeckles are found only in specific cell types and stress granules form specifically in response to certain stress conditions. Adapted from (Hirose et al., 2022).

1.2 Stress granules

Stress granules (SGs) represent one of the two major types of cytoplasmic RNP granules. As part of the integrated stress response, assembly of SGs is highly conserved across diverse species. Initially identified as cytoplasmic aggregates in tomato plant cells under heat shock conditions (Nover et al., 1983), SGs were subsequently observed in yeast and mammalian cells, indicating their conserved role across species in response to cellular stress. (Kedersha et al., 1999; Buchan et al., 2009). These dynamic stress-induced RNP granules rapidly form in response to diverse environmental stressors, including heat shock, oxidative stress, and

viral infection and disassemble upon recovery from stress. SGs share many components with messenger RNP (mRNP) in oocytes and embryos (Buchan, 2014), neuronal granules (Costa et al., 2021) and myo-granules in developing muscle (Vogler et al., 2018), suggesting a conserved mechanism of mRNP compartmentalization. Components of SGs include translation initiation factors, a variety of RNA-binding proteins, small ribosomal subunits as well as translationally arrested mRNAs. Their formation is influenced by numerous conditions, including post-translational modifications and molecular interactions. In particular, interactions mediated by IDRs, the specific amino acid composition of these regions, and distinct post-translational modifications, such as methylation, phosphorylation, and glycosylation, play a crucial role in this process (Wang et al., 2018). Structurally, SGs are comprised of a stable core surrounded by a less concentrated and potentially more dynamic shell-like layer (Protter & Parker, 2016). Given their biological importance and their association with various human diseases, SGs have emerged as one of the most intensively studied RNP granules.

1.2.1 Formation of stress granules

SGs are formed as part of the cellular response to various stress conditions that impair bulk translation initiation, leading to the release of messenger ribonucleic acids (mRNAs) from ribosomes. Upon cellular stress, four distinct upstream kinases can phosphorylate the eukaryotic translation initiation factor 2α (eIF2α) at serine 51, therefore preventing the formation of the 43S pre-initiation complex, which results in translation inhibition, mRNA release from polysomes and the subsequent assembly of SGs (Farrell et al., 1977; Kedersha et al., 1999). SG assembly is driven by RNA-binding proteins (RBPs) containing prion-like domains (PLDs) or IDRs which promote protein aggregation. These domains, characterized by low-complexity sequences, facilitate liquid-liquid phase separation, a crucial step in SG assembly. Furthermore, the combination of protein-protein, RNA-protein and RNA-RNA interactions lead to the formation of core structures by oligomerization of individual mRNPs. These cores progressively fuse to form larger SGs, characterized by multiple cores, surrounded by a more dynamic but less concentrated shell layer. The protein and mRNA composition of SGs is highly variable and depends, among others, on the cell type and the nature of the stressor (Anderson and Kedersha, 2008; Emara et al., 2012). Due to the high concentration of components, SGs can modulate a multitude of signal pathways by recruiting essential proteins. Proteomic analyses have identified a set of core components essential for SG assembly. Among these, the paralogs Ras GTPase-activating protein-binding protein 1 (G3BP1) and Ras GTPase-activating protein-binding protein 2 (G3BP2) are crucial for SG formation in mammalian cells, serving as marker proteins unique to this type of RNPs (Kedersha et al., 2005; Buchan and Parker, 2009). Additional core proteins include components of the 48S pre-initiation complexes, such as small ribosomal subunits, eukaryotic translation initiation factors (e.g. eIF3, eIF4E and eIF4G), T-cell intracellular antigen-1 (TIA-1) and poly(A)-binding protein cytoplasmic 1 (PABPC1), which have the capacity to bind to

untranslated mRNAs and to recruit additional proteins through their PLDs and IDRs. These integral proteins act as nucleators of SG formation when overexpressed in the absence of stress (Kedersha et al., 2000; Tourrière et al., 2003).

1.2.2 Function of stress granules

SGs have garnered significant attention due to their critical roles in mRNA localization, translation and degradation as well as their impact on signaling pathways and antiviral responses. The leading hypothesis in the field suggests that SGs function as temporary RNA storage sites, enabling associated transcripts to either re-enter the translational pool or be targeted for degradation upon stress release (Kedersha and Anderson, 2002; Buchan and Parker 2009). However, the precise functional role of SGs and their potential impact on regulation of gene expression remains unclear. During stress, SGs are thought to regulate translation reprogramming by sequestering non-essential mRNAs while allowing mRNAs that encode proteins essential for the stress response to remain available for translation (Kedersha and Anderson, 2002). This mechanism enables rapid changes in the cellular proteome in order to adjust to cellular needs. In addition to their role in storing untranslated mRNAs, SGs can modulate signaling pathways by sequestering numerous signaling proteins. This sequestration can divert these proteins from their canonical functions, potentially altering cellular processes such as metabolism, growth, and survival (Kedersha et al., 2013). Moreover, dysregulation of SG dynamics, whether through excessive formation or impaired clearance, has been linked to pathological protein aggregation in neurodegenerative diseases (Li et al., 2013; Ramaswami et al., 2013). Therefore, as a prototypical non-membrane-bound organelle, SGs serve as an excellent model for elucidating the molecular mechanisms that govern the assembly of phase-separated cellular compartments.

1.2.3 Role of stress granules in diseases

Increasing evidence suggests that mutations leading to functional impairment of biomolecular condensates are often associated with pathological changes in a range of diseases, including cancer, ischemic events, neurodegenerative diseases, viral infections, autoimmune diseases and even in aging processes. Among the different types of MLOs, SGs are particularly implicated in the progression of neurodegenerative disorders and myopathies. Several amyotrophic lateral sclerosis (ALS) studies demonstrated that mutations in SG-related proteins such as TIA1, FUS, and heterogeneous nuclear ribonucleoprotein A1 (hnRNPA1) result in increased SGs self-assembly within neurons. Under pathological conditions, SGs undergo a transition from a liquid-like to a solid state, whereby they serve as nucleation sites for stable and irreversible amyloid-structures. This can ultimately result in dysregulation of RNA processing and signaling pathways or impairment of protein degradation pathways (Ling et al., 2013). The 43-kDa TAR DNA-binding protein (TDP-43) is one key component of these protein aggregates observed in neurodegenerative diseases (Arai et al., 2006; Neumann et al., 2006). Under physiological conditions, TDP-43 is predominantly localized in the nucleus, where it

plays an essential role in regulating RNA splicing and maintaining mRNA stability (Lagier-Tourenne et al., 2010; Da Cruz and Cleveland, 2011). However, in degenerating neurons of ALS patients, TDP-43 is abnormally depleted from the nucleus and instead forms large cytoplasmic aggregates, driving disease progression. In addition, TDP-43 also undergoes several disease-specific posttranslational modifications, including hyperphosphorylation, ubiquitination, and cleavage (Kwon et al., 2007).

Adult cardiomyocytes, like terminally differentiated, post-mitotic neurons, share common characteristics, including a highly restricted capacity for division and regeneration. Therefore, they are particularly susceptible to both intrinsic and extrinsic stressors, including mutations that affect nuclear-localized proteins (Wolozin et al., 2019). Recently, dysregulated RNP granules have been linked to myocardial pathobiology and heart failure, particularly in the context of congenital dilated cardiomyopathy (DCM). In DCM patients, abnormal aggregation of RNP granules has been observed within the cytoskeleton of cardiomyocytes. Notably, the pathogenic R636S mutation in nuclear RNA-binding motif protein 20 (RBM20) promotes the accumulation of aberrant RNP granules within the sarcoplasm, linking these structures to myocardial pathobiology and the development of heart failure (Schneider et al., 2020).

SGs have also been implicated in cancer, where they function as part of a stress-adaptive strategy that enables tumor cells to modulate signaling pathways and metabolism, thereby enhancing survival under adverse conditions (Ivanov et al., 2019). Chemotherapeutic agents such as doxorubicin, bortezomib, cisplatin, and etoposide, which are commonly used in cancer therapy, are known to induce SG formation in tumor cells. This contributes to resistance against the cytotoxic effects of these drugs (Asadi et al., 2021). Additionally, SGs also participate in cellular defense mechanisms during viral infections by regulating viral replication and host responses (Guan et al., 2023).

1.3 Processing bodies

Processing bodies (P-bodies) represent the second major type of cytoplasmic RNP granules, playing key roles in the regulation of RNA turnover and gene expression repression. Initially identified in yeast, these structures are conserved across a wide range of organisms, including plants, fungi, and animals, highlighting their fundamental cellular functions (Bashkirov et al., 1997; Coller et al., 2001). P-bodies consist of components associated with RNA decay machinery, mRNA silencing and translationally repressed mRNAs (Sheth and Parker, 2003). Although they are constitutive cellular structures, their density can be dynamically modulated under stress conditions that inhibit translation initiation or impair RNA degradation (Kedersha et al., 2005; Teixiera et al., 2005). However, some conflicting reports indicate that their primary function may be to store, rather than degrade, mRNA (Hubstenberger et al., 2017). Spatiotemporal interaction of P-bodies with SGs were observed in both yeast and mammalian cells, indicating a dynamic mRNA cycle involving mRNP remodeling and bidirectional

exchanged between these condensates. P-body assembly into higher-order complexes relies on scaffold proteins such as mRNA-Decapping-Enzym 1A (DCP1A) and Enhancer of Decapping 4 (EDC4), which facilitate multivalent interactions that drive phase separation and condensate maturation. Genetic depletion of classical P-body components reduces the formation of both constitutive and stress-induced P-bodies, underscoring their essential and non-redundant roles in preserving condensate structure and function.

1.4 Paraspeckles

Paraspeckles (PSs) are one type of nuclear granules located in the interchromatin space of the nucleoplasm in mammalian cells (Fox et al., 2002). They are thought to form through LLPS and are involved in a variety of essential cellular functions, including RNA processing, regulation of DNA transcription, and control of the cell cycle. PSs are composed of a specific set of RBPs, including Splicing Factor Proline- And Glutamine-Rich (SFPQ), Non-POU Domain-Containing Octamer Binding Protein (NONO), FUS, TATA-Box Binding Protein Associated Factor 15 (TAF15), Ewing Sarcoma protein (EWS) and RNA-Binding Motif Protein 14 (RBM14), which are organized around the architectural long non-coding RNA (lncRNA), nuclear paraspeckle assembly transcript 1 (*Neat1*, also known as *MEN-ε/β or VINC-1*) (Hennig et al., 2015). These dynamic structures can assemble and disassemble in response to changes in cellular conditions, such as mitosis, stress responses and cell apoptosis (McCluggage and Fox, 2021). PSs regulate gene expression by retaining RNAs containing inverted repeats within the nucleus and by sequestering specific transcription factors. Notably, mitochondrial dysfunction can affect *Neat1* expression and PS formation, highlighting a potential link between PS dynamics and metabolism alterations. Additionally, PSs have been implicated in DNA repair and apoptosis regulation; alterations in their RNA and protein components have been associated with diseases, including cancer, neurodegenerative disorders, and chronic inflammatory diseases (An et al., 2018; Pisani and Baron, 2020; Azam et al., 2024).

1.5 Proximity-dependent labeling methods to study protein complexes

The most widely used methods for studying the composition of membraneless assemblies are traditional proteomic based methods, such as co-immunoprecipitation and organelle purification. However, these methods have limitations in capturing protein interactions or recruitment events that are transient or occur with rapid dynamics. To overcome these limitations, enzyme-catalyzed proximity labeling is a recently developed method to identify protein-protein interactions with high sensitivity and specificity in living cells. Proximity labeling techniques use engineered peroxidase or biotin ligases that are genetically fused to a protein of interest to covalently tag nearby proteins with biotin or similar labels. This allows identification of proteins in the spatial proximity of the target protein in living cells or tissues. Two commonly used enzymes are engineered ascorbate peroxidase 2 (APEX2) and promiscuous mutant of *Escherichia coli* (*E. coli*) biotin ligase (BioID), along with their variants (Figure 2) (Qin et al., 2021).

Enzyme	Enzyme activity	Source	Mutations	Size	Target	Labeling time	Substrat
BirA	Biotin ligase (promiscuous)	*E.coli*	R118G	35 kDa	Lys	18 h-24 h	Biotin
TurboID	Biotin ligase (promiscuous)	*E.coli*	Q65P, I87V, R118S, E140K, Q141R, S150G, L151P, V160A, T192A, K194I, M209V, M241T, S263P, I305V	35 kDa	Lys	10 min	Biotin
MiniTurbo	Biotin ligase (promiscuous)	*E.coli*	N-terminal aa1-63 deleted (DNA binding domain); Q65P, I87V, R118S, E140K, Q141R, S150G, L151P, V160A, T192A, K194I, M209V, I305V	28 kDa	Lys	10 min	Biotin
APEX2	Ascorbate peroxidase	Soybean	K14D, W41F, E112K, A134P	28 kDa	Tyr, Trp, Cys, His	1 min	Biotin-phenol + H_2O_2

Figure 2 Comparison of engineered proximity-based labeling enzymes.

Characteristics of the different proximity labeling enzymes, indicating type of activity, source, mutations, size, targeted amino acid, recommended labeling time and substrate used.

1.5.1 Biotin Ligase (BioID)

BioID is based on a mutant E. coli ligase BirA (R118G; also called BirA*) that specifically catalyzes the biotinylation of the acetyl-CoA carboxylase by forming an amide bond between reactive biotin and a lysine residue. This mutation within the conserved catalytic domain decreases the affinity to the reactive biotin-intermediate biotinoyl-5'-adenylate (bio-AMP) and allows a premature release of the reactive biotin to react with amines on proximate proteins (Figure 3) (Choi-Rhee et al., 2004; Cronan, 2005). The second generation of BioID (BioID2) is based on a smaller biotin ligase derived from Aquifex aeolicus (A. aeolicus). This variant lacks the DNA-binding domain present in BirA*, thereby reducing potential alterations in the localization and/or function of the enzyme when fused to a target protein. The primary limitation of BioID is the slow kinetics and prolonged labeling time to produce sufficient biotinylated proteins for proteomic analysis. For this reason, two BirA mutants from E. coli - TurboID and miniTurbo - were developed, which reduce the labeling time from 18-24 h to 10 min. These modified enzymes exhibit significantly enhanced catalytic activity and biotinylation efficiency compared to their BioID and BioID2 counterparts. TurboID (35 kDa) harbors 15 mutations relative to wild-type BirA, while the smaller miniTurbo (28 kDa) exhibits an N-terminal domain deletion and 13 mutations (Branon et al., 2018).

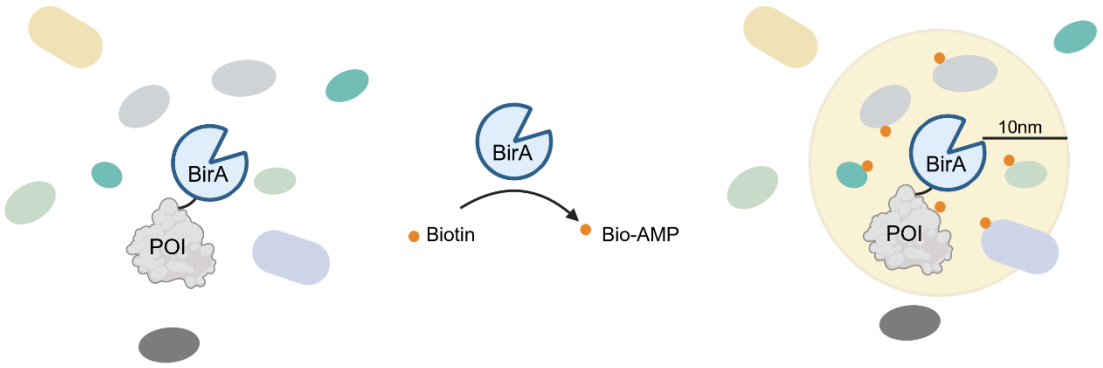

Figure 3 Model of BioID-mediated labeling.

Cellular expression of the biotin ligase (BirA) fused to a protein of interest (POI) facilitates the biotinylation of proximate proteins. The reactive intermediate bio-AMP covalently interacts with amine groups on proteins within an estimated range of 10 nm. Biotinylated proteins can be captured by affinity purification and subsequently identified using mass spectrometry.

1.5.2 Engineered ascorbate peroxidase (APEX)

Engineered ascorbate peroxidase (APEX) was originally created as a genetically encoded reporter enzyme to enable highly specific and high-resolution electron microscopy imaging and proximity labeling in living cells. Its natural purpose in plants is to detoxify hydrogen peroxide by reducing it with ascorbate, but the engineered version was adapted for biotechnological applications requiring robust enzymatic activity in diverse cellular environments. The initial version of APEX exhibited low catalytic activity, prompting the development of a more efficient enzyme via directed protein evolution, which resulted in APEX2, an improved, second-generation enzyme with one additional mutation (A134P). APEX2 uses hydrogen peroxide (H_2O_2) as an oxidant to catalyze the one-electron oxidation of the small-molecule substrate biotin-phenol (BP), generating highly reactive biotin-phenoxyl radicals that form covalent bonds with electron-rich amino acids such as tyrosine, tryptophan and cysteine in proteins located near the APEX2 fusion enzyme (Figure 4) (Hung et al., 2014; Lam et al., 2015; Martell et al., 2012; Rhee et al., 2013). Biotinylated endogenous proteins are subsequently enriched using streptavidin beads and identified by mass spectrometry. This technology combines the advantages of a fast labeling kinetic and high spatial specificity. In particular, APEX2 is the most efficient biotinylation method, with a biotinylation reaction time of 1 min, allowing the capture of even the most transient protein interactions (Rhee et al., 2013; Roux et al., 2012). The spatial resolution achieved by BioID- and APEX2-mediated biotinylation is in the range of 10–20 nm. Notably, BioID approach will result in lower cellular toxicity, whereas the APEX2 system is more suitable for snapshots of a certain proteome due to the short labeling time. Its ability to identify proteins in close proximity to a target protein of interest provides a valuable tool for studying RNP granule biology. In addition, replacement of the substrate biotin-phenol

by biotin-aniline and biotin-naphthylamine will enable APEX2 labeling technique to identify specific RNA molecules in RNPs (Padrón et al., 2019; Zhou et al., 2019).

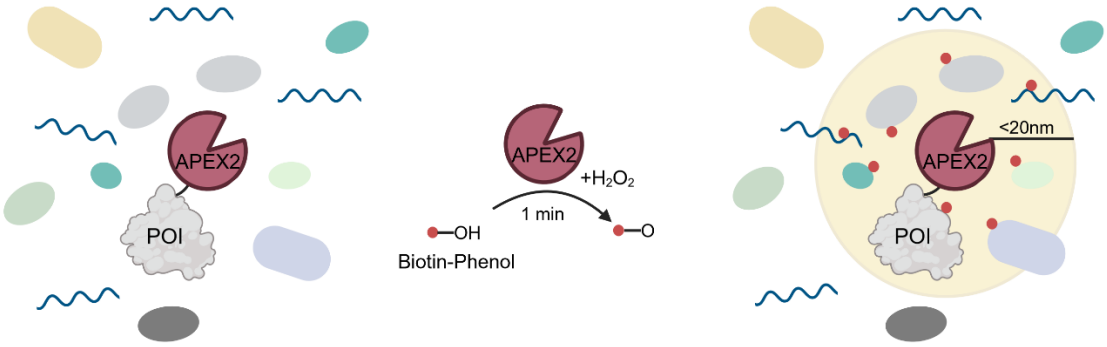

Figure 4 APEX2-mediated proximity biotinylation to identify proteins and RNA components in RNP granules.

The engineered soybean mutant ascorbate peroxidase (APEX2) fused to a protein of interest (POI) or targeted to a subcellular region of interest enables biotin labeling of proteins or RNAs located within a 20 nm radius. The enzyme utilizes supplemented hydrogen peroxide as an oxidant to catalyze the one-electron oxidation of biotin-phenol. The reactive biotin-phenoxyl radical covalently biotinylates electron-rich amino acids of proximate proteins. Biotinylated proteins or RNAs are subsequently enriched through affinity purification using streptavidin-coated beads. Bound proteins are identified by mass spectrometry, whereas bound RNAs are detected by next generation sequencing.

1.6 RNA binding proteins are key players in membraneless organelles

RNA-binding proteins (RBPs) serve as key components of RNP granules and play a pivotal role in various steps in RNA metabolism, such as splicing, transport, stability, and translation of mRNAs. RBPs comprise a large class of over 2,000 proteins that interact with all types of RNAs through one or more RNA-binding domains (RBDs), including the widely studied RNA recognition motif (RRM), K homology (KH) domain, zinc finger, Pumilio (Puf), and DEAD box helicase domains (Corley et al., 2020). In recent years, extensive research has explored the role of RBPs in cardiac function, revealing nearly 400 cardiomyocyte-specific RBPs, predominantly of the RRM-type, many of which have been implicated in the pathogenesis of heart failure (Liao et al., 2016). Notably, the loss of abundant alternative splicing factors, including RBM20 (Guo et al., 2012; Maatz et al., 2014), RBM24 (Yang et al., 2014; Liu et al., 2019; Lu et al., 2022), Muscleblind-like splicing regulator (MBNL1) (Dixon et al., 2015; Kalsotra et al., 2008), RNA Binding Fox-1 Homolog (RBFOX1) and RNA Binding Fox-2 Homolog (RBFOX2) (Wei et al., 2015; Gao et al., 2016), compromises cardiomyocyte function. RBPs can bind to single- or double-stranded RNA and facilitate the assembly of RNP granules. Their ability to drive RNP granule assembly largely depends on encoded IDRs and RBDs, which

enable multivalent interactions. Dysregulation of RBPs or aberrations in phase separation processes have been associated with diseases, such as cancer and most importantly with neurodegenerative disorders, highlighting the critical role of RBPs in maintaining cellular organization and function through biomolecular condensates (Cookson, 2017).

Previously, dysregulated RNP granules have been linked to myocardial pathobiology and heart failure in patients with DCM caused by a mutation in the gene encoding the striated muscle specific RBM20, which results in the accumulation of RBM20 containing sarcoplasmic condensates (Schneider et al., 2021). However, in-depth analysis of RNP formation processes mediated by mutations in additional RBPs within cardiomyocytes is required to gain deeper insights into the molecular mechanisms driving pathogenic RNP granule accumulation that leads to heart failure.

1.6.1 RNA binding protein with multiple splicing is a multifunctional RNA-binding protein

RNA-binding protein with multiple splicing (RBPMS), also known as *hermes* in frog and chicken, is a member of the RRM family, characterized by its ability to bind to specific RNA sequences (tandem CAC motif), including messenger RNAs (mRNAs), microRNAs (miRNAs), and long non-coding RNAs (lncRNAs) (Gerber et al., 1999; Akerberg et al., 2019). The RBPMS family encodes 2 members, RBPMS and RBPMS2, which contain a single RRM of ~80 amino acids that is responsible for both RNA binding and dimerization. The C-terminal region of RBPMS contains an IDR characterized long proline stretches without homology to other proteins (Farazi et al., 2014). The *Rbpms* gene, located on chromosome 8 at position p12, spans over 230 kb in the human genome. In mouse, alternative splicing (AS) generates multiple RBPMS protein isoforms (5 according to UniProt, 4 according to RefSeq, NCBI and at least 19 transcript variants according to AceView), whereas the paralog RBPMS2 is exclusively expressed as a single isoform (Shimamoto et al., 1996). Most commonly expressed isoforms are *Rbpms-203/-213*, which both encode a 197 amino acids (aa) variant 1 (*Rbpmsa*), *Rbpms-201*, encoding a 191 aa variant 2 (*Rbpmsc*) and *Rbpms-202*, which encodes a 220 aa variant 3 (*Rbpmsb*). All reported splicing variants share the same first 5 exons, suggesting a common core promotor for transcriptional regulation. However, the isoforms differ in their C-terminus, encoded by exon 8 in variant 1, exons 8-10 in variant 2 and exon 7 in variant 3 (Figure 5). These variations in sequence correspond to functional diversification; the RNA recognition element (RRE) of RBPMS which consists of tandem CAC motifs separated by a spacer of approximately 1–12 nucleotides, is conserved among various species including Drosophila and Caenorhabditis elegans (Farazi et al., 2014; Ray et al., 2013; Soufari and Mackereth, 2017). RBPMS is broadly expressed across multiple tissues, with particularly high levels in retinal ganglion cells (RGCs), smooth muscle cells and in the vertebrate heart, where it plays a crucial role in RNA splicing, stability and transport (Gerber et al.,1999; Piri et al.,

2006). Its paralog, RBPMS2, shares 67% amino acid identity with RBPMS, varying mostly in their N- and C-terminal regions. Functionally, RBPMS predominantly localizes to the nucleus, whereas RBPMS2 is primarily found in the cytoplasm (Shimamoto et al., 1996).

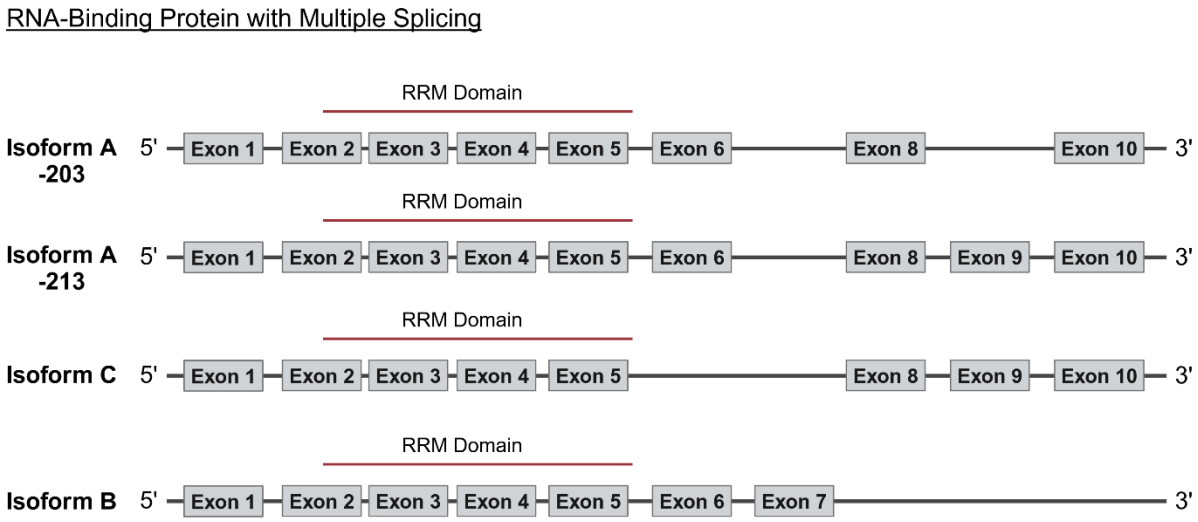

Figure 5 Schematic view of RNA-Binding Protein with Multiple Splicing (RBPMS) isoforms A, B and C.

RBPMS encodes multiple splicing variants by alternative splicing at the 3' end. Schematic illustration of the exon organization of the three previously described RBPMS isoforms (A, B and C), highlighting the positioning of the RNA recognition motif (RRM) domain within each isoform.

1.6.2 Biological roles of RBPMS

RBPMS is an RNA-binding proteins that play critical roles in several aspects of RNA metabolism and gene regulation, including transcription, degradation, transport, stability and splicing (Rabelo-Fernández et al., 2022). Similar to other nucleocytoplasmic or cytoplasmic mRNA-binding proteins, RBPMS re-localizes to cytoplasmic SGs under oxidative stress conditions suggesting a supporting function of RBPMS for mRNA localization in large and/or multinucleated cells where it is preferentially expressed (Farazi et al., 2014). Within these complexes, RBPMS regulates the stability, localization, and translation of RNAs by modulating interactions with other RNP components, such as RBPs, ribonucleases, and RNA helicases. Furthermore, RBPMS is recruited to P-bodies, where it facilitates mRNA decay by binding to CCR4-NOT transcription complex subunit 2 (CNOT2), a component of the CCR4-NOT deadenylation complex (Rambout et al., 2016).

Manipulations of RBPMS levels during embryogenesis suggested functions in *Xenopus laevis* oocyte maturation (Zearfoss et al., 2004), heart and kidney development (Gerber et al., 2002) as well as retinal ganglion cell development (Hörnberg at al., 2013).

Moreover, RBPMS has been identified as a critical splicing regulator in differentiated vascular smooth muscle cells (SMCs) by directly regulating AS of numerous components of the actin

cytoskeleton and focal adhesion machinery, which are important for SMC phenotype-specific function. In addition, RBPMS modulates the splicing of various regulators involved in transcription and splicing, including myocardin, a key transcription factor in SMCs (Nakagaki-Silva et al., 2019; Jacob et al., 2024).

A recent study reported that *Rbpms* is required for normal heart development in mice and constitutive loss-of function mutants result in a premature onset of cardiomyocyte binucleation, ultimately leading to non-compaction cardiomyopathy. Intriguingly, RBPMS-deficient human cardiomyocytes exhibit comparable defects in cytokinesis by mediating isoform switching of the heart-enriched LIM domain protein Pdlim5 (Gan et al., 2023).

1.6.3 RBPMS dysregulation and cancer

Pathology expression data from the Human Protein Atlas indicate that RBPMS exhibits moderate to strong nuclear staining in the majority of endometrial, ovarian, testicular, renal, and pancreatic carcinomas, with occasional cases observed in melanomas and cervical, breast, and lung cancers. Only a limited number of studies support these findings by examining the role of RBPMS dysregulation in cancer. Increased levels of RBPMS suppress cell proliferation, migration and invasion ability of ovarian cancer cells (Rabelo-Fernández et al., 2022). Furthermore, in both cultured cells and mouse xenograft models, RBPMS inhibits the growth and migratory capacity of breast cancer cells through its interaction with the transcription factors c-Fos or Smad3 (Sun et al., 2006).

1.7 Pathophysiological mechanisms of doxorubicin-induced cardiotoxicity

Anthracyclines represent one of the most effective chemotherapy agents employed in the treatment of sarcomas, lymphoma, leukemia and breast cancer. Doxorubicin, a widely used anthracycline, is a potent antitumor drug, however it has been associated with the onset of cardiomyopathy, a severe and often irreversible complication (Rochette et al., 2015). Doxorubicin-induced cardiomyopathy is characterized by the loss of cardiomyocytes, leading to impaired cardiac function and potentially life-threatening consequences. Notably, both children under 4 years and adults over 65 are at increased risk of developing cardiotoxicity (Henriksen, 2018; Bhagat and Kleinerman, 2020).

The mechanisms underlying doxorubicin-induced cardiomyopathy remain incompletely understood. Proposed mechanisms include oxidative stress, mitochondrial dysfunction, cardiomyocyte apoptosis, and inflammation (Van der Zanden et al., 2012; Rawat et al., 2021). Moreover, the enzyme topoisomerase II beta (Top2b), which prevents DNA double-strand breaks (DSBs) induced by cellular stress, has been directly implicated in this process. Top2b is the predominant isoform expressed in cardiomyocytes, whereas the alpha isoform (Top2a) is mainly found in proliferating cells. Doxorubicin primarily targets Top2b by intercalating into DNA, thereby inhibiting its binding and catalytic activity. This interaction stabilizes a ternary

Top2b-doxorubicin-DNA cleavage complex, which leads to the formation of DSBs and ultimately results in cell death (Zhang et al., 2012). Doxorubicin-treated cardiomyocytes exhibit ultrastructural alterations including mitochondrial damage and vacuolization, increased DSBs, and heightened apoptosis (Chatterjee at al., 2010). The absence of Top2b has been shown to attenuate the cardiotoxic effects associated with doxorubicin treatment, displaying reduced levels of DSBs and apoptosis. Intriguingly, the Top2b mediates doxorubicin-induced reduction of the ejection fraction, a clinical hallmark of cardiomyopathy caused by the drug. These findings highlight a mechanistic link between Top2b activity and the progression of doxorubicin-induced cardiac dysfunction (Zhang et al., 2012). At the cellular and molecular levels, these effects manifest clinically as symptoms such as heart failure, arrhythmias, and reduced cardiac function, which may emerge acutely during treatment or years later. The morphological and functional cardiac abnormalities associated with this condition closely resemble those observed in dilated cardiomyopathy, including ventricular and atrial enlargement, reduced left ventricular ejection fraction, and impaired contractile function. Strategies for the prevention and treatment of doxorubicin-induced cardiomyopathy remain limited, thereby underscoring the need for the development of novel therapeutic approaches with the objective of mitigating the risk of cardiotoxicity in patients undergoing chemotherapy.

Dexrazoxane (Zinecard, also known as ICRF-187) is a clinically approved cardioprotective agent used to reduce or prevent the development of doxorubicin-induced cardiotoxicity (Hasinoff, 1998). Its proposed mechanisms of action include acting as a potent iron chelator, which inhibits the formation of anthracycline-iron complexes and, in turn, reduces the subsequent generation of reactive oxygen species (ROS). In addition, dexrazoxane interferes with the formation of anthracycline-Top2 DNA cleavage complexes, thereby reducing DNA damage in cardiac cells (Hasinoff et al., 1995; Lyu et al., 2007). Multiple clinical trials have demonstrated the efficacy of the agent in reducing the incidence of cardiotoxicity, including left ventricular dysfunction, heart failure, and cardiac death, in patients receiving anthracycline-based chemotherapy. Importantly, dexrazoxane does not compromise the antitumor efficacy or increase the non-cardiac toxicity of chemotherapy regimens (Speyer et al., 1988; Wexler et al., 1996; Swain et al., 1997; Lipshultz et al., 2004; Hensley et al., 2009).

1.8 Cardiomyopathy

Cardiomyopathies represent a diverse group of myocardial diseases with heterogeneous etiologies. These conditions are broadly categorized into two main groups: primary (intrinsic) and secondary (extrinsic) cardiomyopathies. Primary cardiomyopathies are confined to the cardiac muscle and result from genetic mutations or acquired abnormalities. In contrast, secondary cardiomyopathies arise due to myocardial damage caused by systemic disorders, including myocardial ischemia, inflammation, infections, or heightened drug toxicity. The most

common types of primary cardiomyopathies comprise dilated cardiomyopathy and myocarditis (Maron et al., 2006).

1.8.1 Dilated cardiomyopathy

Dilated cardiomyopathy (DCM) represents the second most prevalent form of primary cardiomyopathy. Clinically, it is characterized by dilation and enlargement of the left or both ventricles, accompanied by ventricular wall thinning and increased left ventricular mass (Weintraub et al., 2017; McNally et al., 2017). This structural remodeling leads to impaired cardiac function, manifesting as reduced stroke volume and cardiac output, as well as abnormalities in ventricular filling. Additionally, elevated end-diastolic pressure, increased cardiac preload and afterload are clinical characteristics of DCM (Holubarsch et al., 1996; Saks et al., 2006). Unlike myocarditis, which is primarily an inflammatory disorder, DCM is typically a heterogenous, often idiopathic condition. The primary etiology of DCM involves genetic mutations affecting cytoskeletal and sarcomeric proteins. Recent research has identified defective AS mechanisms as contributory factors, particularly missense mutations in splicing regulators RBM20 (Guo et al., 2012), RBM24 (Liu et al., 2019) and RBFOX1 (Gao et al., 2016), which induce pathological mis-splicing of numerous myocardial transcripts in familial DCM cases. In addition to genetic causes, environmental factors, infectious agents, and exposure to cardiotoxic substances contribute to the development of secondary DCM.

1.8.2 Myocarditis

Myocarditis is an acute or chronic inflammatory response of the myocardium mostly triggered by viral infection, although bacterial, protozoal or fungal pathogens, as well as exposure to toxic substances, have also been implicated as causative factors (Lampejo et al., 2021; Tschöpe et al., 2021). Pathologically, myocarditis is characterized by focal or diffuse infiltration of mononuclear cells within the myocardial tissue and is typically categorized into 3 stages: an acute phase caused by viral entry and replication, a subacute phase defined by inflammatory cell infiltration and a chronic phase associated with cardiac dysfunction and structural remodeling. The clinical manifestations are heterogeneous, ranging from asymptomatic or mild symptoms to severe cardiac damage, potentially resulting in cardiogenic shock and life-threatening arrhythmias (Maron et al., 2006; Taqueti et al., 2006; Caforio et al., 2013). Notably, myocarditis can be manifest as acute heart failure and, in some cases, progress to the development of DCM (Fabre et al., 2006).

1.9 Aim of the study

The RNA-binding protein RBPMS contributes to various fundamental RNA metabolism-based functions, including mRNA splicing, transport and stability. In addition to these functions, RBPMS has been observed to relocalize to cytoplasmic SGs in response to oxidative stress. SGs are membraneless RNP assemblies composed of RNA and proteins that form during translational repression and have been implicated in pathological aggregates observed in

neurodegenerative diseases. However, in the context of the cardiovascular system, the turnover, composition and (patho)physiological role of RNP granules remain poorly characterized. A detailed study of RNP granule-mediated disease progression caused by RBPs in cardiomyocytes, may uncover underlying molecular and cellular mechanisms. Such insights might facilitate the development of novel therapeutic strategies to counteract or neutralize these persistently evolving biomolecular condensates. The main aim of this study was to examine the (patho)physiological role of RBPMS-positive RNP granules in the heart, with particular focus on their function under both physiological and cardiac stress conditions. In this context, particular attention was focused on stress induced by the anthracycline chemotherapeutic agent doxorubicin, owing to its well-documented cardiotoxic effects. Doxorubicin-induced cardiomyopathy remains a major clinical challenge, especially among pediatric and young adult cancer patients, due to the current lack of effective preventive strategies, thereby significantly limiting the broader therapeutic use of this drug. To address this aspect, proximity-dependent biotinylation combined with affinity purification assay (APEX2) was employed to visualize and characterize the composition of RBPMS-associated RNPs in cardiomyocytes under baseline and stress conditions. Additionally, mouse models with cardiac-specific knockout and overexpression of RBPMS (isoform A and B) were used to assess isoform-specific contributions to granule biogenesis and turnover. Furthermore, interaction partners of RBPMSA and RBPMSB were identified in cardiomyocytes to better understand the distinct functions and subcellular localization dynamics of each isoform. Finally, molecular biological analysis tools were exploited to determine transcriptomic changes induced by doxorubicin treatment.

2. Material and Methods

2.1 Material

Table 1 Cell lines

Cell line	Company	Catalog no.
Human embryonic kidney cell line (293T-HEK)	ATCC	CRL-11268TM
HL-1 Cardiac Muscle Cell Line	Sigma-Aldrich	SCC065

Table 2 Chemicals and Reagents

Enzyme	Company	Catalog no.
Agar 100 Resin Kit	Agar Scientific Ltd	AGR1031
Agarose	Carl Roth	2267
Ammonium persulfate	Sigma-Aldrich	A3678
Aprotinin	Sigma-Aldrich	10820
Benzamidine	Acros-organics	401790050
Biotin (≥99%)	Sigma-Aldrich	B4501-100MG
Biotinyl tyramide	Merck	SML2135
Bis-Tris	AppliChem	A1025,0500
Bovine serum albumin (BSA)	Thermo Fisher Scientific	BP 1605
Bovine serum albumin solution (BSA)	Sigma-Aldrich	A7284-500ML
Bromphenol blue	Merck	1081220005
Calcium chloride x $2H_2O$	Carl Roth	5239.2
Cisplatin	Merck	232120
Claycomb medium	Sigma-Aldrich	51800C
DAPI (4', 6-diamidino-2-phenylindole)	Thermo Fisher Scientific	D1306
Deoxycholic acid	Fluka	30970
Dexrazoxane	Santa Cruz Biotechnology	SC-252669
Dimethyl sulfoxide (DMSO)	Sigma-Aldrich	D-4540
Disodium hydrogen phosphate (Na2HPO4)	Merck	6580.0500
Doxorubicin hydrochloride	Santa Cruz Biotechnology	SC-200923
1,4-Dithiothreit (DTT)	Carl Roth	6908.2
Dulbecco's modified eagle's medium high glucose	Sigma-Aldrich	D5796
Dulbecco's Modified Eagle's Medium-high glucose + GlutaMAX	Gibco	42430-025
EDTA	Carl Roth	8040.3
EGTA	Sigma-Aldrich	E3889
Ethanol (100%)	Carl Roth	K928.3
Ethanol denatured	Carl Roth	9065.4
Ethidium bromide solution (1 %)	AppliChem	A1152,0100
FSC 22 Frozen Section Compound	Leica	75806-668
Fetal bovine serum	Sigma-Aldrich	F2442
Fetal calf serum	Sigma-Aldrich	F2442

Fibronectin (HL-1 cells)	Sigma-Aldrich	F1141
Fibronectin	PromoCell	C-43050
Formaldehyd 37%	Sigma-Aldrich	F1635
Gelatin from porcine skin	Sigma-Aldrich	G1890
Glucose	Carl Roth	X997.2
L-Glutamine	Sigma-Aldrich	G7513
L-Glutamine-penicillin-streptomycin solution	Sigma-Aldrich	G6784-100ML
Glutaraldehyde	Sigma-Aldrich	G5882
Glycerin (87%)	Merck	1.04094.2500
Glycine	Sigma-Aldrich	15527
HEPES	Carl Roth	9105.3
Hydrochloric acid (37%)	Carl Roth	4625.1
Hydrogen peroxide solution 30% (w/w)	Sigma-Aldrich	H1009-100ML
Isopropanol	Carl Roth	6752.4
Leukemia inhibitory factor	Merck	LIF1050
Leupeptin	Thermo Fisher Scientific	78435
Liberase™	Roche	05401151001
Lipofectamine 2000 reagent	Thermo Fisher Scientific	11668019
Lithium chloride	Carl Roth	P007.1
Magnesium chloride x $6H_2O$	Carl Roth	2189.1
2-Mercaptoethanol	Sigma-Aldrich	97622
Methanol	Carl Roth	4627.5
Mitomycin-C	Sigma-Aldrich	M4287
Mowiol 4-88	Merck	3186101
100x non-essential amino acid	Gibco	11140050
Nonidet P40	Fluka	74385
Norepinephrine	Sigma-Aldrich	A0937
4 x NuPAGE™ LDS Sample Buffer	Thermo Fisher Scientific	NP0008
Paraformaldehyde	Carl Roth	0335.4
Penicillin-Streptomycin (10,000 U/mL)	Thermo Fisher Scientific	15140122
Phenylmethylsulfonyl fluoride (PMSF)	Sigma-Aldrich	P7626
Potassium chloride (KCl)	Carl Roth	6781.3
Potassium bicarbonate (KHCO3)	Merck	1.04854.0500
Potassium dihydrogen phosphate (KH2PO4)	Carl Roth	P018.1
Puromycin dihydrochloride	Sigma-Aldrich	9620
Red Alert™ 10x	Merck	71078-3
RNaseZAP™	Sigma-Aldrich	SLBQ7780V
RNasin Plus	Promega	A515.1
Rotiphorese® Gel 40 (29:1)	Carl Roth	K015.2
Roti® Quant	Carl Roth	2326.3
Skim milk powder	Fluka	K305.1
Sodium azide (NaN3)	Carl Roth	1.06329.0500
Sodium bicarbonate (NaHCO3)	Merck	3957.2
Sodium chloride (NaCl)	Carl Roth	1.06504.0100
Sodium dodecyl sulfate (SDS)	Carl Roth	70166

Sodium deoxycholate	Merck	9097.1
Sodium L-ascorbate	Sigma-Aldrich	A4034
Streptavidin magnetic beads	Pierce	88817
Sucrose	Carl Roth	9097.1
TEMED (Tetramethylethylenediamine)	Carl Roth	5429.2
Tris	Carl Roth	6683.1
Triton-X 100	Carl Roth	R0531
TRIzol Reagent	Invitrogen	15596026
Trolox ((+/−)-6-Hydroxy-2,5,7,8-tetramethylchromane-2-carboxylic acid)	Sigma-Aldrich	238813
Trypsin Inhibitor	Sigma-Aldrich	T6522
TurboFect transfection reagent	Thermo Fisher Scientific	822184.0500
Tween-20	Merck	9713.3

Table 3 Buffer Solutions

Buffer	Composition
10% APS	Dilute 10 g APS in 100 mL Aqua dest.
5% BSA	Dilute 5 g BSA in 100 mL 1 x TBS-T
Cardiomyocyte isolation calcium-free buffer	113 mM NaCl; 4.7 mM KCl; 0.6 mM KH2PO4; mM Na2HPO4; 1.2 mM MgSO4 x 7H_2O; 12 mM NaHCO3; 10 mM KHCOS; 10 mM HEPES; 30 mM taurine; 10 mM 1 2,3-butanedionemonoxime; 5.5 mM glucose
Cardiomyocyte isolation enzyme buffer	0.25 mg/ml Liberase™ DH; 0.14 mg/ml trypsin; 12.5 µmol CaCl2 in calcium-free buffer
Cardiomyocyte isolation stop buffer 1	10% FCS; 12.5 µM CaCl2 in enzyme buffer
Cardiomyocyte isolation stop buffer 2	5% FCS; 12.5 µM CaCl2 in enzyme buffer
Cardiomyocyte cell culture medium	M199 cell culture medium supplemented with 5 mM creatinine x H_2O; 2 mM L-carnitine x HCl; 5 mM taurine; 25 mM HEPES; 1% penicillin/streptavidin; 10% fetal calf serum; 1% insulin-transferrin-sodium selenite media supplement, pH 7.3.
Extraction buffer	100 mM Tris-HCl, pH 8.0; 10 mM EDTA; 10% SDS
Immunofluorescence blocking buffer	0.1% BSA in 1x PBS
Mass Spec Buffer A	0.1% formic acid
Mass Spec Buffer B	80% acetonitrile; 0.1% formic acid
5% Immunoblot blocking solution	Dilute 5 g skim milk/ BSA in 100 mL 1 x TBS-T
10x Phosphate buffered saline (PBS), pH 7.4	Dilute 80 g NaCl; 2 g KCl; 14.4 g Na2HPO4; 2.4 g KH2PO4 in 800 mL Aqua dest.; adjust pH to 7.4; refill to 1000 mL with Aqua dest.
1x Phosphate buffered saline (PBS), pH 7.4	100 mL 10x PBS + 900 mL Aqua dest.; adjust pH to 7.4
Radio-Immunoprecipitation assay buffer (RIPA) lysis buffer, pH 8.0	50 mM Tris, pH 7,4; 150 mM NaCl; 1% NP-40; 0.5% sodium deoxycholate; 0.1% SDS
10% SDS	Dilute 10 g SDS in 100 mL Aqua dest.

50x Tris-acetat-EDTA (TAE)	Dilute 242 g Tris Base; 57.1 mL acetic acid; 100 mL 0.5 M EDTA, pH 8.0 in 1000 mL Aqua dest.
10x Tris-buffered saline (TBS), pH 7.6	0.2 M Tris, 1.4 M NaCl
1x Tris-buffered saline (TBS)	100 mL 10 x TBS + 900 mL Aqua dest.
1x Tris-buffered saline + Tween 20 (TBS/T)	100 mL 10 x TBS + 900 mL Aqua dest. + 0.1% Tween®20
TENS lysis buffer	1 M Tris/HCl, pH 8.0; 0.5 M EDTA, pH 8.0; 4 M NaCl; 20% SDS
10x Tris-EDTA (TE)	100 mM Tris-Cl; 10 mM EDTA, pH 8.0
1x Tris-EDTA (TE)	100 mL 10x TE + 900 mL Aqua dest.
20x Transfer buffer	Dilute 163.2 g Bicine; 209.6 g Bis-Tris; 12 g EDTA in 1000 mL Aqua dest.
1x Transfer buffer	250 mL 20 x transfer buffer; 1000 mL methanol; 3750 mL Aqua dest.
1 M Tris, pH 8.0	Dilute 12.1 g Tris in 80 mL MilliQ H_2O.; adjust pH to 8.0; refill to 100 mL with Aqua dest.

Table 4 Solutions and buffers for proximity labeling

Solution/ buffer	Stock concentration/ components
Biotin	10 mM in DMSO
Biotin-phenol	500 mM in DMSO
Hydrogen peroxide (H_2O_2)	100 mM in PBS
Sodium azide	1 M in dH_2O
Sodium l-ascorbate	1 M in dH_2O
Trolox	500 mM in DMSO
Quencher solution	10 mM sodium ascorbate; 5 mM Trolox; 10 mM sodium azide in DPBS
Lysis buffer	10 mM sodium azide, 10 mM sodium ascorbate, 5 mM Trolox in RIPA lysis buffer supplemented with 1x protease Inhibitors and 1 mM PMSF

Biotin, biotin-phenol and sodium azide stock solutions were prepared and stored at -20 °C or -80 °C. The H_2O_2 solution was freshly prepared from a 30% (w/w) solution. Sodium ascorbate, Trolox, quencher solution and supplemented lysis buffers were prepared freshly.

Table 5 Kits

Kit	Company	Catalog No.
CloneExpress Ultra One Step Cloning Kit	Vazyme Biotech Co., Ltd	C115
Direct-zol™ RNA-Kit	Zymo Research	R2052
Mouse Neonatal Cardiomyocyte Isolation Kit	Miltenyi Biotec	130-100-825
Neonatal Heart Dissociation Kit	Miltenyi Biotec	130-098-373
Super Signal™ West Pico Chemiluminescent Substrate kit	Thermo Fisher Scientific	PI34080

Table 6 Ready-to-use Buffer Solutions

Buffer	Company	Catalog no.
2x Taq Master mix	Vazyme biotech	P111/P112
NuPAGE™ MES SDS Running Buffer	Thermo Fisher Scientific	NP000202
NuPAGE™ MOPS SDS Running Buffer	Thermo Fisher Scientific	NP000102
TaqMan™ Gene Expression Master Mix	Applied Biosystems™	10525395

Table 7 Composition of gel electrophoresis 9% Bis-Tris Polyacrylamid gel (PAA)

Reagent	Separation gel (9%)	Stacking gel (5%)
Aqua dest.	2.9 mL	0.96 mL
3.5x Bis-Tris (pH 6.5-6.8)	2.0 mL	0.5 mL
PAA 30% (37.5:1)	2.1 mL	0.29 mL
10% APS	25 µl	8 µl
TEMED (> 99%)	7 µl	3 µl

Table 8 Marker

Marker	Company/Composition
Protein Marker VI (10 - 245) prestained BC	PanReac AppliChem
PUC Marker	Homemade

Primary antibodies

Table 9 Primary antibodies for immunoblotting

Primary antibody	Dilution	Company	Catalog no.
anti-GAPDH	1:1000	Cell Signaling	2118
anti-RBPMS	1:1000	Sigma-Aldrich	HPA056999
anti-(CGY)FP	1:1000	Evrogen	AB121
anti-TurboGFP	1:1000	Evrogen	AB513
anti-V5	1:1000	Abcam	ab9116
anti-α-Tubulin	1:1000	Sigma-Aldrich	T6074

Table 10 Primary antibodies for immunofluorescence staining

Primary antibody	Dilution	Company	Catalog no.
anti-G3BP	1:1000	Abcam	ab56574
anti-RBPMS	1:1000	Sigma-Aldrich	HPA056999
anti-DCP1A	1:1000	Sigma-Aldrich	WH0055802M6
anti-PABP	1:1000	Proteintech	10970-1-AP
anti-SFPQ	1:1000	Proteintech	67129-1-Ig

anti-TDP-43	1:1000	Thermo Fisher Scientific	MA5-27828
anti-α-sarcomeric-Actinin	1:1000	Sigma-Aldrich	A7811
anti-V5	1:500	Abcam	ab9116
anti-TurboGFP	1:250	Evrogen	AB513
anti-(CGY)FP	1:250	Evrogen	AB121
anti-Phalloidin-FITC	1:250	Sigma-Aldrich	P5282
anti-Phalloidin-TRITC	1:300	Sigma-Aldrich	P1951
anti-SQSTM1/p62	1:250	Abcam	ab56416
DAPI	1:1000	Thermo Fisher Scientific	D1306

Secondary antibodies

Table 11 Secondary antibodies for immunoblotting

Secondary antibody	Dilution	Company	Catalog no.
Goat-anti-mouse IgG, HRP	1:1000	Thermo Fisher Scientific	31430
Goat-anti-rabbit IgG, HRP	1:1000	Thermo Fisher Scientific	31460

Table 12 Secondary antibodies for immunofluorescence staining

Secondary antibody	Dilution	Company	Catalog no.
anti-mouse Alexa 488	1:1000	Invitrogen	A11001
anti-mouse Alexa 594	1:1000	Invitrogen	A11005
anti-rabbit Alexa 594	1:1000	Invitrogen	A11012
anti-mouse Alexa 633	1:1000	Thermo Fisher Scientific	A21126
anti-rabbit Alexa 647	1:1000	Thermo Fisher Scientific	A21246
anti-rabbit Cy3	1:400	Dianova	711-165-152
anti-mouse Cy5	1:500	Dianova	715-175-150

Table 13 TaqmMan assay qRT-PCR probes

Name	Assay ID	Species
Rbpms	Mm00803908_m1	mouse
Gapdh	Mm99999915_g1	mouse

Table 14 Enzymes

Enzyme	Company	Catalog no.
Proteinase K	Carl Roth	7528.2
SuperScript™ II Reverse Transcriptase including 5 x	Thermo Fisher Scientific	18064014

First strand buffer, 0.1 M DTT		
Trypsin-EDTA	Thermo Fisher Scientific	R001100
Trypsin	Sigma-Aldrich	T0303
TrypsinL	Thermo Fisher Scientific	12604013

Table 15 Protease Inhibitors

Inhibitor	Company	Catalog no.
Aprotinin	Sigma-Aldrich	10820
Leupeptin	Sigma-Aldrich	L8511-5MG
Sodium fluoride (NaF)	Sigma-Aldrich	S7920-100G
Sodium orthovanadate (Na3Vo4)	Sigma-Aldrich	450243
Phenylmethylsulfonyl fluoride (PMSF)	Sigma-Aldrich	P7626

Table 16 Primers for genotyping

PCR	Primer Description	Sequence
Rosa-CAG	Rosa-CAG-for Rosa-CAG-rev Rosa-WT-rev	CTT GCT CTC CCA AAG TCG CTC TGA G ACC GTA AGT TAT GTA ACG CGG AAC TCC CTT TAA GCC TGC CCA GAA GAC TCC C
Cre	Cre-for Cre-rev	CGA CCA GGT TCG TT CAC TCA TGG CAG GCT AAG TGC CTT CTC TAC ACC
RBPMSB-APEX2	RosaPA-5-homology-for Rosa26-CAG-geno-rev2	TCT GCT GCC TCC TGG CTT CT GCG GAA CTC CAT ATA TGG GCT ATG A
APEX2	RosaPA-5-homology-for Rosa26-CAG-geno-rev2	TCT GCT GCC TCC TGG CTT CT GCG GAA CTC CAT ATA TGG GCT ATG A
Rbpmsb-KO	R1V3KO-r1 R1V3KO-f2 R1V3-intern-R2	TACTAAAGCACAGGCTGGCTAGGCG ATCTTGGCCGTGTGCCTCACTGG TCCCAGCCTGGACCAATACATTCGACA
RBPMSA-GFP	Rosa-CAG-for Rosa-CAG-rev Rosa-WT-rev	CTT GCT CTC CCA AAG TCG CTC TGA G ACC GTA AGT TAT GTA ACG CGG AAC TCC CTT TAA GCC TGC CCA GAA GAC TCC C
RBPMSB-GFP	Rosa-CAG-for Rosa-CAG-rev Rosa-WT-rev	CTT GCT CTC CCA AAG TCG CTC TGA G ACC GTA AGT TAT GTA ACG CGG AAC TCC CTT TAA GCC TGC CCA GAA GAC TCC C

Table 17 Genotyping protocols

PCR	Primer	Program	Fragment size
XMLC2-Cre	Cre-for Cre-rev	94°C 4:00 94°C 0:30 66°C 0:30 72°C 0:45 Go to 2, repeat 35x 72°C 5:00	Transgene 244 bp

		12°C ∞	
ROSA-CAG	ROSA-CAG-for ROSA-CAG-rev ROSA-wt-rev	94°C 3:00 94°C 0:30 57°C 0:30 72°C 0:30 Go to 2, repeat 35x 72°C 5:00 12°C ∞	Wildtype 249 bp Transgene 325 bp
RBPMSB-APEX2	RosaPA-5-homology-for: Rosa26-CAG-geno-rev2	94°C 3:00 94°C 0:30 57°C 0:30 72°C 0:30 Go to 2, repeat 35x 72°C 5:00 12°C ∞	Wildtype 249 bp Transgene 325 bp
APEX2	RosaPA-5-homology-for: Rosa26-CAG-geno-rev2	94°C 3:00 94°C 0:30 57°C 0:30 72°C 0:30 Go to 2, repeat 35x 72°C 5:00 12°C ∞	Wildtype 249 bp Transgene 325 bp
Rbpmsb-KO	R1V3KO-r1 R1V3KO-f2 R1V3-intern	94°C 3:00 94°C 0:30 57°C 0:30 72°C 0:30 Go to 2, repeat 32x 72°C 5:00 12°C ∞	Wildtype 354bp Transgene 170-230 bp

Table 18 Equipment

Equipment	Company
Agarose gel electrophoresis chamber	Peqlab
BioDoc analyzer	Bio-Rad
BioAnalyzer 2100	Agilent
Centrifuges	Eppendorf
Cell culture plates/ dishes	Greiner Bio-one
ChemiDoc™ MP Imaging System	Bio-Rad
Cold Plate for Tissue Embedding System	Leica
Coverslips	Carl Roth
Cryostat	Leica
Eppendorftubes, 0.5 mL, 1.0 mL, 2.0 mL	Eppendorf
Filter tips (10 µL, 20 µL, 100 µL, 1000 µL)	Thermo Fisher Scientific
Fridge/Freezer	Bosch
Gelsystems (Mini, Maxi)	VWR
GentleMACS Octo Dissociator with Heaters	Miltenyi Biotec
Greiner 96 well plates, polystyrene	Thermo Fisher Scientific
Greiner centrifuge tubes, 15 mL, 50mL	Sigma-Aldrich
Heating block	IKA Labortechnik
LabChip Gx Touch 24 Nucleic Acid Analyzer	Perkin Elmer
Micro centrifuge	Carl Roth
Mini centrifuge	Carl Roth
Multimode Microplate Reader	BERTHOLD Technologies
Nanodrop 2000/2000c spectrophotometer	Thermo Fisher Scientific
Nitrocellulose membranes	Invitrogen
PCR Cycler	Bio-Rad
PCR strips	Star Lab Group
pH meter	HANNA instruments
Pipettes	Rainin
Prescision cover glasses (High Prescision Cover Glasses 170+-5µm. No. 1.5H) 18 x 18 mm	Paul Marienfeld GmbH & Co. KG
Protein LoBind Tubes	Eppendorf
Power Supply	Carl Roth, Bio-Rad
RNaseZap	Sigma-Aldrich
Scales / Precision Balances	KERN, Sartorius
Sonicator	BANDELIN SONOPLUS
StepOnePlus™ Real-Time PCR System	Thermo Fisher Scientific
SuperFrost Plus slides	Menzel-Glaeser
Swing mill	Retsch
Thermocyclers for PCR	Bio-Rad
Thermomixer comfort	Eppendorf
ThermoMixer	Eppendorf
Tips (10 µL, 20 µL, 100 µL, 1000 µL)	Greiner Bio-One
Tissue cell culture plate	VWR
Tissue homogenizer	POLYTRON
Universal Oven	Memmert
UV-Transilluminator	INTAS
Vibrating mill	Retsch, MM301
Vortex mixer	Scientific Industries, Inc.

Waterbath	Leica
XCell SureLock™ Mini-Cell and XCell II™ Blot Module	Thermo Fisher Scientific

Table 19 Software

Software	**Company**
Adobe Illustrator 2022	Adobe Systems Incorporated
BLAST	NCBI
CAT	Computer Administriertes Tierhaus (MPG)
Ensembl Genome Browser	European Molecular Biology Laboratory's European Bioinformatics Institute (EMBL-EBI)
Excel, PowerPoint, Word	Microsoft
Gimp-2.8	GIMP
Graph Pad Prism 9.0	Graph Pad Software, Inc.
Image J / Fiji	Wayne Rasband
Image Lab	Bio-Rad Laboratories
Integrated Genome Browser (IGV)	Broad Institute
Leica confocal software 2.61 LAS X	Leica microsystems
MaxQuant (1.5.3.12)	MPG
Seqbuilder 17.3	DNASTAR Lasergene
StepOne Software v2.3	Thermo Fisher Scientific

2.2 Methods

2.2.1 Animal experimentation

Experiments involving animal health care and treatments were performed in agreement with institutional guidelines and the German animal welfare law. Each experiment was approved by the local governmental animal protection committee (Regierungspräsidium Darmstadt, B2/1125). All mice used in this study were housed in individually ventilated cages (Aero Cage – mM) accompanied with environmental enrichment under specific pathogen-free conditions in the Animal House Facility of the Max Planck Institute for Heart and Lung Research, Bad Nauheim, Germany. Circadian rhythm was maintained by keeping the animals in the dark from 6 pm to 7 am including 1 h of dawn. Age-matched littermates were used for individual experiments. The number of mice used in each experiment is indicated in the corresponding figure legend.

2.2.2 Engineering of genetically modified mice

2.2.2.1 Generation of knock-in mice by targeting the ROSA26 locus in mouse ES cells

Constitutive overexpression mouse strains were generated using ROSA site-specific gene knock-in (Figure 6). Therefore, cDNA for each gene of interest (GOI) was inserted downstream of the loxP-flanked STOP cassette in the modified ROSA26 targeting locus by which the SA-site of pBigT was replaced by a synthetic CAG promotor (Srinivas et al., 2001). The genes of interest were PCR-amplified to introduce NheI and NotI sites and cloned into pBigT-CAG vector. The generated pBigT-CAG-GOI cassette was subcloned in PacI and AscI site of the pRosa26-PA construct. The final construct, containing an antibiotic neomycin resistance selection cassette, a lacZ cassette, and two *loxP* sites, was electroporated into V6.5 F1 hybrid ES cells (gift from Rudi Jaenisch, RRID:CVCL_C865) and targeted stem cell clones were selected by G418 treatment and screened by PCR, with 5' genotyping performed using EcoRV digestion. Positive ES cell clones were injected into C57BL/6 blastocysts to obtain chimeric mice, which were backcrossed to the C57BL/6 background to generate transgenic mice harboring a single mutant allele. Conditional Cre-mediated overexpression of GOI in the myocardium was achieved by crossbreeding with XMLC2-Cre transgenic mice. Aged-matched wildtype littermates with Cre-recombinase expression were used as appropriate control mice in all experiment. The GOIs to be inserted into the ROSA26 locus are either RBPMSA-GFP, RBPMSB-GFP, GFP or RBPMSB-V5-APEX2-NES-GFP, RBPMSB-HA-T2A-V5-APEX2-NES-GFP. ESC cell culture and transgenic service were performed by Sonja Krüger and Susanne Kreutzer (MPI-HLR, Bad Nauheim, Germany).

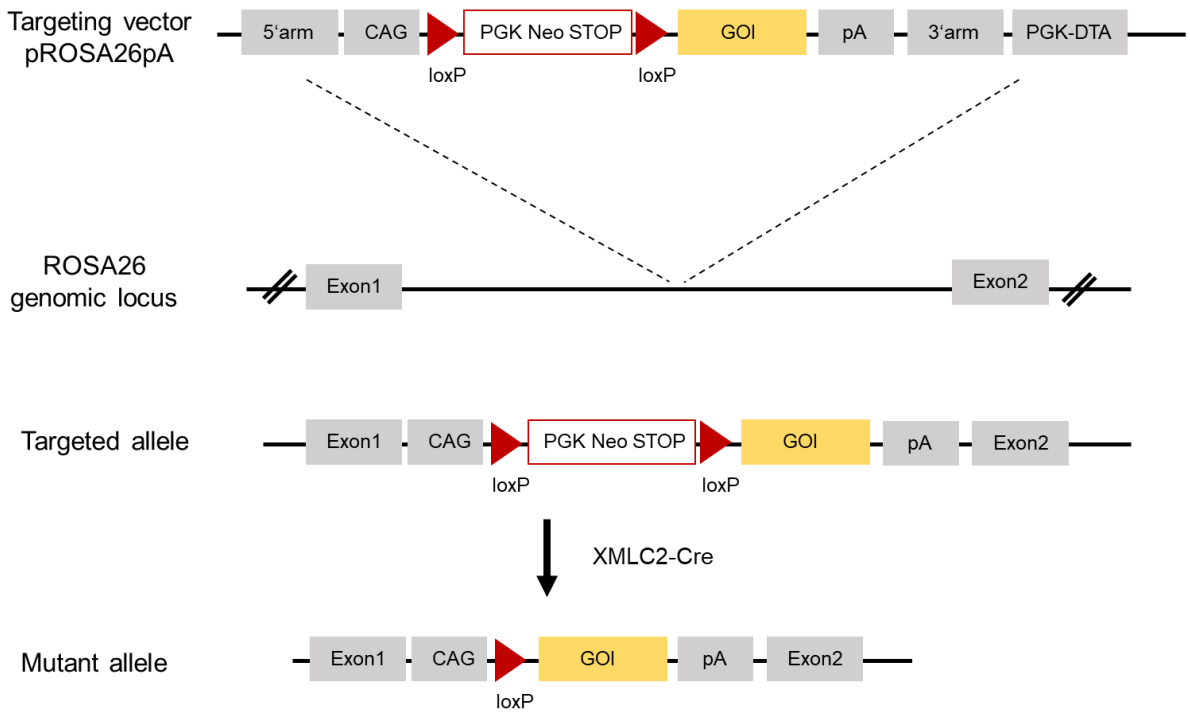

Figure 6 Schematic illustration of targeting the ROSA26 locus in mouse ES cells.

The targeting vector contains the CAG promoter, a loxP-flanked STOP sequence and cDNA for the GOI, which is inserted via homologous recombination into the ROSA26 locus. Overexpression is achieved upon Cre recombinase-mediated excision of the STOP cassette. CAG: enhancer promoter; PGK: phosphoglycerate kinase promoter, Neo: neomycin resistance gene as positive selection marker; GOI: gene of interest; pA: polyadenylation sites.

2.2.2.2 Generation of constitutive *Rbpmsb* knockout mice

Constitutive *Rbpmsb* knockout mice were generated using the CRISPR-Cas9 genome editing system. Therefore, two guide RNAs (gRNAs) targeting the last exon of *Rbpmsb* (ENSMUST00000033995) were cloned into the pSpCas9(BB)-2A-Puro (PX459) plasmid using BbsI restriction sites. Both gRNA plasmids were co-transfected into V6.5 F1 hybrid ES cells using Lipofectamine 3000, followed by puromycin selection to enrich for transfected cells. Candidate mutant ES cell clones were screened by PCR amplification of the target region using primers flanking the gRNA target sites. Deletion of exon 6 was confirmed by Sanger sequencing, which revealed frameshift mutations and premature stop codons resulting from non-homologous end joining (NHEJ) repair. Positive ES cell clones were injected into C57BL/6 blastocysts to obtain chimeric mice, which were backcrossed to the C57BL/6 background to generate transgenic mice harboring a single mutant allele.

2.2.3 Organ isolation

Animals were either sacrificed by combined carbon dioxide anesthesia and cervical dislocation or cervical dislocation following isoflurane exposure. Immediately post-euthanasia, a midline

thoracotomy was performed to rapidly excise the heart. The left ventricular of the heart was perfused with 1x PBS to clear residual blood components prior to downstream analyses.

2.2.4 Extraction of genomic DNA for genotyping from murine ear punches and tail biopsies

For genotyping, ear or tail biopsies of transgenic mice were first digested in 500 µL tail lysis buffer, supplemented with 5 µL Proteinase K (20 mg/mL), at 56°C overnight. The next day, digested ear/tail pieces were centrifuged at 14,000 rpm for 10 min and decanted into a new tube containing 500 µL isopropanol. Genomic DNA was precipitated by inverting the tubes. Following centrifugation at 14,000 rpm for 20 min, supernatants were removed, and the genomic DNA-containing pellets washed in 500 µL 70% ethanol, followed by centrifugation at 14,000 rpm for 5 min. Finally, genomic DNA was air-dried at RT for 1h, resuspended in 300 µL 1x TE buffer, and dissolved by incubation at 56°C overnight.

2.2.5 Genotyping of transgenic mice

Genotyping PCRs were performed with self-designed primers purchased from Merck/Sigma-Aldrich, as indicated in Table 16 using appropriate cycling conditions (Table 17). The master mix for one PCR reaction was prepared as followed:

Reagent	**Volume (µl)**
2x Taq Master	10
Primer 1 (for)	0.5
Primer 2 (rev)	0.5
Primer 3 (wt)	0.5
Genomic DNA	1.5
ddH_2O	10
Total	23

PCR products were loaded on a 2% agarose gel, dissolved in 1x TAE buffer, supplemented with ready-to-use ethidium bromide solution and ran for 30-45 min at 150-200 V, depending on the size of the gel. Double-stranded DNA was visualized under UV light and documented with a BioDoc analyzer.

2.2.6 RNA isolation from cells for qRT-PCR and RNA-Seq

Cells were homogenized by adding 1 mL of Trizol along with an autoclaved metal bead to an Eppendorf tube, followed by processing in a vibrating mill at maximum intensity for 5 min. RNA was then extracted from cells using the Direct-zol RNA Miniprep Kit according to the manufacturer's instructions, diluted in RNase-free TE and stored at -80°C until further usage.

2.2.7 cDNA synthesis and qRT-PCR

Complementary DNA (cDNA) was reverse transcribed from 1 µg of total RNA using the PrimeScript™ RT reagent Kit according to manufacturer's instructions.

Following cDNA synthesis RT-qPCR, was used for qualitative and quantitative analysis of the expression of specific genes. qPCR was performed with TaqMan Gene Expression Master Mix and fluorophore-labeled (FAM) TaqMan probes (TaqMan Gene Expression Assays) purchased from Applied Biosystems. qPCR reactions were processed on a StepOnePlus real-time PCR instrument and relative expressions were calculated using the ΔΔCt method. Each sample set was performed in technical triplicates and normalized to VIC-labeled Gapdh or ACTB as internal housekeeping gene controls. The master mix for one 10 µl qRT-PCR reaction was prepared as followed:

Reagents	**Volume**
TaqMan™ Gene expression master mix	5.0 µL
TaqMan™ gene specific probe (FAM-dye)	0.5 µL
TaqMan™ housekeeping gene probe (VIC-dye)	0.5 µL
cDNA (diluted 1:100 in ddH_2O)	4.0 µL
Total	10 µL

2.2.8 RNA seq

RNA sequencing and related bioinformatic analysis was performed by Dr. Stefan Günther (MPI-HLR, Bad Nauheim, Germany). RNA and library preparation integrity was verified with a BioAnalyzer 2100 or LabChip Gx Touch 24 Nucleic Acid Analyzer. 0,8 – 1 µg of total RNA was used as input for SMARTer Stranded Total RNA Sample Prep Kit - HI Mammalian (Clontech). Trimmomatic version 0.39 was employed to trim reads after a quality drop below a mean of Q15 in a window of 5 nucleotides and keeping only filtered reads longer than 15 nucleotides (Bolger et al., 2014). Trimmed and filtered reads were aligned versus mouse genome version mm10 (Ensembl release 101) using STAR 2.7.9a (Dobin et al., 2013). Following alignment, BAM files were processed to remove duplicates using Picard 3.0.0 (Picard: A set of tools (in Java) for working with next-generation sequencing data in the BAM format). Additionally, multi-mapping, ribosomal, and mitochondrial reads were filtered out. Gene-level read counts were determined using featureCounts 2.0.4 by aggregating reads mapping to exons while excluding those overlapping multiple genes (Liao et al., 2014, featureCounts: an efficient general-purpose program for assigning sequence reads to genomic features). Alignments were filtered to remove: duplicates with Picard 3.0.0 (Picard: A set of tools (in Java) for working with next

generation sequencing data in the BAM format), multi-mapping, ribosomal, or mitochondrial reads. Gene counts were established with featureCounts 2.0.4 by aggregating reads overlapping exons excluding those overlapping multiple genes (Liao et al.,2014). The raw count matrix was normalized with DESeq2 version 1.36.0 (Love et al.,2014). Contrasts were created with DESeq2 based on the raw count matrix. Genes were classified as significantly differentially expressed at average count > 5, multiple testing adjusted p-value < 0.05, and -0.585 < log2FC > 0.585. The Ensemble annotation was enriched with UniProt data (Activities at the Universal Protein Resource (UniProt)).

2.2.9 Cell culture experiments

2.2.9.1 Human Embryonic Kidney Cells (HEK293T)

HEK293T cells were cultured in high glucose DMEM containing 10% fetal bovine serum (FBS) and 1% penicillin/streptomycin/glutamine (PSG) at 37°C in humified atmosphere with 10% CO_2 and passaged at 70-80% confluency. Therefore, cells were washed 3 times with 1x PBS and incubated with 1x Trypsin-EDTA in 1x PBS at 37°C for 3-5 min. After complete detachment of the cell layer, trypsin was inactivated with 2 volumes of pre-warmed complete growth media and cell suspension was transferred to the 15 mL tubes and gently centrifuged at 300g for 5 min. After removing the supernatant, cell pellet was gently resuspended in appropriate amount pre-warmed complete growth medium and seeded to a culture dish.

2.2.9.2 HL-1 cells

HL-1 cells were cultured on gelatin/fibronectin-coated plates and maintained in Claycomb medium supplemented with 10% HL-1 cell screened FBS, 100 µg/ml PS, 0.1 mM Norepinephrine and 2 mM L-Glutamine. The medium was changed every 24-48 h. HL-1 cells were grown at 37°C in an atmosphere of 5% CO_2 and 95% air. Once the cells reached confluence, they were split 1:2 or 1:3, using Trypsin-EDTA and Trypsin Inhibitor which is designated as a passage. Cells were used for a maximum of 15 passages.

2.2.9.3 Murine embryonic stem cells

V6.5 mouse embryonic stem cells (ESC) were maintained on mouse embryonic fibroblast feeder layer at 37°C, 5% CO_2 with daily media exchange. Media contained Dulbecco's Modified Eagle's Medium-high glucose + GlutaMAX, supplemented with 10% PSG, 15% FBS, 0.1 mM 2-Mercaptoethanol, 0.1 mM non-essential amino acids and 1000 U/ml Leukemia inhibitory factor (LIF). Slides were coated with 0.1% Gelatin when seeded for IF staining.

2.2.10 Plasmid transfection

Subconfluent HEK293 cells or HL-1 cells were transiently transfected with 6 µg individual plasmid DNA using either TurboFect or Lipofectamine2000 transfection reagent according to the manufacturer's protocol. The medium was substituted approximately 24 h post-transfection, and cells were harvested for downstream analyses 48 h post-transfection.

2.2.11 Drug treatment

To study the effects of different stressors *ex vivo*, neonatal and adult cardiomyocytes were treated for different time points (1 h-24 h) with doxorubicin (0.1 µM, 1 µM), hydrogen peroxide (H_2O_2; 350 µM), cisplatin (100 µM) and tumor necrosis factor-alpha (TNF-α; 5 ng/ml). DMSO treated cells served as an appropriate control for doxorubicin-treated cells.

2.2.12 Protein extraction and immunoblot analysis

Immunoblot analysis was performed accordingly to standard protocols. In brief, cells or tissue were collected, lysed by homogenization in RIPA buffer, supplemented with protease inhibitors and PMSF, followed by sonication for 20 sec at cycle 3, power 30%. Next, cell or tissue homogenates were clarified by centrifugation at 14,000 rpm for 10 min at 4 °C. Supernatant, representing the cytoplasmic protein fraction, was transferred to a fresh Eppendorf tube and protein concentration was determined using Biorad® DC protein assay kit following manufacturer´s instructions. 10 – 20 µg of proteins in 4x Laemmli buffer were boiled at 95°C for 5 min and separated by SDS-PAGE. The separated proteins were blotted onto nitrocellulose membranes, followed by RedAlert™ staining to verify successful protein transfer. Nitrocellulose membranes were blocked in either 5% skim milk / TBS-T or 5% BSA/TBS-T for 30 min shaking at RT and probed with specific primary antibodies shaking overnight at 4°C. The following day, the membrane was washed by shaking 5 times for 5 min each using 1x TBS-T at RT, followed by incubation with peroxidase-conjugated secondary antibodies for at least 1 h shaking at RT. The membrane was then subsequently washed through shaking at RT 5 times for 5 min each using 1x TBS-T. Finally, proteins were visualized by chemiluminescence using the Super Signal® West Pico Chemiluminescent Substrate kit on a ChemiDoc™ MP Imaging System. Densitometric analysis of the chemiluminescence signals was carried out using the ImageLab software to quantify the relative protein expression. Absolute protein expressions were calculated by normalization to loading control.

2.2.13 Generation of RBPMSB-APEX2 and APEX2 constructs

The RBPMSB-APEX2-V5-NES-copGFP expression construct was generated through a multi-step molecular cloning strategy. First, the murine *Rbpmsb* open reading frame (ORF) was amplified via PCR using primers RBPMSB-fusion-for and RBPMSB-fusion-rev. Concurrently, the V5-APEX2-NES fusion plasmid was PCR-amplified from the pcDNA3.1_V5-APEX2-NES plasmid (Addgene # 49386) with primers V5-APEX2-for and V5-APEX2-rev. These two PCR products were fused through overlap extension PCR using primers RBPMS-APEX-for and RBPMS-APEX-fusion-rev to generate the RBPMSB-V5-APEX2-NES fragment. This intermediate product was subsequently fused to copGFP through a second round of overlap extension PCR using RBPMS-APEX-for and APEX-GFP-rev primers. The final amplicon, encoding RBPMSB-APEX2-V5-NES-copGFP, was ligated into the modified pCAG-IRES-puro

backbone vector (restriction sites: PacI and AscI) using the ClonExpress Ultra One Step Cloning. To generate the RBPMSB-HA-T2A-APEX2-NES-copGFP construct, a synthetic T2A peptide sequence was inserted via overlap extension PCR. The HA-tagged RBPMSB-T2A was amplified using RBPMS-APEX-for and RBPMS-T2A-rev, while the downstream APEX2-NES-copGFP region was amplified using primers RBPMS-T2A-for and APEX-GFP-rev for RBPMSB-T2A-APEX2-NES-copGFP. These two fragments were subsequently fused to produce the final RBPMSB-HA-T2A-APEX2-NES-copGFP construct.

2.2.14 APEX2 proximity labeling

HEK293 cells were seeded in 6-well plates one day prior to labeling to reach ~80–90% confluency. Cells were either left untreated or subjected to heat stress at 46°C for 30 min. Biotin-phenol (BP) was added to the culture medium at a final concentration of 500 µM for 30 min at 37°C, concurrently with stress induction. APEX2-mediated labeling was initiated by adding 1 mM hydrogen peroxide for 1 min at RT. Cells were washed 5x with a quencher solution and collected using cell scrapers, pelleted by centrifugation at 300 x g for 10 min, and either resuspended in cold lysis buffer or stored at -80°C for further processing.

Protein levels were determined with the Pierce 660 nm Protein Assay following manufacturer's instruction. Prior to pull down, magnetic beads coated with streptavidin were equilibrated with lysis buffer containing 10 mM sodium ascorbate, 5 mM Trolox, 10mM sodium azide and protease inhibitors for a total of three washes. Proximity dependent biotin affinity capture was performed by incubating 1 mg/mL of clarified cell lysate with 50 µL beads on a rotating wheel overnight at 4°C. Beads were washed twice with lysis buffer, once with 1 M KCL, once with 0.1 M Na_2CO_3, once with 2 M Urea in 10 mM Tris-HCL (pH 8.0) and twice with lysis buffer. Biotinylated proteins were eluted by boiling streptavidin coated beads in 1 x NuPAGE® LDS sample buffer supplemented with 2 mM biotin and 20 mM dithiodreithol (DTT) and boiled at 95°C for 5 min, followed by SDS-PAGE, and in-gel digestion coupled to LC-MS/MS to identify protein interaction partners in close proximity to the fusion construct. APEX2 analysis was performed using technical triplicates for each condition.

2.2.15 Identification of protein interaction partners of RBPMSA and RBPMSB

GFP-tagged RBPMS variants were generated as C-terminally tagged versions (RBPMSA-GFP& RBPMSB-GFP) using the pCAG-IRES-Puro vector, which also served to produce the GFP control construct. Stable polyclonal mouse ES cell clones were generated by electroporation in murine V6.5 ES cells and puromycin selection. Stable expression of GFP-fusion constructs was tested by western blot analysis using an anti-GFP antibody. For GFP pulldown experiments, mESCs were cultured on feeder cells and trypsinized for harvesting. To deplete feeder cells, mESC and feeder cells were pre-plated for 1 h on a 10 cm cell culture dish. Supernatant mESCs were lysed for the mass spectrometry based interactome screen

using GFP-Trap® (Chromotek) according to the manufactor´s protocol. Collected magnetic agarose beads, which bind fusion protein and the corresponding interactome, were analyzed by liquid chromatography-mass spectrometry.

2.2.16 Liquid chromatography/tandem mass spectrometry (LC-MS/MS) analysis

Beads were processed using off bead digest, followed by using reductive dimethylation and liquid chromatography/tandem mass spectrometry (LC/MS^2) analysis as described (Deutschmeyer et al., 2019), but used version 1.6.0.1 of the MaxQuant suite of algorithms (Cox and Mann, 2008; Cox et al., 2011) and a murine canonical and isoforms uniprot database (The UniProt Consortium, 2007; downloaded 2017/08/17; 90200 entries) (Bairoch et al., 2007). Downstream data analysis and plotting was performed using an R (R Core Team, 2020) and limma (Ritchie et al., 2015) based analysis pipeline (https://github.com/bhagwataditya/autonomics), including a Fisher exact test against the detectome for over-representation with respect to GO (Ashburner et al., 2000) and KEGG (Kanehisa et al., 2012) categories.

2.2.17 Isolation of mouse embryonic fibroblasts

Mouse embryonic fibroblasts (MEFs) were isolated from RBPMSB-APEX2$^{+/-}$Cre^{neg} and RBPMSB-APEX2$^{+/-}$Cre^{pos} mice and the corresponding controls APEX2$^{+/-}$Cre^{neg} and APEX2$^{+/-}$Cre^{pos} at embryonic day (E) 13.5 as described by Jozefczuk et al., 2012. Briefly, pregnant mice were sacrificed by cervical dislocation, embryos isolated and placed separately into a fresh petri dish containing ice-cold 1x PBS. The umbilical cord and the hematopoietic tissue together with the tubular intestine were removed from each embryo and the bulk of the CNS was trimmed off by dissecting away the head above the level of the oral cavity. A small piece of the tail was saved for DNA extraction and genotyping. Each remaining embryo was transferred to a tissue culture hood, placed in a 100 mm dish containing 5 mL of 0.25% trypsin-EDTA, and minced with a sterile scalpel for 2 min. After incubation for 10 min at 37°C, individual cells were separated by extensive pipetting and further incubation at 37°C for 10 min. After adding 5 mL of DMEM, supplemented with 10% FCS and 1% L-glutamine-penicillin-streptomycin, MEFs were spin down at 1,000 rpm for 5 min, and the supernatant was carefully aspirated off. The cell pellets were re-suspended in 10 mL DMEM supplemented with 10% FCS and 1% L-glutamine- penicillin-streptomycin, and plated to a new 100 mm dish. MEFs were maintained at 37°C and 5 % CO_2 and considered to be at passage at this stage.

2.2.18 Isolation of mouse neonatal cardiomyocytes

Timed matings were set up to collect mouse hearts from pups at postnatal days P0-P2 for cardiomyocytes isolation. Pups were decapitated using sterile scissors, after which the thoracic cavity was accessed by opening the sternum. The hearts were carefully excised and immediately transferred to a bacterial dish containing ice-cold 1x PBS. Subsequently, lung

tissue, major blood vessels, and atrial structures were removed to obtain purified ventricular tissue. Cardiomyocyte dissociation was performed using the Neonatal Heart Dissociation Kit in combination with the gentleMACS Octo Dissociator with Heaters, following the manufacturer's instructions. After dissociation, the cardiomyocyte fraction was then isolated using the Mouse Neonatal Cardiomyocyte Isolation Kit according to the manufacturer's protocol. The freshly isolated cardiomyocytes were either processed for RNA and protein extraction or used for cell culture experiments. For culturing, cells were gently resuspended in DMEM supplemented with 5% FCS and 1% P/S/G. The cells were then seeded onto fibronectin-precoated culture dishes or chamber slides (coated with 10% fibronectin in DPBS) and maintained at 37°C in a humidified incubator with 5% CO_2.

2.2.19 Isolation of adult cardiomyocytes

Cardiomyocytes were isolated from murine hearts by enzymatic digestion using a Langendorf system as previously described by O'Connell et al., 2007. In brief, dissected hearts were cannulated via the aorta and arrested by retrograde perfusion with calcium-free buffer. Cannulated hearts were enzymatically digested by perfusion with enzyme buffer solution and cut off from the cannula. Atria were separated, and ventricles were minced in stop buffer 1. After gentle pipetting, myocytes were at 500 rpm centrifuged for 1 min and cell pellets, containing the cardiomyocyte fraction, were resuspended in stop buffer 2. The calcium content of the cell suspension was then stepwise adjusted to 1 mM and cardiomyocyte-containing cell pellets were re-suspended in M199 cell culture medium, supplemented with 5 mM creatinine x H_2O, 2 mM L-carnitine x HCl, 25 mM HEPES, 1% penicillin/streptavidin, 10% FCS, and 1% insulin-transferrin-sodium selenite media supplement, adjusted to pH 7.3. Isolated cardiomyocytes were seeded on cell culture dishes or chamber slides pre-coated with laminin (10 µg/µL laminin in MEM media) and cultured at 37°C and 5% CO_2.

2.2.20 Immunofluorescence staining of cells and tissues

Cells were seeded and processed on Nunc Lab-Tek Chamber slides. Cells were fixed in 4% PFA / 1x PBS for 15 min at RT. After three washing steps in 1x PBS, samples were permeabilized in 0.05% Triton X-100 / 1x PBS for 15 min. Another three times washing steps with 1x PBS were performed before incubating the samples in a blocking solution containing 0.1% BSA in 1x PBS for 30 min to reduce non-specific antibody binding. Afterwards, cells were incubated overnight at 4°C with primary antibodies, which were diluted in a blocking solution. The next day, samples were washed 3 times in 1x PBS for 5 min each at RT, followed by incubation with the respective secondary antibodies diluted in the blocking solution, for 2 h at RT. After three washing steps in 1x PBS for 5 min each, nuclei were counterstained with 4',6-diamidino-2-phenylindole (DAPI), diluted 1:1000 in blocking solution, for 5-10 min. Finally, cells

were again washed for another 3 times with 1x PBS, mounted in Mowiol 4-88, covered with glass slides and analyzed using a fluorescence microscope.

2.2.21 Human myocardial biopsies

Human myocardial tissue samples were obtained from left ventricular biopsies of transplanted hearts. Immediately after tissue procurement, cardiac biopsies were shock frozen in liquid nitrogen, stored at - 80°C and processed for molecular analysis and immunohistochemistry. All patients delivered a prospective written informed consent for research use of cardiac tissues to comply with the requirements of the Medical Council in Hesse, Germany, and the institutional ethics guidelines of the Kerckhoff-Klinik, Bad Nauheim, Germany. The study was approved by the ethics committee of the Medical Council in Hesse, Germany. The responsible person at the clinic is Dr. Manfred Richter.

2.2.22 Image acquisition and processing

Stained cells and cardiac tissue sections were analyzed using a confocal microscope Leica TCS SP8 Confocal or a Leica TCS SP8 Multiphoton. All settings for laser excitation, scanning speed and amplification settings were kept constant during each experiment. Sequential scans were stacked and are shown as maximum projection. Images were processed using ImageJ/Fiji software.

2.2.23 Statistical analysis

Number of samples of the certain genotypes is indicated as “n” in figure legends. Every statistical analysis depicted in this work was completed using the Graph Pad Prism software (version 6 or version 9). All data are presented as mean ± SD (standard deviation) and P-values less than 0.05 were considered statistically significant. Unless otherwise stated, statistical significance between groups was assessed using a two-tailed Student’s t-test (2 groups) or ANOVA analysis (> 2 groups). All analyses were based on neither randomization or blinding. No animals were excluded from statistical analysis. All calculations and bar diagrams were done using GraphPad Prism 9.2.0. Venn diagrams were generated using Venny v2.1.0 to examine the overlap among conditions. The Integrative Genomics Viewer (IGV) 2.3.91 was used for the visual exploration of sequencing data and WIlsON R package was used for plotting feature-based sequencing data.

3. Results

3.1 Biomolecular condensate formation in diseased human myocardium

Biomolecular condensates have emerged as critical players in human diseases, particularly in neurodegeneration and cancer. While SGs and their dysregulation are well-characterized in neurodegenerative disorders, their turnover kinetics, composition and (patho)physiological roles in cardiovascular system remain poorly understood. Consequently, we investigated whether RNP condensates in human cardiac tissue possess a distinct composition, aiming to uncover the molecular mechanisms driving pathogenic RNP granule accumulation and its potential role in heart failure. Cardiac biopsies of explanted hearts were obtained from randomly selected human patients suffering from myocarditis or late-end stage dilated cardiomyopathy (DCM). Human heart tissue from patients undergoing surgical correction of aortic stenosis were used as non-heart failure controls.

TDP-43 is the major disease-associated protein involved in the pathogenesis and progression of amyotrophic lateral sclerosis (ALS). In affected neurons, TDP-43 shows a transition from reversible dynamic state to an irreversible, phosphorylated aggregated state, which is strongly associated with neuronal dysfunction and degeneration of ALS patients (Zbinden et al., 2020; Patel et al., 2015). Previous studies reported the presence of abnormal TDP-43 deposition in the myocardium of ALS patients (Mori et al., 2019). Notably, cardiomyocytes of DCM and myocarditis patients were characterized by a rounded morphology and an increased nuclear volume, whereas cardiomyocytes from control tissue showed well-preserved sarcomere structure. Immunostaining with an antibody specifically recognizing the phosphorylated form of TDP-43 revealed short, linear TDP-43 inclusions in cardiomyocytes from aortic stenosis control patients (Figure 7A), whereas large, dense filamentous inclusions of TDP-43 aggregates were found in cardiomyocytes from patients with DCM or myocarditis (Figure 7B, C). In addition to the increased incidence of phosphorylated TDP-43 (pTDP-43) aggregates observed in heart tissue from patients with DCM or myocarditis compared to control samples, the mean density of these aggregates was also found to be significantly higher (Figure 7D).

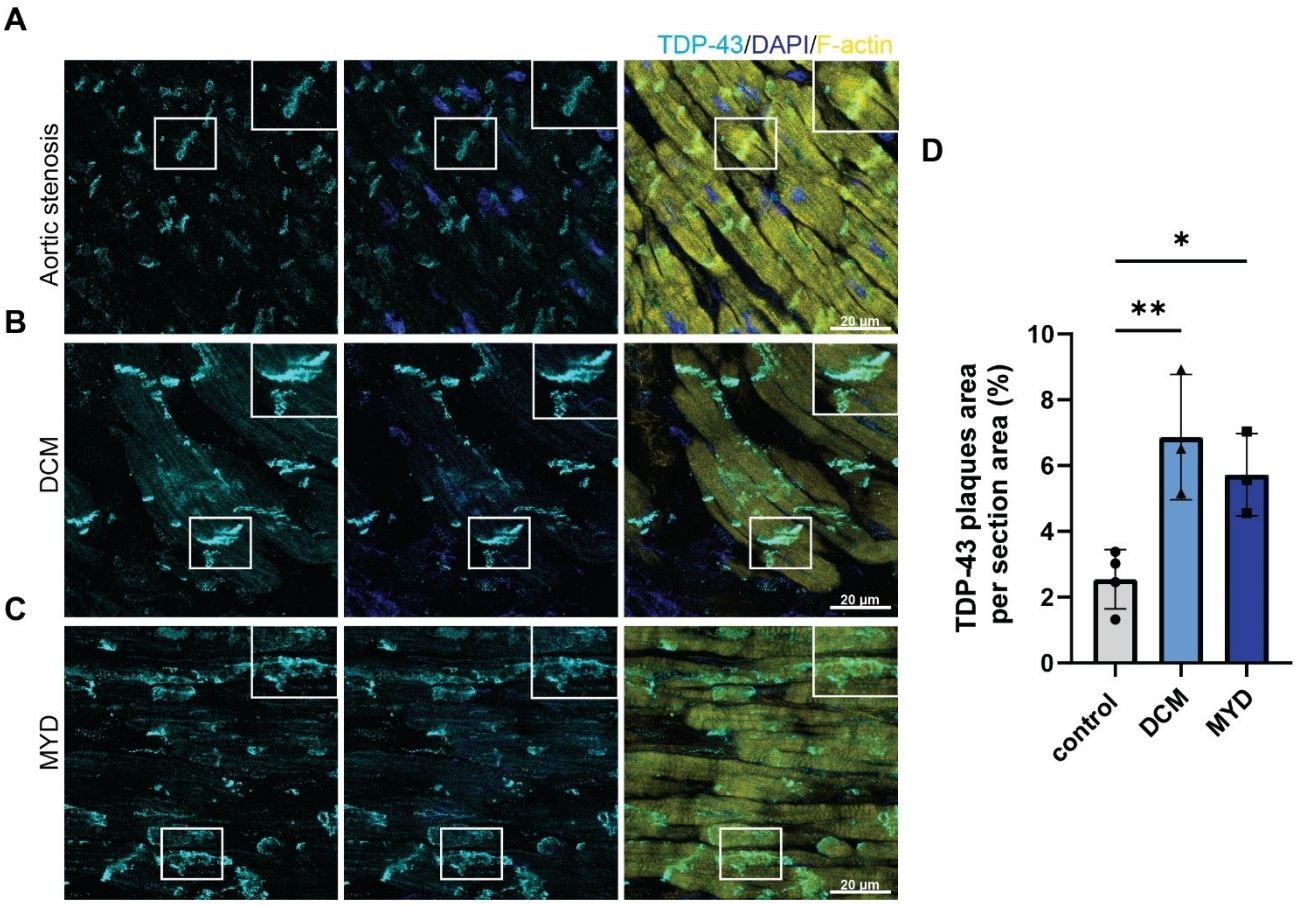

Figure 7 Presence of large, dense, filamentous TDP-43 inclusions in human cardiac biopsies from patients with late-end stage dilated cardiomyopathy and myocarditis. **A-C** Representative confocal images of human cardiac biopsies from patients with aortic stenosis (A), late-end stage dilated cardiomyopathy (DCM) (B) and myocarditis (MYD) (C) stained for TDP-43 (cyan), F-actin (yellow) and nuclear marker DAPI (blue). Scale bar, 20 µm. **D** Quantification of TDP-43 plaque area per longitudinal section area (%) of samples from DCM and myocarditis patients compared to controls**.**

Next, to investigate the potential role of RNPs in cardiovascular disease, we performed immunofluorescence staining for established SG marker proteins. In particular, G3BP1 and PABPC1 were analyzed in heart tissue from diseased and control samples. In human cardiac tissue, biomolecular condensate analysis demonstrated lower G3BP1 levels in controls (Figure 8A), whereas failing hearts displayed a marked accumulation (Figure 8B, C). Cardiomyocytes of late end-stage DCM patients exhibited a higher number of SGs, which were also notably larger in size (Figure 8B). These enlarged SGs invariably contained both key SG components, G3BP1 and PABPC1. In addition to cytoplasmic SGs, large G3BP1-positive puncta were also

observed within the nuclei of cardiomyocytes enriched for SGs (Figure 8B, C), suggesting a potential nuclear involvement in SG-associated pathology.

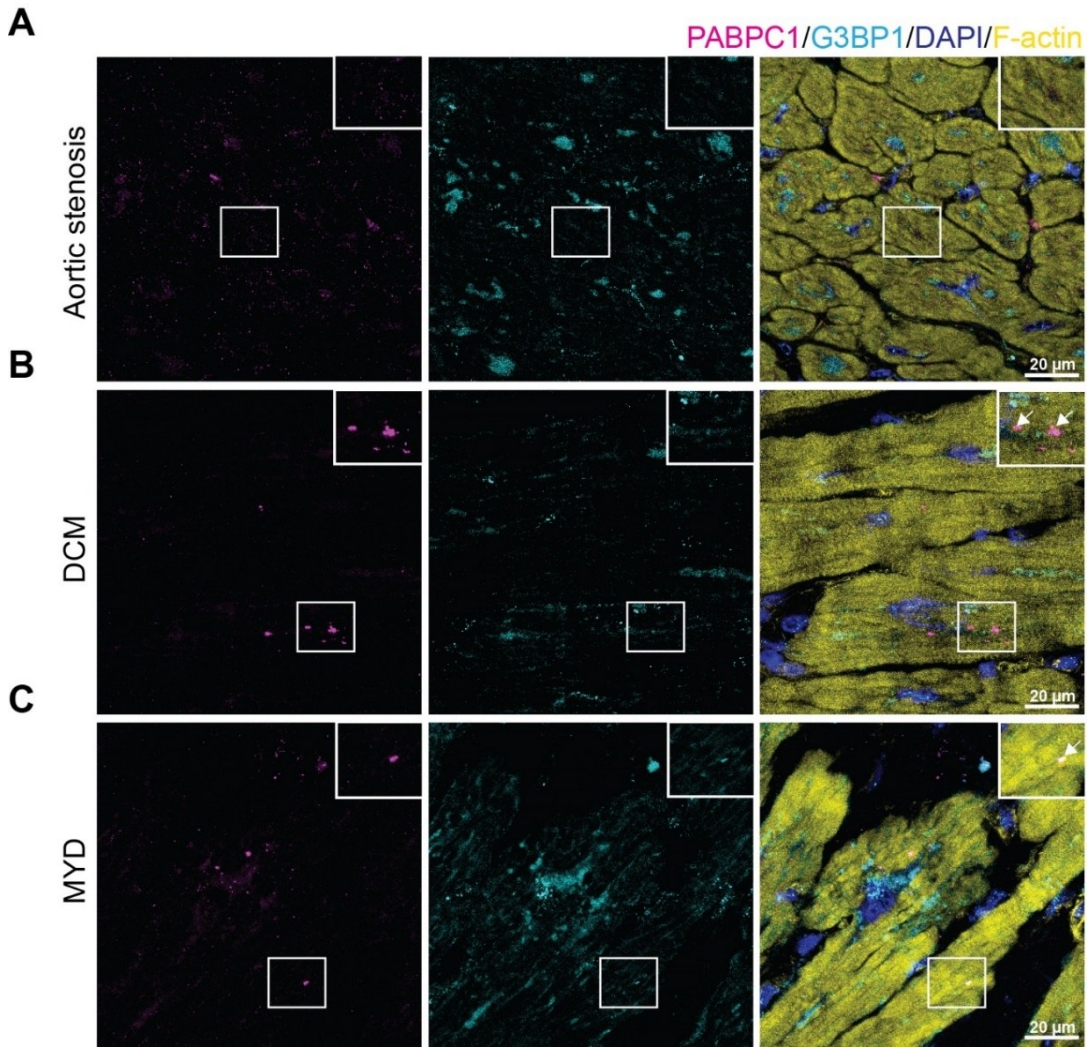

Figure 8 Enhanced stress granules formation in late-end stage dilated cardiomyopathy and myocarditis patients.

A-C Immunofluorescence staining of PABPC1 (magenta), G3BP1 (cyan), F-actin (yellow) and nuclear marker DAPI (blue) in cross-sectioned hearts from control individuals (A) and patients with late-end stage dilated cardiomyopathy (DCM) (B) or myocarditis (MYD) (C). Arrows indicate colocalization of PABPC1 and G3BP1. Scale bar, 20 µm.

Furthermore, colocalization studies of G3BP1 and the aggregate marker p62 indicate that persistent SG accumulation may lead to the formation of aggregate-like structures in stressed cardiomyocytes (Figure 9B, C). These results suggest altered dynamics of SGs and an associated accumulation of misfolded proteins, which may drive their transition from a dynamic to an aberrant, solid-like state. Importantly, in DCM samples, p62 staining exhibited a filamentous pattern with punctate aggregates predominantly localized in the perinuclear

region, corresponding to lysosome-rich areas (Figure 9B, C). Additionally, fat deposits present in cardiac tissue can be detected by their high autofluorescence, especially in the green channel. However, these fat deposits can be clearly distinguished from SGs and p62-positive aggregates by their characteristic structure and generally larger size. This analysis reveals, for the first time, that RNP assemblies are present and altered in diseased human hearts.

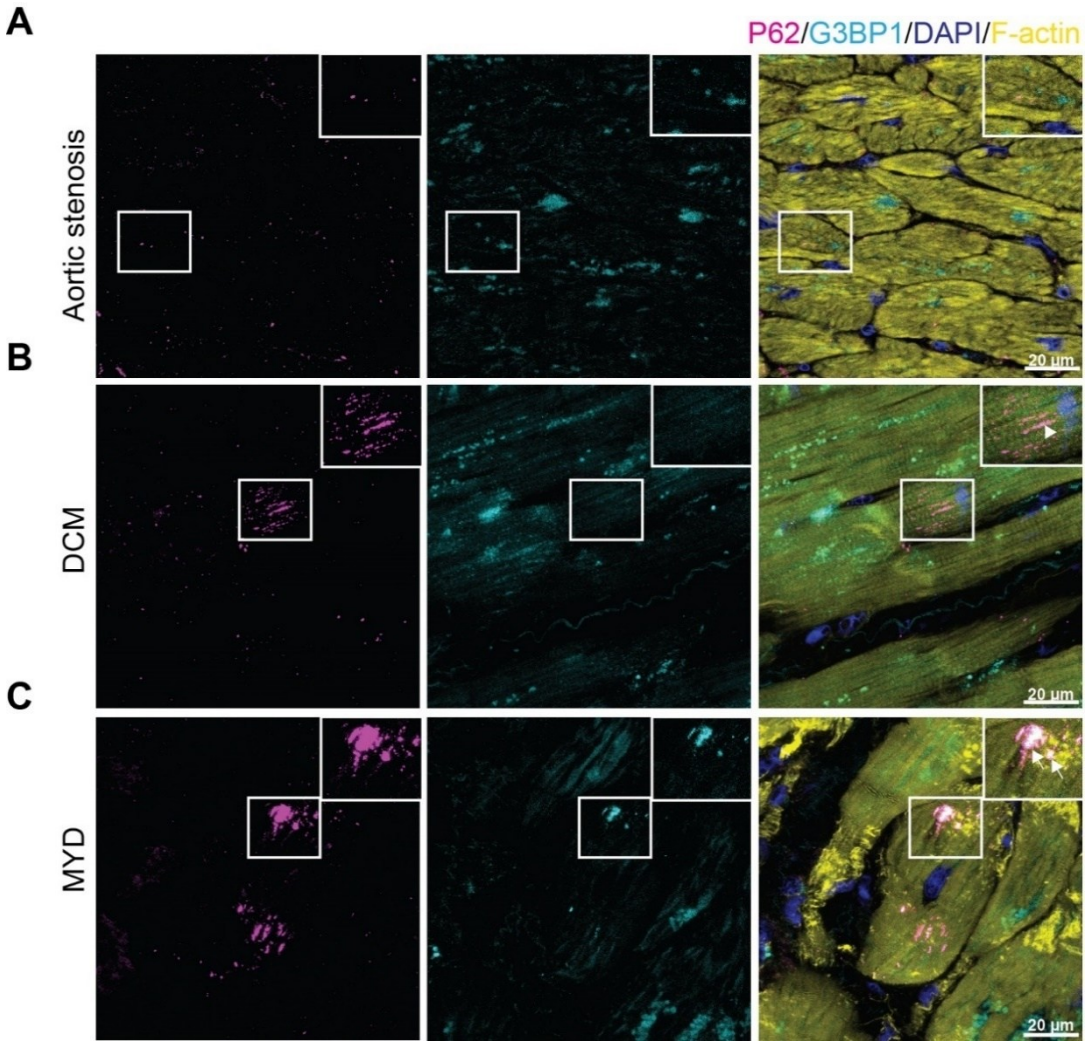

Figure 9 P62 accumulation and colocalization with G3BP1 in cardiomyocytes from patients with late-end stage dilated cardiomyopathy and myocarditis.

A-C Human cardiac biopsies from (A) control individuals and patients with (B) late-end stage dilated cardiomyopathy (DCM) or (C) myocarditis (MYD) were stained for p62 (magenta), G3BP1 (cyan), F-actin (yellow) and nuclear marker DAPI (blue). Arrows indicate colocalization of G3BP1 and p62, arrowhead indicate filamentous aggregation of p62. Scale bar, 20 µm.

3.2 RBPMS abundance and localization is altered in human diseases and animal model

RBPMS is involved in various cellular processes and recent studies have demonstrated that in response to cellular stress, RBPMS undergoes a subcellular localization shift from the nucleus to the cytosol, reflecting its dynamic role in stress-regulated RNA metabolism and cellular adaptation. Under these conditions, RBPMS is recruited to SGs and P-bodies (Rambout et al., 2016). This redistribution suggests a potential role for RBPMS in modulating RNP complex assembly and dynamics. The Mammalian Stress Granules Proteome (MSGP) database is a comprehensive repository detailing experimentally validated proteins localized to mammalian SGs. Based on this database, we extracted and analyzed SG protein expression levels, comparing patients with different neurodegenerative diseases to healthy controls. In particular, this study identified a marked up-regulation of RBPMS expression in the motor cortex of ALS patients, prompting the hypothesis that comparable changes in its expression and subcellular localization may also occur in the heart under pathological conditions. To directly assess a potential correlation between RBPMS protein dynamics and human heart disease, left ventricular biopsies were analyzed for subcellular localization. Interestingly, in the healthy myocardium, RBPMS was predominantly localized to the nuclei of cardiomyocytes (Figure 10A). However, in various subtypes of human heart disease, including DCM and myocarditis, RBPMS subcellular localization switched to the cytoplasm, potentially associating with the actin cytoskeleton and intercalated discs (Figure 10B, C).

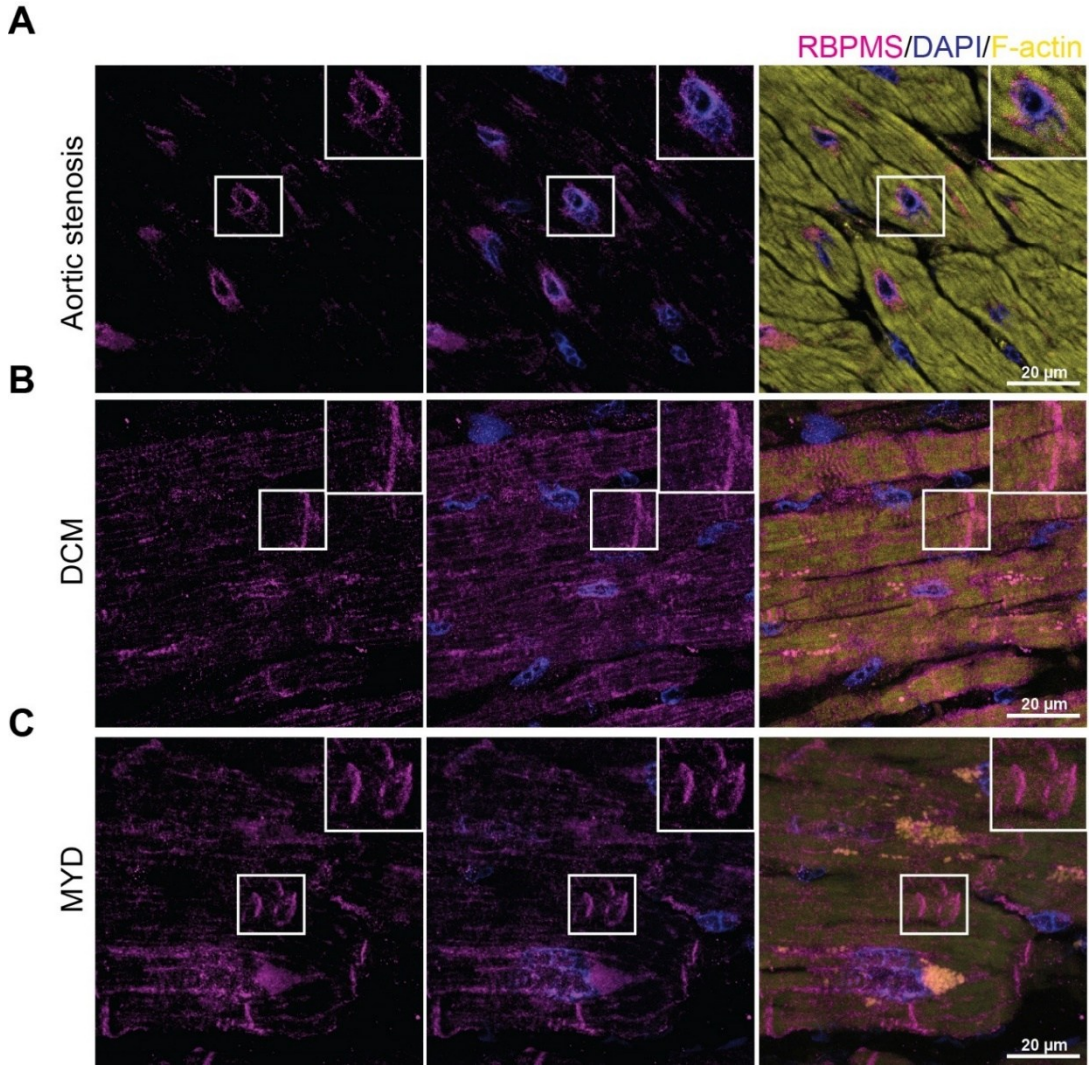

Figure 10 RBPMS mislocalization in cardiomyocytes from patients with late-end stage dilated cardiomyopathy and myocarditis.

A-C Immunofluorescence staining of RBPMS (magenta), F-actin (yellow) and nuclear marker DAPI (blue) in cross-sectioned hearts from control individuals (A) and patients with late-end stage dilated cardiomyopathy (DCM) (B) or myocarditis (MYD) (C). Scale bar, 20 µm.

To further verify this hypothesis, we used a mouse disease model driven by doxycycline-induced overexpression of the inflammatory cytokine Oncostatin M (OSM) in cardiomyocytes ($OSM^{+/-}$). OSM has been demonstrated to promote dedifferentiation of cardiomyocytes and to exacerbate cardiac failure, leading to reduced ejection fraction and reduced fractional shortening. Moreover, RNA sequencing of heart tissue showed increased expression of genes linked to inflammation and fibrotic processes (Jengelley et al., 2022). For this reason, this disease model represents a reasonable model for inflammation. Indeed, studies from our laboratory demonstrated that doxycycline-inducible cardiomyocyte-specific overexpression of OSM in mice resulted in the development of DCM characterized by decreased myocardial wall thickness and dilated ventricles. The observed upregulation of the JAK/STAT3 (P-Stat3) and

Ras/Raf/MEK/Erk (P-Erk1/2) signaling pathways provides evidence of their activation in response to cardiac stress or injury, such as myocardial infarction or inflammation. These pathways play crucial roles in mediating cardioprotective and reparative mechanisms, including the regulation of cell growth, proliferation, differentiation, and adaptive responses, thereby contributing to the maintenance of cardiac function under pathophysiological conditions (Figure 11A). In addition, the protein level of α-tubulin was altered following OSM overexpression, demonstrating a destabilization of microtubule structure as a hallmark of different cardiac pathologies, including cardiac hypertrophy and heart failure (Figure 11B, C). In this context, we investigated the protein levels of RBPMSA and RBPMSB in our OSM disease model and the corresponding littermate controls. Immunoblot analysis of OSM overexpression hearts revealed a significant upregulation of both, RBPMSA and RBPMSB, protein isoforms in comparison to control hearts. This upregulation may indicate attempts to preserve cardiac function through modulation of AS, suggesting a potential role in cardiac pathology. However, RBPMS can also be expressed by immune cells infiltrating the heart tissue during disease. Therefore, the increased protein levels might partially arise from these immune cells rather than cardiomyocytes exclusively. To conclusively determine cell-specific expression, further studies focusing on isolated cardiomyocytes are needed, although efficient isolation from these hearts remains challenging.

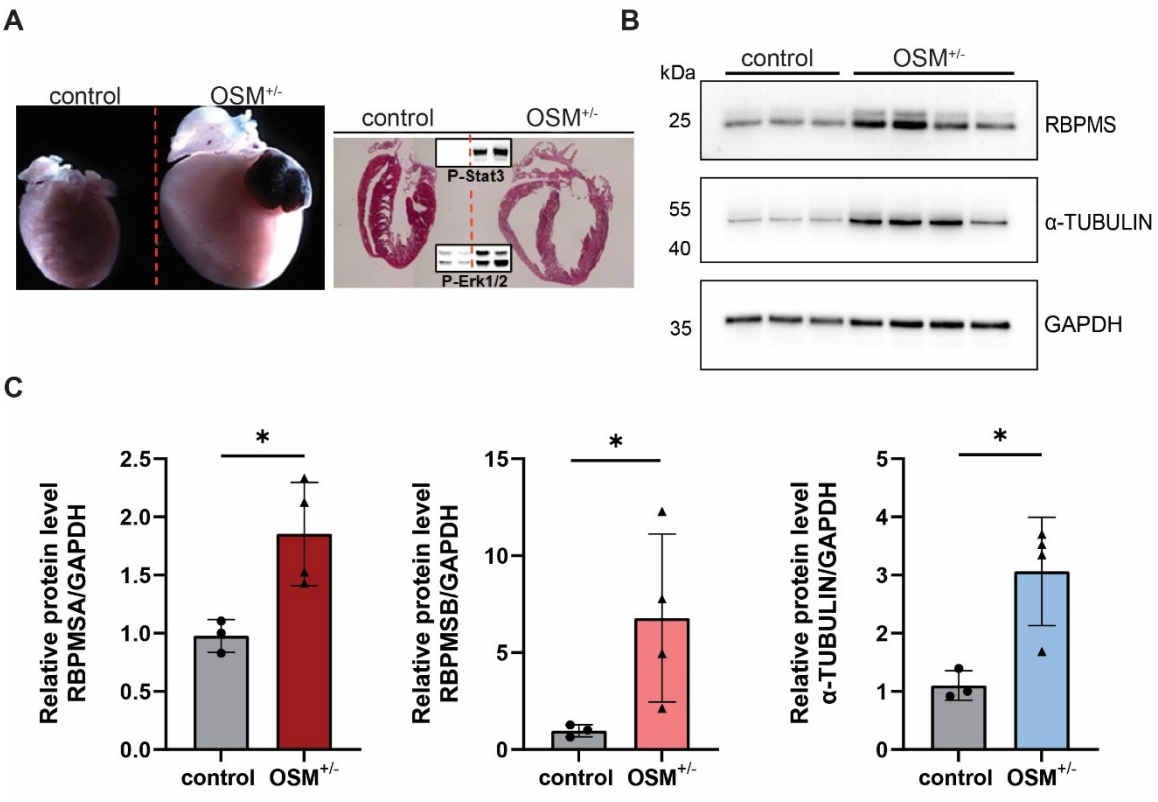

Figure 11 Upregulation of RBPMS in a cardiac inflammation model induced by Oncostatin M overexpression.

A Images of dissected hearts and H&E-stained cross-sections from Oncostatin M (OSM) overexpressing and control hearts and immunoblot analysis of JAK/Stat3 (P-Stat3) und Ras/Raf/MEK/Erk (P-Erk1/2) levels. Mice were analyzed 7 days after doxycycline administration. **B** RBPMSA, RBPMSB and α-Tubulin protein levels in OSM overexpression (n = 4) and control mouse hearts (n = 3). **C** Quantification of RBPMSA, RBPMSB and α-Tubulin protein levels relative to GAPDH expression. Data represent the mean ± SD. Two-tailed unpaired t-test. *P < 0.05. ns = not significant.

3.3 RBPMS localizes to stress granules in cardiomyocytes upon heat shock

Given that RBPMS alters its subcellular localization under cardiac disease conditions, we hypothesized that RBPMS may also contribute to the formation of cytoplasmic granules in isolated cardiomyocytes subjected to stress conditions. To explore the subcellular localization of RBPMS and a potential recruitment to SGs, isolated neonatal cardiomyocytes were subjected to heat shock (46° C for 30 min). Colocalization of RBPMS and the well-known SG marker protein G3BP1 was visualized by immunofluorescence staining and further validated by quantitative colocalization analysis using JACoP. The Pearson correlation coefficient (PCC) confirmed a strong correlation (r = 0.786) compared to controls (r = 0.684). Notably, larger SGs were concentrated in the perinuclear region, suggesting a close interaction with the nucleus to facilitate signaling processes (Figure 12A, B). To gain insight into the composition and dynamics of RNPs in the cardiovascular system, we employed a selected RBPMS isoform as a bait protein to visualize and characterize RNPs. More specifically, the RBPMS isoform B (RBPMSB) which is predominantly localized to the cytoplasm, implying a critical role in SG formation and function.

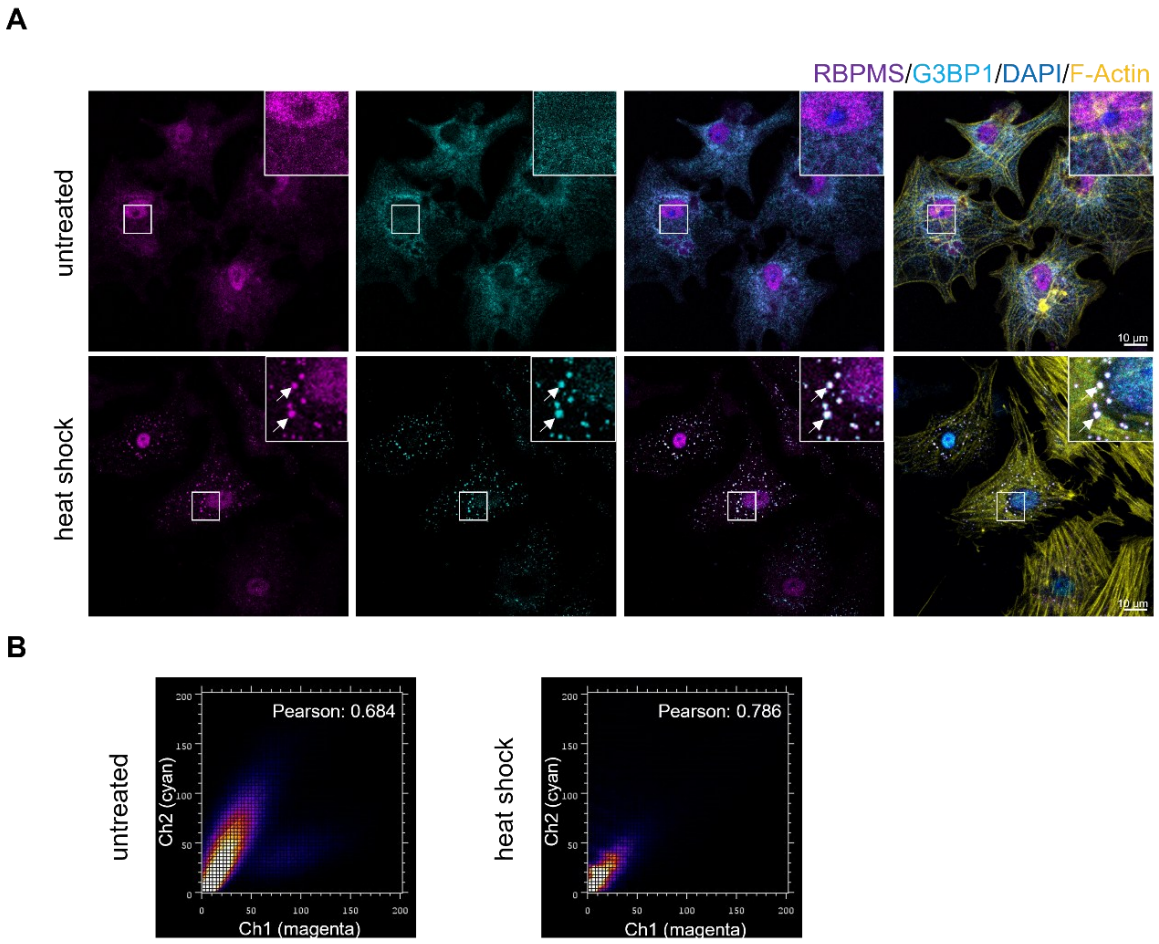

Figure 12 Subcellular localization shift of RBPMS to stress granules in heat-shock treated primary neonatal cardiomyocytes.

A Representative images of murine neonatal cardiomyocytes (P0) under normal and heat shock stress conditions (46°C, 1 h), co-stained with G3BP1 (cyan), RBPMS (magenta), nuclei (DAPI, blue) and F-Actin (yellow). Arrows indicate individual stress granules in which both G3BP1 and RBPMS overlap. Scale bar, 10 µm. **B** Scatter plots of cyan [channel 1 (Ch1)] and magenta [channel 2 (Ch2)] pixel intensities and Pearson's correlation coefficients showing colocalization of the images in A.

3.4 APEX2-based proximity labeling in HEK293T cells identified colocalization of RBPMSB with nuclear chromatin remodelers in stress granules under stress conditions

Recent advanced in methods for determining the composition of membraneless assemblies, including biochemical affinity purification, sorting, and proximity labeling, now make it possible to characterize the protein content of cytoplasmic RNP granules such as SGs and P-bodies (Hubstenberger et al., 2017; Jain et al., 2016; Markmiller et al., 2018). In this study, we combined a proximity labeling approach with quantitative mass spectrometry and RBP-focused

immunofluorescence approach to comprehensively expand our knowledge of the protein composition and dynamics of SGs in the heart. The previously described optimized biotin ligases TurboID or miniTurbo (Branon et al., 2018) and engineered ascorbate peroxidase APEX2 (Hung et al., 2014; Lam et al., 2015; Martell et al., 2012; Rhee et al., 2013) enable the identification of proteins in close proximity to a protein of interest. A comparative analysis was performed between the two optimized biotin ligases and APEX2. Unexpectedly, only a limited subset of proteins biotinylated by TurboID or miniTurbo had been previously identified as SG components (see Appendix Figure 43-45). In conclusion, the latest-generation biotin ligases, TurboID and miniTurbo, enable rapid and efficient biotinylation; however, their excessively high basal activity makes them unsuitable for studying highly dynamic structures such as SGs.

In contrast, APEX2's combination of short labeling time, spatial precision, and compatibility with native environments makes it particularly effective for studying transient interactions in dynamic changing structures like the formation of SGs. To demonstrate the feasibility of APEX2-mediated proximity labeling in mammalian cells, a proof-of-principle experiment was conducted in HEK293T cells. This involved stable transfection with APEX2 fusion construct encoding RBPMSB, which was fused in frame to a carboxyl-terminal V5-tagged engineered variant of soybean ascorbate peroxidase APEX2, hereafter referred to as RBPMSB-APEX2. This construct encodes an additional nuclear export signal (NES) to ensure cytoplasmic localization and a copGFP for visualization (Figure 13A). Previous analysis identified a conserved NES (VFCPLLQQIRF) motif within the mouse and human RBPMSB protein sequences, which potentially mediates the differential subcellular localization of the this RBPMS isoform (Shan et al., 2025). As a control for APEX2-mediated labeling in the entire cytoplasm, a self-cleaving T2A peptide sequence was introduced between the open reading frame of RBPMSB and V5-APEX2-NES-copGFP (hereafter referred to as APEX2). Stable HEK293T lines expressing either RBPMSB-APEX2 or control APEX2 were subsequently established for the proximity labeling studies. In order to validate correct subcellular localization and to ensure that the tagged RBPMSB recapitulates the endogenous distribution, immunofluorescence analysis was performed. Detection of tagged RBPMSB using both the anti-V5 antibody and the copGFP-tag demonstrated exclusive cytoplasmic localization (Figures 13B and 14B). Consistently, the APEX2 fusion protein displayed a diffuse cytoplasmic signal that remained unchanged upon heat shock (Figure 14B). The strategy enables nonspecific labeling of cytoplasmic protein, thereby minimizing the risk of detecting false-positive RBPMSB interaction partners arising from unspecific complex formation, and provides a suitable control for subsequent experiments. Furthermore, immunoblot analysis of total protein extracts corroborated equal protein levels of the respective constructs at the expected molecular size (Figure 13C).

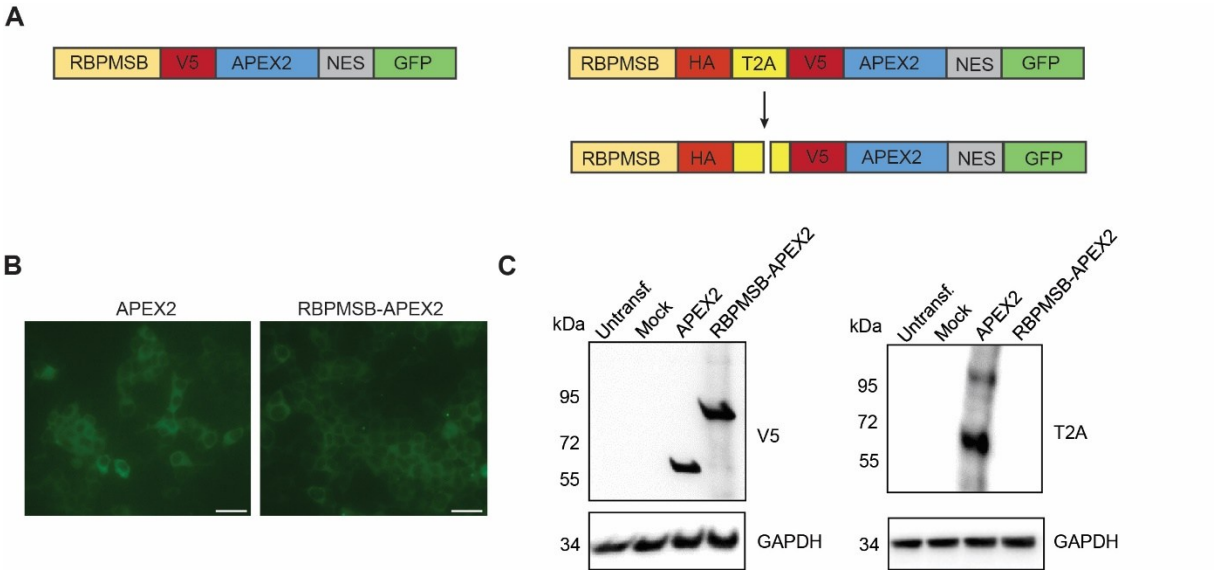

Figure 13 Schematic view and validation of RBPMSB-APEX2 and APEX2 constructs in HEK293T cells for proximity labeling.

A Schematic representation of RBPMSB-V5-APEX2-NES-copGFP (RBPMSB-APEX2) and RBPMSB-T2A-V5-APEX2-NES-copGFP (APEX2). **B** HEK293T cells were stably transfected with fusion plasmids encoding for RBPMSB-APEX2 or APEX2 as indicated. The subcellular localization of the overexpressed proteins was analyzed by direct detection of the copGFP signal by light microscopy. Scale bar, 20 µm. **C** The protein abundances and efficient cleavage of the RBPMSB-APEX2 precursors were confirmed by immunoblotting analysis probed with anti-V5 and anti-T2A antibodies. GAPDH was used as a loading control. Mock= empty vector, untransf. = untransfected control cells.

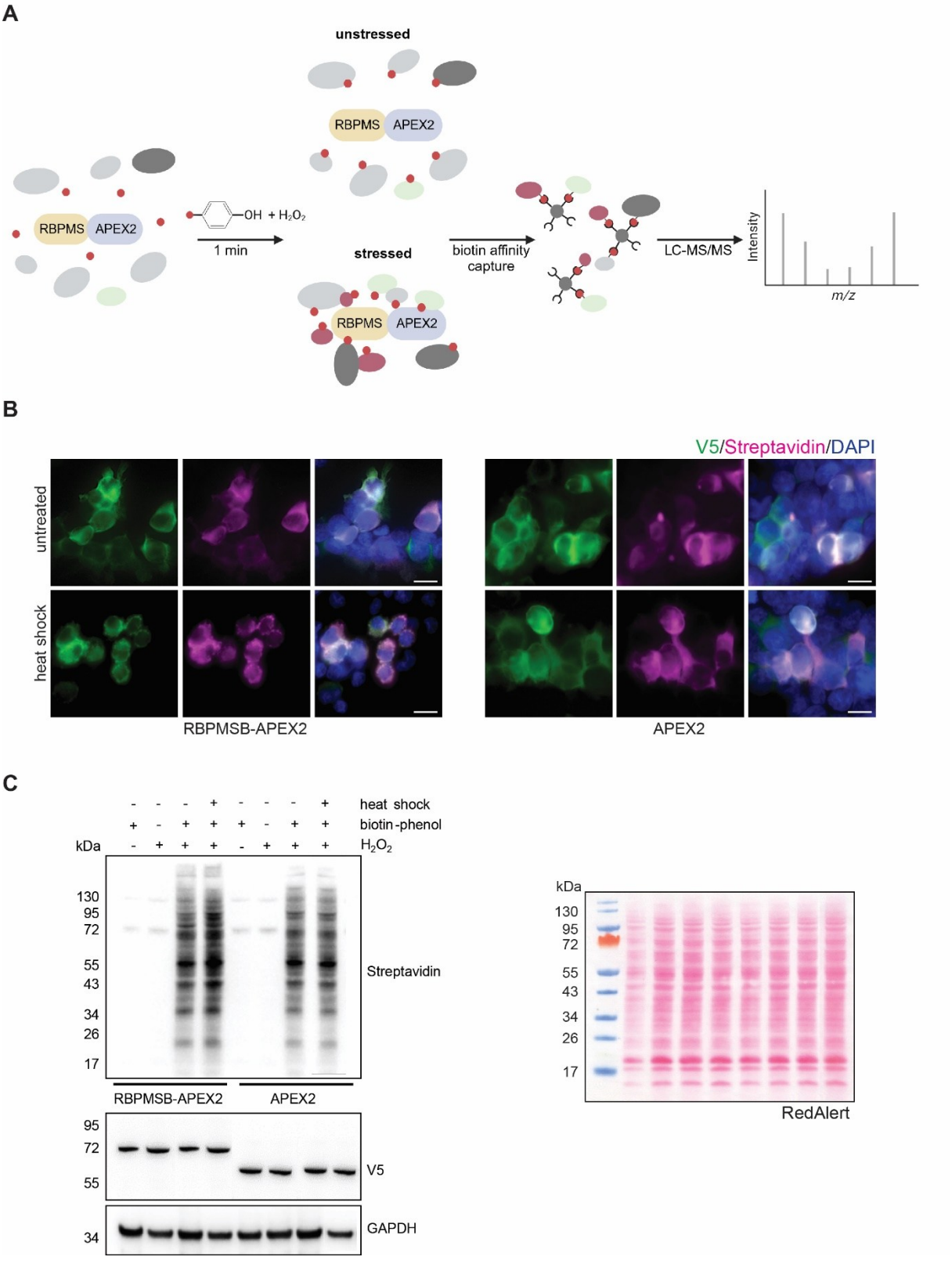

Figure 14 Proximity dependent biotinylation and affinity purification approach to identify the interactome of RBPMSB.

A Schematic view of experimental workflow for APEX2 proximity labeling of proteins with biotin-phenol. HEK293T cells were stably transfected with plasmids encoding RBPMSB-APEX2 and APEX2,

unstressed and heat shock-treated cells were subjected to APEX2-mediated biotinylation. Biotinylated endogenous proteins in close proximity to the fusion protein were isolated by affinity capture on streptavidin-coated beads and identified by LC-MS/MS. **B** Confocal fluorescence imaging of unstressed and heat shocked cells with anti-streptavidin antibody (magenta) to detect biotinylation, anti-V5 antibody (green) and nuclei (DAPI, blue). Scale bar, 10 µm. **C** RedAlert staining (right), streptavidin-HRP analysis of induced protein biotinylation (left) in whole cell lysates displays a broad range of protein bands across various molecular weights and immunoblot analysis probed with anti-V5 antibody. GAPDH served as a loading control.

To identify stress-dependent interactors of RBPMS, we performed a comparative analysis of biotinylated proteins in RBPMSB-APEX2 cells subjected to stress and unstressed conditions. In addition, specificity was achieved by comparing lysates from stressed RBPMSB-APEX2-expressing cells and cells expressing APEX2 alone, which served as a control for normalization. The qualitative control of the APEX2 approach by principal component analysis (PCA) revealed a distinct separation of the different experimental groups (RBPMSB-APEX2, RBPMSB-APEX2 with stress and APEX2 control) (Figure 15A). Mass spectrometry identified putative granule components that included numerous proteins associated with RNA metabolism, along with a substantial proportion of nuclear proteins (Figure 15B). The latter were involved in biological processes such as histone modification, chromatin remodeling, and chromosome organization (Figure 15C, D). These findings are in line with previous studies indicating that numerous molecular components exhibit dual localization and are shuttling between nucleoli and SGs in response to endogenous and environmental signals, thereby controlling cell survival (Mahboubi et al., 2014).

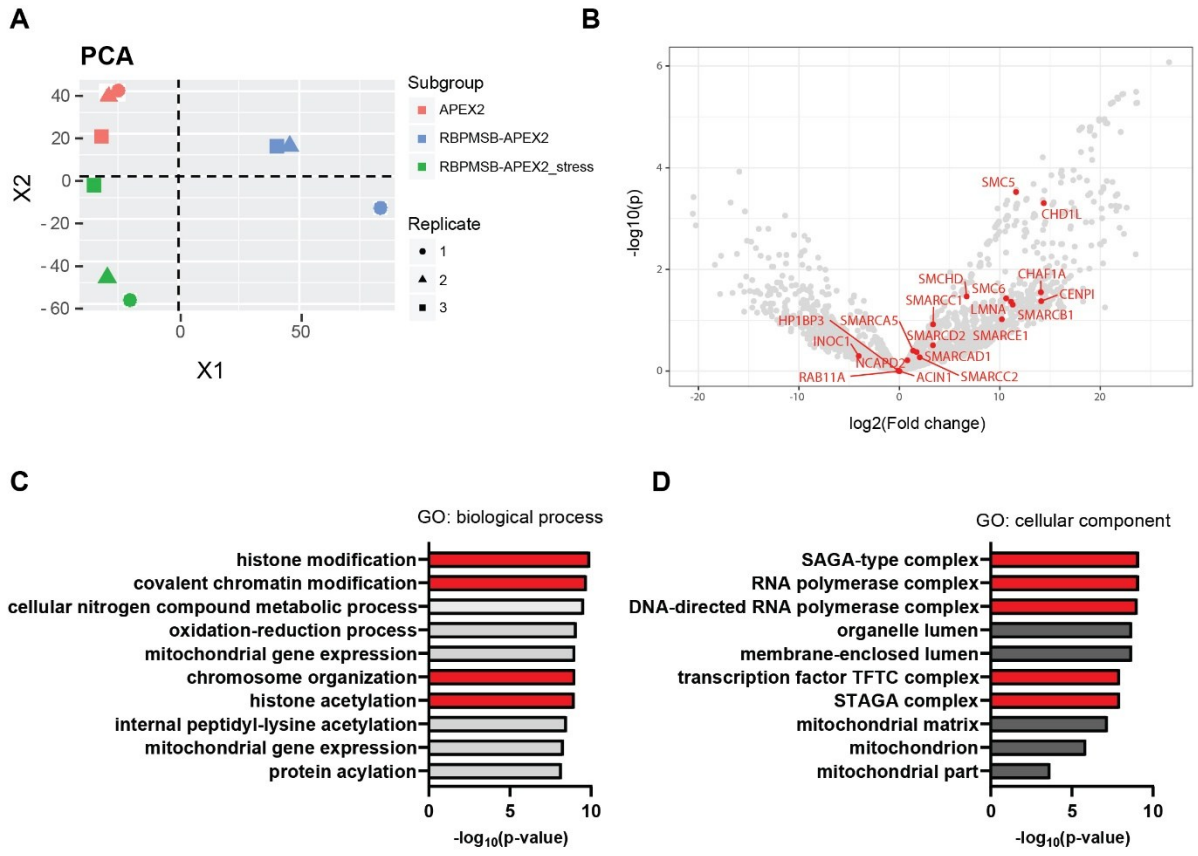

Figure 15 APEX2-mediated proximity labeling of cytoplasmically localized RBPMSB in HEK293T cells identified a subset of nuclear proteins.

A Principal Component Analysis (PCA) of APEX2-mediated proximity labeling indicate the separation of the individual biological replicates (1-3) and different experimental subgroups (RBPMSB-APEX2, RBPMSB-APEX2_stressed and APEX2 control) after streptavidin-pulldown and mass spectrometry (MS) analysis. Scatter within groups is depicted as a percentage in two dimensions (X1, X2). **B** Volcano plot showing proteins biotinylated by RBPMSB-APEX2 in comparison to APEX2. Nuclear proteins are depicted in red. **C, D** Box plots showing the top 10 enriched GO terms for proteins preferentially labeled by RBPMSB-APEX2 upon heat stress. GO terms refer to biological process (C) or cellular component (D). GO terms related to nuclear events are depicted in red.

Among the identified nuclear proteins, SMARCC2 and DNMT3B were selected for experimental validation, as these proteins have not previously been described as components of SGs. SMARCC2 is one of the three core subunits of the large ATP-dependent SWI/SNF chromatin remodeling complex, along with SMARCA2 and SMARCB1. Acting as a DNA-binding protein, it helps recruit the complex to specific genomic regions, thereby promoting chromatin remodeling and regulating gene expression (Li et al., 2022). DNMT3B is a member of the DNA methyltransferase (DNMT) family and plays a critical role in maintaining genomic stability and mediating tissue-specific gene expression patterns (Gao et al., 2022). Upon heat shock exposure, a fraction of SMARCC2 and DNMT3B undergoes a subcellular redistribution,

translocating to the cytosol and assembling into SGs, as evidenced by their colocalization with the SG marker G3BP1 (Figure 16A, B). This observation prompted us to investigate whether stress withdrawal reverts the subcellular switch. Remarkably, upon recovery from heat stress and SG disassembly, SMARCC2 shuttles back into the nucleus (Figure 17). Collectively, these data confirm the reliability of APEX2-mediated proximity labeling and demonstrate its potential as a robust tool for investigating RNP composition.

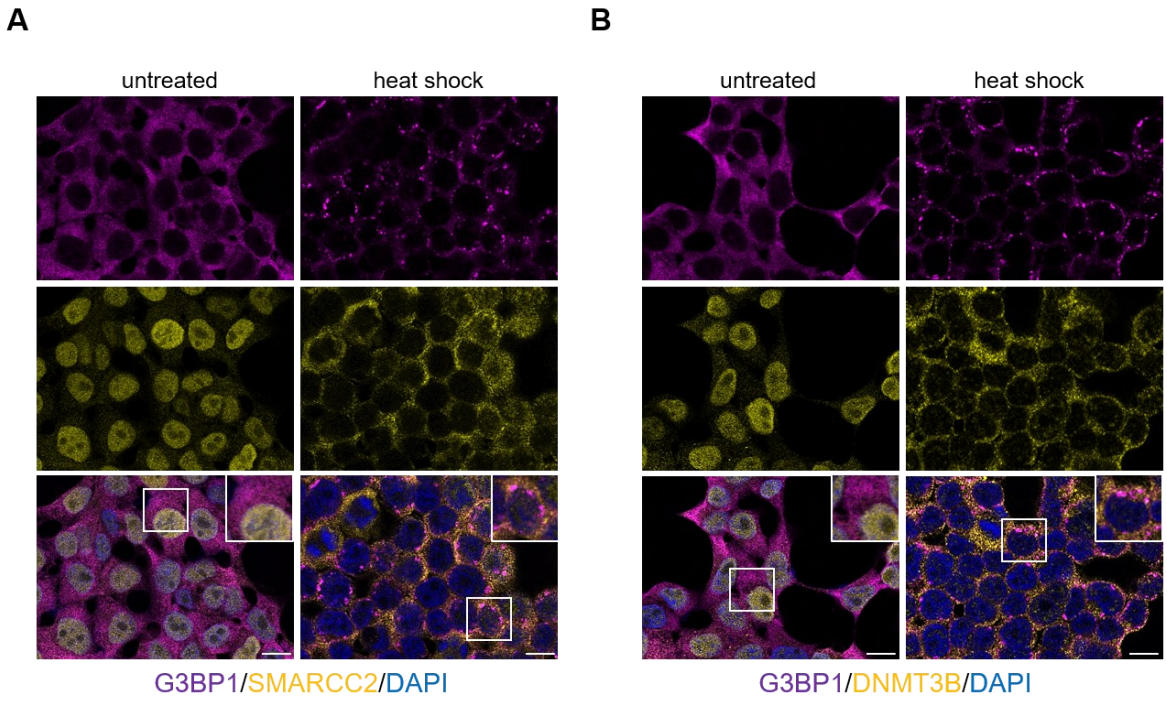

Figure 16 Nuclear proteins SMARCC2 and DNMT3B are recruited to SGs upon heat shock.

A, B Co-staining of untreated and heat-shocked (46°C, 1 h) HEK293T cells with G3BP1 (magenta), SMARCC2 (A) or DNMT3B (B) (yellow) and nuclei (DAPI, blue). Scale bar, 10 µm.

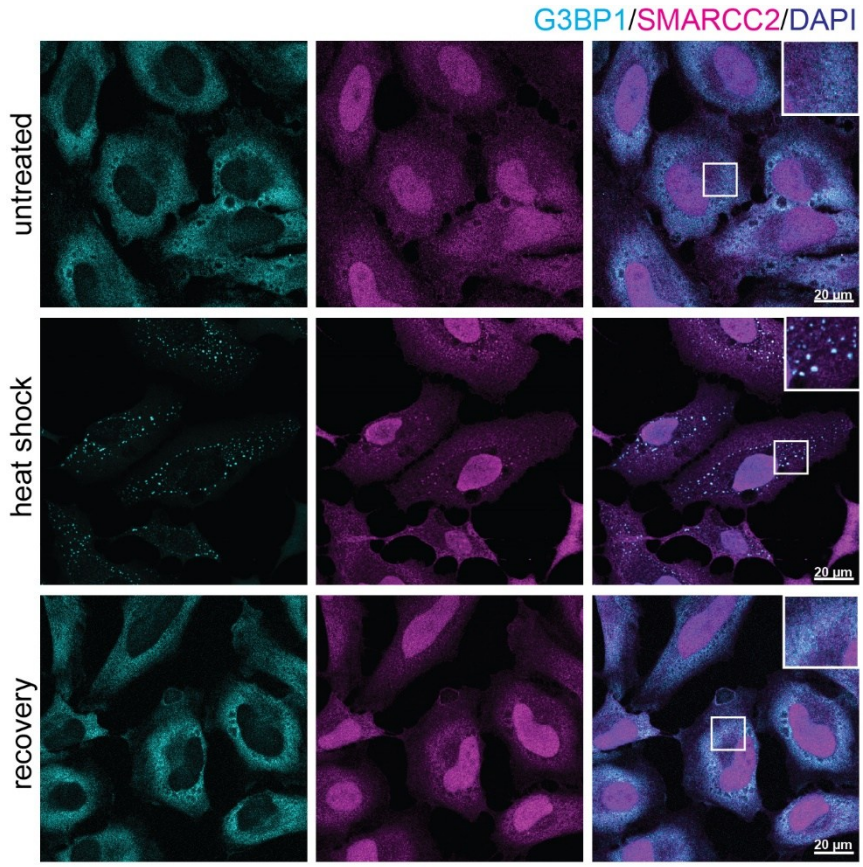

Figure 17 SMARCC2 shuttles between nucleus and cytoplasm in response to heat stress.

Immunofluorescence staining of G3BP1 (cyan), SMARCC2 (magenta) and nuclei (DAPI, blue) in non-treated and heat-shocked (46°C, 30 min) HEK293T cells. After stress exposure, cells were cultured for 1 h at 37°C to initiate the recovery phase. Scale bar, 20 µm.

3.5 Establishing APEX2-mediated proximity labeling in murine HL-1 cell line

In a next step, APEX2-mediated proximity labeling was established in cardiac muscle cell line HL-1 using transient transfection of the (RBPMSB)-APEX2 expression constructs as described above (3.4). Cytoplasmic localization of the APEX-fusion proteins was detected by the copGFP signal. Western blot analysis using an antibody against V5 epitope tag verified comparable expression levels of the fusion and control constructs and calculated molecular weights (Figure 18A, B). In addition, RBPMSB-APEX2 was recruited to SGs in response to heat stress (Figure 18C).

Previous studies demonstrated that HL-1 cells exhibit a relatively low permeability to biotin-phenol (data not shown), necessitating the establishment of a modified labeling protocol to adapt BP and H_2O_2 concentrations. The optimized protocol employs elevated BP (5 mM) and reduced exogenous H_2O_2 (0.5 mM) concentrations, resulting in enhanced biotinylation efficiency and enabling APEX2 labeling in HL-1 cells (Figure 18D, E). Notably, the reduction

in H_2O_2 concentration minimizes cytotoxicity while preserving labeling efficiency, representing a significant methodological advancement.

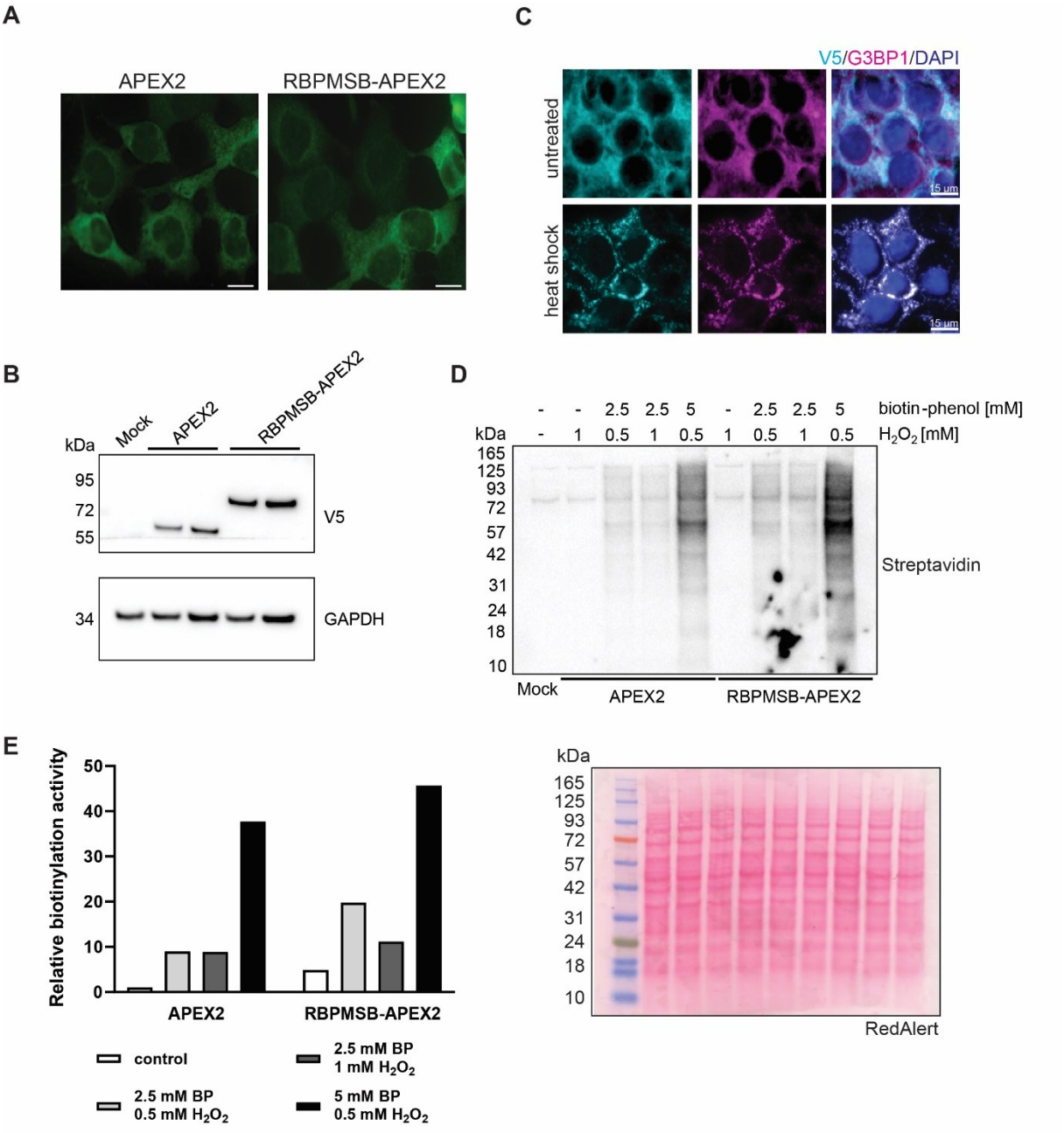

Figure 18 Optimized conditions for APEX2-mediated proximity biotinylation in cardiac HL-1 cells.

A Fluorescence microscopy images detecting copGFP signal of HL-1 cells transiently transfected with RBPMSB-APEX2 and APEX2 fusion constructs. Scale bar, 20 µm. **B** Western blot validation of APEX2 and RBPMSB-APEX2 fusion proteins at calculated molecular weights in transiently transfected HI-1 cells. **C** Representative images of heat-shocked HL-1 cells expressing RBPMSB-APEX2 stained with V5 (cyan), G3BP1 (magenta) and DAPI (blue). Scale bar, 15 µm. **D** HL-1 cells expressing RBPMSB-APEX2 or APEX2 were preincubated with the indicated concentrations of biotin-phenol for 30 min,

followed by the addition of indicated concentration H_2O_2 for 1 min. Whole cell lysates were probed with streptavidin-HRP and **E** the relative biotinylation activity was quantified. RedAlert staining was used for normalization.

In the next step, the optimized protocol was applied to HL-1 cells for proximity-labeling of proteins by RBPMSB-APEX2 or APEX2 control, followed by combined affinity purification and LC-MS/MS. To identify stress-dependent interactors of RBPMS in cardiomyocytes, we performed a comparative analysis of biotinylated proteins in RBPMS-APEX2 cells subjected to stress (heat shock) and those maintained under unstressed conditions. To account for non-specific background labeling, comparative proteomic analysis was performed between lysates derived from stressed RBPMSB-APEX2-expressing cells and APEX2 controls. PCA of the mass spectrometry data revealed distinct variability within the dataset, demonstrating clear separation among the three experimental groups (RBPMSB, RBPMSB_stress and APEX2 control). This analysis clearly indicates that all groups displayed distinct proteomic profiles, with the most pronounced difference observed between APEX2 and RBPMSB-APEX2 in the presence of stress (Figure 19A). Notably, comparison of significantly enriched proteins under heat stress with the Mammalian Stress Granules Proteome (MSGP) database revealed that 23% (27 out of 120) of the RBPMSB-APEX2 interactors under stress conditions are established SG markers/components (Figure 19B, C). Although the majority of biotinylated proteins are enriched for GO terms linked to nuclear functions, including spliceosomal complexes, mRNA processing, and DNA replication, some are also associated with cytoplasmic SGs (Figure 19E, F). Furthermore, RBPMS-APEX2 interactors encompass a minor proportion of known paraspeckle (PS) proteins, representing approximately 15% (18/120) of all enriched proteins (Figure 19B, D). These data indicate a potential link between SGs and the nucleus, through the exchange of proteins, which supports cellular adaptation during stress.

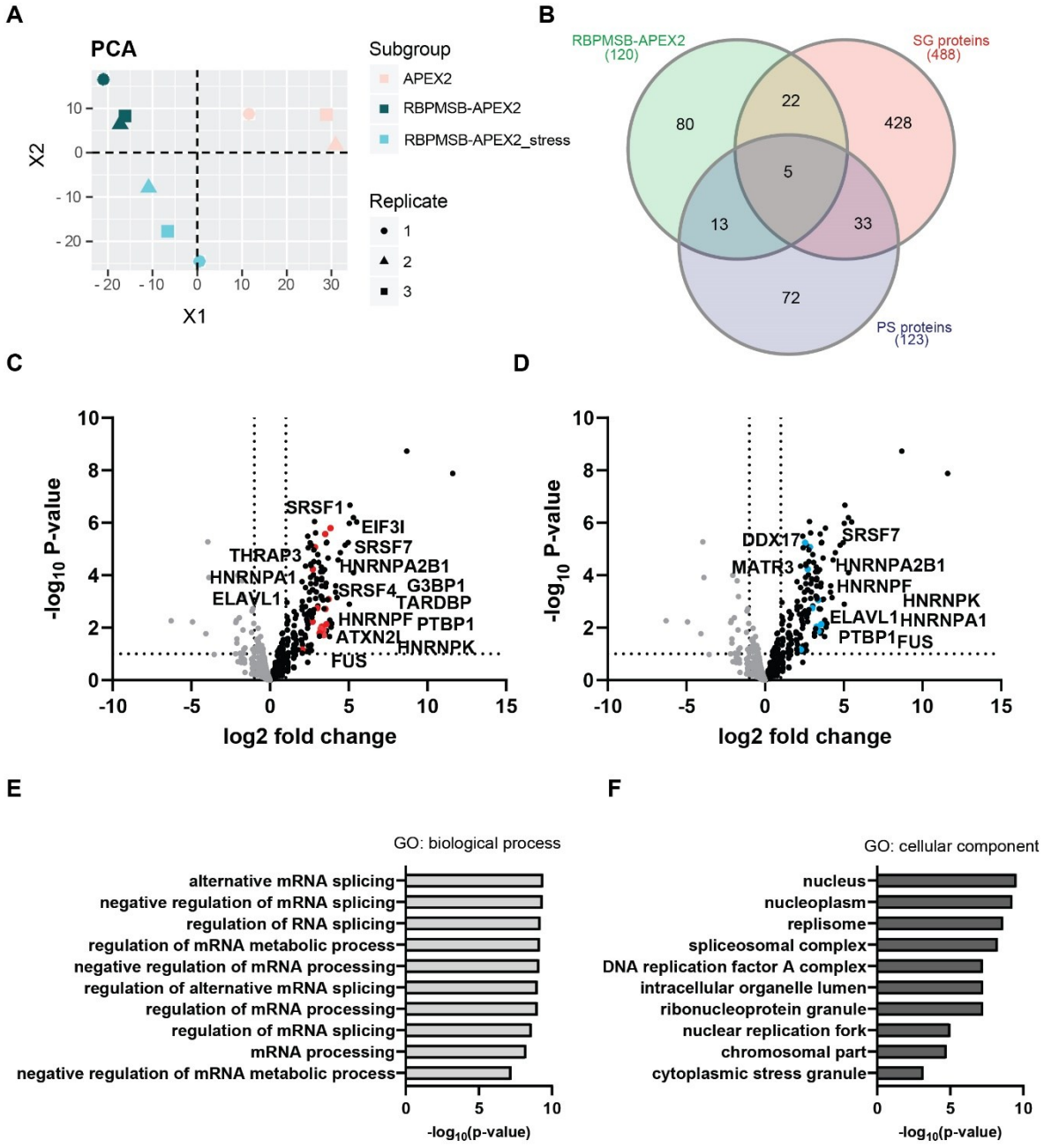

Figure 19 APEX2-mediated proximity labeling of RBPMSB in cardiac HL-1 cells identified stress granules and paraspeckles components.

A Principal component analysis (PCA) depicting separation of the individual biological replicates (1-3) and different experimental groups (RBPMSB-APEX2, RBPMSB-APEX2_stressed and APEX2 control) after streptavidin-pulldown and mass spectrometry (MS) analysis. **B** Venn diagram merging stress-dependent proteins biotinylated by RBPMSB-APEX2 with known stress granule (SG) and paraspeckle (PS) proteins. **C, D** Volcano plot showing proteins biotinylated by RBPMSB-APEX2 upon heat stress (black). Proteins labeled by APEX2 are shown in grey. SG proteins are depicted in red and PS proteins in blue. Adjusted P-values based on the -$\log_{10}$ ratio (y-axis) are plotted against changes based on the log2 ratio (x-axis). **E, F** Box plots showing enriched GO terms of proteins biotinylated by RBPMSB-

APEX2 upon heat stress. GO terms referring to molecular function (E) and cellular component (F) are shown. Only the top 10 GO terms are depicted. Significance was calculated based on the -$\log_{10}$ p-value.

3.6 Establishing a transgenic RBPMSB-APEX2 mouse model to identify SG proteins by *ex vivo* proximity labeling in primary MEFs

To further examine the RBPMSB interactome and SG composition in primary cells, two transgenic APEX2 and RBPMSB-APEX2 mouse lines were generated by introducing the respective APEX2 fusion constructs (as described in 3.4) into the ROSA26 genomic locus. In a first step, these mice were crossbred with CMV-CRE deleter mice to ubiquitously express APEX2 and RBPMSB-APEX2. Crossbreeding with cardiomyocyte-specific *Xenopus laevis myosin light-chain 2* (*XMLC2*)-Cre resulted in conditional activation of APEX2 and RBPMS-APEX2 in cardiomyocytes from embryonic stage onwards (Figure 20A). Both mouse strains were born according to expected mendelian ratios and were viable, indicating that overexpression of the fusion proteins in cardiomyocytes does not cause any adverse effects (data not shown). R26-APEX2 and R26-RBPMSB-APEX2 transgenic mice robustly express APEX2 or RBPMSB-APEX2, as validated by fluorescence microscopy detecting endogenous copGFP signal in whole hearts (Figure 20B) and immunoblotting analysis of isolated mouse embryonic fibroblasts (MEFs) and primary fetal cardiomyocytes using V5 antibody (Figure 20C, D). Notably, our transgenic *ex vivo* APEX2 approach efficiently and robustly biotinylated proteins in MEFs and primary fetal cardiomyocytes under standard labeling conditions (Figure 20E + Figure 21A).

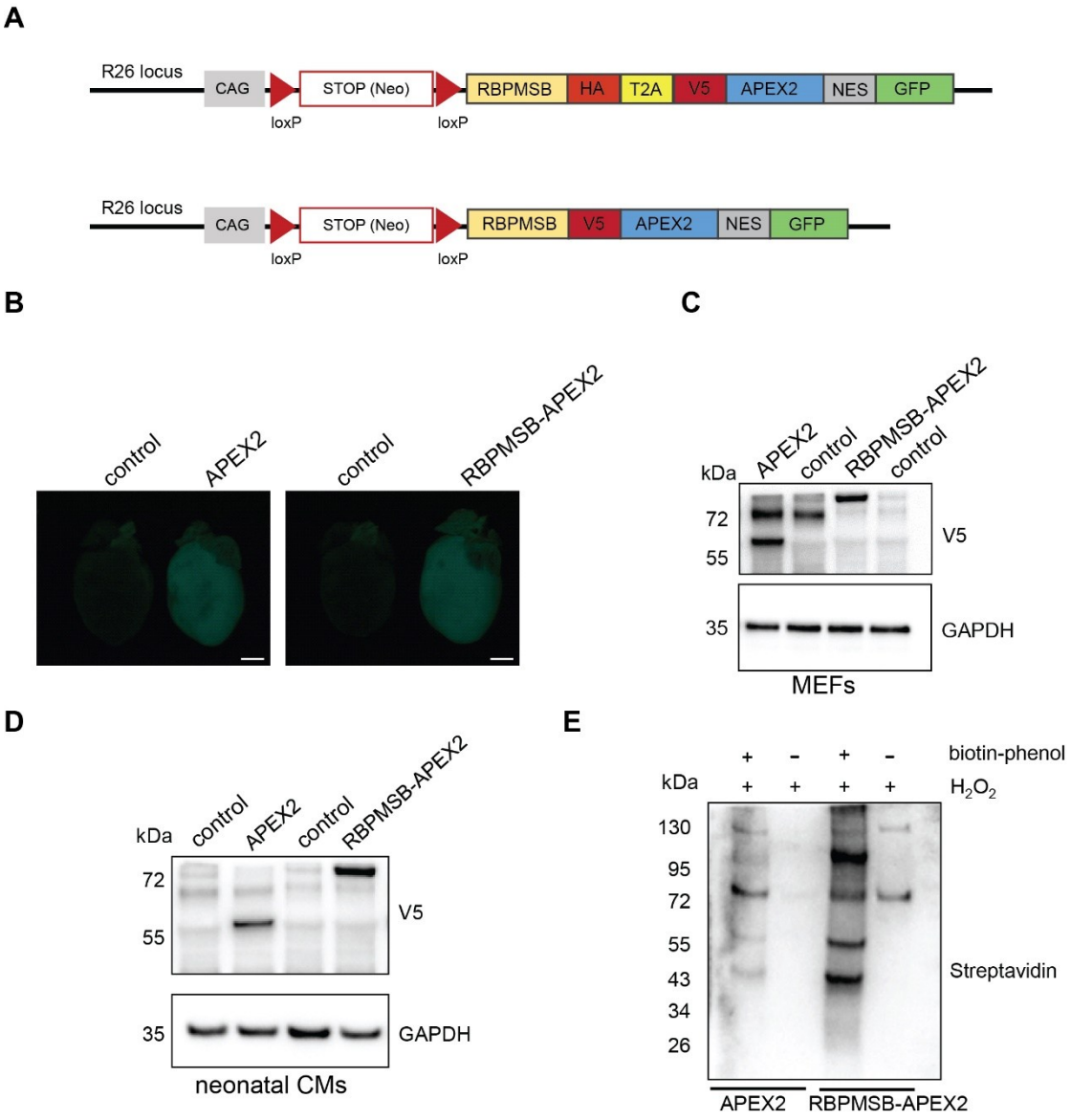

Figure 20 Validation of transgenic (RBPMSB)-APEX2 mouse models.

A Scheme of RBPMSB-V5-APEX2-NES-copGFP (RBPMSB-APEX2) and RBPMSB-T2A-V5-APEX2-NES-copGFP (APEX2) transgenic mouse line, harboring a loxP-flanked Neomycin-(Neo) STOP cassette in the ROSA26 locus, which enables cardiomyocyte-specific expression of the fusion protein after Cre-mediated recombination. Fusion proteins containing V5-tag, the nuclear export signal (NES) and the copGFP-tag. APEX2 mouse line serves as a control for normalization. **B** Images of whole hearts isolated from APEX2$^{+/-}$Cre^{neg}, APEX2$^{+/-}$Cre^{pos}, RBPMSB-APEX2$^{+/-}$Cre^{neg} and RBPMSB-APEX2$^{+/-}$Cre^{pos} adult mice. Scale bar, 1000 µm. **C, D** Representative Western blot using V5 antibody to detect fusion protein abundance in mouse embryonic fibroblasts (MEFs) (C) and isolated neonatal cardiomyocytes (CMs) (D). GAPDH was used as a loading control. **E** Immunoblot of biotinylated proteins from isolated neonatal cardiomyocytes of APEX2$^{+/-}$Cre^{pos} and RBPMSB-APEX2$^{+/-}$Cre^{pos} mice.

Proximity labeling was performed as previously described for other cell types (3.4), using isolated MEFs from APEX2$^{+/-}$Cre^{pos} and RBPMSB-APEX2$^{+/-}$Cre^{pos} embryos The system was validated by Western blot and immunofluorescence staining to confirm expression, activity and correct localization of the fusion proteins (Figure 21A, B). In order to identify heat stress-dependent interactors of RBPMS, we conducted a comparative analysis using the previously reported pipeline (3.4). Heat map analysis of the proteomics profiles indicates variables in this data set, revealing two discrete clusters. The first cluster includes APEX2 and RBPMSB-APEX2 in unstressed cells, while the second cluster encompasses RBPMSB-APEX2 under heat stress. This suggests that under unstressed conditions, APEX2 or RBPMSB-APEX2 share similar protein sets, most likely due to the random distribution of APEX2 or RBPMSB-APEX2 within the cytoplasm. In contrast, significant alterations in candidate protein profiles were detected when comparing non-stress and heat shock conditions (Figure 21C). Mass spectrometry analysis revealed increased number of biotinylated proteins specifically under stress conditions, indicative of enhanced protein density in proximity to RBPMSB, likely due SG assembly (Figure 21D). Furthermore, proteins highly enriched in proximity to RBPMSB-positive granules showed consistent patterns under both experimental conditions - comparing heat-stressed RBPMSB-APEX2 with either APEX2 alone or untreated RBPMSB-APEX2. This consistency further reduces false-positive interactions (background/off-target labeling) and confirms high-confidence, heat stress-dependent interactors (Figure 22A, B).Gene Ontology (GO) term analysis revealed that cytoplasmic SGs was the most significantly enriched term upon heat shock stress. Furthermore, gene set enrichment analysis demonstrated that the majority of the identified proteins were involved in key cellular processes, including the regulation of gene expression, metabolic processes, and translation (Figure 22C, D). Interestingly, comparison and integration of the biotinylated proteins following heat shock treatment from HEK293 cells, HL1 cells and primary MEFs revealed that the majority of identified proteins were unique to each cell type. This is likely due to incomplete capture of low or differential abundant proteins within these cell types (Figure 22E). In summary, these data illustrate that the RBPMSB interactome comprises numerous well-characterized SG components in response to heat stress, while also highlighting substantial cell-type-specific diversity in SG composition.

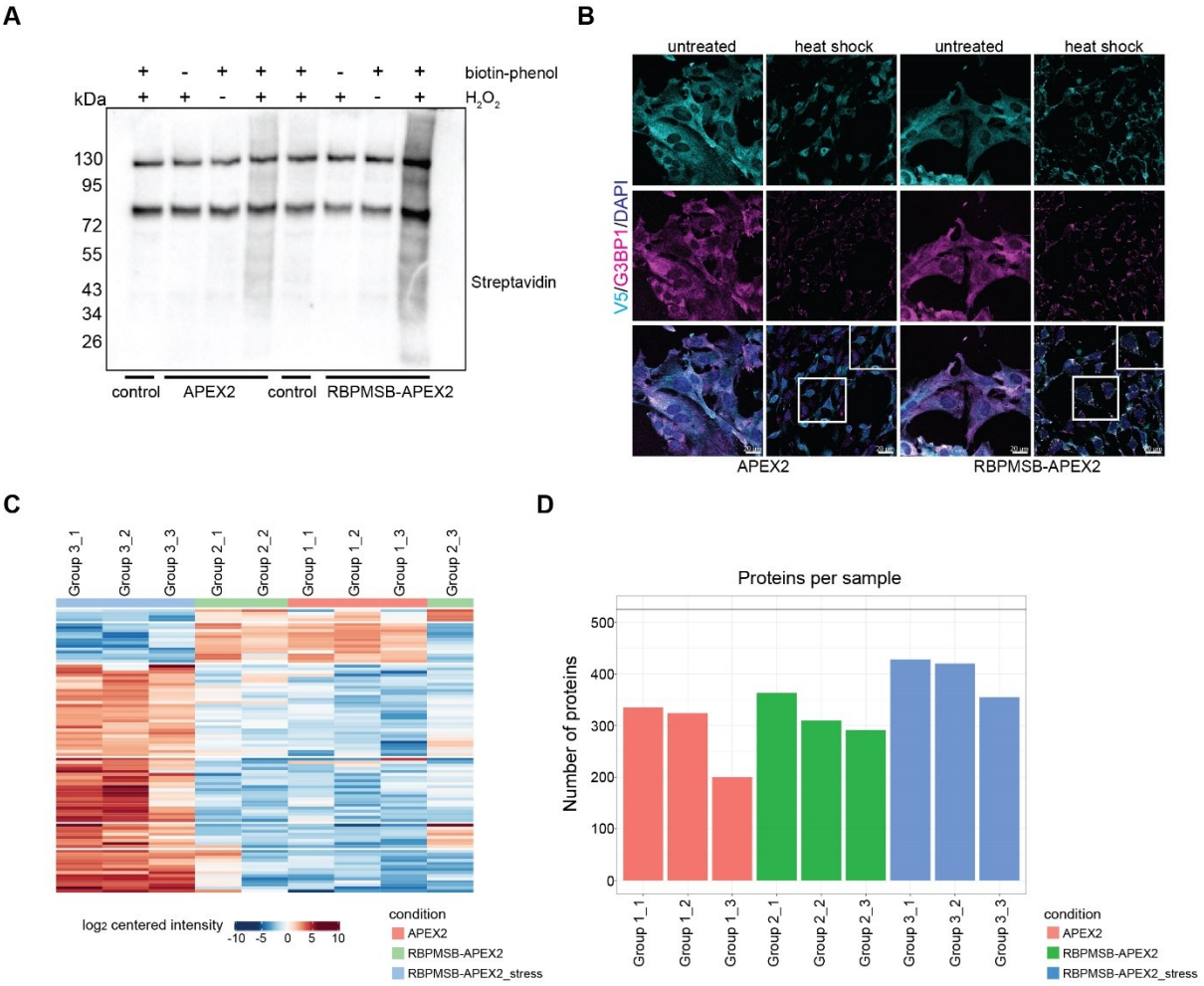

Figure 21 *Ex vivo* APEX2 proximity labeling of RBPMSB in mouse embryonic fibroblasts.

A Representative streptavidin-HRP blot of biotinylated proteins in cultured primary mouse embryonic fibroblasts (MEFs) isolated from RBPMSB-APEX2$^{+/-}$Cre^{neg} and RBPMSB-APEX2$^{+/-}$Cre^{pos} mouse embryos at embryonic day (E) 13.5 and the corresponding controls APEX2$^{+/-}$Cre^{neg} and APEX2$^{+/-}$Cre^{pos}. Primary MEFs were incubated with 500 µM biotin-phenol and labeling was initiated with 1 mM H_2O_2. **B** Confocal images of MEFs isolated from APEX2$^{+/-}$Cre^{pos} and RBPMSB-APEX2$^{+/-}$Cre^{pos} mouse embryos at embryonic day (E) 13.5. MEFs were cultured at 37°C (control) or treated with heat stress (46°C/ 1 h) to induce SG formation. Immunofluorescence labeling using V5 (cyan), G3BP1 (magenta) antibodies and counterstaining with nuclear marker (DAPI, blue). Scale bar, 20 µm. **C** Heat map depicting all identified proteins labeled either by APEX2 and RBPMSB-APEX2 under normal condition or by RBPMSB-APEX2 under stress conditions. **D** Abundance of identified proteins in the different experimental settings APEX2, RBPMSB-APEX2 under basal conditions and RBPMSB-APEX2 upon stress.

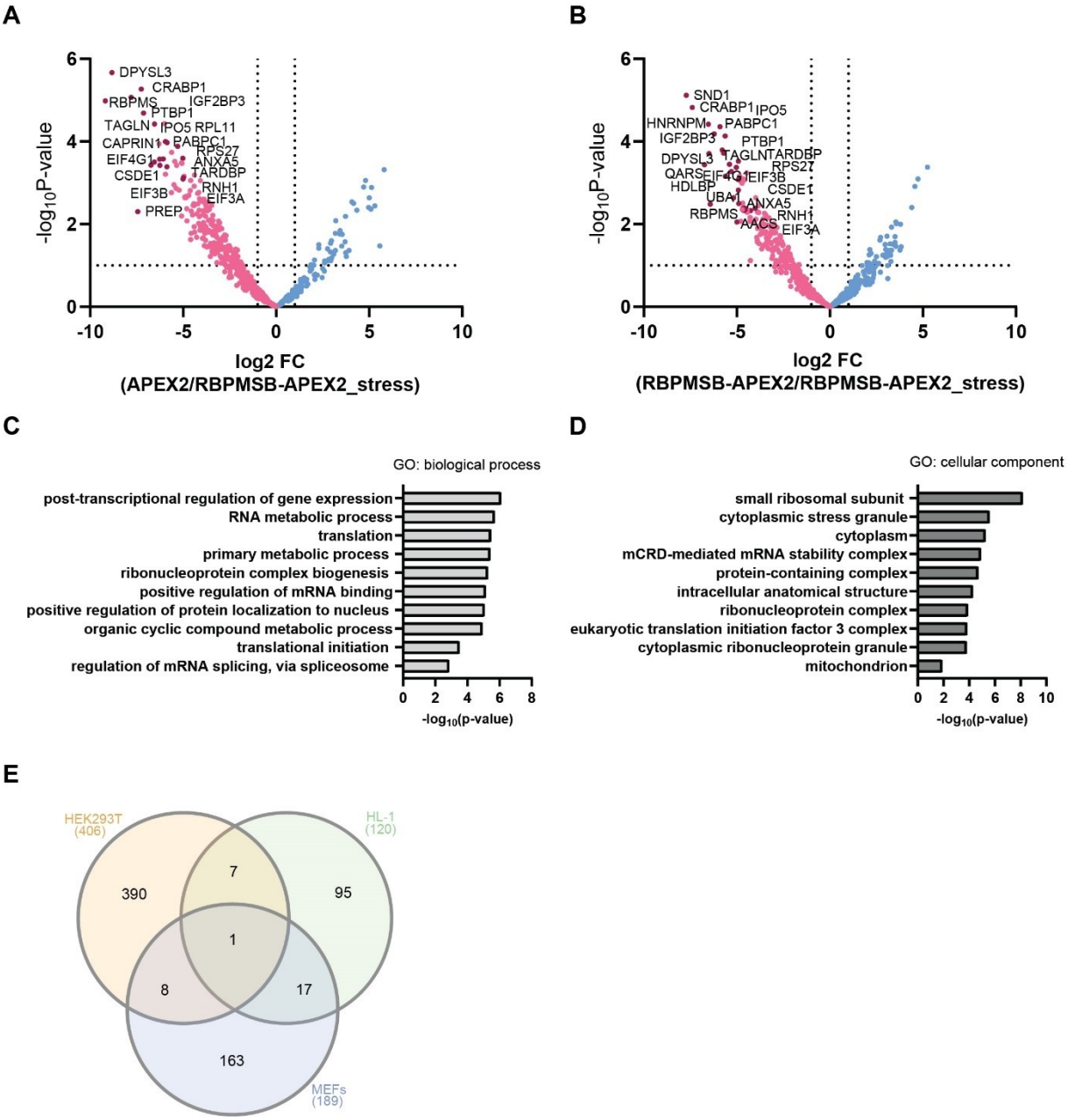

Figure 22 Analysis of APEX2-mediated proximity labeling of RBPMSB in heat stressed mouse embryonic fibroblasts.

A, B Volcano plots depicting detected biotinylated proteins by APEX2 and RBPMSB-APEX2 labeling upon heat stress (A) (n=3) or RBPMSB-APEX2 under basal conditions versus RBPMSB-APEX2 upon heat stress (B) (n=3). **C, D** Box plots showing GO term enrichment for proteins preferentially labeled in RBPMSB-APEX2 expressing mouse embryonic fibroblasts (MEFs) under heat shock in comparison to untreated control cells. GO terms refer to biological process (C) or cellular component (D). Only the top 10 GO terms are shown. Significance was calculated based on the $-\log_{10}$ p-value. **E** Venn diagram comparing APEX2 hits identified in HEK293T cells, HL-1 cells and MEFs treated with heat shock.

3.7 Different cellular stressors result in altered subcellular localization of RBPMS

Several cytotoxic drugs are known to induce cardiotoxic effects, leading to long-term morbidity. Doxorubicin is a highly effective anti-cancer drug widely used to treat a broad spectrum of adult and pediatric malignancies, including a variety of solid tumors, breast cancer, Hodgkin's disease, Kaposi's sarcoma, neuroblastoma, and soft tissue sarcomas. However, doxorubicin administration causes cumulative dose-dependent cardiotoxicity in many patients ranging from changes in myocardial structure and function to severe cardiomyopathy and congestive heart failure, which can lead to heart transplantation or death (Chatterjee et al., 2010). At high doses, cardiotoxicity often occurs within a few months, whereas low doses rarely cause deterioration of ventricular function in the first year after therapy (Von Hoff et al., 1979). Notably, different doses of doxorubicin activate different regulatory mechanisms in hepatoma cells, specifically chronic exposure to high doses induces apoptosis, whereas lower doses lead to senescence and late death by mitotic catastrophe (Eom et al., 2005). Given the dose- and time-dependent effects of doxorubicin, we first examined the subcellular localization of RBPMS over time in HEK293T cells treated with low (0.1 µM) or high (1 µM) concentrations of doxorubicin. In untreated cells, RBPMS predominantly localized to the nucleus (Figure 23A). A low doxorubicin concentration induced the assembly of SGs and the recruitment of RBPMS after 6 h and 24 h of stress exposure (Figure 23B, D). Remarkably, elevated doses of doxorubicin triggered a distinct redistribution of RBPMS, with pronounced nuclear accumulation evidenced by its colocalization with the nuclear DNA marker DAPI (Figure 23C, D). High-dose treatment also induced morphological alterations, including cell shrinkage and rounding-features consistent with apoptotic progression. In conclusion, doxorubicin treatment led to a switch in the subcellular localization of RBPMS but not G3BP1 in a dose-dependent manner, underscoring the specificity of RBPMS redistribution in response to differential drug exposure.

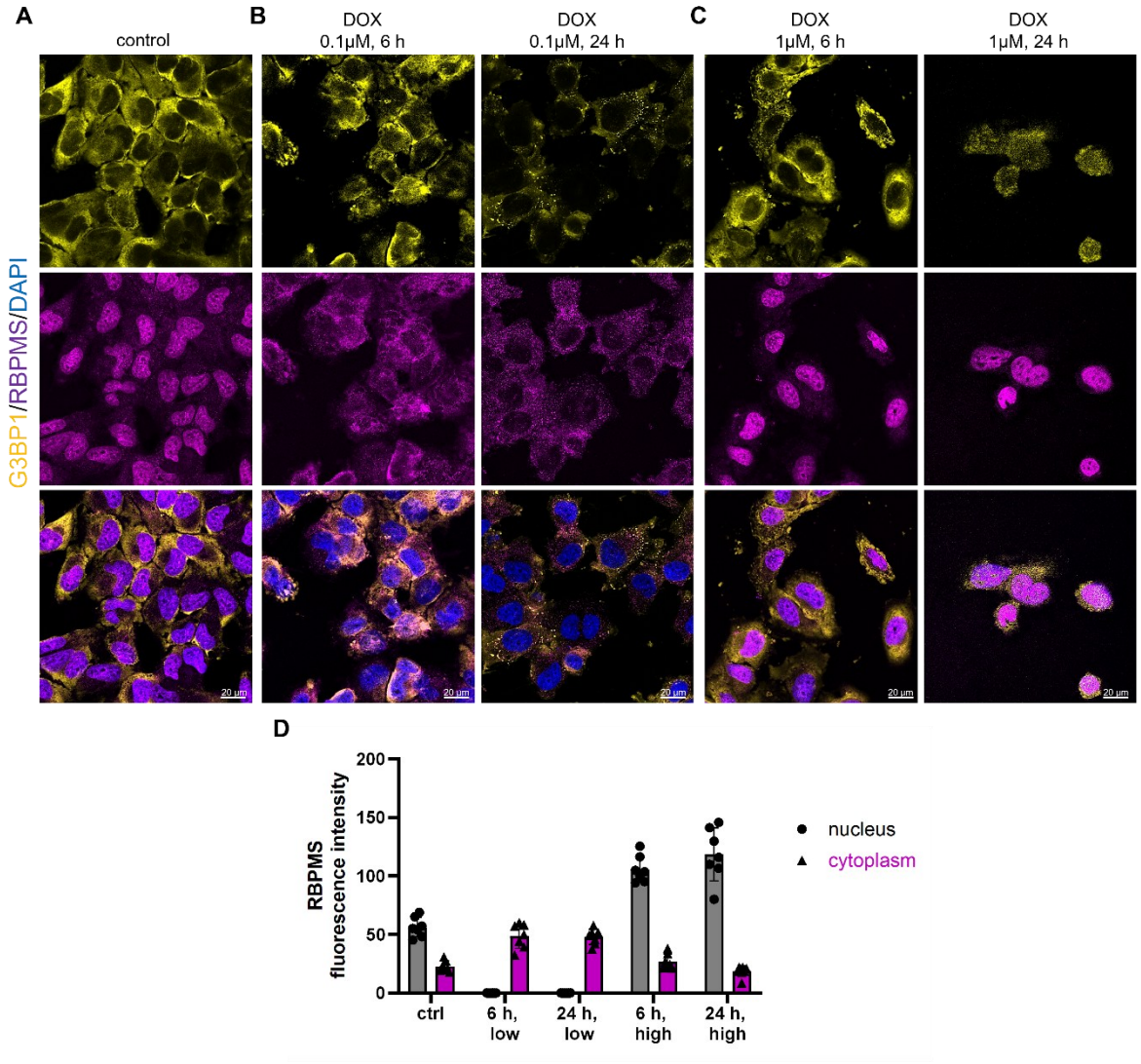

Figure 23 Doxorubicin dosage-dependent localization of RBPMS in HEK293T cells. **A-C** Counterstaining of HEK293T cells with G3BP1 (yellow), RBPMS (magenta) and nuclei (DAPI, blue) following low (0.1 µM) or high (1 µM) dosage of doxorubicin (DOX) at different time points. Untreated cells were used as controls (ctrl). Scale bar, 20 µm. **D** Fluorescence intensity of RBPMS staining in the nucleus and cytoplasm of HEK293T cells with and without doxorubicin treatment.

Doxorubicin imposes substantial stress on cardiac tissue, making it an important model for investigating underlying pathophysiological mechanisms. Therefore, I explored the potential role of RBPMS in response to cytotoxic drug treatment in isolated wild-type neonatal cardiomyocytes. First, the spatiotemporal dynamics and subcellular localization of doxorubicin within cells were assessed at various time points by monitoring its intrinsic autofluorescence as a readout in fixed primary cells. Within 3 h of treatment, doxorubicin exhibited a fine punctate distribution within the cell nuclei (Figure 24A, B). By 24 h, it reorganized into larger, condensed

aggregates that overlapped with chromatin-dense nuclear regions (Figure 24C). This redistribution coincided with the appearance of cytoplasmic SGs, suggesting a temporal link between nuclear drug accumulation and cellular stress responses.

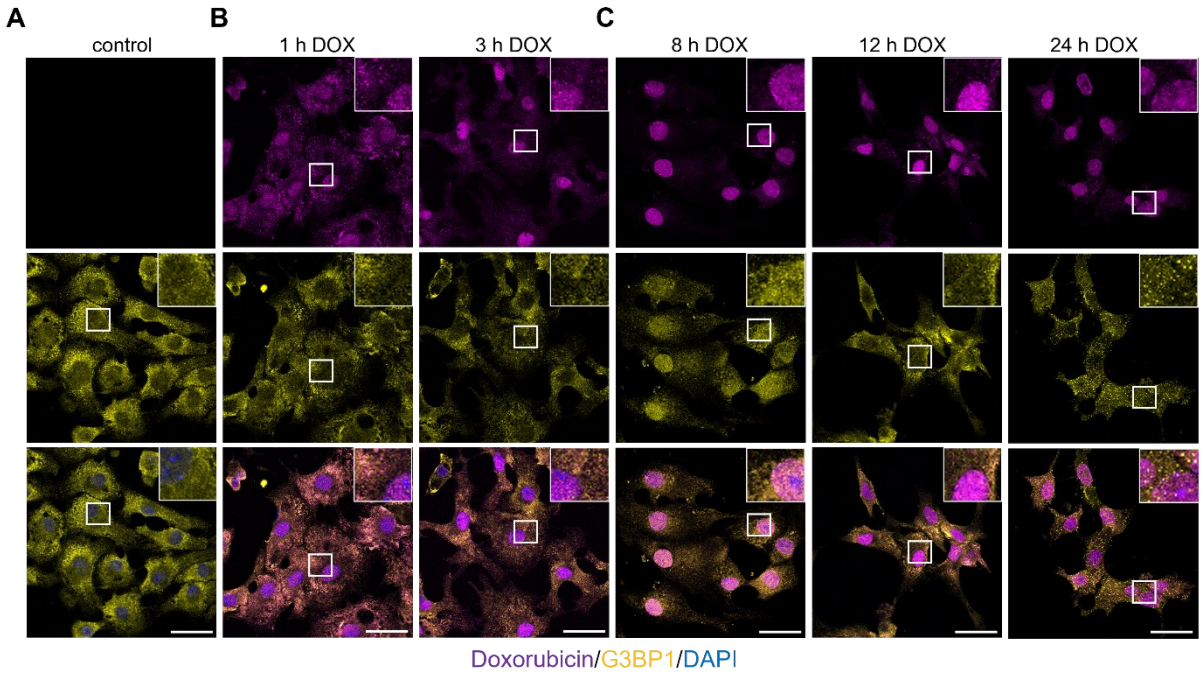

Figure 24 Dynamics of doxorubicin accumulation in neonatal cardiomyocytes.

A-C Representative fluorescence microscopy images showing the intrinsic fluorescence of doxorubicin (magenta) and G3BP1 (yellow) in P0/P1 neonatal isolated cardiomyocytes from wild-type mice treated with and without doxorubicin (DOX; 1 µM) at different time points. Cardiomyocytes were counterstained with F-Actin (green) and nuclear stain DAPI (blue). Scale bar, 20 µm.

Semi-quantitative RT-PCR and Western blot analysis indicate that RBPMSA and RBPMSB represent the two most abundant *Rbpms* isoforms. The fact that RBPMSA is primarily localized in the nucleus whereas RBPMSB is predominantly enriched in the cytoplasm prompted us to examine whether the two isoforms contribute to the same or distinct types of RNP granules. To monitor RBPMS localization and function in cardiomyocytes, murine GFP-tagged RBPMSA or RBPMSB was conditionally overexpressed from the ROSA26 locus using the cardiomyocyte-specific XMLC2-Cre. Mice with cardiomyocyte-specific overexpression of RBPMSA-GFP or RBPMSB-GFP survived until advanced age without any severe phenotype (data not shown). Surprisingly, immunofluorescence staining revealed a recruitment of both, RBPMSA and RBPMSB to nuclear and cytoplasmic speckles in response to various stress stimuli. Specifically, in response to heat shock, RBPMSB forms foci exclusively in the cytosol, whereas doxorubicin treatment leads to the formation of speckles in both compartments, the nucleus and the cytosol. In contrast, RBPMSA exhibited distinct localization patterns in response to different stress stimuli. Upon heat shock, RBPMSA showed a rather moderate

accumulation of foci in the cytoplasm, in contrast to doxorubicin treatment, which resulted in a restricted recruitment to nuclear speckles (Figure 25A, B). This observation suggests that RBPMS might alter subcellular localization in a context-dependent manner such as cellular stress conditions, thereby adapting its function to cellular demands, with the two isoforms fulfilling distinct functional roles.

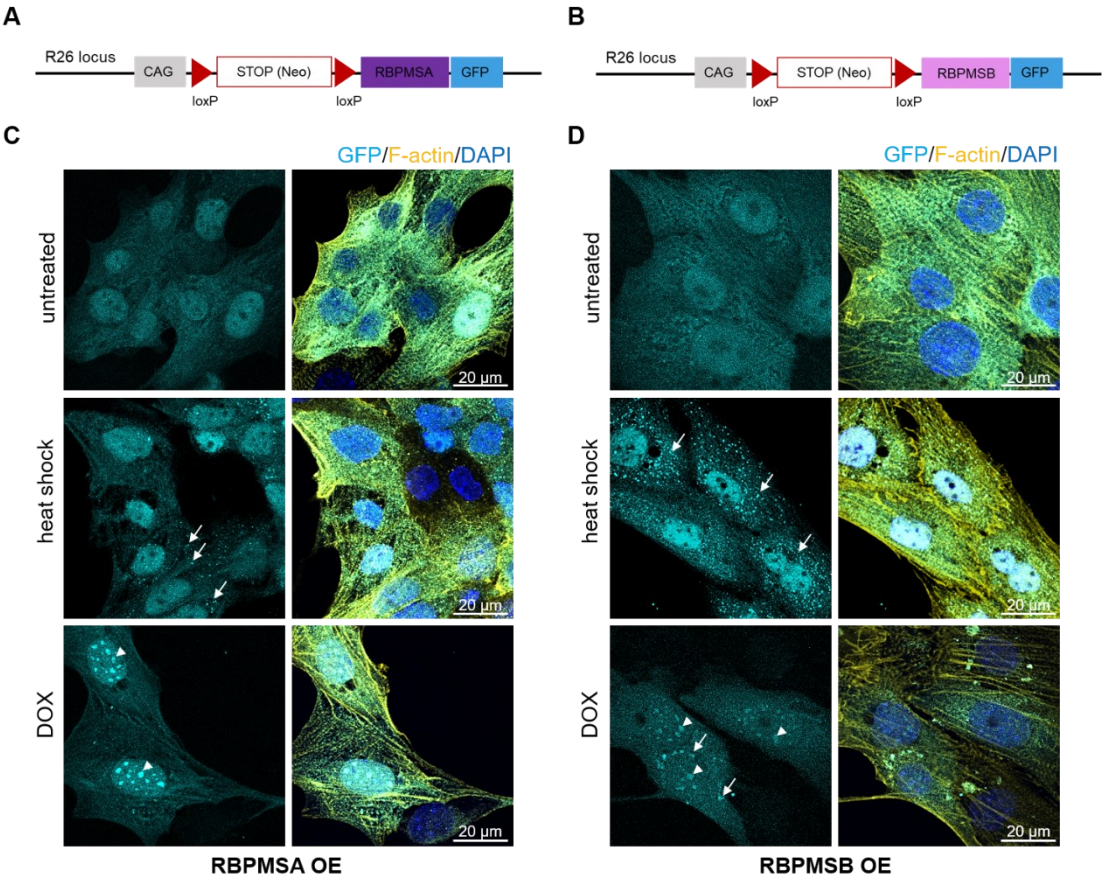

Figure 25 RBPMSA and RBPMSB form distinct cytoplasmic and nuclear speckles in response to various stress stimuli.

A, B Scheme of RBPMSA-GFP (A) and RBPMSB-GFP (B) transgenic overexpression mouse lines, harboring a loxP-flanked Neo-STOP cassette and a GFP-tagged murine RBPMSA or RBPMSB in the ROSA26 locus. **C, D** Immunofluorescence staining of GFP (cyan), F-actin (yellow) and nuclei (DAPI, blue) in isolated mouse neonatal cardiomyocytes (P0) overexpressing GFP-tagged RBPMSA (C) or RBPMSB (D). Cells were treated with either heat shock (1 h, 46°C) or doxorubicin (DOX) (1 µM, 24 h). Untreated neonatal cardiomyocytes were used as a negative control. Both isoforms are components of both, nuclear (arrowheads) and cytosolic (arrows) RNP granules, under different stress conditions. Scale bar, 20µm.

To gain deeper insights into the dynamics of RBPMSA and RBPMSB granule formation, we performed a time-course analysis by treating primary neonatal cardiomyocytes with doxorubicin for various time periods. Since RBPMSB is involved in two different RNP granule types, we proposed that an initial cytoplasmic granule formation may be followed by a

subsequent formation of nuclear foci. To test this hypothesis, we made use of isolated primary neonatal cardiomyocytes which overexpress GFP-tagged RBPMSB. Neonatal cardiomyocytes employed oscillating RBPMSB-containing RNP granules during doxorubicin treatment, initiating first in cytoplasmic SG formation, as indicated by the colocalization of the fusion protein with G3BP1. Subsequently RBPMSB displayed dual localization in both SGs and the nucleus, characterized by a punctate distribution within the interchromatin space (Figure 26A, B). Interestingly, extended exposure to doxorubicin led to a predominant nuclear accumulation of RBPMSB-GFP, while a minor fraction remained in the cytosol (Figure 26B, C). RBPMSB-GFP-positive foci partially overlapped with doxorubicin, indicating that both are associated with DNA damage and nuclear remodeling, suggesting a potential functional connection between them. This colocalization with doxorubicin may facilitate the self-assembly of RBPMSB-GFP into phase-separated condensates.

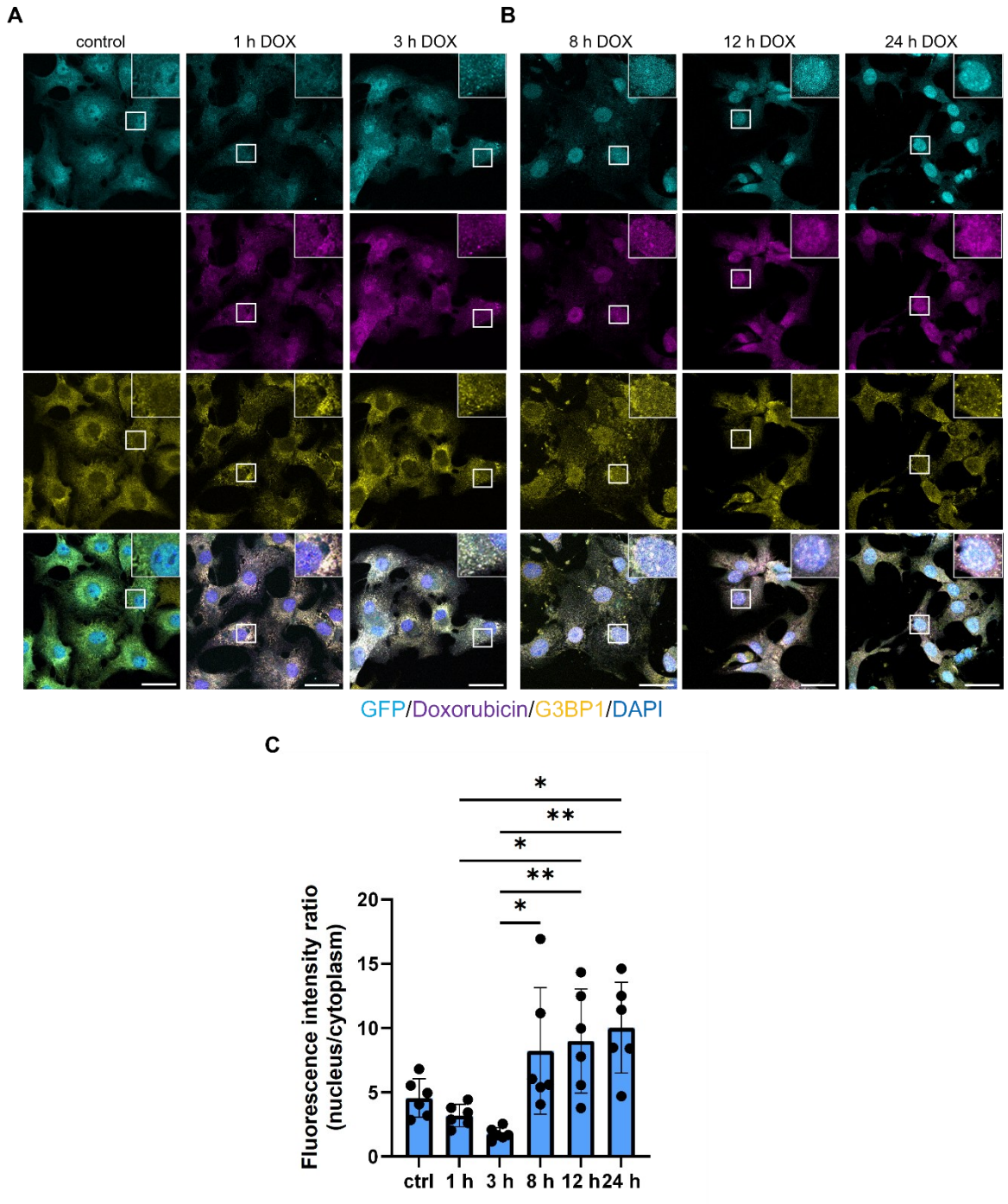

Figure 26 Dynamics of RBPMSB speckle formation upon doxorubicin treatment in neonatal cardiomyocytes.

A, B Representative confocal images of GFP (cyan), doxorubicin autofluorescence (magenta) and G3BP1 (yellow) in P0/P1 neonatal cardiomyocytes isolated from RBPMSB-GFP overexpressing mice. Cells treated with or without doxorubicin (DOX; 1 µM) at different time points. Cardiomyocyte nuclei were counterstained with DAPI (blue). Scale bar, 20 µm. **C** Quantitative analysis of the nuclear-to-cytoplasmic fluorescence intensity ratio in P0/P1 neonatal cardiomyocytes overexpressing RBPMSB-GFP. (n=6; 20 cells per group).

Dexrazoxane (Zinecard, also known as ICRF-187) is a clinically approved cardioprotective agent used to mitigate doxorubicin-induced cardiotoxicity by preventing the formation of Top2 cleavable complexes and promoting the degradation of Top2b (Andoh, 1998; Hellmann, 1998). To assess whether dexrazoxane can attenuate doxorubicin-induced biomolecular condensate formation in neonatal cardiomyocytes and to elucidate the underlying molecular mechanisms, primary neonatal cardiomyocytes were pretreated with dexrazoxane prior to doxorubicin exposure. Surprisingly, dexrazoxane pretreatment failed to inhibit the formation of doxorubicin-induced condensates. Intriguingly, RBPMS and G3BP1 were found to colocalize within both cytoplasmic and nuclear foci following treatment (Figure 27). These findings suggest that nuclear condensate formation is primarily driven by doxorubicin's ability to intercalate into DNA and/or its induction of ROS, which in turn causes oxidative DNA lesions and strand breaks.

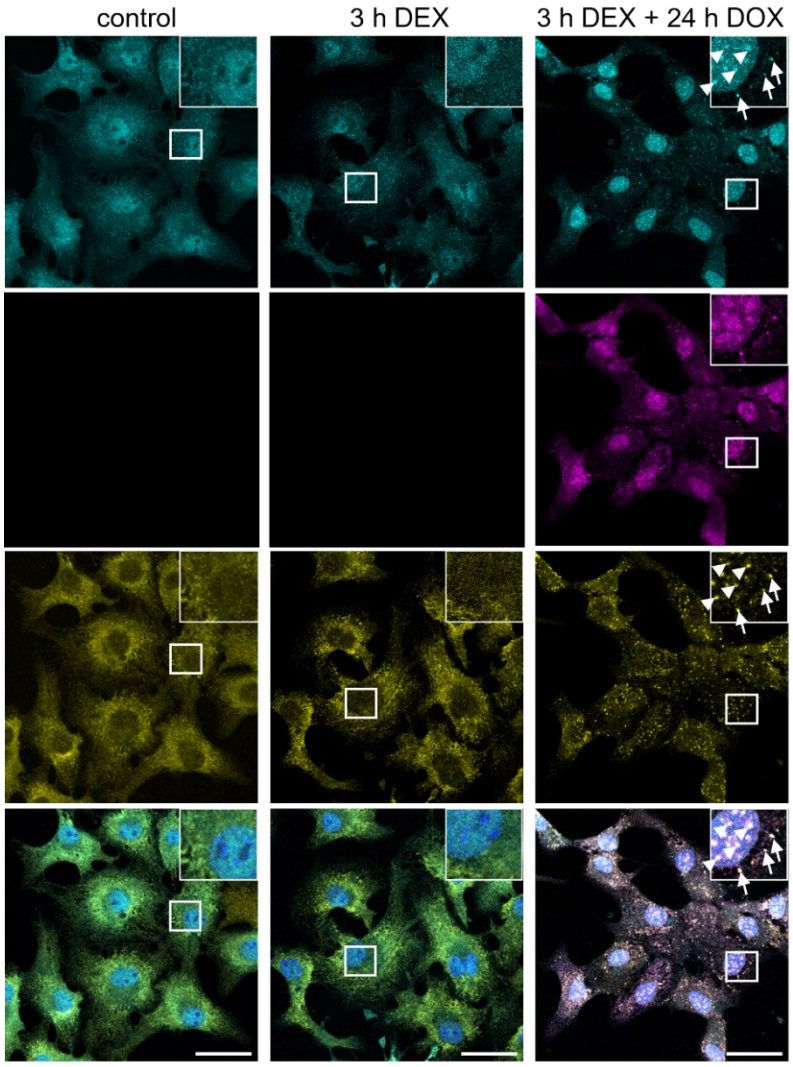

Figure 27 Doxorubicin-induced condensates are independent of Top2b in neonatal cardiomyocytes.

Representative confocal microscopy images showing RBPMSB-GFP fusion protein (cyan), intracellular autofluorescence of doxorubicin (magenta) and G3BP1 (yellow) in P0/P1 neonatal isolated cardiomyocytes from RBPMSB-GFP overexpressing mice. Primary cells were pre-treated with dexrazoxane (DEX) for 3 h prior to doxorubicin (DOX) treatment (1 µM) for 24 h. Cardiomyocytes were counterstained with nuclear stain DAPI (blue). Arrowheads indicate nuclear foci and arrows mark cytoplasmic SGs. Arrows Scale bar, 20 µm.

To exclude the possibility that the nuclear localization of RBPMS fusion proteins arises from GFP dimerization or from non-physiological protein abundance due to overexpression, we utilized an endogenously C-terminal-tagged transgenic mouse reporter strain. The V5-tagged RBPMSB allows us to monitor the localization of one of the two most abundant isoforms under different stress conditions. In line with our previous findings from GFP-tagged RBPMS fusion proteins, the V5-tagged endogenous RBPMSB isoform exhibits a dynamic relocalization upon doxorubicin exposure. Specifically, after 3 h of treatment, RBPMSB assembles into cytoplasmic granules, while at 24 h, a pronounced nuclear accumulation occurs, characterized by the formation of granular foci within interchromatin (DNA-depleted regions) (Figure 28).This congruence between the endogenous reporter line and the GFP-tagged results underscores the physiological relevance of RBPMSB's stress-induced redistribution.

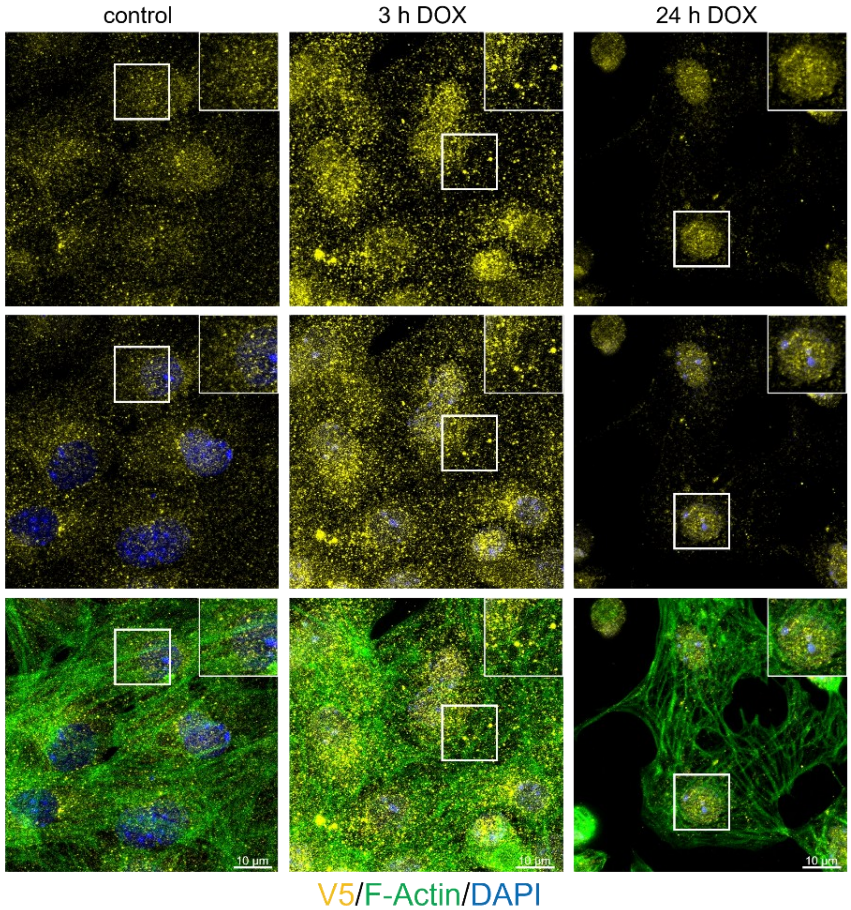

Figure 28 V5-tagged RBPMSB expressed from the endogenous locus forms speckles in the cytoplasm and nucleus upon doxorubicin treatment.

Representative immunofluorescent images of P0/P1 isolated neonatal cardiomyocytes treated with doxorubicin (DOX; 1 µM) for different time periods and untreated control. Primary cells were stained with V5 antibody to detect tagged RBPMSB (yellow), F-Actin (green) and nuclear stain DAPI (blue). Scale bar, 10 µm.

Doxorubicin is a genotoxic reagent that induces DNA damage primarily through the generation of DNA double-strand breaks (DSBs) (Renu et al., 2018). This mechanism raised the question of whether the nuclear localization of RBPMS observed during doxorubicin treatment reflects a general response to genotoxic stress or arises from properties specific to doxorubicin. Given that doxorubicin was the first stressor shown to induce RBPMS recruitment to nuclear speckles, we subsequently investigated speckle formation in cardiomyocytes under exposure to additional ROS-inducing agents, including hydrogen peroxide (H_2O_2), cisplatin and tumor necrosis factor-alpha (TNF-α) - all of which are known to cause DSBs and activate apoptosis signaling pathways. This approach allowed examination of whether RBPMS speckle formation represents a generalized response to diverse oxidative stressors in cardiomyocytes. Short-term exposure (2 h) to all stressors induced transient cytosolic granule formation (Figure 29A, B), while prolonged treatment (24 h) led to nuclear speckle assembly (Figure 29A, C). Unexpectedly, G3BP1 exhibited nuclear translocation following extended exposure to cisplatin, H_2O_2 or TNF-α. SG assembly occurred universally within 2 h of treatment but dissipated as RBPMS and G3BP1 redistributed to nuclear foci (Figure 29A-C). In conclusion, RBPMS consistently undergoes subcellular relocalization in response to various stressors, suggesting a fundamental role in regulating the dynamics of RNP complexes. This function appears to be integral to cellular adaptation under oxidative stress or genotoxic stress preceding apoptosis, rather than representing a response specific to doxorubicin. Furthermore, stressor dose-dependent effects bifurcate cellular signal pathways: at low stress levels, distinct biochemical mechanisms may be activated that support cellular adaptation and survival, while elevated oxidative stress likely initiate signaling cascades shifting the cellular response toward damage, inflammation, and cell death. This duality suggests that the specific outcome depends on both the intensity and duration of the stress experienced by the cell.

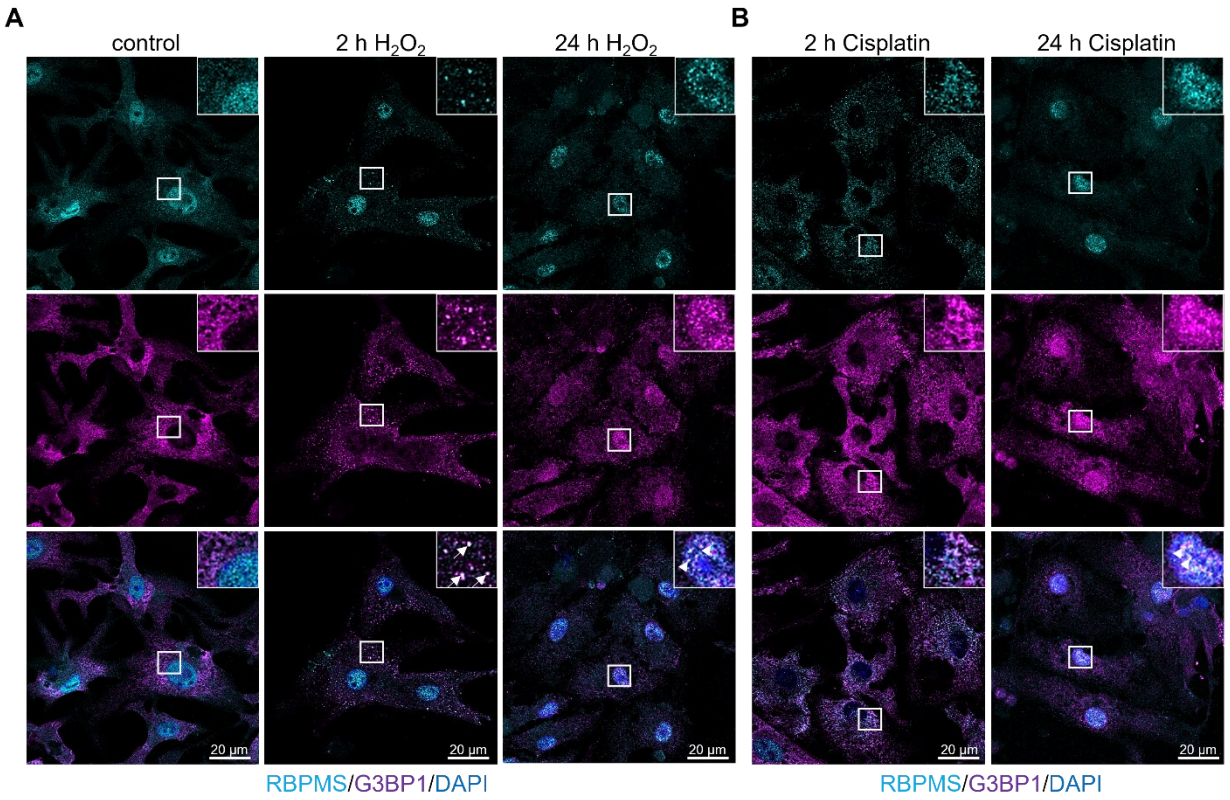
A
control
2 h H_2O_2
24 h H_2O_2
B
2 h Cisplatin
24 h Cisplatin
20 µm
RBPMS/G3BP1/DAPI
RBPMS/G3BP1/DAPI

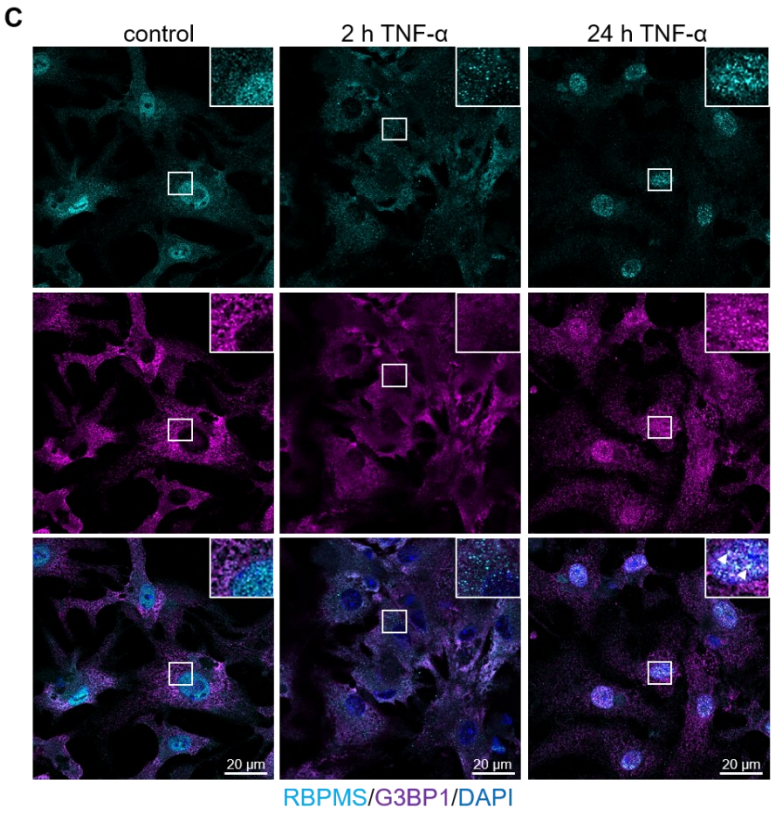
C
control
2 h TNF-α
24 h TNF-α
20 µm
RBPMS/G3BP1/DAPI

Figure 29 RBPMS exhibits dynamic subcellular redistribution under stress conditions.
A-C Representative confocal microscopy images of RBPMS (cyan), G3BP1 (magenta) and nuclei (DAPI, blue) in P0/P1 isolated neonatal cardiomyocytes. Cells were treated with 350 µM H_2O_2 (A) 100 µM Cisplatin (B) or 5 ng/ml TNF-α (C) for 2 h or 24 h and compared with untreated cells (control). Arrows indicate cytoplasmic granules; arrowheads mark nuclear granules. Scale bar, 20 µm.

3.8 Identification of a novel *Rbpms* isoform in cardiomyocytes upon doxorubicin treatment

The RBPMS gene is expressed in multiple alternatively spliced transcript variants encoding distinct protein isoforms. This isoform diversity likely confers functional versatility, thereby enabling RBPMS proteins to engage in a wide range of cellular processes and to adapt dynamically to distinct cellular signals. The most commonly expressed isoforms encompass RBPMSA and RBPMSB. Both share an identical N-terminal region of 176 amino acids encoded by six common exons, but differ in their C-terminal sequences, which are encoded by exon 8 in RBPMSA and by exon 7 in RBPMSB (Shimamoto et al., 1996). To resolve how RBPMS dynamics relate to the relative abundance of its isoforms, we analyzed the distribution of *Rbpms* mRNA variants in neonatal wild-type cardiomyocytes under basal and following doxorubicin treatment. Semi-quantitative RT-PCR using two primer pairs targeting the alternatively spliced exons across all predicted transcripts revealed six distinct splicing events that give rise to the *Rbpms* isoforms (Figure 30A-C). Among these, *Rbpmsa* (*Rbpms-203/-213*), encoding a 197aa variant, and *Rbpmsb* (*Rbpms-202*) encoding a 220aa variant, were the most abundantly expressed isoforms, while *Rbpmsc* (*Rbpms-201*) represents a distinct isoform characterized by the skipping of exon 6. Interestingly, doxorubicin treatment significantly altered the relative abundance of *Rbpms* isoforms, resulting in marked downregulation of *Rbpmsa* and *Rbpmsb* (Figure 30D). In contrast, doxorubicin treatment led to the upregulation of a novel isoform, *Rbpmsd*, which has not yet been annotated. RT-PCR combined with Sanger sequencing revealed the inclusion of a putative poison exon X, which has not been annotated in in the mouse genome so far. This novel exon X locates within the canonic intronic region flanked by exon 7 and exon 8. Cross-species transcriptome analysis demonstrated that the poison exon is highly conserved across different species, although it is still not annotated, suggesting that its inclusion may serve specific regulatory functions under stress conditions.

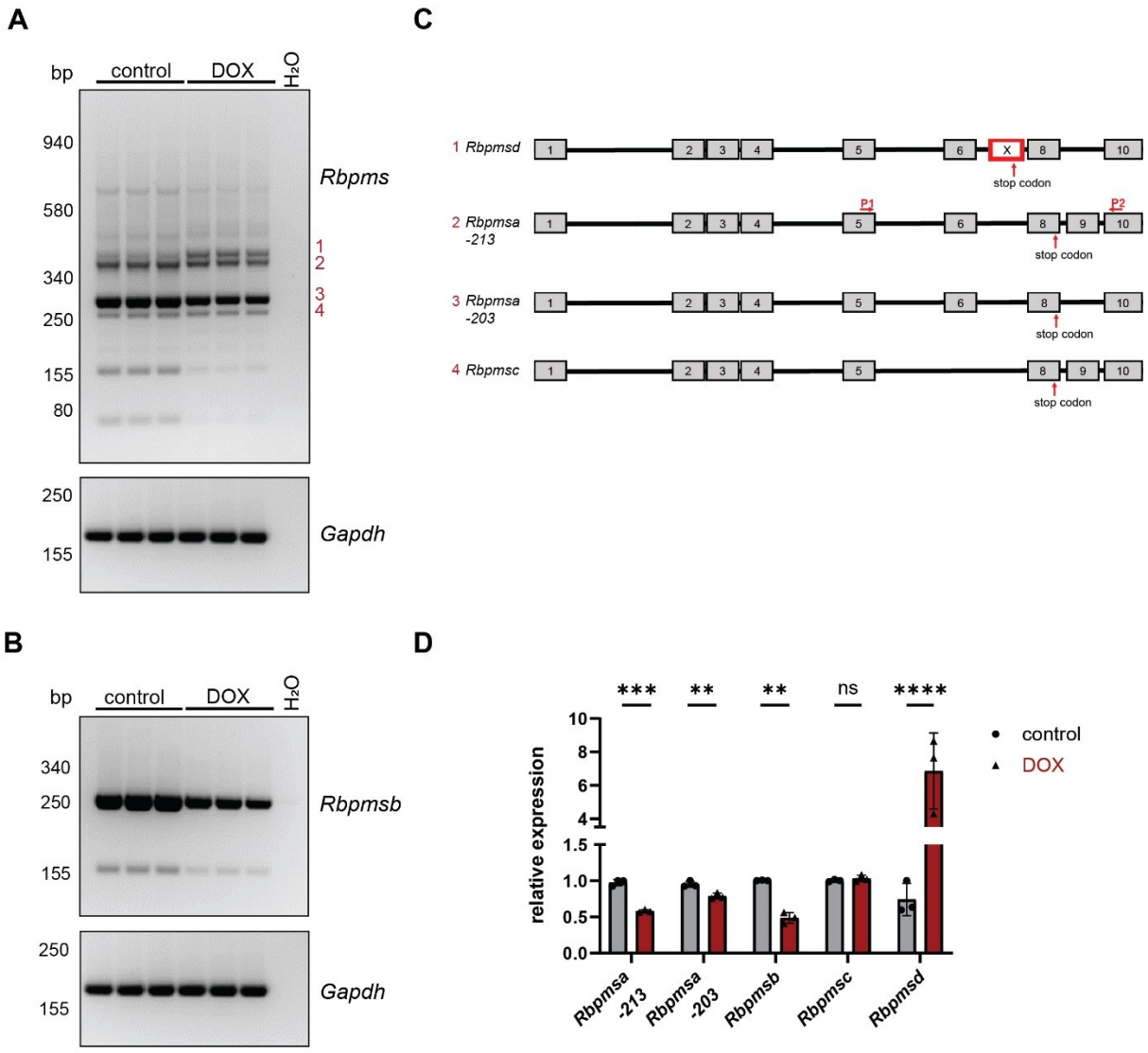

Figure 30 Doxorubicin alters the ratio of *Rbpms* splice events and results in the enhanced expression of a novel *Rbpmsd* isoform.

A, B Splice variants of mouse *Rbpms* in isolated neonatal cardiomyocytes treated with or without doxorubicin (DOX; 1 µM for 24 h) assessed by semi-quantitative RT-PCR. *Gapdh* served as a loading control. **C** Schematic representation of *Rbpms* transcripts generated by alternative splicing at the 3'end. Arrows indicate the position of primers used for semi-quantitative RT-PCR. **D** Quantitative analysis of the relative expression levels among distinct *Rbpms* isoforms. Data represent the mean ± SD. Two-way ANOVA with Bonferroni's multiple comparisons test. **P < 0.01; ***P < 0.001; ****P < 0.0001. ns = not significant.

In order to selectively amplify the full-length open reading frame (ORF) of *Rbpmsd*, specific primers were designed to span the start and stop codon of *Rbpmsd* (Figure 31A). Semi-quantitative RT-PCR amplified a single 627 bp fragment, consistent with the predicted ORF length. As expected, *Rbpmsd* transcript levels were significantly elevated in doxorubicin-treated cells compared to untreated controls (Figure 31B, C), and the novel *Rbpms* isoform was confirmed by Sanger sequencing. To ascertain whether *Rbpmsd* levels are solely regulated at the transcriptional level or also at translational level, immunoblot analysis will be performed in the future.

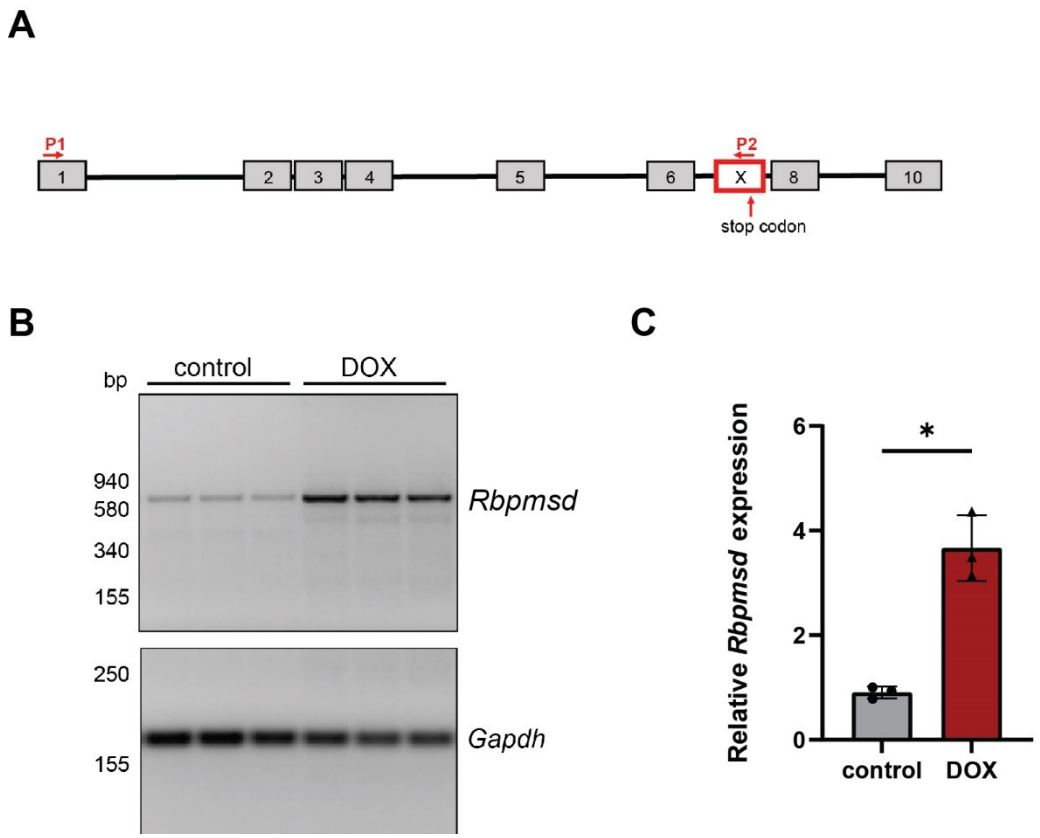

Figure 31 Validation of a de novo identified *Rbpmsd* isoform in neonatal cardiomyocytes.

A Scheme depicting the novel identified isoform of RBPMS. Arrows indicate the position of the primers used for **B** validation of *Rbpmsd* isoform by semi-quantitative RT-PCR in wild-type neonatal cardiomyocytes and **C** corresponding quantification. *Gapdh* served as a loading control. Data represent the mean ± SD. Unpaired t-test with Welch's correction. *P < 0.05.

Next, to assess and compare the mRNA expression profile of *Rbpms* isoforms in the adult stage, we employed semi-quantitative RT-PCR on primary adult cardiomyocytes from wild-type mice under basal conditions and under doxorubicin treatment. Consistent with observations in neonatal cardiomyocytes, *Rbpmsa* and *Rbpmsb* expression was markedly

decreased in response to doxorubicin (Figure 32A-C). In contrast, the *Rbpmsc* isoform displayed a significant upregulation following doxorubicin treatment, suggesting that distinct *Rbpms* isoforms may differentially influence anthracycline sensitivity in cardiomyocytes (Figure 32A, C). However, PCR analysis demonstrated amplification of only the *Rbpmsa*, *Rbpmsb* and *Rbpmsc* isoforms, while the *Rbpmsd* isoform was not detected in adult cardiomyocytes (Figure 32A, B). Taken together, these data demonstrate the existence of a novel *Rbpms* isoform encoding a putative 207aa RBPMS protein variant in neonatal but not in adult cardiomyocytes that is highly induced upon doxorubicin treatment. However, the molecular and physiological function of this isoform remains unknown.

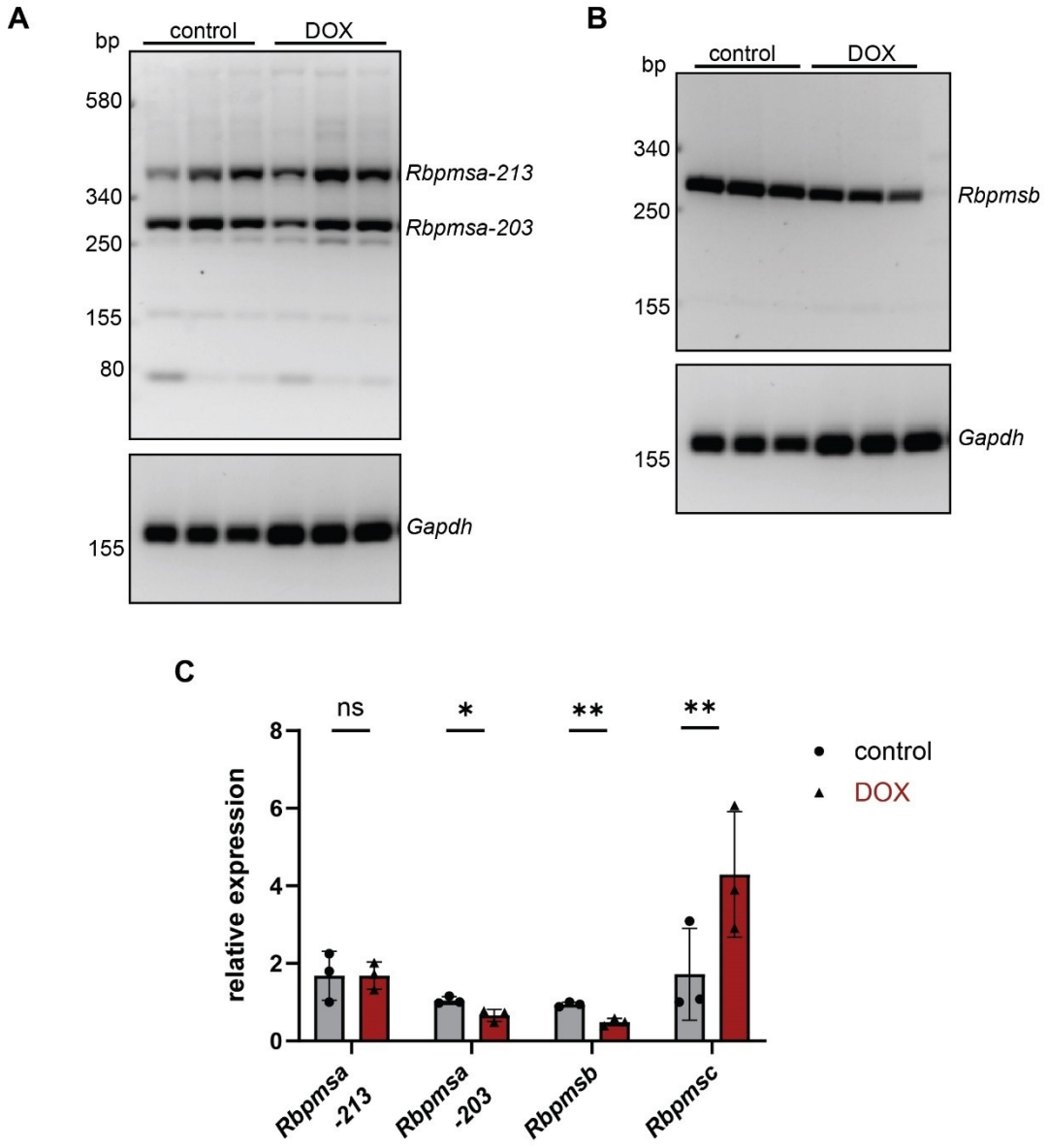

Figure 32 Primary adult cardiomyocytes do not express the *Rbpmsd* isoform.

A, B Splice variants of mouse *Rbpms* in isolated adult cardiomyocytes from wild-type mice treated with or without doxorubicin (DOX; 1 µM for 24 h) assessed by semi-quantitative RT-PCR. *Gapdh* served as

a loading control. **C** Quantification of relative expression levels of *Rbpmsa*, *Rbpmsb* and *Rbpmsc* isoforms. Data represent the mean ± SD. Two-way ANOVA with Bonferroni's multiple comparisons test. *P < 0.05; **P < 0.01.

Given that RBPMS acts as a splicing factor that may autoregulate its own AS, we asked whether increased expression of *Rbpmsa* and *Rbpmsb* could affect the relative abundance of RBPMS isoform. To this end, we overexpressed GFP-tagged RBPMSA and RBPMSB from the ROSA26 locus combined with the embryonic cardiomyocyte-specific XMLC2-Cre. RT-qPCR analysis using gene-specific TaqMan probes confirmed a significant increase in the mRNA levels of *Rbpmsa* and *Rbpmsb*, thereby validating their overexpression (Figure 33A, B). Notably, overexpression of RBPMSA in adult cardiomyocytes augmented endogenous *Rbpmsb* mRNA levels (Figure 33C). In parallel, elevated RBPMSB protein levels led to increased endogenous *Rbpmsa* mRNA levels, without affecting the expression of other isoforms (Figure 33D). These findings suggest that the regulation of isoform equilibrium is governed by a complex network of autoregulatory mechanisms.

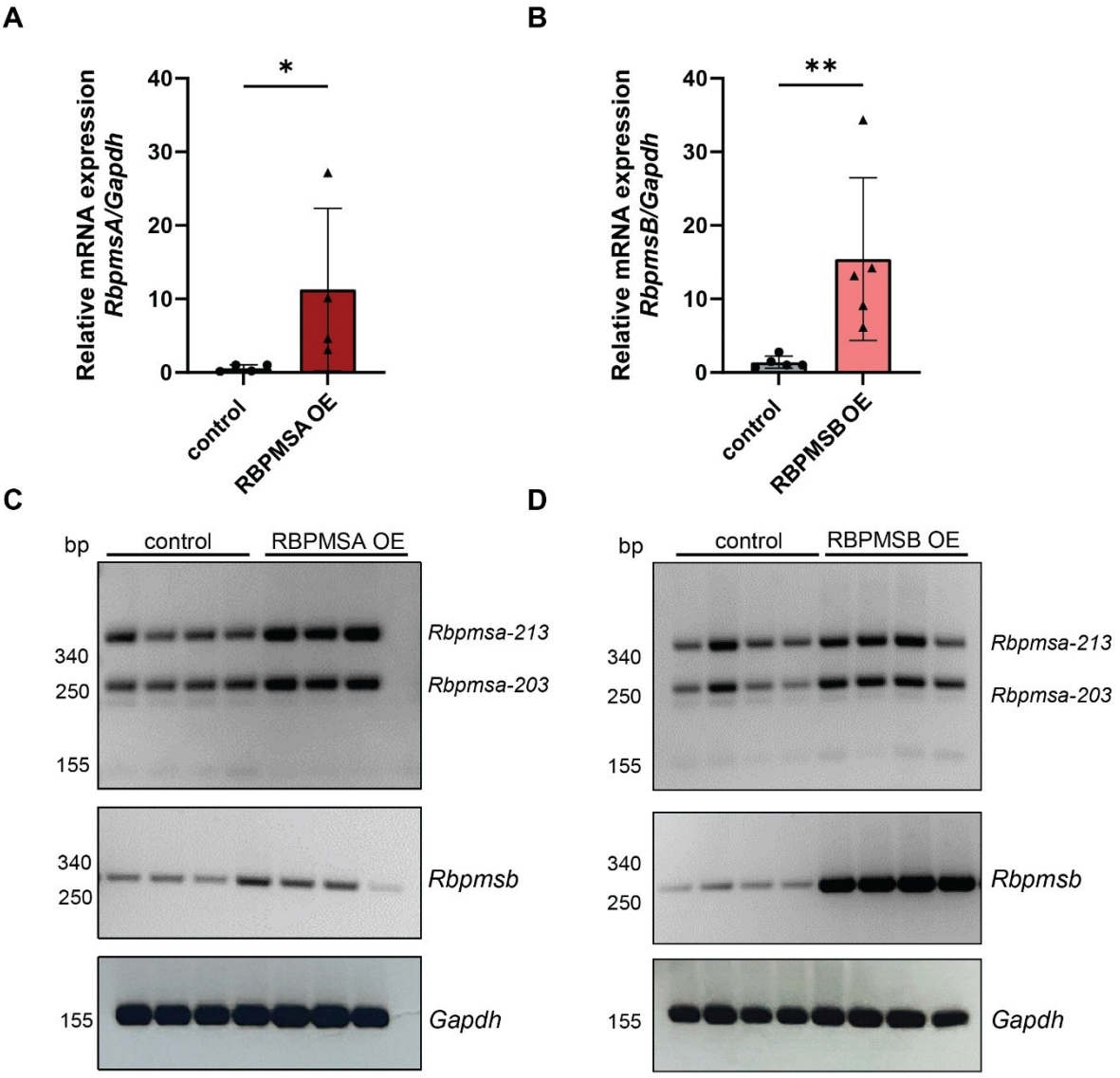

Figure 33 Autoregulation of RBPMS isoforms suggests a feedback network in primary adult cardiomyocytes.

A Quantitative RT-PCR analysis of cardiomyocytes isolated from RBPMSA-GFP overexpressing and control mice to assess *Rbpmsa* expression levels. n = 4 for each group. **B** Quantitative RT-PCR analysis of cardiomyocytes isolated from RBPMSB-GFP overexpressing and control mice to assess *Rbpmsb* expression levels. n = 5 for each group. **C, D** Splice variants of mouse *Rbpms* in isolated adult cardiomyocytes from RBPMSA (C) or RBPMSB (D) overexpressing mice assessed by semi-quantitative RT-PCR. *Gapdh* served as a loading control. Data represent the mean ± SD. One-tailed unpaired t-test. *P < 0.05; **P < 0.01.

3.9 Transcriptomic and alternative splicing changes in doxorubicin-treated cardiomyocytes

Doxorubicin treatment of neonatal cardiomyocytes led to pronounced changes in subcellular localization of RBPMS and is associated with increased inclusion of a poison exon in *Rbpms*

transcripts, suggesting a broader impact on AS, specifically promoting poison or cryptic exon inclusion. To explore this, mRNA analysis of doxorubicin-treated and untreated neonatal and adult cardiomyocytes was performed. PCA of gene expression data revealed distinct clusters, indicating substantial transcriptomic differences between both experimental groups following doxorubicin exposure (Figure 34A). This analysis demonstrates pronounced changes in the transcriptome profile following doxorubicin treatment compared to control cardiomyocytes. Differential expression analysis identified 13,984 differentially expressed genes (DEGs), with 7,184 genes upregulated and 6,800 downregulated, underscoring the profound impact of doxorubicin on gene expression (Figure 34B). Upregulated genes were enriched for biological processes such as metabolism and translation, while downregulated genes were primarily involved in DNA repair mechanisms and cell cycle regulation. Additionally, genes encoding tricarboxylic acid (TCA) cycle enzymes were upregulated, suggesting an early compensatory response to reduced intracellular ATP levels (Figure 34C, D). In adult cardiomyocytes, 11.841 DEGs were detected, comprising 5944 upregulated and 5897 downregulated genes. Among these genes, 3778 upregulated and 3993 downregulated genes were commonly expressed in neonatal and adult cardiomyocytes, indicating both common and stage-specific transcriptomic responses to doxorubicin (Figure 34E, F). Importantly, several essential cardiac splicing factors, including RBPMS, displayed altered expression levels upon doxorubicin treatment, with distinct patterns observed between neonatal and adult cardiomyocytes. These findings suggest distinct developmental stage-specific mechanisms of action in response to doxorubicin treatment (Figure 34G, H), reflected by the differential regulation of specific splicing factors, and resulting in global changes of alternative splicing networks. This aligns with previous reports demonstrating that doxorubicin exposure results in global gene expression and AS changes driven by altered expression of RBPs.

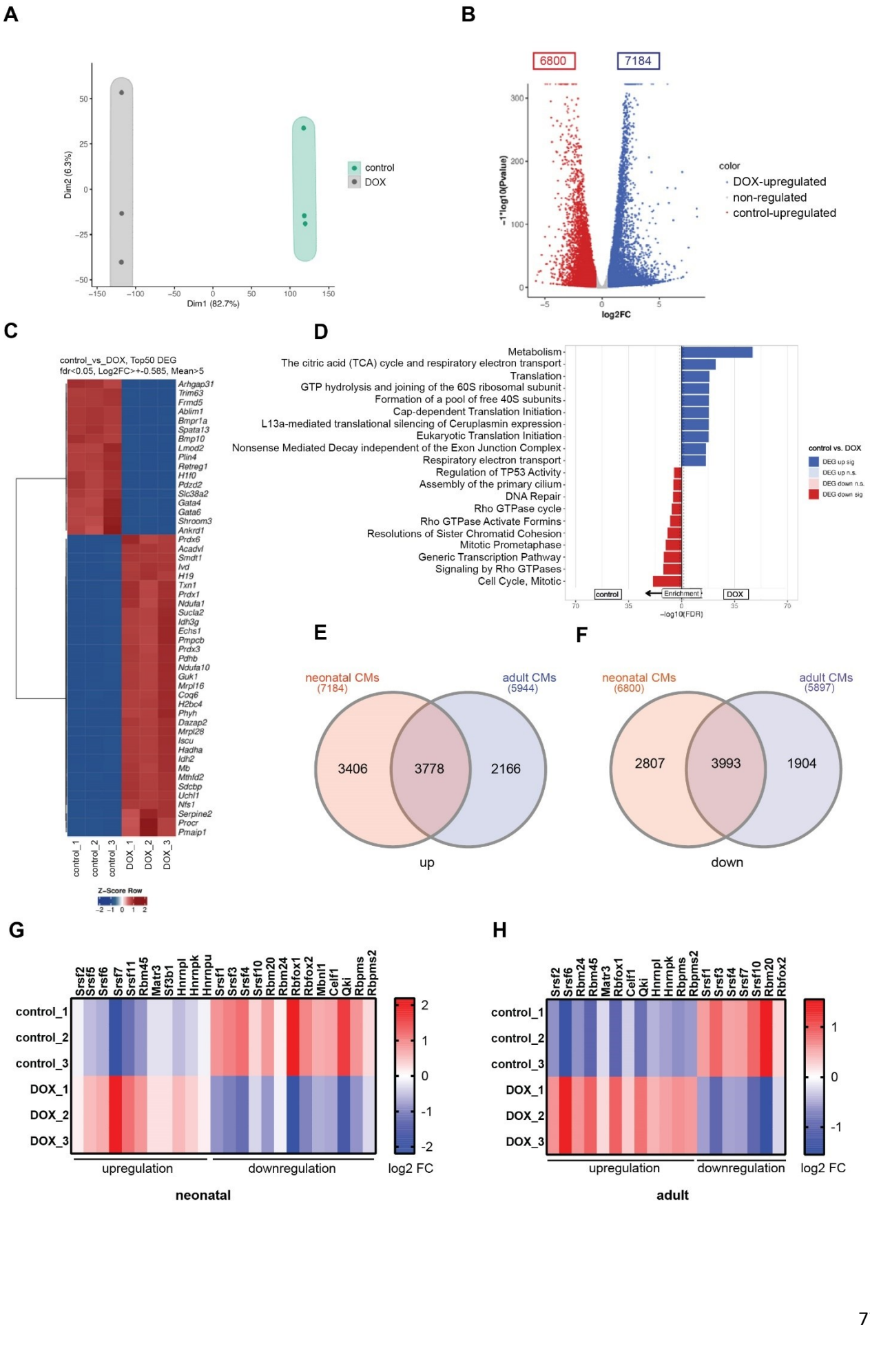
A
Dim2 (6.3%)
Dim1 (82.7%)
control
DOX
B
6800
7184
-1*log10(Pvalue)
log2FC
color
DOX-upregulated
non-regulated
control-upregulated
C
control_vs_DOX, Top50 DEG
fdr<0.05, Log2FC>+-0.585, Mean>5
Arhgap31
Trim63
Frmd5
Ablim1
Bmpr1a
Spata13
Bmp10
Lmod2
Plin4
Retreg1
H1f0
Pdzd2
Slc38a2
Gata4
Gata6
Shroom3
Ankrd1
Prdx6
Acadvl
Smdt1
Ivd
H19
Txn1
Prdx1
Ndufa1
Sucla2
Idh3g
Echs1
Pmpcb
Prdx3
Pdhb
Ndufa10
Guk1
Mrpl16
Coq6
H2bc4
Phyh
Dazap2
Mrpl28
Iscu
Hadha
Idh2
Mb
Mthfd2
Sdcbp
Uchl1
Nfs1
Serpine2
Procr
Pmaip1
control_1
control_2
control_3
DOX_1
DOX_2
DOX_3
Z-Score Row
D
Metabolism
The citric acid (TCA) cycle and respiratory electron transport
Translation
GTP hydrolysis and joining of the 60S ribosomal subunit
Formation of a pool of free 40S subunits
Cap-dependent Translation Initiation
L13a-mediated translational silencing of Ceruplasmin expression
Eukaryotic Translation Initiation
Nonsense Mediated Decay independent of the Exon Junction Complex
Respiratory electron transport
Regulation of TP53 Activity
Assembly of the primary cilium
DNA Repair
Rho GTPase cycle
Rho GTPase Activate Formins
Resolutions of Sister Chromatid Cohesion
Mitotic Prometaphase
Generic Transcription Pathway
Signaling by Rho GTPases
Cell Cycle, Mitotic
control vs. DOX
DEG up sig
DEG up n.s.
DEG down n.s.
DEG down sig
control
Enrichment
DOX
-log10(FDR)
E
neonatal CMs
(7184)
adult CMs
(5944)
3406
3778
2166
up
F
neonatal CMs
(6800)
adult CMs
(5897)
2807
3993
1904
down
G
Srsf2
Srsf5
Srsf6
Srsf7
Srsf11
Rbm45
Matr3
Sf3b1
Hnrnpl
Hnrnpk
Hnrnpu
Srsf1
Srsf3
Srsf4
Srsf10
Rbm20
Rbm24
Rbfox1
Rbfox2
Mbnl1
Celf1
Qki
Rbpms
Rbpms2
control_1
control_2
control_3
DOX_1
DOX_2
DOX_3
upregulation
downregulation
log2 FC
neonatal
H
Srsf2
Srsf6
Rbm24
Rbm45
Matr3
Rbfox1
Celf1
Qki
Hnrnpl
Hnrnpk
Rbpms
Rbpms2
Srsf1
Srsf3
Srsf4
Srsf7
Srsf10
Rbm20
Rbfox2
control_1
control_2
control_3
DOX_1
DOX_2
DOX_3
upregulation
downregulation
log2 FC
adult

Figure 34 Doxorubicin treatment of neonatal cardiomyocytes induces massive gene expression changes.

A Principal component analysis (PCA) depicting separation of the individual replicates and clustering of untreated and doxorubicin-treated neonatal wild-type cardiomyocytes. **B** Volcano plot representation of differential gene expression analysis between untreated and doxorubicin-treated wild-type neonatal cardiomyocytes. Values are blotted for statistical significance (P-value, y-axis) and magnitude of expression change (log2 fold change, x-axis). Genes were considered differently expressed if they exhibited ≥ 5 counts, log2FC <> ± 0,585 and P-value ≤ 0,05. **C** Heat map showing the top 50 most significantly differentially expressed genes (DEGs) in doxorubicin-treated neonatal cardiomyocytes. **D** Gene ontology (GO) term enrichment analysis of DEGs between control and doxorubicin-treated neonatal cardiomyocytes. **E, F** Venn diagrams merging differential expression sets of two conditions [doxorubicin-treated neonatal cardiomyocytes (CMs) and adult CMs] for upregulated (E) and downregulated (F) DEGs (DEGs: basemean ≥ 5, log2fc ± 0,585, padj ≤ 0,05). **G, H** Heat map illustrating the differential expression (>log2 fold change) of genes encoding splicing factor proteins in neonatal (G) and adult (H) cardiomyocytes treated with and without doxorubicin (1 µM, 24 h).

Genome-wide AS analysis of RNA-seq data identified exonic splicing events in 8,241 genes, each containing one or more significantly regulated altered exon-exon junctions (adjusted p-value > 0.05) between treated and untreated cardiomyocytes. GO enrichment analysis was performed to determine the functional relevance of these genes. The majority of genes with altered exon-exon junctions belong to the category splicing factors and are primarily associated with pathways critical to cardiac biology, including metabolism, cardiac muscle contraction, cytoskeleton organization, cell cycle regulation, DNA damage response, and cell death. Additionally, GO term analysis revealed that many of these genes play crucial roles in ribonucleoprotein granules and nuclear bodies, including nuclear speckles (Figure 35A, B). Evaluation of *Rbpms* mRNA expression in control and doxorubicin-treated neonatal cardiomyocytes revealed elevated sequencing reads mapping to intron 6 of the *Rbpms* gene and the inclusion of exon X, a poison cassette exon (PCE) containing a potential premature termination codon (PTC) (Figure 35C). This finding aligns with our previous observations and suggests alterations in transcriptional or post-transcriptional regulation of *Rbpms*. Importantly, we observed that doxorubicin treatment induces the inclusion of PCE in several splicing factors. To illustrate this phenomenon, we selected two specific examples, *Srsf7* and *Rbm39*. Quantitative analysis of exon-exon junction reads demonstrated that doxorubicin treatment enhances the inclusion of a previously reported PCE in *Srsf7* transcripts. Furthermore, elevated read coverage in both PCE-flanking introns (3a and 3b) as well as intron 5, indicate an intron retention event upon doxorubicin treatment (Figure 35D). Bioinformatics analysis further revealed the inclusion of a PCE in *Rbm39* mRNA, resulting in an isoform containing a putative PTC potentially targeted for degradation via nonsense-mediated decay (NMD).

Additionally, doxorubicin treatment induced the retention of introns 2, 3, and 4 within *Rbm39* transcripts (Figure 35E). This study provides the first evidence that doxorubicin triggers a global alternative splicing (AS) response, characterized by widespread inclusion of poison cassette exons (PCEs) in neonatal cardiomyocytes. In summary, these splicing alterations contribute to the adaptive AS response following doxorubicin treatment. Such modifications likely have functional implications for the expression and activity of key splicing regulators, including RBPMS. Future research should focus on experimentally validating selected DEGs and splicing events to confirm these observations.

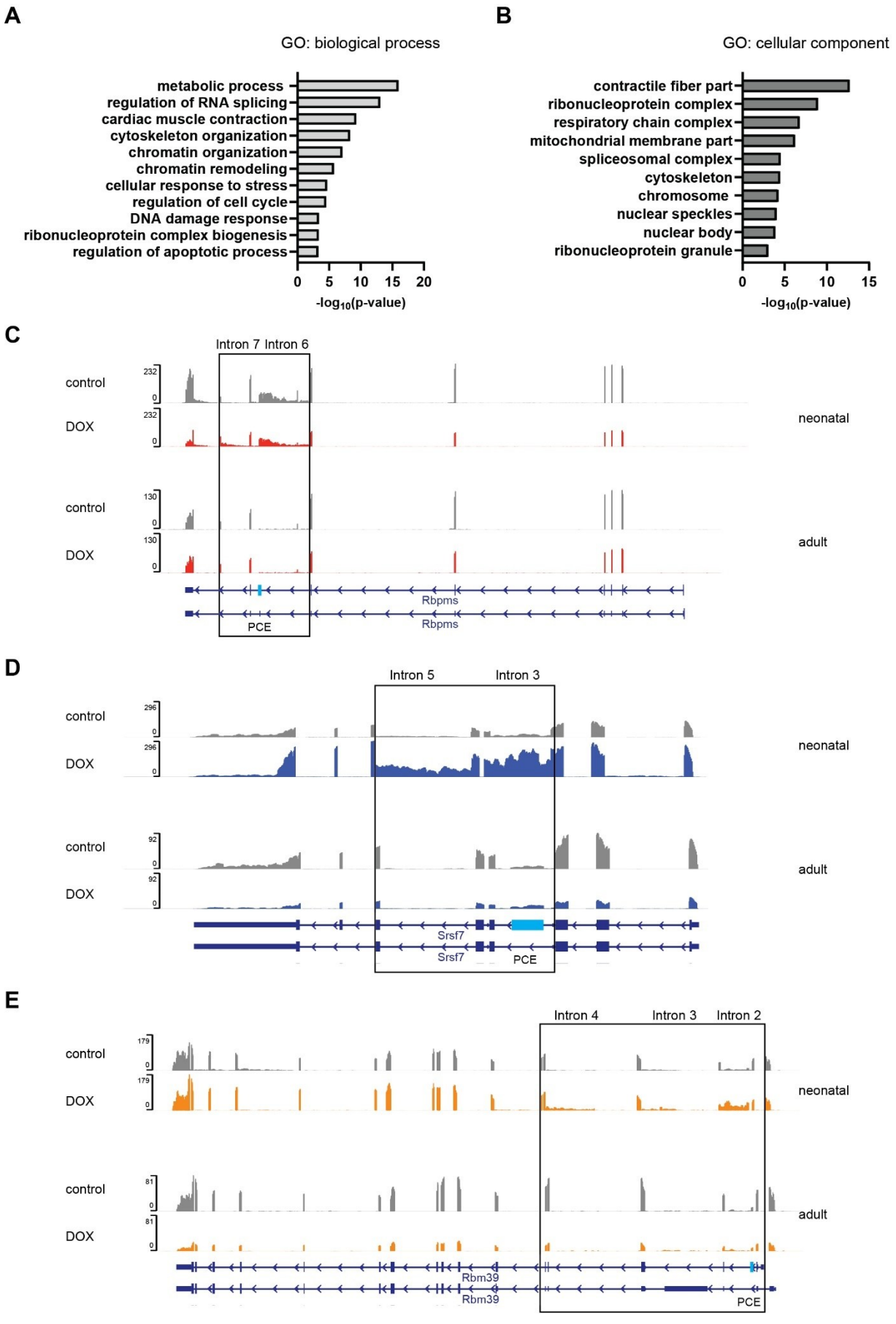
A
GO: biological process
metabolic process
regulation of RNA splicing
cardiac muscle contraction
cytoskeleton organization
chromatin organization
chromatin remodeling
cellular response to stress
regulation of cell cycle
DNA damage response
ribonucleoprotein complex biogenesis
regulation of apoptotic process
0 5 10 15 20
-log10(p-value)
B
GO: cellular component
contractile fiber part
ribonucleoprotein complex
respiratory chain complex
mitochondrial membrane part
spliceosomal complex
cytoskeleton
chromosome
nuclear speckles
nuclear body
ribonucleoprotein granule
0 5 10 15
-log10(p-value)
C
Intron 7 Intron 6
control
DOX
control
DOX
neonatal
adult
Rbpms
Rbpms
PCE
D
Intron 5
Intron 3
control
DOX
control
DOX
neonatal
adult
Srsf7
Srsf7
PCE
E
Intron 4
Intron 3
Intron 2
control
DOX
control
DOX
neonatal
adult
Rbm39
Rbm39
PCE

Figure 35 Doxorubicin treatment promotes aberrant splicing in neonatal cardiomyocytes but not in adult cardiomyocytes.

A, B Gene ontology (GO) term enrichment of genes exhibiting alternative splicing events in control and doxorubicin-treated neonatal cardiomyocytes. GO terms are shown for cellular component (A) or biological process (B) categories. Significance of GO term enrichment is represented as the $-\log_{10}$ p-value. **C-E** Integrative genomics viewer (IGV) snapshots of the RBPMS (C), SRSF7 (D) and RBM39 (E) gene loci displaying RNA sequencing data from untreated and doxorubicin (DOX)-treated neonatal and adult cardiomyocytes. Increased read coverage for intronic regions is indicated by black boxes. Location of poison cassette exons (PCEs) are marked in cyan.

3.10 Distinct RBPMS isoforms interact with components of different membraneless organelles

In order to identify interaction partners of the two most abundant RBPMS isoforms, RBPMSA and RBPMSB, a GFP-based protein interaction screen was conducted. To this end, stable integrated mouse embryonic stem (mES) cell lines overexpressing C-terminal GFP-tagged RBPMSA and RBPMSB were generated. Pure GFP overexpressing mES cells served as control in all related experiments. All experiments were performed in an undifferentiated mESC state. Immunoblot analysis of the immunoprecipitated fractions showed that GFP-tagged RBPMSA and RBPMSB fusion proteins were enriched in the pulldown, demonstrating the efficient and specific immunoprecipitation of both isoforms from cell extracts (Figure 36A).

Immunoprecipitated proteins were gel extracted, trypsin digested, and identified by LC-MS/MS. Although RBPMSA and RBPMSB differ in the corresponding C-terminal regions as well as in isoform specific subcellular localizations, the majority of binding partners are shared between both isoforms. RBPMSA primarily interacts with cytoplasmic SG and P-body components, including G3BP1, G3BP2 and ELAV-like RNA-binding proteins 1 (ELAV1/ HuR) and 2 (ELAVL2/ HuB). In addition to cytoplasmic proteins, RBPMSA also associates with nuclear PS members Non-POU domain-containing octamer-binding protein (NONO), Splicing factor, proline- and glutamine-rich (SFPQ) and RNA-binding motif protein 14 (RBM14) (Figure 36B). Gene Ontology terms related to ribonucleoprotein granules and P-bodies are enriched in RBPMSA overexpressing mES cells, compared to control cells (Figure 36C). In contrast, the RBPMSB-interactors are predominantly associated with the mitochondrial matrix, with a notable enrichment of cytoskeleton-related proteins (Figure 36D-F). In conclusion, these findings indicate that both isoforms are involved in the regulation of cytoplasmic RNP assemblies, including SG and P-body formation. Moreover, RBPMSA primarily associates with components of nuclear bodies, particularly PS, while RBPMSB is likely involved in mitochondrial metabolism or in mediating interaction between membrane-bound organelles and membraneless condensates.

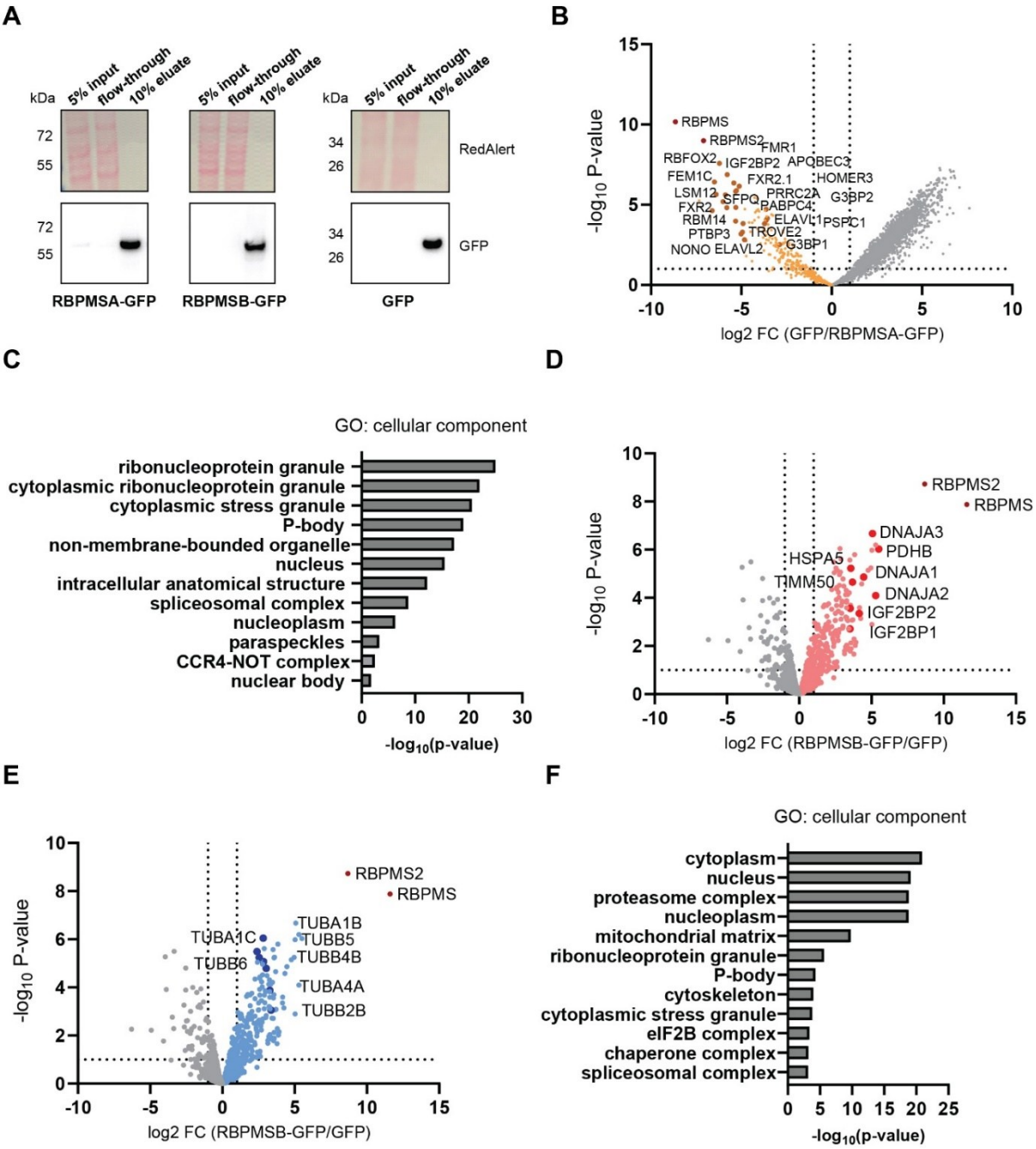

Figure 36 GFP-based interactome screen of RBPMSA and RBPMSB in undifferentiated mouse embryonic stem cells.

A Immunoblot analysis of GFP-pulldown of RBPMSA, RBPMSB or GFP in overexpressing mouse embryonic stem cells probed with anti-GFP antibody. **B** Volcano plot representation of differentially abundant proteins in mouse embryonic stem cells expressing RBPMSA-GFP versus GFP. **C** Box plots showing the top 12 enriched GO terms for proteins enriched for RBPMSA-GFP versus GFP control. GO terms refer to cellular component. **D, E** Volcano plot representation of proteomic analysis in mouse embryonic stem cells expressing RBPMSB-GFP versus GFP. Mitochondria-associated proteins are depicted in red (D) and microtubule proteins are shown in blue (E). **F** Box plots display the 12 most

significantly enriched GO terms for proteins that are specifically enriched for RBPMSB-GFP compared to GFP control. GO terms refer to cellular component.

To further elucidate the roles of the individual isoforms in cardiomyocytes, we performed an interaction partner screen to identify their specific binding networks. For this purpose, C-terminal GFP-tagged RBPMSA or RBPMSB isoforms was conditionally overexpressed from the ROSA26 locus using a heart-specific Cre-driver. Immunoprecipitation of whole-heart tissue lysates from 12-week-old mice using an anti-GFP antibody resulted in efficient target enrichment, as verified by subsequent Western blot analysis (Figure 37A). Furthermore, qualitative control of the pulldown by PCA demonstrated distinct separation of the different experimental groups (RBPMSA, RBPMSB and control) and a low variance across biological replicates (Figure 37B). The two isoforms shared approximately 70% of their identified binding partners, indicating considerable functional overlap (Figure 37C, D). Analysis of interaction partners yielded nearly identical top ten enriched GO terms, primarily associated with RNA stability and splicing regulation. In addition, terms related to translation, metabolism and gene expression were significantly enriched, underscoring the multifunctional roles of RBPMS (Figure 38A, B). Notably, both interactome screens identified multiple RNA-binding proteins belonging to the heterogeneous nuclear ribonucleoproteins (hnRNPs) family, along with other ubiquitously expressed splicing regulators, including Polypyrimidine tract-binding protein 1 (PTBP1) and Muscleblind-like protein 1 (MBNL1), which were highly enriched relative to control samples. These factors are key components of ribonucleoprotein complexes, which further emphasizes a potential role of RBPMS in the assembly of cytoplasmic RNP granules by mediating mRNA localization and translational regulation in cardiomyocytes (Figure 38C).

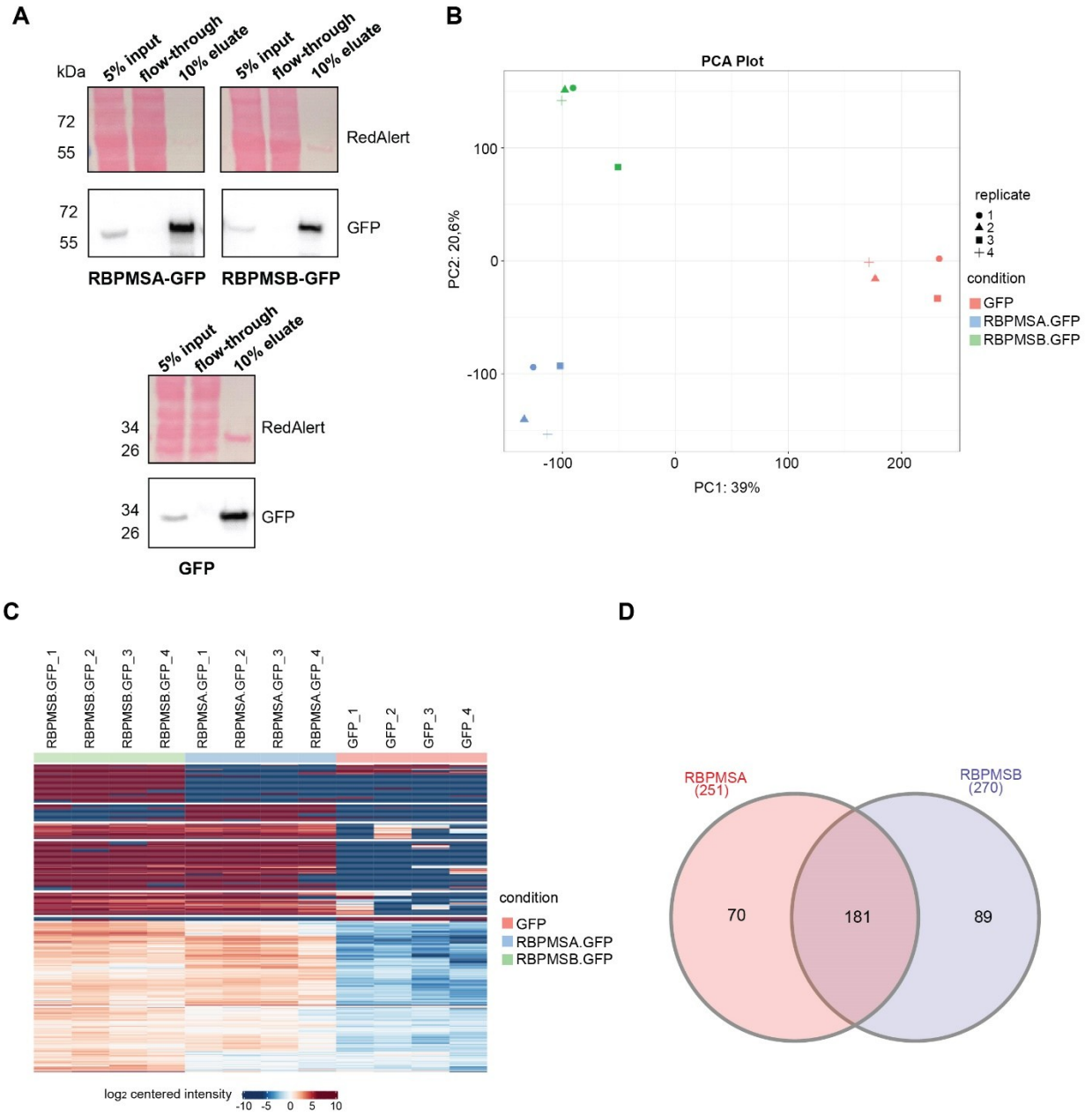

Figure 37 RBPMSA and RBPMSB share a common set of interaction partners in the murine heart.

A Immunoblot analysis of GFP-pulldown fractions from heart lysates of adult mice overexpressing RBPMSA-GFP, RBPMSB-GFP or GFP, probed with anti-GFP antibody to confirm efficient enrichment of the tagged proteins. **B** Two-dimensional principal component analysis (PCA) of mass spectrometry (MS) data from GFP-pulldowns, showing clustering of individual replicates (n=4 per group) and distinct separation of the different experimental groups (RBPMSA-GFP, RBPMSB-GFP, GFP). **C** Heat map depicting all proteins identified in RBPMSA-GFP and RBPMSB-GFP pulldown fractions compared to GFP controls. **D** Venn diagram illustrating overlapping and unique interactions identified for RBPMSA and RBPMSB isoforms.

Mass spectrometry analysis targeting the divergent C-terminal regions of RBPMSA and RBPMSB revealed reciprocal interactions between the two isoforms. Specifically, ectopically expressed RBPMSA was found to interact with endogenous RBPMSB, and vice versa, ectopic RBPMSB interacts with endogenous RBPMSA (Figure 38D). Of note, RBPMS2 was highly enriched in both datasets, suggesting that RBPMSA, RBPMSB and RBPMS2 act together to accomplish certain functions. Interestingly, RBPMSA predominantly interacted with RBPs that are well-established components of PS and are also implicated in DNA repair mechanisms, including SFPQ, NONO, Paraspeckle component 1 (PSPC1), RNA-binding protein FUS and TATA box-binding protein-associated factor 15 (Taf15) (Figure 38C, E). Analogous to RBPMS, these proteins also harbor extensive intrinsically disordered regions (IDRs), which confer biophysical properties that facilitate LLPS from the soluble cytoplasmic milieu and simultaneously increase their thermodynamic susceptibility to aberrant aggregation under pathological contexts. Notably, among RBPMSA interactors, we identified heterogeneous nuclear ribonucleoprotein U-like 1 (hnRNPUL1), a multifunctional protein involved in nucleocytoplasmic RNA transport and mRNA processing, that has recently emerged as a key regulator of DNA damage response pathways. This association points to a potential role of RBPMSA in DNA damage signaling and nuclear speckle organization. In contrast, the interactome of RBPMSB was enriched in a wide spectrum of RNA-binding proteins, SG components, as well as proteins linked to mitochondrial and ribosomal functions, consistent with the predominantly cytoplasmic localization of this isoform (Figure 38F). These results strengthen our hypothesis that both RBPMS isoforms contribute to cytoplasmic RNP granule formation, particularly in the context of SGs. Moreover, the enrichment of SG-associated proteins in the RBPMS interactome, even under non-stressed conditions in cardiomyocytes, underscores a potential role for these isoforms in the maintenance and regulation of RNP granules under basal conditions.

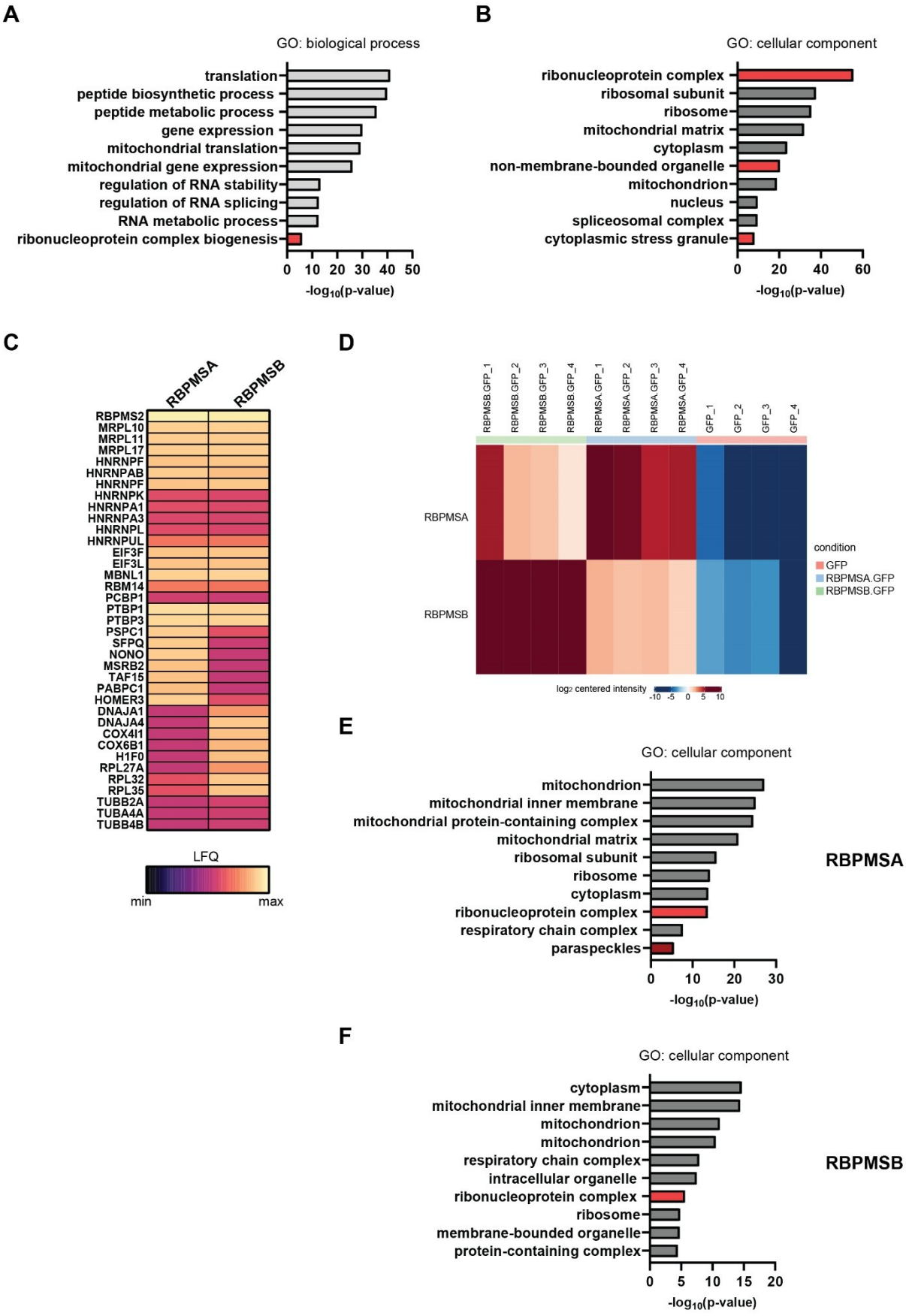
A
GO: biological process
translation
peptide biosynthetic process
peptide metabolic process
gene expression
mitochondrial translation
mitochondrial gene expression
regulation of RNA stability
regulation of RNA splicing
RNA metabolic process
ribonucleoprotein complex biogenesis
0 10 20 30 40 50
-log10(p-value)
B
GO: cellular component
ribonucleoprotein complex
ribosomal subunit
ribosome
mitochondrial matrix
cytoplasm
non-membrane-bounded organelle
mitochondrion
nucleus
spliceosomal complex
cytoplasmic stress granule
0 20 40 60
-log10(p-value)
C
RBPMSA
RBPMSB
RBPMS2
MRPL10
MRPL11
MRPL17
HNRNPF
HNRNPAB
HNRNPF
HNRNPK
HNRNPA1
HNRNPA3
HNRNPL
HNRNPUL
EIF3F
EIF3L
MBNL1
RBM14
PCBP1
PTBP1
PTBP3
PSPC1
SFPQ
NONO
MSRB2
TAF15
PABPC1
HOMER3
DNAJA1
DNAJA4
COX4I1
COX6B1
H1F0
RPL27A
RPL32
RPL35
TUBB2A
TUBA4A
TUBB4B
LFQ
min
max
D
RBPMSB.GFP_1
RBPMSB.GFP_2
RBPMSB.GFP_3
RBPMSB.GFP_4
RBPMSA.GFP_1
RBPMSA.GFP_2
RBPMSA.GFP_3
RBPMSA.GFP_4
GFP_1
GFP_2
GFP_3
GFP_4
RBPMSA
RBPMSB
condition
GFP
RBPMSA.GFP
RBPMSB.GFP
log2 centered intensity
-10 -5 0 5 10
E
GO: cellular component
mitochondrion
mitochondrial inner membrane
mitochondrial protein-containing complex
mitochondrial matrix
ribosomal subunit
ribosome
cytoplasm
ribonucleoprotein complex
respiratory chain complex
paraspeckles
0 10 20 30
-log10(p-value)
RBPMSA
F
GO: cellular component
cytoplasm
mitochondrial inner membrane
mitochondrion
mitochondrion
respiratory chain complex
intracellular organelle
ribonucleoprotein complex
ribosome
membrane-bounded organelle
protein-containing complex
0 5 10 15 20
-log10(p-value)
RBPMSB

Figure 38 Enrichment analysis of RBPMSA and RBPMB interaction partners in the heart.
A, B Box plots displaying the top 10 enriched GO terms for proteins significantly enriched in RBPMSA-GFP and RBPMSB-GFP pulldown samples compared to GFP control. **C** Heat map showing selected candidates of the RBPMSA and RBPMSB interactome screen. **D** Heat map showing interaction of RBPMSA and RBPMSB isoforms. **E, F** Box plots showing the top 10 enriched GO terms for proteins enriched for either RBPMSA-GFP (E) or RBPMSB-GFP (F) versus GFP control. GO terms representing cellular components (B, E; F) or biological processes (A) are shown. GO terms associated with RNP complex formation are depicted in red. Significance was calculated based on the $-\log_{10}$ p-value.

3.11 Constitutive deletion of *Rbpmsb* in mice does not cause phenotypic alterations under physiological conditions

To determine the predominant function of *Rbpmsb in vivo*, constitutive *Rbpmsb* knockout mice were generated via CRISPR/Cas9-mediated deletion of exon 7, which encodes critical functional domains of this isoform. Homozygous *Rbpms*-KO mice (*Rbpmsb*-KO$^{-/-}$) were obtained from heterozygous (*Rbpmsb*-KO$^{+/-}$) intercrosses at Mendelian ratios of 25%, confirming no embryonic lethality. *Rbpmsb* mutant mice were maintained in the inbred C57BL/6J genetic background. Immunoblot analysis of isolated cardiomyocytes confirmed a complete loss of the RBPMS protein isoform in *Rbpmsb*-KO hearts, accompanied by a significant elevation of RBPMSA protein levels (Figure 39B-D). The increased expression of RBPMSA may serve as a compensatory response to preserve functions common to both isoforms ,or alternatively, deletion of the final exon of RBPMSB could shift splicing preferences, thereby favoring production of *Rbpmsa* transcripts. Remarkably, homozygous *Rbpmsb* mutant mice are viable and do not display gross cardiac morphological abnormalities under physiological conditions. At one year of age, heart-to-body weight (HW/BW), heart weight-to-tibial length (HW/TL) and body weight-to-tibial length (BW/TL) ratios showed no significant differences compared to littermate controls (*Rbpms*-KO$^{+/+}$)(Figure 39A, E).

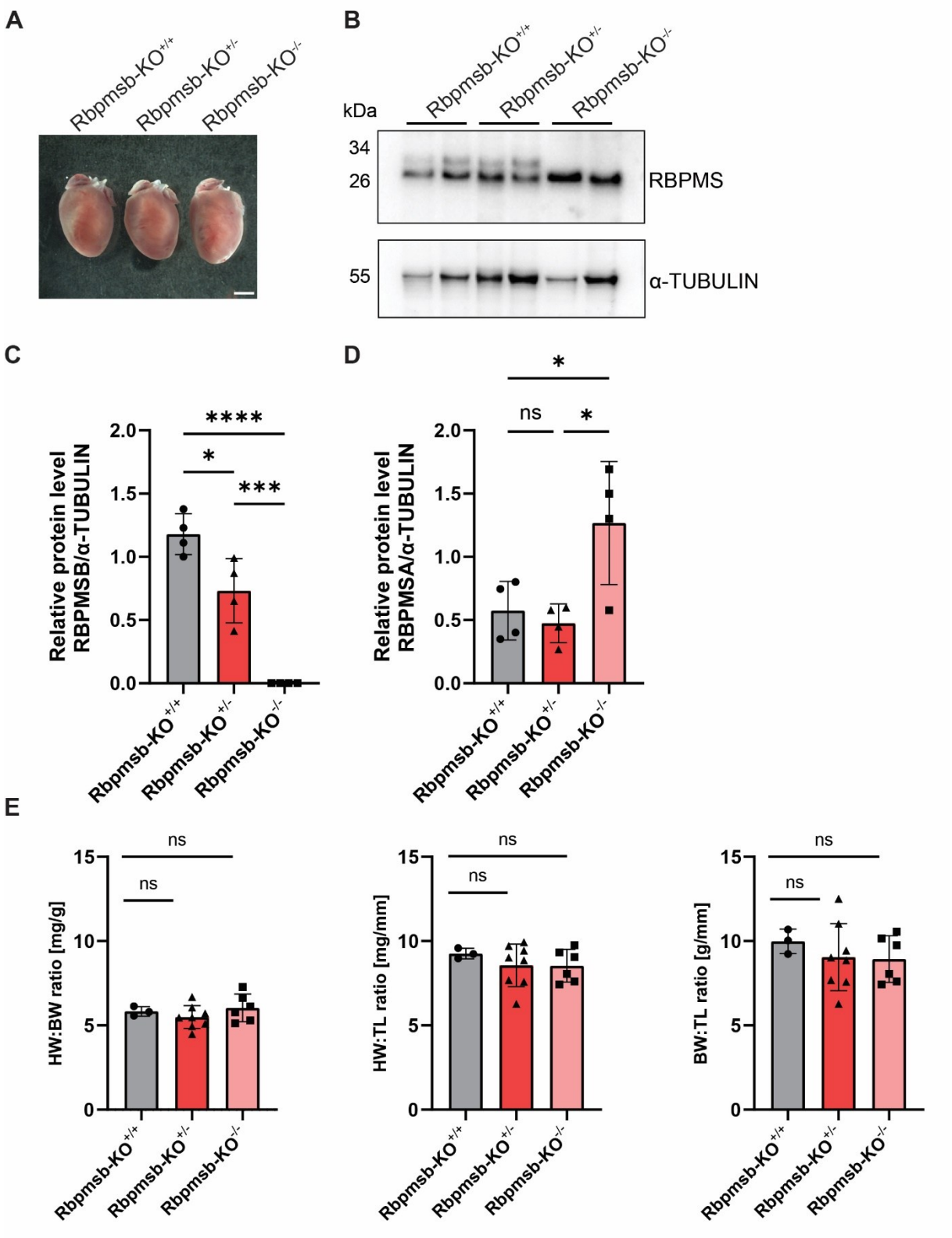

Figure 39 Inactivation of *Rbpmsb* does not affect heart morphology.

A Images of adult mouse hearts from wild-type (*Rbpmsb*$^{+/+}$; WT, n=3), heterozygous (*Rbpmsb*$^{+/-}$; Het, n=8), and homozygous knockout (*Rbpmsb*$^{-/-}$; KO, n=7) animals. **B** Immunoblot analysis of RBPMSA and RBPMSB protein levels in heart tissue and **C, D** quantification of protein abundance normalized to

α-TUBULIN. n = 4 for each group. **E** Effects of *Rbpmsb* deletion on heart weight-to-body weight (HW:BW), heart weight-to-tibia length (HW:TL) and body weight-to- tibia length (BW:TL) ratios in WT (n=3), Het (n=8) and KO (n=7) mice. Data represent the mean ± SD. Statistical significance was determined by two-way ANOVA with Bonferroni's multiple comparisons test. ns = not significant, *P < 0.05; ***P < 0.001; ****P < 0.0001.

3.12 Constitutive *Rbpmsb* loss impairs nuclear accumulation of SFPQ in doxorubicin-treated mice

The nucleus is comprised of numerous different nuclear bodies. PSs represent a category of nuclear bodies located in the interchromatin space of mammalian nuclei, labeled by SFPQ (Fox et al., 2002). Given that *Rbpmsb*-KO mutants did not exhibit overt abnormalities in cardiac morphology, we next investigated functional consequences of *Rbpmsb* inactivation under stress conditions. Considering the interaction between RBPMS and components of PSs, we postulated a potential function of RBPMS in these nuclear bodies. To ascertain whether loss of the cytoplasmic RBPMSB isoform affects the nuclear accumulation, distribution or localization of the remaining RBPMS isoforms, co-immunostaining of RBPMS and PS marker SFPQ was performed. These experiments were conducted in isolated adult cardiomyocytes from control (*Rbpmsb*-KO$^{+/+}$) and knockout (*Rbpmsb*-KO$^{-/-}$) mice under both basal conditions and following doxorubicin treatment. Immunofluorescence analysis revealed an increased nuclear RBPMS signal intensity 5 h after doxorubicin treatment, which persisted at 24 h (Figure 40A-C). Surprisingly, *Rbpmsb* deletion significantly attenuated accumulation of SFPQ in the nucleus (Figure 38D), suggesting a regulatory role of RBPMS in nuclear phase separation processes, potentially influencing the nuclear import of SFPQ and the assembly/maintenance of PSs in response to cellular stress.

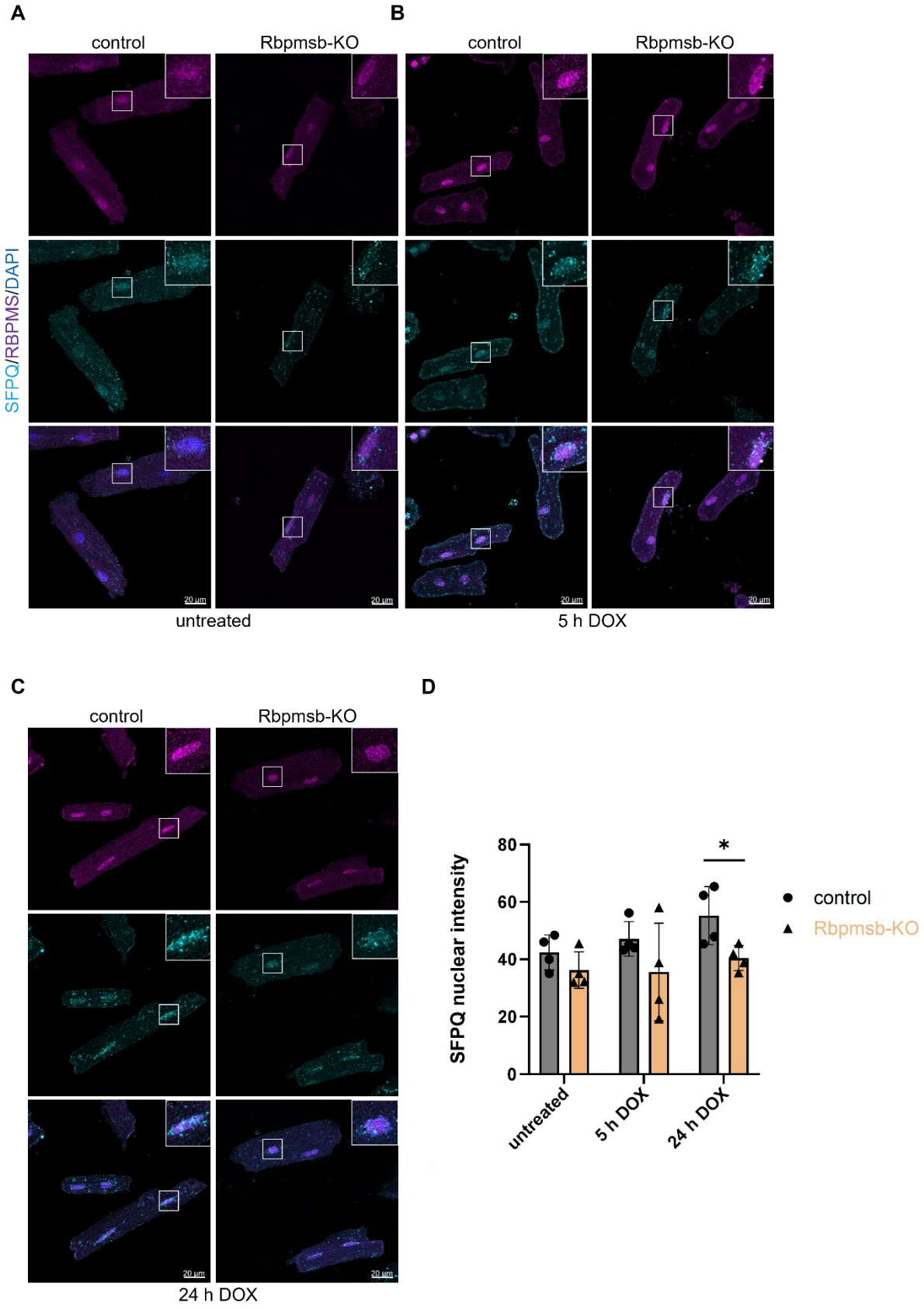

Figure 40 Loss of *Rbpmsb* attenuate nuclear accumulation of SFPQ upon doxorubicin treatment.

A-C Immunofluorescence staining of RBPMS (magenta), SFPQ (cyan) and nuclei (DAPI, blue) in isolated adult cardiomyocytes from *Rbpmsb*-KO$^{+/+}$ (control) and *Rbpmsb*-KO$^{-/-}$ (Rbpmsb-KO) mice.

Cardiomyocytes were treated r without (control) (A) or with 1 µM doxorubicin for 5 h (B) or 24 h (C). Scale bar, 20 µm. **D** Quantification of SFPQ staining intensity within the nucleus. Data represent the mean ± SD. Two-way ANOVA with Bonferroni's multiple comparisons test. *P < 0.05.

Given that loss of *Rbpmsb* affects SFPQ nuclear accumulation, we next investigated whether elevated RBPMS protein levels influence nuclear speckle formation under cardiac stress conditions. Isolated adult cardiomyocytes overexpressing GFP-tagged RBPMSB showed an increased nuclear RBPMS accumulation after doxorubicin treatment compared to controls. Remarkably, under standard conditions SFPQ, is diffusely distributed throughout the nucleus (Figure 41A), however following doxorubicin treatment it redistributed into nuclear puncta that colocalized with RBPMSB-GFP. This reorganization of SFPQ occurred at an earlier time point in cardiomyocytes overexpressing RBPMS compared to controls, indicating an accelerated recruitment to nuclear puncta (Figure 41B, C). Concomitantly, these cells displayed reduced nuclear accumulation of doxorubicin, suggesting decreased intercalation into DNA. In control samples, prolonged exposure of doxorubicin resulted in increased nuclear staining intensity in the green channel (GFP). Although imaging settings were optimized to minimize bleed-through, some crosstalk is expected because of the strong intrinsic fluorescence of doxorubicin, which is typically detected in the red channel. Based on these findings, we propose that RBPMS not only plays a role in cytoplasmic granules, as previously reported, but may also contribute to nuclear body formation under stress conditions.

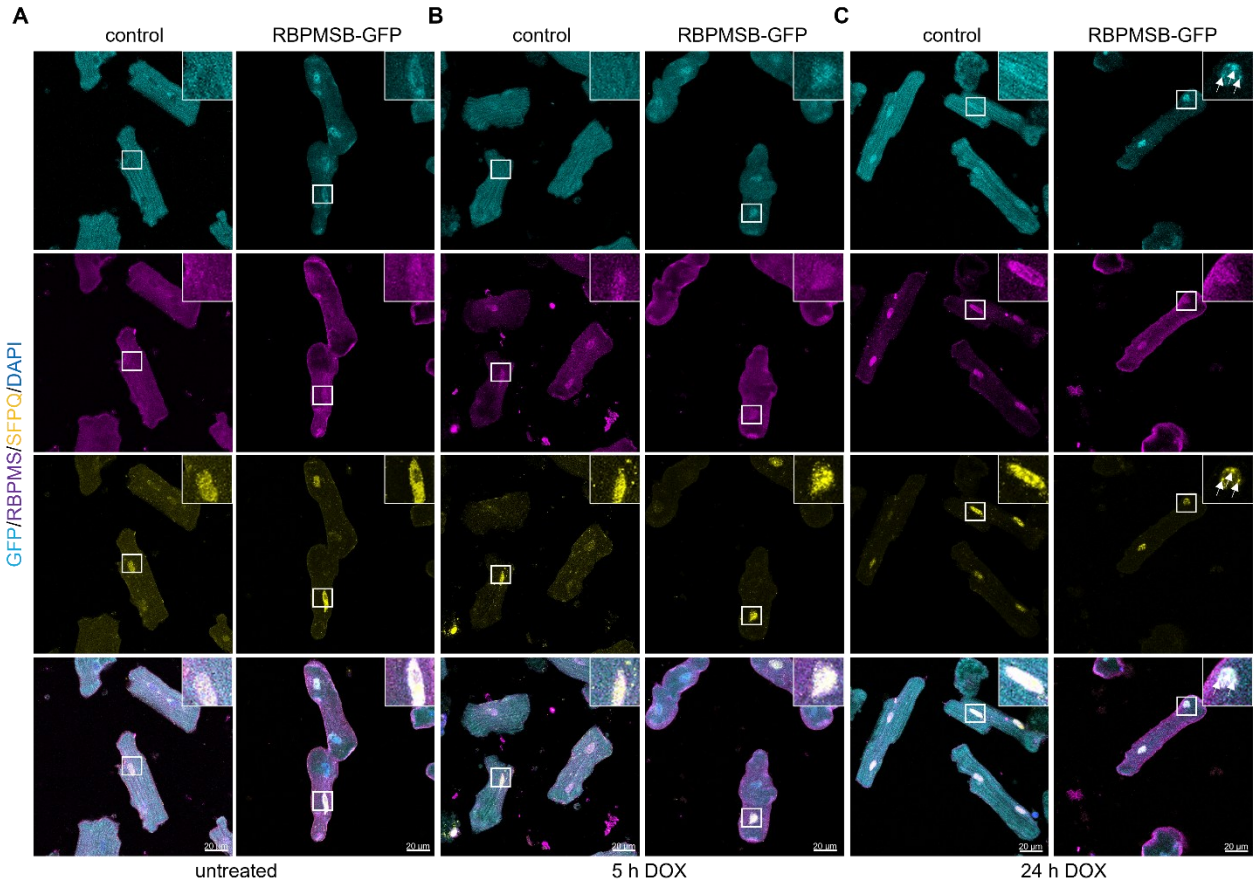

Figure 41 Dynamic RBPMSB speckle formation upon doxorubicin treatment in isolated adult cardiomyocytes.

A-C Fluorescence microscopy images of GFP (cyan), RBPMS (magenta), SFPQ (yellow) and nuclei (DAPI, blue) in isolated adult cardiomyocytes from control and RBPMSB-GFP mice. Cardiomyocytes were treated with or without 1 µM doxorubicin for 5 h or 24 h. Arrow indicates colocalization of SFPQ and RBPMSB-GFP. Scale bar, 20 µm.

3.13 Deletion of *Rbpmsb* mitigates doxorubicin-induced DNA damage in adult cardiomyocytes

Doxorubicin intercalates into the DNA and inhibits topoisomerase activity, thereby inducing DNA double-strand breaks (DSBs) (Austin et al., 1998). These DSBs elicit phosphorylation of key regulators of cell cycle progression and DNA repair, including histone H2AX at Ser139 (Lavin et al., 2007). Since prolonged, high-dose doxorubicin treatment induces speckle formation, we next investigated whether this phenomenon could be attributed to the induction of DSBs in cardiomyocytes, potentially driving nuclear speckle assembly. To address this, we employed the phosphorylated form of histone H2AX (γ-H2AX), which serves as a well-established marker of the DNA damage response (DDR) triggered by DNA DSBs, and is widely regarded as a reliable indicator of such lesions (Rogakou et al., 1998). Treatment with

doxorubicin (1 µM) markedly increased γ-H2AX protein levels in both control and the *Rbpmsb*-KO cells. Notably, deletion of RBPMSB substantially attenuated the γ-H2AX response observed in control cells, implying more efficient DNA repair and reduced DNA damage in the absence of RBPMSB (Figure 42A, B). In line with the observed downregulation of *Rbpms* mRNA levels, RBPMS protein abundance was also diminished following doxorubicin treatment. Interestingly, loss of *Rbpmsb* resulted in a significant upregulation of RBPMSA levels (Figure 42C, D). Collectively, these data demonstrate that RBPMS might function in DNA repair through direct interaction of RBPMSA with DBHS proteins and via functional compensation between RBPMS isoforms.

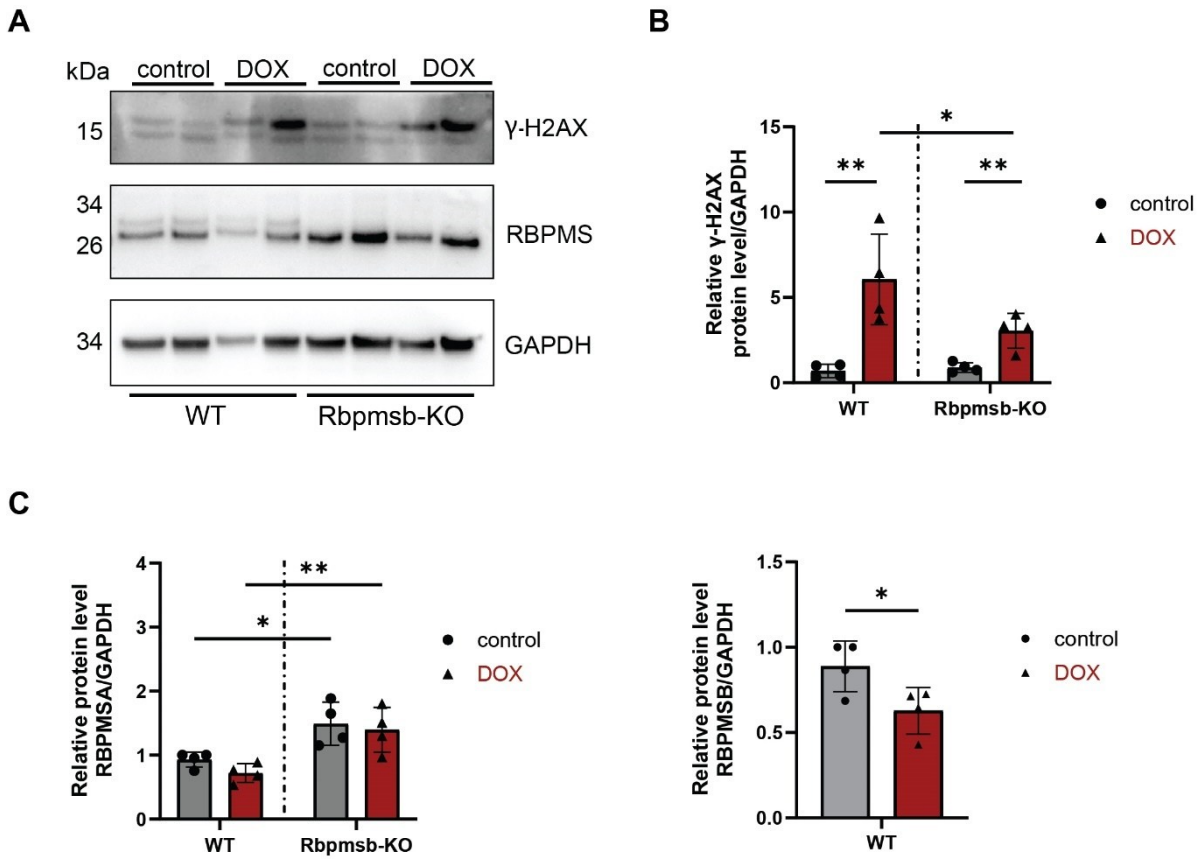

Figure 42 Doxorubicin treatment causes DNA double-strand breaks in isolated adult cardiomyocytes.

A Immunoblot analysis of phosphorylated histone H2AX (γ-H2AX), RBPMSA and RBPMSB in primary isolated adult cardiomyocytes from wild-type and *Rbpmsb* knockout mutants without or with doxorubicin treatment (DOX; 1µM) for 24 h. **B, C** Quantification of γ-H2AX (B), RBPMSA and RBPMSB (C) protein levels relative to GAPDH expression. n = 3 each group. Data represent the mean ± SD. Two-way ANOVA with Bonferroni's multiple comparisons test. *P < 0.05; **P < 0.01.

4. Discussion

4.1 Stress granule dysregulation in human heart diseases

4.1.1 TDP-43 and RBPMS proteinopathies in cardiovascular diseases

Cytoplasmic aggregation and mislocalization of RBPs have emerged as defining features of neurodegenerative diseases, including amyotrophic lateral sclerosis (ALS), frontotemporal lobar dementia (FTLD) and Alzheimer's disease (AD) (Conlon et al., 2017; Nussbacher et al., 2019). Two prominent examples are TDP-43 and FUS, both of which have been linked to the development and progression of ALS. These ubiquitously expressed RBPs demonstrate altered nucleocytoplasmic localization, transitioning from the nucleus to the cytoplasm, where they aggregate under pathological conditions. While the presence of TDP-43 aggregates in the central nervous system is well established in ALS and FTLD, only a few studies have addressed TDP-43 aggregation in skeletal and cardiac muscle of patients with ALS and neuromuscular diseases, and there is a paucity of research on TDP-43 aggregates in heart diseases (Cykowski et al., 2018; Mori et al., 2019). Two types of phosphorylated TDP-43 (pTDP-43) aggregates - dense filamentous and short linear inclusions - in skeletal and cardiac muscle were identified, both of which share immunohistochemical features with TDP-43 inclusions found in the central nervous system of ALS patients. Thus, pTDP-43 aggregates in skeletal and cardiac muscle serve as a marker of myogenic degeneration in ALS and other neuromuscular disorders (Mori et al., 2019). This study demonstrates that TDP-43 undergoes disease-specific posttranslational modifications and accumulates on large cytoplasmic aggregates, a phenomenon not limited to neurodegenerative diseases, but also occurs in heart diseases such as late-end stage dilated cardiomyopathy (DCM) and myocarditis. Thus, while neuronal TDP-43 pathology is a hallmark of neurodegenerative disorders, the presence of cytoplasmic TDP-43 proteinopathies may also be characteristic of certain cardiomyopathies. However, the precise role of cytoplasmic TDP-43 in the pathogenesis of these cardiac proteinopathies remains unclear and warrants further investigation.

Our findings suggest that mislocalization of nuclear RNA-binding proteins may represent a shared pathogenic principle in cardiomyopathies. Like TDP-43, RBPMS is predominantly nuclear under basal conditions, yet disease-associated cytoplasmic redistribution points to a disruption of RNA metabolism and stress adaptation. Whether this reflects a loss of essential nuclear functions, a toxic gain-of-function through cytoplasmic aggregation, or some combination of both, remains unresolved. The parallels to TDP-43 proteinopathies in neurodegeneration raise the intriguing possibility that cardiomyopathies may likewise belong to a broader class of “RNA-binding proteinopathies.” In this context, RBPMS mislocalization could impair splicing regulation, perturb SG dynamics, and compromise the ability of cardiomyocytes to withstand physiological and pathological stress. Importantly, increased

RBPMS expression and mislocalization in diseased tissue suggests potential clinical utility as a biomarker of disease progression or as a therapeutic target. Elucidating how RBPMS localization is regulated, by post-translational modification, interaction partners, or mutations, will be key to understanding its contribution to cardiac pathology and to exploring whether restoration of RNA-binding protein homeostasis can modify disease outcomes.

4.1.2 Aberrant stress granule dynamics in cardiovascular diseases

This study demonstrates that proteinaceous inclusions in the myocardium of DCM and myocarditis patients mainly contain SG proteins, suggestive of SG-related pathological changes. In cardiomyocytes, constant protein turnover is particularly vital due to high basal metabolic and mechanical stress (Jacot et al., 2011). Prolonged cellular stress and disease-induced mutations in SG-associated RBPs can promote the formation of aberrant SGs and/or impair their disassembly, ultimately resulting in pathological protein aggregation. Consequently, we hypothesized that SGs may serve as a source of cytoplasmic TDP-43 aggregates in cardiomyocytes of failing hearts. Our data further support this concept by demonstrating increased SG formation in diseased myocardial tissue. This observation implies that chronic cardiac stress enhances SG assembly, which in turn may facilitate the aggregation of nuclear RBPs such as TDP-43. Indeed, cytoplasmic TDP-43 inclusions colocalizes with SG proteins in primary neurons under cellular stress, and mutations in TDP-43 lead to increased association with SGs and impaired SG dynamics (Li et al., 2013). Importantly, aberrant SG dynamics not only contribute to pathological protein inclusion formation but may also interfere with RNA processing, thereby compromising the adaptive capacity of cardiomyocytes under stress. In this context, dysregulated SGs could represent a critical nodal point linking environmental stress, genetic predisposition, and proteostasis failure in the progression of cardiomyopathy.

Recent studies have shown that SGs may participate in the pathogenesis of neurodegenerative diseases such as ALS and Alzheimer disease (Li et al., 2013). We hypothesized that SG may similarly be implicated in other chronic pathological conditions affecting the cardiovascular system, including myocarditis and DCM. Our study reveals that SGs accumulate in cardiomyocytes during myocarditis and DCM. Autophagy is pivotal for maintaining SG homeostasis by mediating the degradation of both physiological and pathological SGs (Chitiprolu et al., 2018; Guo et al., 2014). The autophagy receptor p62 (SQSTM1) localizes in close proximity to SGs and interacts with the canonical SG marker G3BP1 upon arsenite-induced stress, establishing a direct link between SGs and the autophagic pathway. Notably, p62 knockout results in substantial accumulation of SGs during the recovery phase following stress exposure (Yang et al., 2023). In human cardiovascular disease samples, we observed a marked upregulation of p62 expression that colocalizes with

enlarged G3BP1-positive foci, suggesting the pathological conversion of aberrant ribonucleoprotein (RNP) granules into cytotoxic aggregate-like inclusions within stressed cardiomyocytes. Given the role of autophagy in the clearance of RNP granules (Buchan et al., 2013), the elevated p62 levels likely reflect defective clearance mechanisms, implying that pathological SG accumulation may overwhelm autophagy pathways, leading to cellular dysfunction. TDP-43, a known regulator of autophagy, is also implicated in autophagic dysfunction when mutated (Bose et al., 2011; Filimonenko et al., 2007). Collectively, our findings expand the understanding of pathological SG formation and suggest a potential regulatory role for p62 in SG homeostasis within cardiomyopathies. The modulation of SG formation and clearance through p62 presents a promising avenue for therapeutic interventions in cardiovascular diseases. In summary, our study was the first to characterize SGs in the human cardiovascular system. While SGs confer protection under acute stress conditions, their persistent activation in heart diseases like DCM and myocarditis emphasizes the need for a deeper understanding of their function and the development of targeted therapies.

4.2 Robust APEX2-mediated labeling enables protein proximity mapping in murine HL-1 cardiomyocytes

Previous studies have employed the APEX2 proximity labeling technique to gain novel biological insights across various cellular contexts, including membraneless organelles formed by phase separation. APEX2 enables high-resolution mapping of protein and RNA environments by catalyzing the biotinylation of molecules in close proximity to a protein of interest, thereby facilitating the identification of localized and transient interactions within specific subcellular compartments. Consequently, this approach has proven particularly valuable for investigating the dynamics of SG formation and disassembly across various cell lines and primary cells, revealing significant insights into SG composition and identifying potential regulatory targets involved in SG biogenesis and function (Markmiller et al., 2018; Zhou et al., 2019; Tan et al., 2020). Despite these advances, the SG proteome in cardiomyocytes remains uncharacterized. In this study, we established the first optimized protocol for APEX2-mediated proximity labeling in the HL-1 cardiac cell line, overcoming critical barriers to membrane permeability of biotin-phenol. The refined methodology significantly improves biotinylation efficiency, enabling high-resolution mapping of the SG proteome and revealing increased interactome complexity.

The APEX2-proximity labeling uncovered numerous splicing factors as components of RBPMS-positive foci that assemble in HL-1 cardiomyocytes following heat shock. In the heart, splicing factors regulate the functional properties of cardiomyocytes by modulating AS of multiple genes, particularly those encoding sarcomeric proteins (Weeland et al., 2015). This

regulation enables the heart to adapt to changing demands under conditions of stress or disease. Several studies have demonstrated that specific serine/arginine-rich (SR) splicing factors, including SRSF1, SRSF3, and SRSF7, are recruited to SGs during stress, temporarily reducing their nuclear availability and altering splicing patterns (Twyffels et al., 2011; Anil More et al., 2020; Jayabalan et al., 2016). This aligns with observations that splicing is globally inhibited during mammalian heat stress response (Shalgi et al., 2014). Encoded RNA-binding domains in these factors, are essential for their cytoplasmic translocation and SG incorporation, facilitating the sequestration of splicing-associated transcripts within these structures. An illustrative example of the necessity of RNA-binding for nuclear export is SRSF1, which requires intact RRMs (Twyffels et al., 2011). These present findings corroborate earlier reports of stress-induced nucleocytoplasmic redistribution of RBPs and their role in translational repression.

Moreover, our APEX2 approach identified numerous previously uncharacterized SG-associated proteins [76% (93/120)] in the murine HL-1 cardiomyocyte cell line, highlighting the cell type-specific complexity of SG composition. Previous studies employing commonly used cell lines such as HEK293T or U2OS likely missed certain cardiac-specific proteins due to their absence in these non-cardiac cell types. This underscores the tissue-specific adaptations of SGs, as the discovery of cardiac-enriched proteins indicates unique SG compositions that may contribute to organ-specific vulnerability under stress. The composition of SGs depends on both the cell type and the specific stress encountered, with cell type accounting for approximately 20% of their variability. Notably, neuronal cells display a particularly complex repertoire of proteins within their SGs, reflecting specialized functional demands (Markmiller et al., 2019). Different cell types may recruit distinct sets of proteins to SGs, suggesting a specialized stress response that supports specific cellular functions and survival mechanisms.

Furthermore, using a combination of APEX2 proximity labeling and immunoprecipitation experiments, we identified several SG-associated proteins as potential interactors or proximal partners of RBPMS under non-stress conditions, indicating that SG stability may be supported by enhanced basal protein-protein interactions . Recent studies have proposed that certain SG-associated proteins can pre-assemble even in the absence of stress, forming complexes that locally concentrate RBPs and prime cells for rapid SG formation upon stress exposure (Wheeler et al., 2016; Baymiller et al., 2023). For instance, core SG components have been shown to interact within the neurites of human iPSC-derived motor neurons prior to arsenic exposure. Furthermore, uninjured or growing axons in the peripheral nervous system contain interactomes that include HuR, TIA1, and G3BP1, all well-characterized SG constituents (Sahoo et al., 2018). Consistent with previous findings, our current data demonstrate preexisting and constitutive proximity interactions among core SG components in unstressed

cardiomyocytes. Such interactions likely serve as precursors, facilitating the efficient and rapid assembly of SGs and enabling dynamic regulation of translation in response to cellular stress.

The perinuclear localization of SGs may have functional importance in mRNA regulation, given their role as dynamic hubs of mRNA metabolism (Kedersha et al., 2002). This positioning suggests a close functional interplay with nuclear processes, particularly as several regulatory RBPs shuttle between the nucleus and SGs in response to stress conditions (Zhang et al., 2019; Mahboubi et al., 2014). Proximity localization to the nucleus could enhance signaling efficiency by minimizing diffusion distances for proteins that mediate cross-compartment communication. Moreover, nuclear transport mechanisms are modulated during stress: importin α, a key mediator of nuclear import, accumulates in the nucleus, while importin α/β-dependent nuclear import is downregulated during heat shock as an adaptive response to environmental stress (Furuta et al., 2004; Miyamoto et al., 2004). The modulation of nuclear import efficiency may contribute to the dynamic redistribution of proteins between nuclear compartment and cytosolic SGs, further underscoring the functional significance of SG localization in the perinuclear region. Experimental approaches using export inhibitors such as Leptomycin B or Selinexor could clarify whether stress-induced cytoplasmic retention results from impaired nuclear import or active cytoplasmic sequestration.

4.3 RBPMS exhibits a dual role in stress granules and nuclear bodies under stress conditions

4.3.1 RBPMS isoforms mediate stress granule dynamics and DNA damage modulation in response to doxorubicin-induced cardiotoxicity

The subcellular localization of RBPMS isoforms determines their distinct functional roles. RBPMSA, which is predominantly nuclear, is primarily involved in the regulation of AS, whereas RBPMSB, mainly localized in the cytoplasm, likely contributes to RNA stability and trafficking. This functional segregation highlights specialized roles in RNA metabolism and cellular stress responses. Intriguingly, RBPMS encodes a putative IDR domain in addition the single RRM domain, which facilitates higher-order oligomerization and is essential for its splicing regulatory activity and phase separation properties. The IDR enables RBPMS to participate in the assembly of RNP granules, including SGs. Indeed, RBPMS has been reported to translocate to SGs in response to oxidative stress in HEK293T cells (Farazi et al., 2014). In accordance with these observations, this study demonstrates that RBPMS colocalizes with the SG marker G3BP1 in isolated cardiomyocytes under stress conditions. Moreover, treatment with doxorubicin, a topoisomerase II beta (Top2b) inhibitor that induces DNA double-strand breaks (DSBs), promotes the formation of discrete nuclear puncta by RBPMS. Consistently, increased RBPMSA levels in *Rbpmsb* isoform-deficient cardiomyocytes might indicate functional redundancy of the different RBPMS isoforms, which is accompanied

by a reduction in DSB-induced phosphorylated histone H2A (γ-H2AX) and a decreased number of SFPQ-positive nuclear granules. These findings point to a potential role for RBPMS in PS formation and DDR. Importantly, the transgenic mice used in these studies are viable, supporting the compensatory role of RBPMS isoforms in cardiac function. NEAT1 overexpression promotes DNA damage repair and mitigates doxorubicin-induced cardiotoxicity (Adriaens et al., 2016; Liu et al., 2019). To confirm a direct association with PS, future studies should employ NEAT1 fluorescent *in situ* hybridization (FISH) in conjunction with RBPMS immunofluorescence microscopy.

Notably, 24 h post-treatment, we observed a significant overlap between condensed chromatin (DNA condensates) and doxorubicin-induced condensates; however, RBPMS exhibited only partial colocalization with these structures within the interchromatin space. Consequently, the sequestration of doxorubicin into nuclear granules may reduce its local concentration at DNA target sites, thereby diminishing DNA damage. Moreover, previous reports have demonstrated that doxorubicin promotes LLPS (Garg et al., 2024) and preferentially accumulates within heterochromatin, promotes the formation of liquid condensates by heterochromatin protein 1 (HP1) and induces the formation of doxorubicin-H1 fibrous condensates through its interaction with histone H1. (Wang et al., 2023). It is also plausible that doxorubicin may interact with other histones or chromatin-associated proteins, further contributing to chromatin reorganization and phase separation.

Doxorubicin triggers a DNA damage response (DDR) and apoptosis, resulting in transcriptomic changes that disrupt mitochondrial biogenesis in cardiomyocytes. One of the primary mechanisms underlying these effects is the inhibition of Top2, which, together with the generation of reactive oxygen species (ROS), substantially contributes to DNA damage and cardiotoxicity (Zhang et al., 2012). Consistent with our observations, treatment of cardiomyocytes with doxorubicin resulted in increased levels of phosphorylated histone H2A (γ-H2AX), a marker of DSBs. Dexrazoxane (Zinecard, ICRF-187), a clinically approved cardioprotectant, functions as a Top2 catalytic inhibitor (Andoh, 1998), induces proteasomal degradation of Top2b in H9C2 cardiomyocytes and can partially protect doxorubicin-induced DNA damage (Andoh, 1998; Lyu et al., 2007). However, the results in this study show that dexrazoxane pre-treatment does not prevent the formation of doxorubicin-induced nuclear condensates in neonatal cardiomyocytes, indicating that these condensates are not dependent on the formation or proteasomal degradation of Top2-DNA complexes but may instead arise as a consequence of apoptosis or may represent a protective cellular response. Chromatin condensates play a crucial protective roles in cellular physiology, particularly by safeguarding genome stability and integrity. A key aspect of their function lies in the regulation of DDR signaling. Remarkably, chromatin condensation alone is sufficient to activate DDR pathways,

thereby integrating these signals into the broader cellular response to DNA damage (Burgess et al., 2014). Chromatin condensates serve as molecular hubs during cellular stress by sequestering regulatory molecules and facilitating DNA repair processes. Notably, recent studies have highlighted the protective roles of paraspeckles (PS)-a class of nuclear bodies involved in gene regulation and stress responses-particularly in neurodegenerative diseases such as ALS (Shelkovnikova et al., 2018). These findings underscore the multifaceted roles of nuclear condensates in cellular defense mechanisms during genotoxic stress.

4.3.2 Paraspeckle-associated RBPMS network regulates cardiac DNA damage response

Mass spectrometry profiling of purified PSs in HEK293T cells revealed a substantial and unexpected proteomic overlap with SGs components, despite the prior assumption that these structures were independent due to their respective confinement to the nucleus and cytoplasm. This finding challenges the assumption that these membraneless organelles are functionally independent and suggests a structural and functional continuum between nuclear and cytoplasmic RNP granules. SGs can sequester several PS-associated proteins that normally suppress PS formation when retained in the nucleus, thereby impacting their gene regulatory functions (An et al., 2019). In this study, we employed mass spectrometry to identify numerous RBPMS interactors in cardiomyocytes, including RBPs with key roles in DDR and PS formation, such as RBM14, SFPQ, NONO, HNRNPA1, HNRNPUL and TAF15. Notably, all these proteins contain aggregation-promoting prion-like domains. The association of RBPMS with these key regulatory proteins suggests a role in modulating cellular responses to genotoxic stress, possibly by influencing DDR signaling pathways and the assembly of nuclear bodies. These proteins also contain IDRs, a common feature of RBPs implicated in neurodegenerative diseases, including ALS (Vance et al., 2009; Couthouis et al., 2011; Chesi et al., 2013; Kim et al., 2013). IDRs are essential for higher-order protein oligomerization and phase separation, facilitating the assembly of membraneless organelles like SGs and nuclear bodies (Yang et al., 2023). Thus, the presence of IDRs is a defining characteristic of many PS-associated proteins. RBM14, is a central interactor in this process, orchestrating the recruitment of additional factors to PS, thereby facilitating their biogenesis. A key function of RBM14 is to mediate the interaction between two core Drosophila behavior/human splicing (DBHS)-family proteins, NONO and SFPQ, which are essential structural components of PSs and are involved in diverse roles in RNA metabolism, DDR, and PS formation (Lim et al., 2020). The SFPQ-NONO heterodimer accumulates at the DNA damage sites, where it interacts with the Ku70/Ku80 complex, an essential component of the nonhomologous end joining (NHEJ) DNA repair pathway and promotes DNA end joining (Alfano et al., 2015). Moreover, under neuropathological conditions, SFPQ has been reported to abnormally accumulate in the

cytoplasm, and maintaining its proper nucleocytoplasmic distribution is crucial for cellular homeostasis and stress response regulation (Ke et al., 2012; Lu et al., 2018). Our findings further support the interaction between RBPMS and SFPQ, as confirmed by proximity-dependent biotinylation, co-immunoprecipitation and immunofluorescence colocalization analysis. Additionally, RBPMS interacts with heterogeneous nuclear ribonucleoprotein U-like (hnRNPUL), underscoring its critical role in the DDR. The identification of these RBPs as RBPMS interactors points to a complex regulatory network that coordinates phase separation and DDR, potentially bridging nuclear and cytoplasmic membraneless organelles during cellular stress responses. Notably, APEX2 proximity labeling revealed that several PS-associated proteins localize near RBPMS in HL-1 cardiomyocytes, but not in HEK293T cells or MEFs, supporting a cardiac-specific role of RBPMS in PS formation and related processes. Collectively, these results support the hypothesis that RBPMS serves as a molecular hub integrating stress signaling, RNA processing, and chromatin organization in the heart. Through its interactions with DDR and PS-associated proteins, RBPMS may drive the dynamic remodeling of nuclear architecture and promote the formation of phase-separated condensates in response to genotoxic stress, thereby enhancing cellular resilience and preserving genome stability in cardiomyocytes.

4.3.3 RBPMS links RNA granule dynamics to mitochondrial function in cardiomyocyte stress adaptation and doxorubicin-induced toxicity

In this study, we observed that doxorubicin treatment initially induces SG formation in the cytoplasm, which is subsequently followed by the assembly of granules within the nucleus. These findings suggest a temporal sequence of RNP granule formation in response to acute stress. Building on this, we propose that SG assembly functions as an immediate adaptive response to acute stress, such as doxorubicin exposure, whereas PSs and other nuclear bodies coordinate longer-term adjustments of cellular processes needed to cope with prolonged stress. Studies have demonstrated that the formation of SGs is essential for initiating and sustaining PS assembly under stress conditions and that these cytoplasmic and nuclear RNP granules are structurally and functionally interconnected (An et al., 2015). SGs are generally regarded as protective structures that support cell survival under diverse stress conditions (Arimoto et al., 2008), whereas PSs enhance cell viability during proteasome inhibition, heat shock, and exposure to foreign double-stranded RNA (dsRNA) (Hirose at al., 2014). PSs are particularly important in safeguarding cells from disruptions in RNA metabolism, thereby strengthening their resilience to oxidative stress and insults linked to neurodegenerative diseases (Shelkovnikova et al., 2018; Wang et al., 2022). The assembly of PSs is dynamically regulated and can be triggered by signals originating from SGs, reflecting a continuum of RNP granule formation that allows cells to efficiently adapt to changing

environmental conditions. This biphasic response involves an initial cytoplasmic wave of SG formation followed by a nuclear wave of PS assembly, enabling both immediate and long-term modulation of gene expression and stress responses (Shelkovnikova et al., 2018). RBPMS localization changes dramatically in a stress-type-dependent manner, however only a fraction of RBPMS relocalizes to nuclear foci. It has been proposed that the core of PSs acts as a site for sequestering specific components, while the surrounding shell is more dynamic and engages with different nucleoplasmic proteins in a manner that depends on the type and function of the PS. Therefore, the different types of PSs may exhibit distinct responses under stress conditions (Arnold et al., 2024). RBPMS isoforms likely interact with components of both the shell and core of PSs. RBPMSA constitutively associates with core PS components under basal conditions, suggesting a fundamental role in maintaining PS structural integrity through RNA-protein interactions with key architectural factors. In contrast, RBPMSB exhibits stress-induced recruitment to PSs and interacts preferentially with stress-responsive elements, potentially facilitating the complete assembly and functional regulation of these nuclear bodies under stress conditions.

HuR has been implicated in the early cellular response to doxorubicin, undergoing phosphorylation-dependent translocation from the nucleus to the cytoplasm (Latorre et al., 2012). Comparable to HuR, RBPMS may undergoes phosphorylation at specific residues adjacent to its RNA recognition motif, which affect its RNA binding affinity or nuclear localization, thereby modulating its dynamics in response to various stress conditions. Publicly available phosphoproteomic datasets have identified multiple phosphorylation sites within RBPMS. In particular, threonine residues at positions 113 and 118, which are adjacent to the RRM domain have been reported as phosphorylation sites (Barnhart et al., 2022).

Intriguingly, our data suggest a close interplay between SGs and membrane-bound organelles, particularly mitochondria. Proteomic analyses indicate that RBPMB may interact with mitochondrial proteins, highlighting a potential molecular interface between these structures. Notably, pathological disruption of SG dynamics in neurodegenerative diseases appears to be tightly linked to mitochondrial dysfunction (Amen et al., 2021), further underscoring the potential interplay between these cellular structures. Our transcriptomic analyses revealed a marked enrichment of mitochondrial gene expression following doxorubicin treatment, with prominent alterations in the tricarboxylic acid (TCA) cycle and electron transport chain - hallmarks of doxorubicin-induced cardiotoxicity. These findings underscore the pivotal role of mitochondrial function in orchestrating the cellular stress response, wherein SGs serve as key regulators of mRNA triage and promoters of cell survival. We propose that mitochondrial dynamics are essential for the proper assembly and function of SGs and speculate that DNA damage accumulation upon doxorubicin treatment disrupts mitochondrial ultrastructure

(Sultana et al., 2006; Valko et al., 2007; Wei et al., 2001), which in turn impair the proper assembly of SGs or lead to the disassembly and nuclear translocation of RBPMS. Thus, the interplay between mitochondria and SGs is likely a key determinant of cellular resilience during stress, and mitochondrial impairment may contribute to the onset of doxorubicin-induced cardiac toxicity by alter SG assembly and dynamics and altering the global stress response. Further studies will be required to elucidate the precise molecular mechanisms underlying these interactions.

4.4 RBPMS acts as a mediator of cellular stress responses

4.4.1 Genotoxic stress-induced redistribution of RBPMS highlights its role in nuclear speckle remodeling

Our findings indicate that the recruitment of RBPMSB into nuclear foci is not specific to doxorubicin treatment but represents a broader response to genotoxic stress. Treatment with agents such as H_2O_2 and cisplatin, which induce oxidative damage and DNA double-strand breaks (DSBs), likewise promotes a redistribution of RBPMS. Prolonged exposure or elevated doses of these agents promote nuclear accumulation of RBPMS rather than its recruitment to cytoplasmic SGs. This redistribution reflects the activation of stress-responsive signaling pathways, most notably the p38 MAPK cascade, which reshapes nuclear bodies and facilitates the recruitment of splicing and RNA processing factors (Sung et al., 2023). Reports show that physiologically relevant H_2O_2 concentrations (0.01 mM-0.4 mM) elicit dose-dependent effects: low concentrations drive senescence, while higher doses induce apoptosis, reflecting the degree of DNA damage (Benhusein et al., 2010). Similarly, cisplatin, a widely used chemotherapeutic agent, triggers mitochondrial dysfunction, DNA damage, and oxidative stress-mediated apoptosis in cardiomyocytes. Its cytotoxicity manifests within 6–24 h, primarily through the formation of platinum-DNA adducts that disrupt replication and impair repair mechanisms.(Qian et al., 2018; Soliman et al., 2018; Shirmanova et al., 2017). Emerging evidence suggests that cisplatin-induced genotoxic stress is not only linked to the regulation of PSs but also to the assembly of SGs. Specifically, cisplatin treatment upregulates the long non-coding RNA NEAT1, which drives PS formation and promotes sequestration of SFPQ and NONO. This, in turn, reprograms the transcription of pro-survival genes while concurrently disrupting DDR pathways. The depletion of SFPQ enhances the transcription of pro-apoptotic genes, thereby promoting cell death (Ru et al., 2018). Consequently, PS formation is a critical determinant of cellular sensitivity to cisplatin.

Genotoxic stress broadly suppresses transcription through RNA polymerase II (RNAPII) degradation, redirecting cellular resources towards stress adaptation and fostering nuclear condensates enriched in SFPQ, NONO, FUS, and TAF15 (Kleimann et al., 2005). In this context, the distinct redistribution of RBPMS under stress suggests functionally divergent roles,

with pro-survival SGs primarily coordinating acute stress responses through repression of non-essential translation, whereas nuclear accumulation is associated with the regulation of apoptosis and DDR. This relocalization represents an adaptive mechanism that promotes efficient management of stress-induced transcripts and supports rapid expression of immediate early genes. Nuclear speckles, which serve as hubs for the storage and modification of splicing factors, are dynamically reorganized during stress to support the processing of stress-responsive transcripts (Sung et al., 2023). Given its function as a splicing regulator, RBPMS likely contributes to the assembly and organization of nuclear speckles by modulating the repertoire and activity of splicing factors within these compartments, thereby orchestrating the dynamic nuclear environment required for efficient gene expression and pre-mRNA processing.

4.4.2 Dynamic nuclear-cytoplasmic shuttling of RBPMS and G3BP1 links phase separation to DNA damage signaling and apoptotic regulation

Intriguingly, the nuclear and cytoplasmic localization of both RBPMS and G3BP1 suggest to be stress-specific. Under acute oxidative stress, these RNA-binding proteins predominantly accumulate in cytoplasmic SGs, facilitating immediate cellular protective responses. In contrast, during prolonged oxidative stress, RBPMS and G3BP1 translocate to the nucleus where they form distinct nuclear foci. These observations align with previous studies demonstrating that the subcellular translocation of G3BP1, particularly its shuttling between the cytoplasm and nucleus, plays a decisive role in regulating apoptosis: cytoplasmic G3BP1 and SG formation generally protect against apoptosis by sequestering pro-apoptotic factors and mRNAs (Takahashi et al., 2013), while nuclear translocation modulates apoptotic signaling pathways, particularly through interactions with p53 and related factors (Mao et al., 2021). Phosphorylation at Ser-149 directs G3BP1 to the nucleus (Tourrière et al., 2003), where it may associate with ribonucleoprotein complexes. Functionally, G3BP1 is classified as a non-canonical helicase and transcription factor, capable of unwinding DNA, RNA, and DNA/RNA hybrid structures (Costa et al., 1999). This activity may underlie its potential function in DNA damage-related processes or apoptosis.

Collectively, these findings will offer novel insights into the role of RBPMS in RNA metabolism, phase separation, and cellular stress responses. Further research is required to clarify the role of RBPMS in the DDR and its potential contributions to disease pathogenesis, particularly in cardiomyocytes. Future studies should specifically investigate the effects of RBPMSA knockout on DDR efficiency in cardiomyocytes, for instance through comet assays, to elucidate its pathophysiological relevance in response to genotoxic stress.

4.5 Doxorubicin reshapes splicing factor networks through poison exon inclusion and intron splicing

4.5.1 Phase separation drives hierarchical coordination of splicing regulators in cardiomyocytes

Genotoxic agents such as doxorubicin exert profound effects on the splicing machinery by altering the expression levels and posttranslational modifications of several splicing regulators, including SR proteins and heterogeneous nuclear ribonucleoproteins (hnRNPs) (Haley et al., 2009; Filippov et al., 2007; Zhou et al., 2013; Martinez-Contreras et al., 2007). These modifications influence the intracellular localization and functional activity of these proteins, thereby modulating AS events. For instance, phosphorylation-induced relocalization of specific kinases can lead to hyperphosphorylation of SR proteins, resulting in alterations in pre-mRNA splicing (Gui et al., 1994; Colwill et al., 1996). In vascular smooth muscle cells (VSMCs), phosphorylation of RBPMS directly downregulates its splicing activity , providing rapid adaptive modulatory mechanism (Barnhardt et al., 2022). RBPMS contains a single RRM and proline-rich IDR that promotes oligomerization and interaction with other RBPs (Teplova et al., 2016). In addition, the IDR facilitates AS regulation, enabling cooperative binding to target RNAs and recruitment of ubiquitous expressed splicing factors such as PTBP1, MBNL1, and QKI (Nakagaki-Silva et al., 2019). In VSMCs, RBPMS acts as a master splicing regulator, controlling the activity of co-regulators such as RBFOX2 and MBNL1 and thereby indirectly influencing downstream AS events that shape the VSMC contractile phenotype. Moreover, RBPMS influences AS of *Mbnl1* and *Mbnl2*, which encode splicing regulators themselves, indicating a hierarchical regulatory network. This regulatory role is not limited to VSMCs but also encompasses cardiac muscle and embryonic stem cells, where RBPMS expression is governed by super-enhancers (Nakagaki-Silva et al., 2019). Indeed, our data indicate that RBPMSA operates as a central hub of AS in the myocardium through interactions with ubiquitously expressed splicing factors such as PTBP1 and hnRNPs and cardiomyocyte-specific splicing factors such as MBNL1 and RBFOX1. By coordinating with other splicing regulators within the nuclear environment, RBPMSA likely acts as a master regulator that fine-tunes cardiac-specific splicing programs critical for myocardial function. Importantly, dysregulation of RBPMSA-mediated splicing has been linked to impaired cardiomyocyte contractility and dilated cardiomyopathy, underscoring its potential involvement in cardiac disease pathogenesis (Gan et al., 2023). Thus, understanding the molecular mechanisms of RBPMSA's splicing regulation may open new avenues for therapeutic strategies targeting AS to treat or prevent cardiac dysfunction and heart failure. These findings suggest that RBPMSA-mediated cardiac splicing does not rely solely on heart-restricted RBPs or unique cofactors. Rather, RBPMS functions as part of a dynamic AS network that includes both specialized

cardiac regulators and core splicing factors broadly expressed across tissues. The IDRs of RBPMS promote phase separation, driving the assembly of nuclear condensates such as PSs and thereby enhancing access to the splicing machinery. Through this capacity to organize nuclear microenvironments, RBPMS not only regulates the splicing of its direct RNA targets but also modulates a wider network of splicing events and other post-transcriptional processes throughout the nucleus.

4.5.2. Novel putative *Rbpmsd* isoform reveals stress-responsive splicing regulation in neonatal cardiomyocytes

Interestingly, we identified previously uncharacterized *Rbpms* isoform, termed *Rbpmsd*, that is expressed in neonatal but not adult cardiomyocytes. This isoform incorporates a poison exon cassette (PCE) and exhibits intron retention, resulting in a transcript harboring a premature termination codon (PTC). Since the PTC is positioned more than 50–55 nucleotides upstream of the final exon-exon junction, the *Rbpmsd* transcript is predicted to be targeted for degradation by the nonsense-mediated decay (NMD) pathway. Moreover, doxorubicin treatment markedly upregulates *Rbpmsd* expression, accompanied by a concomitant reduction in *Rbpmsa* and *Rbpmsb* mRNA levels. Given that RBPMSA and RBPMSB regulate splicing, it is likely that RBPMS, together with its associated splicing factors, promotes PCE skipping under normal conditions to ensure production of functional RBPMS protein. While transcripts containing PTC are typically targeted for degradation via NMD, doxorubicin suppresses NMD machinery, enabling PTC-containing transcripts to evade degradation (Popp et al., 2015). Furthermore, chemotherapeutic stress alters the expression or activity of splicing regulators, promoting PCE inclusion and intron retention. This transcriptome-wide AS reprogramming may act as a buffering mechanism to adapt the proteome under genotoxic stress. Interestingly, alternative splicing coupled with nonsense-mediated decay (AS-NMD) events are highly enriched among splicing regulators. Many of these proteins bind their own transcripts and promote the splicing of nonproductive NMD isoforms, creating an autoregulatory negative feedback loop that maintains protein expression within a self-limiting range (Lareau et al., 2007). The coordinated inclusion of PCEs together with intron retention constitutes an adaptive AS response to doxorubicin exposure, potentially influencing cardiomyocyte survival. This combined perturbation (PCE inclusion plus intron retention) reveals a previously unrecognized dimension of doxorubicin cardiotoxicity, directly linking genotoxic stress to splicing dysregulation in cardiomyocytes. Understanding how RBPMS activity is regulated under genotoxic stress may uncover therapeutic targets to counteract cardiotoxicity.

The minimal size disparity between the protein isoforms (10-13aa), hinders effective resolution by standard Western blotting. To overcome this limitation, two-dimensional gel electrophoresis

(2DE) - which separates proteins by isoelectric point and molecular weight - provides higher resolution for distinguishing these isoforms with minimal mass differences and enables quantification of their stress-dependent expression. Functional assays, such as CRISPR-based isoform-specific knockdowns or knockouts, will clarify the role of *Rbpmsd* in AS regulation and cardiomyocyte survival. These insights may help guide the development of strategies to preserve splicing fidelity during chemotherapy, thereby mitigating the risk adverse cardiac outcomes.

4.5.3. Splicing dysregulation as a central mechanism of doxorubicin cardiotoxicity

Doxorubicin induces extensive gene expression remodeling, including AS events that allow cardiomyocytes to adapt to environmental stress. The observed reduction in RBPMSA and RBPMSB levels is likely arises from PCE inclusion and subsequent degradation of the transcript, a mechanism that mirrors the autoregulatory feedback loops reported for other splicing regulators such as SRSF7 and RBM39 (Campagne et al., 2023). Transient SRSF7 overexpression enhances PCE exon inclusion and triggers NMD-dependent transcript degradation, while prolonged overexpression causes intron retention and nuclear confinement of transcripts, resulting in the formation of regulatory nuclear bodies. (Goenka et al., 2016; Yap et al., 2018). Markedly, RBM39 tightly autoregulates its expression through a negative feedback loop at the pre-mRNA splicing stage by promoting the inclusion of a PCE. This mechanism involves all three RRMs and the arginine-serine-rich domain of RBM39, which coordinate interactions with the spliceosome components and the pre-mRNA to control alternative 3'-splice site selection, ultimately leading to regulated PCE inclusion and transcript degradation. This autoregulatory loop ensures precise control of RBM39 levels in the cell (Campagne et al., 2023).

Strikingly, several essential splicing factors, including SRSF7 and RBM39, exhibit increased intron retention in neonatal but not in adult cardiomyocytes, indicating a potential feedback mechanism in which components of the AS machinery are either self-regulated or modulated by other splicing factors via changes in splicing patterns. This differential regulation may reflect developmental stage-specific control of splicing efficiency, allowing neonatal cells to fine-tune gene expression during maturation. Doxorubicin-induced intron retention may contribute to the loss of specific RBPMS isoforms (*Rbpms-203/-213* and *Rbpms-202*), reinforcing the concept that splicing factors promote the adaptation of gene expression and modulate protein levels through intron retention during cellular stress. Interestingly, several splicing factors implicated in cardiomyopathy exhibit altered expression upon doxorubicin treatment in neonatal cardiomyocytes, including RBM20 (Van den Hoogenhof et al., 2018), QKI (Chen et al., 2021), CELF1 (Ladd et al., 2015), SRSF1 (Xu et al., 2005), and SRSF5 (Zhang et al., 2021).

Specifically, several splicing regulators that promote intron retention, such as *Srsf2*, *Hnrnpl*, *Hnrnpk*, *Sf3b1,* are upregulated following doxorubicin treatment. Furthermore, intron retention serves as a key regulatory mechanism during development: global analyses comparing fetal and adult human hearts reveal that alternative 3′ and 5′ splice site usage, exon skipping, and intron retention account for the majority of AS events, with intron retention and exon skipping being more prevalent in fetal hearts (Li et al., 2013; Wang et al., 2016). The shift toward noncoding isoforms of splicing regulators under stress conditions reflects a coordinated regulatory program rather than a general splicing failure, underscoring the importance of identifying AS switching events. Our findings imply that doxorubicin-induced AS changes, including PCE inclusion and intron retention, may contribute to cardiotoxicity by altering the expression and function of key splicing regulators and their downstream targets.

In addition to protein abundance, subcellular localization is a pivotal determinant of protein function. Under doxorubicin-induced genotoxic stress, RBPMS undergoes relocalization to nuclear granules, particularly via its interaction with SFPQ, implicating it in the regulation of stress-responsive splicing. The presence of RBPMS-positive nuclear foci adjacent to nuclear speckles after doxorubicin treatment further supports the concept of dynamically coordinated splicing regulation (data not shown). This is consistent with functional crosstalk between nuclear speckles and PS, which collaboratively regulate mRNA splicing (Okuda et al., 2025). Stress conditions induce nucleocytoplasmic shuttling of splicing regulators, such as SR proteins (e.g., SRSF1, SRSF3, SRSF7), which translocate to cytoplasmic SGs or nuclear stress bodies. These subcellular redistribution events drive adaptive AS responses and reduce splicing efficiency by sequestering factors into granules, enabling rapid transcriptome and proteome remodeling to prioritize stress adaptation (Ibrahim et al., 2005). Intron retention further modulates post-transcriptional regulation by retaining pre-mRNAs in the nucleus, as observed during heat shock and other stress conditions (Ninomiya et al., 2019; Goenka et al., 2016; Yap et al., 2018).

Previous studies collectively highlight the fundamental principle that cellular responses to oxidative stress are highly cell-type-dependent, varying between terminally quiescent, fully differentiated, and proliferative cells (Cepinskas G., 1994; Flores S. C., 1997; Kaufmann, 1989; Kim et al., 2018; Liu, 1989; Walker P. R., 1991). Notably, children under 4 years exhibit heightened susceptibility to doxorubicin-induced cardiotoxicity compared to adults, reflecting distinct mechanisms of toxicity (Krischke et al., 2016; Lipschultz et al., 1991; Lipschultz et al., 1996; Pratt et al., 1978). In this line, age-dependent differences in doxorubicin-induced apoptosis have been observed. This sensitivity is linked to higher baseline caspase-3 activity and proapoptotic protein expression in immature cardiomyocytes, which sharply decline postnatally. Specifically, acute doxorubicin treatment induces a strong apoptotic response in

neonatal but not mature cardiomyocytes, due to the downregulation of key apoptotic regulators (Shi et al., 2012). Our finding that *Rbpms* isoform expression differs between proliferating neonatal cardiomyocytes and postmitotic adult cardiomyocytes may reflect differentiation stage-specific variations in oxidative stress responses, which could, in turn, influence cellular vulnerability and physiological function. Alternatively, these differences may stem from cell type–specific efficiencies in expressing genes that mediate antioxidant defense (Kim et al., 2018). Proliferating neonatal cardiomyocytes exhibit distinct splicing factor dynamics (e.g., RBM24, QKI, CELF1) under doxorubicin treatment, potentially contributing to their heightened vulnerability. These findings highlight the interplay between developmental stage, stress adaptation, and splicing regulation in shaping cardiac resilience to genotoxic agents.

Finally, this study demonstrates that therapy-induced stress responses, such as those triggered by doxorubicin, are accompanied with downregulation of splicing factors, thereby driving global intron retention and PCE inclusion. These mechanisms enable cardiomyocyte stress adaptation by modulating the activity and stability of key proteins involved in cell survival and drug resistance. The dynamic regulation of RBPMS localization and expression highlights its dual role in autoregulating its own transcripts and modulating AS of mRNA targets. These findings position RBPMS as a critical node the transcriptional and post-transcriptional response to doxorubicin-induced stress, potentially contributing to the drug's cardiotoxic effects. By generating diverse splice variants and assembling into dynamic RNP complexes, RBPMS fine-tunes RNA metabolism and gene expression in a context-dependent fashion, emphasizing its central role in maintaining cellular homeostasis. Core functions such as splicing regulation, mRNA stability, and transport are essential for normal cellular function, and their dysregulation has been implicated in numerous diseases, making them a central focus of biomedical research. Understanding the mechanistic links between RBPMS isoform expression, doxorubicin-induced cardiotoxicity, and adaptive splicing responses may provide novel insights into the pathophysiology of chemotherapy-induced cardiac dysfunction. Future research should focus on targeted strategies to modulate AS in cardiomyocytes. Leveraging CRISPR-based platforms, such as CRISPR-Cas13 or CasRx, to selectively knock down genes and reprogram AS patterns in could help identify key pathological AS targets and clarify their impact on cardiovascular health. Such mechanistic insights hold promise for the development of novel therapeutic strategies aimed at mitigating chemotherapy-induced cardiotoxicity, with important implications for both pediatric and adult oncology patients.

4.6 Future Directions

4.6.1 Identification of SG and PB protein and RNA composition in cardiomyocytes using APEX2 proximity labeling

Given that RBPMS localizes to both SGs and P-bodies, it is crucial to characterize the specific molecular composition of the corresponding RBPMS-positive foci in cardiomyocytes. To address this, APEX2 proximity labeling will be employed, targeting SGs via G3BP1 and P-bodies via DCP1A. This approach will enable the identification of unique and overlapping protein constituents, providing a comprehensive analysis of both specific and shared components between these two granule types. The enzymatic activity of APEX2 fusion constructs targeted to SGs and P-bodies was successfully validated in HEK293T cells by immunoblotting with a V5 antibody and streptavidin-HRP detection (see Appendix Figure 46). Future studies will focus on mapping the stress-dependent interaction partners of RBPMSB within SGs and P-bodies, comparing proliferative (MEFs) and postmitotic cells (cardiomyocytes). This comparative analysis will facilitate the distinction between closely related RNP granules and contribute to a more detailed characterization of cell-type-specific assemblies.

The RNA composition of SGs in cardiomyocytes remains largely unexplored. In addition to proteomic mapping, APEX2-mediated proximity labeling enables transcriptomic analysis by directly biotinylating RNA (APEX-seq) (Zhou et al., 2019). To achieve higher specificity for nucleic acids, a biotin-aniline probe will be utilized to map the transcriptome of SGs, specifically in cardiomyocytes. Candidate target RNAs identified through this approach can be further validated using single-molecule fluorescence in situ hybridization (smFISH) in both murine and human tissues. This integrative strategy will provide a more comprehensive understanding of mRNAs sequestered within SGs, elucidate their regulatory mechanisms, and clarify their roles in cellular homeostasis and disease.

4.6.2 Auto- or cross-regulation of *Rbpms* splicing by additional splicing factors

The present study demonstrates that doxorubicin treatment induces pronounced alterations in AS, including the regulation of RBPMS isoforms. Our findings suggest that RBPMS may autoregulate its own splicing, a mechanism modulated by doxorubicin exposure. Specifically, we propose that doxorubicin enhances the inclusion of exon X, introducing a PTC and triggering NMD, thereby reducing the abundance of functional *Rbpms* transcripts. To test this hypothesis, future studies could employ cycloheximide treatment or UPF1 knockdown to inhibit NMD. These approaches would help determine whether *Rbpmsd* regulation is mediated at the transcriptional level or through post-transcriptional mechanisms, thereby clarifying the

mechanistic interplay between chemotherapy-induced splicing dysregulation and autoregulatory feedback loops in *Rbpms* expression.

Further studies could employ individual-nucleotide resolution UV crosslinking and immunoprecipitation (iCLIP) to systematically map the genome-wide binding sites of RBPMSA and RBPMSB isoforms in mouse cardiomyocytes. Given that RBPMSA is predominantly nuclear and RBPMSB resides in the cytosol, iCLIP applied to nuclear and cytoplasmic fractions, respectively, would provide valuable insights into their isoform-specific regulatory functions. This compartment-specific binding site mapping approach will enable the identification of direct RNA targets of each isoform within their respective subcellular environments. Integrating iCLIP data with transcriptome-wide analyses of AS changes will clarify whether the observed AS events result from direct RBPMS binding to specific motifs (such as CAC elements) or are mediated indirectly through broader regulatory networks. Additionally, complementary RNA-binding motif enrichment analyses could help identify other regulatory factors (e.g., MBNL, PTBP) or stress-responsive RBPs that may cooperate with RBPMS isoforms to fine-tune AS outcomes, particularly under chemotherapeutic stress.

4.6.3 Stress-specific interactome of RBPMSA and RBPMSB

The interaction between RBPMS and PS components under basal physiological conditions warrants further investigation into how the RBPMS protein-protein interaction network adapts to chemotherapeutic stressors such as doxorubicin. If the RBPMS interactome remains largely conserved during doxorubicin exposure, this would support the presence of a stable PS structural core that persists even in the absence of acute cellular stress, thereby positioning RBPMS as a constitutive architectural component of PSs. This hypothesis can be addressed by performing immunoprecipitation coupled with mass spectrometry under both steady-state and doxorubicin-treated conditions. A comparative analysis of the resulting interactomes will determine whether RBPMS retains stable associations with core PS proteins or undergoes stress-induced remodeling of its interaction network. Such an approach will yield valuable insights into the dynamics and functional significance of RBPMS-containing complexes during cellular stress adaptation.

References

1. Adriaens, C., Standaert, L., Barra, J., Latil, M., Verfaillie, A., Kalev, P., Boeckx, B., Wijnhoven, P.W.G., Radaelli, E., Vermi, W., Leucci, E., Lapouge, G., Beck, B., van den Oord, J., Nakagawa, S., Hirose, T., Sablina, A.A., Lambrechts, D., Aerts, S., Blanpain, C., Marine, J.-C. (2016). p53 induces formation of NEAT1 lncRNA-containing paraspeckles that modulate replication stress response and chemosensitivity. *Nat Med 22*, 861–868. https://doi.org/10.1038/nm.4135
2. Akerberg, A.A., Burns, C.E., Burns, C.G. (2019). Exploring the activities of RBPMS proteins in myocardial biology. *Pediatric cardiology 40*, 1410–1418. https://doi.org/10.1007/s00246-019-02180-6
3. Alfano, L., Costa, C., Caporaso, A., Altieri, A., Indovina, P., Macaluso, M., Giordano, A., Pentimalli, F. (2016). NONO regulates the intra-S-phase checkpoint in response to UV radiation. *Oncogene 35*, 567–576. https://doi.org/10.1038/onc.2015.107
4. An, H., Shelkovnikova, T.A. (2019). Stress granules regulate paraspeckles: RNP granule continuum at work. *Cell Stress 3*, 385–387. https://doi.org/10.15698/cst2019.12.207
5. An, H., Tan, J.T., Shelkovnikova, T.A. (2019). Stress granules regulate stress-induced paraspeckle assembly. *Journal of Cell Biology 218*, 4127–4140. https://doi.org/10.1083/jcb.201904098
6. An, H., Williams, N.G., Shelkovnikova, T.A., 2018. NEAT1 and paraspeckles in neurodegenerative diseases: A missing lnc found? Noncoding RNA Res 3, 243–252. https://doi.org/10.1016/j.ncrna.2018.11.003
7. Anderson, P., Kedersha, N. (2008). Stress granules: the Tao of RNA triage. *Trends in Biochemical Sciences 33*, 141–150. https://doi.org/10.1016/j.tibs.2007.12.003
8. Andoh, T. (1998). Bis(2,6-dioxopiperazines), catalytic inhibitors of DNA topoisomerase II, as molecular probes, cardiprotectors and antitumor drugs. *Biochimie 80*, 235–246. https://doi.org/10.1016/S0300-9084(98)80006-0
9. Angel, M., Fleshler, E., Atrash, M.K., Kinor, N., Benichou, J.I.C., Shav-Tal, Y. (2024). Nuclear RNA-related processes modulate the assembly of cytoplasmic RNA granules. *Nucleic Acids Research 52*, 5356–5375. https://doi.org/10.1093/nar/gkae119
10. Änkö, M.-L., Müller-McNicoll, M., Brandl, H., Curk, T., Gorup, C., Henry, I., Ule, J., Neugebauer, K.M. (2012). The RNA-binding landscapes of two SR proteins reveal unique functions and binding to diverse RNA classes. *Genome Biology 13*, R17. https://doi.org/10.1186/gb-2012-13-3-r17
11. Anufrieva, K.S., Shender, V.O., Arapidi, G.P., Pavlyukov, M.S., Shakhparonov, M.I., Shnaider, P.V., Butenko, I.O., Lagarkova, M.A., Govorun, V.M. (2018). Therapy-induced stress response is associated with downregulation of pre-mRNA splicing in cancer cells. *Genome Medicine 10*, 49. https://doi.org/10.1186/s13073-018-0557-y
12. Arai, T., Hasegawa, M., Akiyama, H., Ikeda, K., Nonaka, T., Mori, H., Mann, D., Tsuchiya, K., Yoshida, M., Hashizume, Y., Oda, T., 2006. TDP-43 is a component of ubiquitin-positive tau-negative inclusions in frontotemporal lobar degeneration and amyotrophic lateral sclerosis. Biochemical and Biophysical Research Communications 351, 602–611. https://doi.org/10.1016/j.bbrc.2006.10.093
13. Arimoto, K., Fukuda, H., Imajoh-Ohmi, S., Saito, H., Takekawa, M. (2008). Formation of stress granules inhibits apoptosis by suppressing stress-responsive MAPK pathways. *Nat Cell Biol 10*, 1324–1332. https://doi.org/10.1038/ncb1791
14. Arnold, B., Kessler, L., Okuda, E.K., Riegger, R.J., Cañás, M.C.H., Zebrowska, E., Bakisoglu, C., Nagasse, H.Y., Stanek, D., Dormann, D., Zarnack, K., Heilemann, M.,

Müller-McNicoll, M. (2024). Rapid depletion and super-resolution microscopy reveal an unexpected role of the nuclear-speckle protein SRSF5 in paraspeckle assembly and dynamics during cellular stress. *BioRxiv*. https://doi.org/10.1101/2024.08.11.607506
15. Asadi, M.R., Moslehian, M.S., Sabaie, H., Poornabi, M., Ghasemi, E., Hassani, M., Hussen, B.M., Taheri, M., Rezazadeh, M. (2021). Stress Granules in the Anti-Cancer Medications Mechanism of Action: A Systematic Scoping Review. *Front Oncol 11*, 797549. https://doi.org/10.3389/fonc.2021.797549
16. Ashburner, M., Ball, C.A., Blake, J.A., Botstein, D., Butler, H., Cherry, J.M., Davis, A.P., Dolinski, K., Dwight, S.S., Eppig, J.T., Harris, M.A., Hill, D.P., Issel-Tarver, L., Kasarskis, A., Lewis, S., Matese, J.C., Richardson, J.E., Ringwald, M., Rubin, G.M., Sherlock, G., 2000. Gene ontology: tool for the unification of biology. The Gene Ontology Consortium. Nat Genet 25, 25–29. https://doi.org/10.1038/75556
17. Aulas, A., Fay, M.M., Lyons, S.M., Achorn, C.A., Kedersha, N., Anderson, P., Ivanov, P. (2017). Stress-specific differences in assembly and composition of stress granules and related foci. *Journal of Cell Science jcs*.199240. https://doi.org/10.1242/jcs.199240
18. Aulas, A., Vande Velde, C. (2015). Alterations in stress granule dynamics driven by TDP-43 and FUS: a link to pathological inclusions in ALS? *Front Cell Neurosci 9*, 423. https://doi.org/10.3389/fncel.2015.00423
19. Azam, S., Armijo, K.S., Weindel, C.G., Chapman, M.J., Devigne, A., Nakagawa, S., Hirose, T., Carpenter, S., Watson, R.O., Patrick, K.L., 2024. The early macrophage response to pathogens requires dynamic regulation of the nuclear paraspeckle. Proc Natl Acad Sci U S A 121, e2312587121. https://doi.org/10.1073/pnas.2312587121
20. Azarova, A.M., Lyu, Y.L., Lin, C.-P., Tsai, Y.-C., Lau, J.Y.-N., Wang, J.C., Liu, L.F., 2007. Roles of DNA topoisomerase II isozymes in chemotherapy and secondary malignancies. *Proc Natl Acad Sci U S A 104*, 11014–11019. https://doi.org/10.1073/pnas.0704002104
21. Banani, S.F., Lee, H.O., Hyman, A.A., Rosen, M.K., 2017. Biomolecular condensates: organizers of cellular biochemistry. *Nat Rev Mol Cell Biol 18*, 285–298. https://doi.org/10.1038/nrm.2017.7
22. Banerjee, A., Vest, K.E., Pavlath, G.K., Corbett, A.H., 2017. Nuclear poly(A) binding protein 1 (PABPN1) and Matrin3 interact in muscle cells and regulate RNA processing. *Nucleic Acids Research 45*, 10706–10725. https://doi.org/10.1093/nar/gkx786
23. Barbarics, B., Eildermann, K., Kaderali, L., Cyganek, L., Plessmann, U., Bodemeyer, J., Paul, T., Ströbel, P., Urlaub, H., Tirilomis, T., Lenz, C., Bohnenberger, H., 2021. Proteomic mapping of atrial and ventricular heart tissue in patients with aortic valve stenosis. *Sci Rep 11*, 24389. https://doi.org/10.1038/s41598-021-03907-3
24. Barnabe, N., Butler, M., Hasinoff, B.B., n.d. The effect of the catalytic topoisomerase II inhibitor dexrazoxane (ICRF-187) on CC9C10 hybridoma viability and productivity.
25. Barnhart, M.D., Yang, Y., Nakagaki-Silva, E.E., Hammond, T.H., Pizzinga, M., Gooding, C., Stott, K., Smith, C.W.J., 2022a. Phosphorylation of the smooth muscle master splicing regulator RBPMS regulates its splicing activity. Nucleic Acids Res 50, 11895–11915. https://doi.org/10.1093/nar/gkac1048
26. Barutcu, A.R., Wu, M., Braunschweig, U., Dyakov, B.J.A., Luo, Z., Turner, K.M., Durbic, T., Lin, Z.-Y., Weatheritt, R.J., Maass, P.G., Gingras, A.-C., Blencowe, B.J., 2022. Systematic mapping of nuclear domain-associated transcripts reveals speckles and lamina as hubs of functionally distinct retained introns. Molecular Cell 82, 1035-1052.e9. https://doi.org/10.1016/j.molcel.2021.12.010

27. Bashkirov, V.I., Scherthan, H., Solinger, J.A., Buerstedde, J.-M., Heyer, W.-D., 1997. A Mouse Cytoplasmic Exoribonuclease (mXRN1p) with Preference for G4 Tetraplex Substrates. Journal of Cell Biology 136, 761–773. https://doi.org/10.1083/jcb.136.4.761
28. Baymiller, M., Moon, S.L., 2023. Stress Granules as Causes and Consequences of Translation Suppression. Antioxid Redox Signal 39, 390–409. https://doi.org/10.1089/ars.2022.0164
29. Belger, C., Abrahams, C., Imamdin, A., Lecour, S., 2023. Doxorubicin-induced cardiotoxicity and risk factors. Int J Cardiol Heart Vasc 50, 101332. https://doi.org/10.1016/j.ijcha.2023.101332
30. Benhusein, GhazallaM., Mutch, E., Aburawi, S., Williams, FaithM., 2010. Genotoxic effect induced by hydrogen peroxide in human hepatoma cells using comet assay. Libyan Journal of Medicine 5, 4637. https://doi.org/10.3402/ljm.v5i0.4637
31. Bhagat, A., Kleinerman, E.S., 2020. Anthracycline-Induced Cardiotoxicity: Causes, Mechanisms, and Prevention, in: Kleinerman, E.S., Gorlick, R. (Eds.), Current Advances in Osteosarcoma: Clinical Perspectives: Past, Present and Future. Springer International Publishing, Cham, pp. 181–192. https://doi.org/10.1007/978-3-030-43032-0_15
32. Biamonti, G., Vourc'h, C., 2010. Nuclear Stress Bodies. Cold Spring Harb Perspect Biol 2, a000695. https://doi.org/10.1101/cshperspect.a000695
33. Boeynaems, S., Chong, S., Gsponer, J., Holt, L., Milovanovic, D., Mitrea, D.M., Mueller-Cajar, O., Portz, B., Reilly, J.F., Reinkemeier, C.D., Sabari, B.R., Sanulli, S., Shorter, J., Sontag, E., Strader, L., Stachowiak, J., Weber, S.C., White, M., Zhang, H., Zweckstetter, M., Elbaum-Garfinkle, S., Kriwacki, R., 2023. Phase Separation in Biology and Disease; Current Perspectives and Open Questions. Journal of Molecular Biology 435, 167971. https://doi.org/10.1016/j.jmb.2023.167971
34. Boisvert, F.-M., van Koningsbruggen, S., Navascués, J., Lamond, A.I., 2007. The multifunctional nucleolus. Nat Rev Mol Cell Biol 8, 574–585. https://doi.org/10.1038/nrm2184
35. Bolger, A.M., Lohse, M., Usadel, B., 2014. Trimmomatic: a flexible trimmer for Illumina sequence data. Bioinformatics 30, 2114–2120. https://doi.org/10.1093/bioinformatics/btu170
36. Borcherds, W., Bremer, A., Borgia, M.B., Mittag, T., 2020. How do intrinsically disordered protein regions encode a driving force for liquid-liquid phase separation? Current opinion in structural biology 67, 41. https://doi.org/10.1016/j.sbi.2020.09.004
37. Bose, J.K., Huang, C.-C., Shen, C.-K.J., 2011. Regulation of Autophagy by Neuropathological Protein TDP-43. J Biol Chem 286, 44441–44448. https://doi.org/10.1074/jbc.M111.237115
38. Bosire, R., Fadel, L., Mocsár, G., Nánási, P., Sen, P., Sharma, A.K., Naseem, M.U., Kovács, A., Kugel, J., Kroemer, G., Vámosi, G., Szabó, G., 2022. Doxorubicin impacts chromatin binding of HMGB1, Histone H1 and retinoic acid receptor. Sci Rep 12, 8087. https://doi.org/10.1038/s41598-022-11994-z
39. Brangwynne, C.P., Tompa, P., Pappu, R.V., 2015. Polymer physics of intracellular phase transitions. Nature Phys 11, 899–904. https://doi.org/10.1038/nphys3532
40. Branon, T.C., Bosch, J.A., Sanchez, A.D., Udeshi, N.D., Svinkina, T., Carr, S.A., Feldman, J.L., Perrimon, N., Ting, A.Y., 2018a. Efficient proximity labeling in living cells and organisms with TurboID. Nat Biotechnol 36, 880–887. https://doi.org/10.1038/nbt.4201
41. Branon, T.C., Bosch, J.A., Sanchez, A.D., Udeshi, N.D., Svinkina, T., Carr, S.A., Feldman, J.L., Perrimon, N., Ting, A.Y., 2017. Directed evolution of TurboID for

efficient proximity labeling in living cells and organisms. https://doi.org/10.1101/196980
42. Buchan, J.R., 2014. mRNP granules. RNA Biol 11, 1019–1030. https://doi.org/10.4161/15476286.2014.972208
43. Buchan, J.R., Parker, R., 2009. Eukaryotic stress granules: the ins and outs of translation. Mol Cell 36, 932–941. https://doi.org/10.1016/j.molcel.2009.11.020
44. Bugger, H., Guzman, C., Zechner, C., Palmeri, M., Russell, K.S., Russell, R.R., 2011. UNCOUPLING PROTEIN DOWNREGULATION IN DOXORUBICIN INDUCED HEART FAILURE IMPROVES MITOCHONDRIAL COUPLING BUT INCREASES REACTIVE OXYGEN SPECIES GENERATION. Cancer Chemother Pharmacol 67, 1381–1388. https://doi.org/10.1007/s00280-010-1441-7
45. Burgess, R.C., Burman, B., Kruhlak, M., Misteli, T., 2014. Activation of DNA damage response signaling by condensed chromatin. Cell Rep 9, 1703–1717. https://doi.org/10.1016/j.celrep.2014.10.060
46. Busà, R., Geremia, R., Sette, C., 2010. Genotoxic stress causes the accumulation of the splicing regulator Sam68 in nuclear foci of transcriptionally active chromatin. Nucleic Acids Research 38, 3005–3018. https://doi.org/10.1093/nar/gkq004
47. Caforio, A.L.P., Pankuweit, S., Arbustini, E., Basso, C., Gimeno-Blanes, J., Felix, S.B., Fu, M., Heliö, T., Heymans, S., Jahns, R., Klingel, K., Linhart, A., Maisch, B., McKenna, W., Mogensen, J., Pinto, Y.M., Ristic, A., Schultheiss, H.-P., Seggewiss, H., Tavazzi, L., Thiene, G., Yilmaz, A., Charron, P., Elliott, P.M., European Society of Cardiology Working Group on Myocardial and Pericardial Diseases, 2013. Current state of knowledge on aetiology, diagnosis, management, and therapy of myocarditis: a position statement of the European Society of Cardiology Working Group on Myocardial and Pericardial Diseases. Eur Heart J 34, 2636–2648, 2648a–2648d. https://doi.org/10.1093/eurheartj/eht210
48. Campagne, S., Jutzi, D., Malard, F., Matoga, M., Romane, K., Feldmuller, M., Colombo, M., Ruepp, M.-D., Allain, F.H.-T., 2023. Molecular basis of RNA-binding and autoregulation by the cancer-associated splicing factor RBM39. Nat Commun 14, 5366. https://doi.org/10.1038/s41467-023-40254-5
49. Cao, J., Wei, Z., Nie, Y., Chen, H.-Z., 2024. Therapeutic potential of alternative splicing in cardiovascular diseases. eBioMedicine 101. https://doi.org/10.1016/j.ebiom.2024.104995
50. Carvill, G.L., Mefford, H.C., 2020. Poison exons in neurodevelopment and disease. Current Opinion in Genetics & Development, Molecular and Genetic Bases of Disease 65, 98–102. https://doi.org/10.1016/j.gde.2020.05.030
51. Chabot, B., n.d. hnRNP and hnRNP-Like Proteins in Splicing Control: Molecular Mechanisms and Implication in Human Pathologies.
52. Chatterjee, K., Zhang, J., Honbo, N., Karliner, J.S., 2010. Doxorubicin Cardiomyopathy. Cardiology 115, 155–162. https://doi.org/10.1159/000265166
53. Chen, X., Liu, Ying, Xu, C., Ba, L., Liu, Z., Li, Xiuya, Huang, J., Simpson, E., Gao, H., Cao, D., Sheng, W., Qi, H., Ji, H., Sanderson, M., Cai, C.-L., Li, Xiaohui, Yang, L., Na, J., Yamamura, K., Liu, Yunlong, Huang, G., Shou, W., Sun, N., 2021. QKI is a critical pre-mRNA alternative splicing regulator of cardiac myofibrillogenesis and contractile function. Nat Commun 12, 89. https://doi.org/10.1038/s41467-020-20327-5
54. Chitiprolu, M., Jagow, C., Tremblay, V., Bondy-Chorney, E., Paris, G., Savard, A., Palidwor, G., Barry, F.A., Zinman, L., Keith, J., Rogaeva, E., Robertson, J., Lavallée-Adam, M., Woulfe, J., Couture, J.-F., Côté, J., Gibbings, D., 2018. A complex of C9ORF72 and p62 uses arginine methylation to eliminate stress granules by autophagy. Nature Communications 9, 2794. https://doi.org/10.1038/s41467-018-05273-7

55. Choi-Rhee, E., Schulman, H., Cronan, J.E., 2004. Promiscuous protein biotinylation by Escherichia coli biotin protein ligase. Protein Science 13, 3043–3050. https://doi.org/10.1110/ps.04911804
56. Coller, J.M., Tucker, M., Sheth, U., Valencia-Sanchez, M.A., Parker, R., 2001. The DEAD box helicase, Dhh1p, functions in mRNA decapping and interacts with both the decapping and deadenylase complexes. RNA 7, 1717–1727. https://doi.org/10.1017/s135583820101994x
57. Colwill, K., Pawson, T., Andrews, B., Prasad, J., Manley, J.L., Bell, J.C., Duncan, P.I., 1996. The Clk/Sty protein kinase phosphorylates SR splicing factors and regulates their intranuclear distribution. EMBO J 15, 265–275.
58. Conlon, E.G., Manley, J.L., 2017a. RNA-binding proteins in neurodegeneration: mechanisms in aggregate. Genes Dev 31, 1509–1528. https://doi.org/10.1101/gad.304055.117
59. Cookson, M.R., 2017. RNA-binding proteins implicated in Neurodegenerative diseases. Wiley Interdiscip Rev RNA 8, 10.1002/wrna.1397. https://doi.org/10.1002/wrna.1397
60. Corbet, G.A., Parker, R., 2020. RNP Granule Formation: Lessons from P-Bodies and Stress Granules. Cold Spring Harb Symp Quant Biol 040329. https://doi.org/10.1101/sqb.2019.84.040329
61. Corley, M., Burns, M.C., Yeo, G.W., 2020. How RNA binding proteins interact with RNA: molecules and mechanisms. Mol Cell 78, 9–29. https://doi.org/10.1016/j.molcel.2020.03.011
62. Costa, I.D., Buchanan, C.N., Zdradzinski, M.D., Sahoo, P.K., Smith, T.P., Thames, E., Kar, A.N., Twiss, J.L., 2021. The functional organization of axonal mRNA transport and translation. Nat Rev Neurosci 22, 77–91. https://doi.org/10.1038/s41583-020-00407-7
63. Cronan, J.E., 2005. Targeted and proximity-dependent promiscuous protein biotinylation by a mutant Escherichia coli biotin protein ligase. The Journal of Nutritional Biochemistry 16, 416–418. https://doi.org/10.1016/j.jnutbio.2005.03.017
64. Cruz-Garcia, Y., Barkovits, K., Kohlhaas, M., Pickel, S., Gulentz, M., Heindl, C., Pfeiffer, K., Eder-Negrin, P., Maack, C., Marcus, K., Kuhn, M., Miranda-Laferte, E., 2022. Nanoenviroments of the β-Subunit of L-Type Voltage-Gated Calcium Channels in Adult Cardiomyocytes. Front Cell Dev Biol 9, 724778. https://doi.org/10.3389/fcell.2021.724778
65. Cui, N., Wu, F., Lu, W., Bai, R., Ke, B., Liu, T., Li, L., Lan, F., Cui, M., 2019. Doxorubicin-induced cardiotoxicity is maturation dependent due to the shift from topoisomerase IIα to IIβ in human stem cell derived cardiomyocytes. J Cell Mol Med 23, 4627–4639. https://doi.org/10.1111/jcmm.14346
66. Cox, J., Mann, M., 2008. MaxQuant enables high peptide identification rates, individualized p.p.b.-range mass accuracies and proteome-wide protein quantification. Nat Biotechnol 26, 1367–1372. https://doi.org/10.1038/nbt.1511
67. Cox, J., Neuhauser, N., Michalski, A., Scheltema, R.A., Olsen, J.V., Mann, M., 2011. Andromeda: a peptide search engine integrated into the MaxQuant environment. J Proteome Res 10, 1794–1805. https://doi.org/10.1021/pr101065j
68. Cykowski, M.D., Powell, S.Z., Appel, J.W., Arumanayagam, A.S., Rivera, A.L., Appel, S.H., 2018a. Phosphorylated TDP-43 (pTDP-43) aggregates in the axial skeletal muscle of patients with sporadic and familial amyotrophic lateral sclerosis. Acta Neuropathologica Communications 6, 28. https://doi.org/10.1186/s40478-018-0528-y
69. Da Cruz, S., Cleveland, D.W., 2011. Understanding the role of TDP-43 and FUS/TLS in ALS and beyond. Current Opinion in Neurobiology, Neurobiology of disease 21, 904–919. https://doi.org/10.1016/j.conb.2011.05.029

70. Dao, T.P., Rajendran, A., Galagedera, S.K.K., Haws, W., Castañeda, C.A., 2023. Short N-terminal disordered regions and the proline-rich domain are major regulators of phase transitions for full-length UBQLN1, UBQLN2 and UBQLN4. bioRxiv 2023.09.27.559790. https://doi.org/10.1101/2023.09.27.559790
71. Das, R.K., Ruff, K.M., Pappu, R.V., 2015. Relating sequence encoded information to form and function of intrinsically disordered proteins. Current opinion in structural biology 32, 102. https://doi.org/10.1016/j.sbi.2015.03.008
72. De Boer, E.M.J., Orie, V.K., Williams, T., Baker, M.R., De Oliveira, H.M., Polvikoski, T., Silsby, M., Menon, P., van den Bos, M., Halliday, G.M., van den Berg, L.H., Van Den Bosch, L., van Damme, P., Kiernan, M., van Es, M.A., Vucic, S., 2021. TDP-43 proteinopathies: a new wave of neurodegenerative diseases. J Neurol Neurosurg Psychiatry 92, 86–95. https://doi.org/10.1136/jnnp-2020-322983
73. De Bruin, R.G., Rabelink, T.J., van Zonneveld, A.J., van der Veer, E.P., 2017. Emerging roles for RNA-binding proteins as effectors and regulators of cardiovascular disease. European Heart Journal 38, 1380–1388. https://doi.org/10.1093/eurheartj/ehw567
74. De Silva, H.C., Lin, M.Z., Phillips, L., Martin, J.L., Baxter, R.C., 2019. IGFBP-3 interacts with NONO and SFPQ in PARP-dependent DNA damage repair in triple-negative breast cancer. Cell Mol Life Sci 76, 2015–2030. https://doi.org/10.1007/s00018-019-03033-4
75. Deng, S., Yan, T., Jendrny, C., Nemecek, A., Vincetic, M., Gödtel-Armbrust, U., Wojnowski, L., 2014. Dexrazoxane may prevent doxorubicin-induced DNA damage via depleting both Topoisomerase II isoforms. BMC Cancer 14, 842. https://doi.org/10.1186/1471-2407-14-842
76. De Oliveira Freitas Machado, C., Schafranek, M., Brüggemann, M., Hernández Cañás, M.C., Keller, M., Di Liddo, A., Brezski, A., Blümel, N., Arnold, B., Bremm, A., Wittig, I., Jaé, N., McNicoll, F., Dimmeler, S., Zarnack, K., Müller-McNicoll, M., 2023a. Poison cassette exon splicing of SRSF6 regulates nuclear speckle dispersal and the response to hypoxia. Nucleic Acids Research 51, 870–890. https://doi.org/10.1093/nar/gkac1225
77. Deutschmeyer, V., Breuer, J., Walesch, S.K., Sokol, A.M., Graumann, J., Bartkuhn, M., Boettger, T., Rossbach, O., Richter, A.M., 2019. Epigenetic therapy of novel tumour suppressor ZAR1 and its cancer biomarker function. Clin Epigenetics 11, 182. https://doi.org/10.1186/s13148-019-0774-2
78. Dixon, D.M., Choi, J., El-Ghazali, A., Park, S.Y., Roos, K.P., Jordan, M.C., Fishbein, M.C., Comai, L., Reddy, S., 2015. Loss of muscleblind-like 1 results in cardiac pathology and persistence of embryonic splice isoforms. Sci Rep 5, 9042. https://doi.org/10.1038/srep09042
79. Dobin, A., Davis, C.A., Schlesinger, F., Drenkow, J., Zaleski, C., Jha, S., Batut, P., Chaisson, M., Gingeras, T.R., 2013. STAR: ultrafast universal RNA-seq aligner. Bioinformatics 29, 15–21. https://doi.org/10.1093/bioinformatics/bts635
80. Dornfeld, K., Bjork, J., Folkert, G., Skildum, A., Wallace, K.B., n.d. Mitochondrial activities play a pivotal role in regulating cell cycle in response to doxorubicin. Cell Cycle 20, 1067–1079. https://doi.org/10.1080/15384101.2021.1919839
81. Emara, M.M., Fujimura, K., Sciaranghella, D., Ivanova, V., Ivanov, P., Anderson, P., 2012. Hydrogen peroxide induces stress granule formation independent of eIF2α phosphorylation. Biochem Biophys Res Commun 423, 763–769. https://doi.org/10.1016/j.bbrc.2012.06.033
82. Eom, Y.-W., Kim, M.A., Park, S.S., Goo, M.J., Kwon, H.J., Sohn, S., Kim, W.-H., Yoon, G., Choi, K.S., 2005. Two distinct modes of cell death induced by doxorubicin:

apoptosis and cell death through mitotic catastrophe accompanied by senescence-like phenotype. Oncogene 24, 4765–4777. https://doi.org/10.1038/sj.onc.1208627
83. Erhardt, S., Stoecklin, G., 2020. The heat's on: nuclear stress bodies signal intron retention. EMBO J 39, e104154. https://doi.org/10.15252/embj.2019104154
84. Fabre, A., Sheppard, M.N., 2006. Sudden adult death syndrome and other non-ischaemic causes of sudden cardiac death. Heart 92, 316–320. https://doi.org/10.1136/hrt.2004.045518
85. Fagg, W.S., Liu, N., Fair, J.H., Shiue, L., Katzman, S., Donohue, J.P., Ares, M., 2017. Autogenous cross-regulation of Quaking mRNA processing and translation balances Quaking functions in splicing and translation. Genes Dev 31, 1894–1909. https://doi.org/10.1101/gad.302059.117
86. Farah, N., Dresner, H.S., Searles, K.J., Winiarsky, R., Moosikasuwan, M., Cajigas, A., Hahm, S., Steinberg, J.J., 2000. Cisplatin DNA Adduct Detection and Depurination Measured by 32P DNA Radiolabeling and Two-Dimensional Thin-Layer Chromatography: A Time and Concentration Study. Cancer Investigation 18, 314–326. https://doi.org/10.3109/07357900009012174
87. Farazi, T.A., Leonhardt, C.S., Mukherjee, N., Mihailovic, A., Li, S., Max, K.E.A., Meyer, C., Yamaji, M., Cekan, P., Jacobs, N.C., Gerstberger, S., Bognanni, C., Larsson, E., Ohler, U., Tuschl, T., 2014b. Identification of the RNA recognition element of the RBPMS family of RNA-binding proteins and their transcriptome-wide mRNA targets. RNA 20, 1090–1102. https://doi.org/10.1261/rna.045005.114
88. Farrell, P.J., Balkow, K., Hunt, T., Jackson, R.J., Trachsel, H., 1977. Phosphorylation of initiation factor eIF-2 and the control of reticulocyte protein synthesis. Cell 11, 187–200. https://doi.org/10.1016/0092-8674(77)90330-0
89. Filimonenko, M., Stuffers, S., Raiborg, C., Yamamoto, A., Malerød, L., Fisher, E.M.C., Isaacs, A., Brech, A., Stenmark, H., Simonsen, A., 2007. Functional multivesicular bodies are required for autophagic clearance of protein aggregates associated with neurodegenerative disease. J Cell Biol 179, 485–500. https://doi.org/10.1083/jcb.200702115
90. Fortune, J.M., Osheroff, N., 2000. Topoisomerase II as a target for anticancer drugs: When enzymes stop being nice, in: Progress in Nucleic Acid Research and Molecular Biology. Academic Press, pp. 221–253. https://doi.org/10.1016/S0079-6603(00)64006-0
91. Fox, A.H., 2018. A mitochondria–paraspeckle crosstalk. Nat Cell Biol 20, 1108–1109. https://doi.org/10.1038/s41556-018-0207-z
92. Fox, A.H., Lam, Y.W., Leung, A.K.L., Lyon, C.E., Andersen, J., Mann, M., Lamond, A.I., 2002. Paraspeckles: A Novel Nuclear Domain. Current Biology 12, 13–25. https://doi.org/10.1016/S0960-9822(01)00632-7
93. Freibaum, B.D., Messing, J., Yang, P., Kim, H.J., Taylor, J.P., 2021. High-fidelity reconstitution of stress granules and nucleoli in mammalian cellular lysate. J Cell Biol 220, e202009079. https://doi.org/10.1083/jcb.202009079
94. Furuta, M., Kose, S., Koike, M., Shimi, T., Hiraoka, Y., Yoneda, Y., Haraguchi, T., Imamoto, N., 2004. Heat-shock induced nuclear retention and recycling inhibition of importin α. Genes to Cells 9, 429–441. https://doi.org/10.1111/j.1356-9597.2004.00734.x
95. Gallina, I., Colding, C., Henriksen, P., Beli, P., Nakamura, K., Offman, J., Mathiasen, D.P., Silva, S., Hoffmann, E., Groth, A., Choudhary, C., Lisby, M., 2015. Cmr1/WDR76 defines a nuclear genotoxic stress body linking genome integrity and protein quality control. Nat Commun 6, 6533. https://doi.org/10.1038/ncomms7533
96. Gan, P., Wang, Z., Bezprozvannaya, S., McAnally, J.R., Tan, W., Li, H., Bassel-Duby, R., Liu, N., Olson, E.N., 2023. RBPMS regulates cardiomyocyte contraction and

cardiac function through RNA alternative splicing. Cardiovasc Res 120, 56–68. https://doi.org/10.1093/cvr/cvad166
97. Gao, C., Ren, S., Lee, J.-H., Qiu, J., Chapski, D.J., Rau, C.D., Zhou, Y., Abdellatif, M., Nakano, A., Vondriska, T.M., Xiao, X., Fu, X.-D., Chen, J.-N., Wang, Y., n.d. RBFox1-mediated RNA splicing regulates cardiac hypertrophy and heart failure. J Clin Invest 126, 195–206. https://doi.org/10.1172/JCI84015
98. Gao, L., Emperle, M., Guo, Y., Grimm, S.A., Ren, W., Adam, S., Uryu, H., Zhang, Z.-M., Chen, D., Yin, J., Dukatz, M., Anteneh, H., Jurkowska, R.Z., Lu, J., Wang, Y., Bashtrykov, P., Wade, P.A., Wang, G.G., Jeltsch, A., Song, J., 2020. Comprehensive structure-function characterization of DNMT3B and DNMT3A reveals distinctive de novo DNA methylation mechanisms. Nat Commun 11, 3355. https://doi.org/10.1038/s41467-020-17109-4
99. Gao, X., Kong, L., Lu, X., Zhang, G., Chi, L., Jiang, Y., Wu, Y., Yan, C., Duerksen-Hughes, P., Zhu, X., Yang, J., 2014b. Paraspeckle Protein 1 (PSPC1) Is Involved in the Cisplatin Induced DNA Damage Response—Role in G1/S Checkpoint. PLoS One 9, e97174. https://doi.org/10.1371/journal.pone.0097174
100. Garg, A., Kumar, G., Singh, V., Sinha, S., 2024. Doxorubicin catalyses self-assembly of p53 by phase separation. Curr Res Struct Biol 7, 100133. https://doi.org/10.1016/j.crstbi.2024.100133
101. Garloff, V., Krüger, T., Brakhage, A., Rubio, I., 2023. Control of TurboID-dependent biotinylation intensity in proximity ligation screens. Journal of Proteomics 279, 104886. https://doi.org/10.1016/j.jprot.2023.104886
102. Gerber, W.V., Vokes, S.A., Zearfoss, N.R., Krieg, P.A., 2002. A Role for the RNA-Binding Protein, hermes, in the Regulation of Heart Development. Developmental Biology 247, 116–126. https://doi.org/10.1006/dbio.2002.0678
103. Gerber, W.V., Yatskievych, T.A., Antin, P.B., Correia, K.M., Conlon, R.A., Krieg, P.A., 1999. The RNA-binding protein gene, hermes, is expressed at high levels in the developing heart. Mechanisms of Development 80, 77–86. https://doi.org/10.1016/S0925-4773(98)00195-6
104. Giudice, J., Xia, Z., Wang, E.T., Scavuzzo, M.A., Ward, A.J., Kalsotra, A., Wang, W., Wehrens, X.H.T., Burge, C.B., Li, W., Cooper, T.A., 2014. Alternative splicing regulates vesicular trafficking genes in cardiomyocytes during postnatal heart development. Nat Commun 5, 3603. https://doi.org/10.1038/ncomms4603
105. Goenka, A., Sengupta, S., Pandey, R., Parihar, R., Mohanta, G.C., Mukerji, M., Ganesh, S., 2016. Human satellite-III non-coding RNAs modulate heat-shock-induced transcriptional repression. J Cell Sci 129, 3541–3552. https://doi.org/10.1242/jcs.189803
106. Goody, P.R., Hosen, M.R., Christmann, D., Niepmann, S.T., Zietzer, A., Adam, M., Bönner, F., Zimmer, S., Nickenig, G., Jansen, F., 2020. Aortic Valve Stenosis. Arteriosclerosis, Thrombosis, and Vascular Biology 40, 885–900. https://doi.org/10.1161/ATVBAHA.119.313067
107. Grosch, M., n.d. The function of paraspeckle components in pluripotency maintenance and differentiation.
108. Grosch, M., Ittermann, S., Shaposhnikov, D., Drukker, M., 2020. Chromatin-Associated Membraneless Organelles in Regulation of Cellular Differentiation. Stem Cell Reports 15, 1220–1232. https://doi.org/10.1016/j.stemcr.2020.10.011
109. Guan, Y., Wang, Y., Fu, X., Bai, G., Li, X., Mao, J., Yan, Y., Hu, L., 2023. Multiple functions of stress granules in viral infection at a glance. Frontiers in Microbiology 14, 1138864. https://doi.org/10.3389/fmicb.2023.1138864
110. Gui, J.F., Tronchère, H., Chandler, S.D., Fu, X.D., 1994. Purification and characterization of a kinase specific for the serine- and arginine-rich pre-mRNA

splicing factors. Proc Natl Acad Sci U S A 91, 10824–10828. https://doi.org/10.1073/pnas.91.23.10824
111. Guo, H., Chitiprolu, M., Gagnon, D., Meng, L., Perez-Iratxeta, C., Lagace, D., Gibbings, D., 2014. Autophagy supports genomic stability by degrading retrotransposon RNA. Nat Commun 5, 5276. https://doi.org/10.1038/ncomms6276
112. Guo, W., Schafer, S., Greaser, M.L., Radke, M.H., Liss, M., Govindarajan, T., Maatz, H., Schulz, H., Li, S., Parrish, A.M., Dauksaite, V., Vakeel, P., Klaassen, S., Gerull, B., Thierfelder, L., Regitz-Zagrosek, V., Hacker, T.A., Saupe, K.W., Dec, G.W., Ellinor, P.T., MacRae, C.A., Spallek, B., Fischer, R., Perrot, A., Özcelik, C., Saar, K., Hubner, N., Gotthardt, M., 2012. RBM20, a gene for hereditary cardiomyopathy, regulates titin splicing. Nat Med 18, 766–773. https://doi.org/10.1038/nm.2693
113. Han, J., Ding, J.-H., Byeon, C.W., Kim, J.H., Hertel, K.J., Jeong, S., Fu, X.-D., 2011. SR Proteins Induce Alternative Exon Skipping through Their Activities on the Flanking Constitutive Exons. Mol Cell Biol 31, 793–802. https://doi.org/10.1128/MCB.01117-10
114. Harley, J., Clarke, B.E., Patani, R., 2021. The Interplay of RNA Binding Proteins, Oxidative Stress and Mitochondrial Dysfunction in ALS. Antioxidants 10, 552. https://doi.org/10.3390/antiox10040552
115. Harmon, T.S., Holehouse, A.S., Rosen, M.K., Pappu, R.V., 2017. Intrinsically disordered linkers determine the interplay between phase separation and gelation in multivalent proteins. eLife 6, e30294. https://doi.org/10.7554/eLife.30294
116. Hartl, F.U., Bracher, A., Hayer-Hartl, M., 2011. Molecular chaperones in protein folding and proteostasis. Nature 475, 324–332. https://doi.org/10.1038/nature10317
117. Hasenson, S.E., Shav-Tal, Y., 2020. Speculating on the Roles of Nuclear Speckles: How RNA-Protein Nuclear Assemblies Affect Gene Expression. BioEssays 42, 2000104. https://doi.org/10.1002/bies.202000104
118. Hasinoff, B.B., 1998. Chemistry of dexrazoxane and analogues. Semin Oncol 25, 3–9.
119. Hasinoff, B.B., Kuschak, T.I., Yalowich, J.C., Creighton, A.M., 1995. A QSAR study comparing the cytotoxicity and DNA topoisomerase II inhibitory effects of bisdioxopiperazine analogs of ICRF-187 (dexrazoxane). Biochem Pharmacol 50, 953–958. https://doi.org/10.1016/0006-2952(95)00218-o
120. Hellmann, K., 1998. Overview and historical development of dexrazoxane. Semin Oncol 25, 48–54.
121. Hennig, S., Kong, G., Mannen, T., Sadowska, A., Kobelke, S., Blythe, A., Knott, G.J., Iyer, K.S., Ho, D., Newcombe, E.A., Hosoki, K., Goshima, N., Kawaguchi, T., Hatters, D., Trinkle-Mulcahy, L., Hirose, T., Bond, C.S., Fox, A.H., 2015. Prion-like domains in RNA binding proteins are essential for building subnuclear paraspeckles. J Cell Biol 210, 529–539. https://doi.org/10.1083/jcb.201504117
122. Henriksen, P.A., 2018. Anthracycline cardiotoxicity: an update on mechanisms, monitoring and prevention. Heart 104, 971–977. https://doi.org/10.1136/heartjnl-2017-312103
123. Hensley, M.L., Hagerty, K.L., Kewalramani, T., Green, D.M., Meropol, N.J., Wasserman, T.H., Cohen, G.I., Emami, B., Gradishar, W.J., Mitchell, R.B., Thigpen, J.T., Trotti, A., von Hoff, D., Schuchter, L.M., 2009. American Society of Clinical Oncology 2008 clinical practice guideline update: use of chemotherapy and radiation therapy protectants. J Clin Oncol 27, 127–145. https://doi.org/10.1200/JCO.2008.17.2627
124. Hillman, R.T., Green, R.E., Brenner, S.E., 2004c. An unappreciated role for RNA surveillance. Genome Biology 5, R8. https://doi.org/10.1186/gb-2004-5-2-r8
125. Hirose, T., Ninomiya, K., Nakagawa, S., Yamazaki, T., 2023. A guide to membraneless organelles and their various roles in gene regulation. Nat Rev Mol Cell Biol 24, 288–304. https://doi.org/10.1038/s41580-022-00558-8

126.Hochberg-Laufer, H., Schwed-Gross, A., Neugebauer, K.M., Shav-Tal, Y., 2019. Uncoupling of nucleo-cytoplasmic RNA export and localization during stress. Nucleic Acids Res 47, 4778–4797. https://doi.org/10.1093/nar/gkz168
127.Hodgson, R., Huang, W.-P., Kumar, V., An, H., Chalakova, Z., Rayment, J., Ellis, B.C.S., Stender, E.G.P., van Vugt, J.J.F.A., Sequencing Consortium, P.M.A., Locker, N., Pitout, I., Fletcher, S., Cooper-Knock, J., Shelkovnikova, T., 2024. TDP-43 is a Master Regulator of Paraspeckle Condensation. https://doi.org/10.2139/ssrn.4721338
128.Holubarsch, C., Ruf, T., Goldstein, D.J., Ashton, R.C., Nickl, W., Pieske, B., Pioch, K., Lüdemann, J., Wiesner, S., Hasenfuss, G., Posival, H., Just, H., Burkhoff, D., 1996. Existence of the Frank-Starling mechanism in the failing human heart. Investigations on the organ, tissue, and sarcomere levels. Circulation 94, 683–689. https://doi.org/10.1161/01.cir.94.4.683
129.Hornberg, H., Wollerton-van Horck, F., Maurus, D., Zwart, M., Svoboda, H., Harris, W.A., Holt, C.E., 2013. RNA-Binding Protein Hermes/RBPMS Inversely Affects Synapse Density and Axon Arbor Formation in Retinal Ganglion Cells In Vivo. Journal of Neuroscience 33, 10384–10395. https://doi.org/10.1523/JNEUROSCI.5858-12.2013
130.Hörnberg, H., Wollerton-van Horck, F., Maurus, D., Zwart, M., Svoboda, H., Harris, W.A., Holt, C.E., 2013. RNA-binding protein Hermes/RBPMS inversely affects synapse density and axon arbor formation in retinal ganglion cells in vivo. J Neurosci 33, 10384–10395. https://doi.org/10.1523/JNEUROSCI.5858-12.2013
131.Hu, R., Qian, B., Li, A., Fang, Y., 2022. Role of Proteostasis Regulation in the Turnover of Stress Granules. Int J Mol Sci 23, 14565. https://doi.org/10.3390/ijms232314565
132.Huang, W.-P., Ellis, B.C.S., Hodgson, R.E., Sanchez Avila, A., Kumar, V., Rayment, J., Moll, T., Shelkovnikova, T.A., 2024. Stress-induced TDP-43 nuclear condensation causes splicing loss of function and STMN2 depletion. Cell Reports 43, 114421. https://doi.org/10.1016/j.celrep.2024.114421
133.Huang, Z., Zhang, H., Huang, C., Yi, R., Zhang, X., Ma, K., Huang, W., Wu, Q., Zhuang, Y., Liu, J., Liu, W., Guo, Y., Kang, X., Hu, X., Bai, X., Chen, Z., 2024. Cytoplasmic Aggregates of Splicing Factor Proline-Glutamine Rich Disrupt Nucleocytoplasmic Transport and Induce Persistent Stress Granules. Journal of Cellular and Molecular Medicine 28, e70261. https://doi.org/10.1111/jcmm.70261
134.Hubstenberger, A., Courel, M., Bénard, M., Souquere, S., Ernoult-Lange, M., Chouaib, R., Yi, Z., Morlot, J.-B., Munier, A., Fradet, M., Daunesse, M., Bertrand, E., Pierron, G., Mozziconacci, J., Kress, M., Weil, D., 2017. P-Body Purification Reveals the Condensation of Repressed mRNA Regulons. Mol Cell 68, 144-157.e5. https://doi.org/10.1016/j.molcel.2017.09.003
135.Huelsenbeck, S.C., Schorr, A., Roos, W.P., Huelsenbeck, J., Henninger, C., Kaina, B., Fritz, G., 2012. Rac1 Protein Signaling Is Required for DNA Damage Response Stimulated by Topoisomerase II Poisons*. Journal of Biological Chemistry 287, 38590–38599. https://doi.org/10.1074/jbc.M112.377903
136.Humphrey, J., Birsa, N., Milioto, C., McLaughlin, M., Ule, A.M., Robaldo, D., Eberle, A.B., Kräuchi, R., Bentham, M., Brown, A.-L., Jarvis, S., Bodo, C., Garone, M.G., Devoy, A., Soraru, G., Rosa, A., Bozzoni, I., Fisher, E.M.C., Mühlemann, O., Schiavo, G., Ruepp, M.-D., Isaacs, A.M., Plagnol, V., Fratta, P., 2020. FUS ALS-causative mutations impair FUS autoregulation and splicing factor networks through intron retention. Nucleic Acids Res 48, 6889–6905. https://doi.org/10.1093/nar/gkaa410
137.Hung, V., Zou, P., Rhee, H.-W., Udeshi, N.D., Cracan, V., Svinkina, T., Carr, S.A., Mootha, V.K., Ting, A.Y., 2014. Proteomic Mapping of the Human Mitochondrial

Intermembrane Space in Live Cells via Ratiometric APEX Tagging. Molecular Cell 55, 332–341. https://doi.org/10.1016/j.molcel.2014.06.003
138. Hyman, A.A., Weber, C.A., Jülicher, F., 2014b. Liquid-Liquid Phase Separation in Biology. Annu. Rev. Cell Dev. Biol. 30, 39–58. https://doi.org/10.1146/annurev-cellbio-100913-013325
139. Ibrahim, A.Y., Khaodeuanepheng, N.P., Amarasekara, D.L., Correia, J.J., Lewis, K.A., Fitzkee, N.C., Hough, L.E., Whitten, S.T., 2023. Intrinsically disordered regions that drive phase separation form a robustly distinct protein class. Journal of Biological Chemistry 299. https://doi.org/10.1016/j.jbc.2022.102801
140. Ibrahim, E.C., Schaal, T.D., Hertel, K.J., Reed, R., Maniatis, T., 2005. Serine/arginine-rich protein-dependent suppression of exon skipping by exonic splicing enhancers. Proc Natl Acad Sci U S A 102, 5002–5007. https://doi.org/10.1073/pnas.0500543102
141. Ivanov, P., Kedersha, N., Anderson, P., 2019. Stress Granules and Processing Bodies in Translational Control. Cold Spring Harb Perspect Biol 11, a032813. https://doi.org/10.1101/cshperspect.a032813
142. Jacob, A.G., Moutsopoulos, I., Petchey, A., Kollyfas, R., Knight-Schrijver, V.R., Mohorianu, I., Sinha, S., Smith, C.W.J., 2024. RNA binding protein with multiple splicing (RBPMS) promotes contractile phenotype splicing in human embryonic stem cell–derived vascular smooth muscle cells. Cardiovascular Research cvae198. https://doi.org/10.1093/cvr/cvae198
143. Jacot, J.G., Martin, J.C., Hunt, D.L., 2010. Mechanobiology of Cardiomyocyte Development. J Biomech 43, 93. https://doi.org/10.1016/j.jbiomech.2009.09.014
144. Jain, S., Wheeler, J.R., Walters, R.W., Agrawal, A., Barsic, A., Parker, R., 2016. ATPase-Modulated Stress Granules Contain a Diverse Proteome and Substructure. Cell 164, 487–498. https://doi.org/10.1016/j.cell.2015.12.038
145. Janero, D.R., Hreniuk, D., Sharif, H.M., 1993. Hydrogen peroxide-induced oxidative stress to the mammalian heart-muscle cell (cardiomyocyte): Nonperoxidative purine and pyrimidine nucleotide depletion. Journal of Cellular Physiology 155, 494–504. https://doi.org/10.1002/jcp.1041550308
146. Jang, Y., Elsayed, Z., Eki, R., He, S., Du, K.-P., Abbas, T., Kai, M., 2020. Intrinsically disordered protein RBM14 plays a role in generation of RNA:DNA hybrids at double-strand break sites. Proceedings of the National Academy of Sciences 117, 5329–5338. https://doi.org/10.1073/pnas.1913280117
147. Jayabalan, A.K., Sanchez, A., Park, R.Y., Yoon, S.P., Kang, G.-Y., Baek, J.-H., Anderson, P., Kee, Y., Ohn, T., 2016. NEDDylation promotes stress granule assembly. Nat Commun 7, 12125. https://doi.org/10.1038/ncomms12125
148. Jengelley, D.H.A., Wang, M., Narasimhan, A., Rupert, J.E., Young, A.R., Zhong, X., Horan, D.J., Robling, A.G., Koniaris, L.G., Zimmers, T.A., 2022. Exogenous Oncostatin M Induces Cardiac Dysfunction, Musculoskeletal Atrophy, and Fibrosis. Cytokine 159, 155972. https://doi.org/10.1016/j.cyto.2022.155972
149. Jo, M., Lee, S., Jeon, Y.-M., Kim, S., Kwon, Y., Kim, H.-J., 2020. The role of TDP-43 propagation in neurodegenerative diseases: integrating insights from clinical and experimental studies. Exp Mol Med 52, 1652–1662. https://doi.org/10.1038/s12276-020-00513-7
150. Jo, Y., Jang, J., Song, D., Park, H., Jung, Y., 2022. Determinants for intrinsically disordered protein recruitment into phase-separated protein condensates. Chem. Sci. 13, 522–530. https://doi.org/10.1039/D1SC05672G
151. Jozefczuk, J., Drews, K., Adjaye, J., 2012. Preparation of mouse embryonic fibroblast cells suitable for culturing human embryonic and induced pluripotent stem cells. J Vis Exp 3854. https://doi.org/10.3791/3854

152.Kai, M., 2016. Roles of RNA-Binding Proteins in DNA Damage Response. International Journal of Molecular Sciences 17, 310. https://doi.org/10.3390/ijms17030310
153.Kalsotra, A., Xiao, X., Ward, A.J., Castle, J.C., Johnson, J.M., Burge, C.B., Cooper, T.A., 2008. A postnatal switch of CELF and MBNL proteins reprograms alternative splicing in the developing heart. Proc Natl Acad Sci U S A 105, 20333–20338. https://doi.org/10.1073/pnas.0809045105
154.Kanehisa, M., Goto, S., Sato, Y., Furumichi, M., Tanabe, M., 2012. KEGG for integration and interpretation of large-scale molecular data sets. Nucleic Acids Res 40, D109-114. https://doi.org/10.1093/nar/gkr988
155.Kawaguchi, T., Tanigawa, A., Naganuma, T., Ohkawa, Y., Souquere, S., Pierron, G., Hirose, T., 2015. SWI/SNF chromatin-remodeling complexes function in noncoding RNA-dependent assembly of nuclear bodies. Proceedings of the National Academy of Sciences 112, 4304–4309. https://doi.org/10.1073/pnas.1423819112
156.Ke, Y.D., Dramiga, J., Schütz, U., Kril, J.J., Ittner, L.M., Schröder, H., Götz, J., 2012. Tau-mediated nuclear depletion and cytoplasmic accumulation of SFPQ in Alzheimer's and Pick's disease. PLoS One 7, e35678. https://doi.org/10.1371/journal.pone.0035678
157.Kedersha, N., Anderson, P., 2007. Mammalian stress granules and processing bodies. Methods Enzymol 431, 61–81. https://doi.org/10.1016/S0076-6879(07)31005-7
158.Kedersha, N., Anderson, P., 2002. Stress granules: sites of mRNA triage that regulate mRNA stability and translatability. Biochemical Society Transactions 30.
159.Kedersha, N., Cho, M.R., Li, W., Yacono, P.W., Chen, S., Gilks, N., Golan, D.E., Anderson, P., 2000. Dynamic Shuttling of Tia-1 Accompanies the Recruitment of mRNA to Mammalian Stress Granules. J Cell Biol 151, 1257–1268. https://doi.org/10.1083/jcb.151.6.1257
160.Kedersha, N., Gupta, M., Li, W., Miller, I., Anderson, P., 1999a. RNA-Binding Proteins Tia-1 and Tiar Link the Phosphorylation of Eif-2α to the Assembly of Mammalian Stress Granules. J Cell Biol 147, 1431–1442. https://doi.org/10.1083/jcb.147.7.1431
161.Kedersha, N., Ivanov, P., Anderson, P., 2013. Stress granules and cell signaling: more than just a passing phase? Trends Biochem Sci 38, 10.1016/j.tibs.2013.07.004. https://doi.org/10.1016/j.tibs.2013.07.004
162.Kedersha, N., Stoecklin, G., Ayodele, M., Yacono, P., Lykke-Andersen, J., Fritzler, M.J., Scheuner, D., Kaufman, R.J., Golan, D.E., Anderson, P., 2005. Stress granules and processing bodies are dynamically linked sites of mRNP remodeling. J Cell Biol 169, 871–884. https://doi.org/10.1083/jcb.200502088
163.Keiten-Schmitz, J., Wagner, K., Piller, T., Kaulich, M., Alberti, S., Müller, S., 2020a. The Nuclear SUMO-Targeted Ubiquitin Quality Control Network Regulates the Dynamics of Cytoplasmic Stress Granules. Molecular Cell 79, 54-67.e7. https://doi.org/10.1016/j.molcel.2020.05.017
164.Kelly, C., Kiltschewskij, D.J., Leong, A.J.W., Haw, T.J., Croft, A.J., Balachandran, L., Chen, D., Bond, D.R., Lee, H.J., Cairns, M.J., Sverdlov, A.L., Ngo, D.T.M., 2025. Identifying common pathways for doxorubicin and carfilzomib-induced cardiotoxicities: transcriptomic and epigenetic profiling. Sci Rep 15, 4395. https://doi.org/10.1038/s41598-025-87442-5
165.Kleiman, F.E., Wu-Baer, F., Fonseca, D., Kaneko, S., Baer, R., Manley, J.L., 2005. BRCA1/BARD1 inhibition of mRNA 3' processing involves targeted degradation of RNA polymerase II. Genes Dev 19, 1227–1237. https://doi.org/10.1101/gad.1309505

166.Klein, I.A., Boija, A., Afeyan, L.K., Hawken, S.W., Fan, M., Dall'Agnese, A., Oksuz, O., Henninger, J.E., Shrinivas, K., Sabari, B.R., Sagi, I., Clark, V.E., Platt, J.M., Kar, M., McCall, P.M., Zamudio, A.V., Manteiga, J.C., Coffey, E.L., Li, C.H., Hannett, N.M., Guo, Y.E., Decker, T.-M., Lee, T.I., Zhang, T., Weng, J.-K., Taatjes, D.J., Chakraborty, A., Sharp, P.A., Chang, Y.T., Hyman, A.A., Gray, N.S., Young, R.A., 2020. Partitioning of cancer therapeutics in nuclear condensates. Science (New York, N.Y.) 368, 1386. https://doi.org/10.1126/science.aaz4427
167.Knowles, R.B., Sabry, J.H., Martone, M.E., Deerinck, T.J., Ellisman, M.H., Bassell, G.J., Kosik, K.S., 1996. Translocation of RNA Granules in Living Neurons. J. Neurosci. 16, 7812–7820. https://doi.org/10.1523/JNEUROSCI.16-24-07812.1996
168.Königs, V., de Oliveira Freitas Machado, C., Arnold, B., Blümel, N., Solovyeva, A., Löbbert, S., Schafranek, M., Ruiz De Los Mozos, I., Wittig, I., McNicoll, F., Schulz, M.H., Müller-McNicoll, M., 2020. SRSF7 maintains its homeostasis through the expression of Split-ORFs and nuclear body assembly. Nat Struct Mol Biol 27, 260–273. https://doi.org/10.1038/s41594-020-0385-9
169.Konorev, E.A., Vanamala, S., Kalyanaraman, B., 2008. Differences in Doxorubicin-Induced Apoptotic Signaling in Adult and Immature Cardiomyocytes. Free Radic Biol Med 45, 1723–1728. https://doi.org/10.1016/j.freeradbiomed.2008.09.006
170.Krischke, M., Hempel, G., Völler, S., André, N., D'Incalci, M., Bisogno, G., Köpcke, W., Borowski, M., Herold, R., Boddy, A.V., Boos, J., 2016. Pharmacokinetic and pharmacodynamic study of doxorubicin in children with cancer: results of a "European Pediatric Oncology Off-patents Medicines Consortium" trial. Cancer Chemother Pharmacol 78, 1175–1184. https://doi.org/10.1007/s00280-016-3174-8
171.Kubin, T., Pöling, J., Kostin, S., Gajawada, P., Hein, S., Rees, W., Wietelmann, A., Tanaka, M., Lörchner, H., Schimanski, S., Szibor, M., Warnecke, H., Braun, T., 2011. Oncostatin M Is a Major Mediator of Cardiomyocyte Dedifferentiation and Remodeling. Cell Stem Cell 9, 420–432. https://doi.org/10.1016/j.stem.2011.08.013
172.Kushner, J., Papa, A., Marx, S.O., 2021. Use of Proximity Labeling in Cardiovascular Research. JACC Basic Transl Sci 6, 598–609. https://doi.org/10.1016/j.jacbts.2021.01.005
173.Kwon, S., Zhang, Y., Matthias, P., 2007. The deacetylase HDAC6 is a novel critical component of stress granules involved in the stress response. Genes Dev 21, 3381–3394. https://doi.org/10.1101/gad.461107
174.Lagier-Tourenne, C., Polymenidou, M., Cleveland, D.W., 2010. TDP-43 and FUS/TLS: emerging roles in RNA processing and neurodegeneration. Hum Mol Genet 19, R46–R64. https://doi.org/10.1093/hmg/ddq137
175.Lam, S.S., Martell, J.D., Kamer, K.J., Deerinck, T.J., Ellisman, M.H., Mootha, V.K., Ting, A.Y., 2015. Directed evolution of APEX2 for electron microscopy and proteomics. Nat Methods 12, 51–54. https://doi.org/10.1038/nmeth.3179
176.Lampejo, T., Durkin, S.M., Bhatt, N., Guttmann, O., 2021. Acute myocarditis: aetiology, diagnosis and management. Clin Med (Lond) 21, e505–e510. https://doi.org/10.7861/clinmed.2021-0121
177.Langer, S.W., 2014. Dexrazoxane for the treatment of chemotherapy-related side effects. Cancer Manag Res 6, 357–363. https://doi.org/10.2147/CMAR.S47238
178.Lareau, L.F., Brooks, A.N., Soergel, D.A.W., Meng, Q., Brenner, S.E., 2007. The coupling of alternative splicing and nonsense-mediated mRNA decay. Adv Exp Med Biol 623, 190–211. https://doi.org/10.1007/978-0-387-77374-2_12
179.Latorre, E., Tebaldi, T., Viero, G., Spartà, A.M., Quattrone, A., Provenzani, A., 2012b. Downregulation of HuR as a new mechanism of doxorubicin resistance in breast cancer cells. Molecular Cancer 11, 13. https://doi.org/10.1186/1476-4598-11-13

180.Lellahi, S.M., Rosenlund, I.A., Hedberg, A., Kiær, L.T., Mikkola, I., Knutsen, E., Perander, M., 2018. The long noncoding RNA NEAT1 and nuclear paraspeckles are up-regulated by the transcription factor HSF1 in the heat shock response. J Biol Chem 293, 18965–18976. https://doi.org/10.1074/jbc.RA118.004473
181.Li, C., Wang, T., Gu, J., Qi, S., Li, J., Chen, L., Wu, H., Shi, L., Song, C., Li, H., Zhu, L., Lu, Y., Zhou, Q., 2022. SMARCC2 mediates the regulation of DKK1 by the transcription factor EGR1 through chromatin remodeling to reduce the proliferative capacity of glioblastoma. Cell Death Dis 13, 1–14. https://doi.org/10.1038/s41419-022-05439-8
182.Li, K., Wang, Z., 2021. Speckles and paraspeckles coordinate to regulate HSV-1 genes transcription. Commun Biol 4, 1–10. https://doi.org/10.1038/s42003-021-02742-6
183.Li, R., Yan, G., Li, Q., Sun, H., Hu, Y., Sun, J., Xu, B., 2012. MicroRNA-145 Protects Cardiomyocytes against Hydrogen Peroxide (H2O2)-Induced Apoptosis through Targeting the Mitochondria Apoptotic Pathway. PLoS One 7, e44907. https://doi.org/10.1371/journal.pone.0044907
184.Li, W., Lin, W.-D., Ray, P., Lan, P., Schmidt, W., 2013. Genome-wide detection of condition-sensitive alternative splicing in Arabidopsis roots. Plant Physiol 162, 1750–1763. https://doi.org/10.1104/pp.113.217778
185.Li, W., Wang, Y., 2023b. Stress granules: potential therapeutic targets for infectious and inflammatory diseases. Front Immunol 14, 1145346. https://doi.org/10.3389/fimmu.2023.1145346
186.Li, Y.R., King, O.D., Shorter, J., Gitler, A.D., 2013b. Stress granules as crucibles of ALS pathogenesis. Journal of Cell Biology 201, 361–372. https://doi.org/10.1083/jcb.201302044
187.Liao, Y., Castello, A., Fischer, B., Leicht, S., Föehr, S., Frese, C.K., Ragan, C., Kurscheid, S., Pagler, E., Yang, H., Krijgsveld, J., Hentze, M.W., Preiss, T., 2016b. The Cardiomyocyte RNA-Binding Proteome: Links to Intermediary Metabolism and Heart Disease. Cell Reports 16, 1456–1469. https://doi.org/10.1016/j.celrep.2016.06.084
188.Liao, Y., Smyth, G.K., Shi, W., 2014. featureCounts: an efficient general purpose program for assigning sequence reads to genomic features. Bioinformatics 30, 923–930. https://doi.org/10.1093/bioinformatics/btt656
189.Lim, Y.W., James, D., Huang, J., Lee, M., 2020. The Emerging Role of the RNA-Binding Protein SFPQ in Neuronal Function and Neurodegeneration. International Journal of Molecular Sciences 21, 7151. https://doi.org/10.3390/ijms21197151
190.Linders, A.N., Dias, I.B., López Fernández, T., Tocchetti, C.G., Bomer, N., Van der Meer, P., 2024c. A review of the pathophysiological mechanisms of doxorubicin-induced cardiotoxicity and aging. npj Aging 10, 1–9. https://doi.org/10.1038/s41514-024-00135-7
191.Lindquist, S., 1981. Regulation of protein synthesis during heat shock. Nature 293, 311–314. https://doi.org/10.1038/293311a0
192.Ling, S.-C., Polymenidou, M., Cleveland, D.W., 2013. Converging Mechanisms in ALS and FTD: Disrupted RNA and Protein Homeostasis. Neuron 79, 416–438. https://doi.org/10.1016/j.neuron.2013.07.033
193.Lipshultz, S.E., Colan, S.D., Gelber, R.D., Perez-Atayde, A.R., Sallan, S.E., Sanders, S.P., 1991. Late Cardiac Effects of Doxorubicin Therapy for Acute Lymphoblastic Leukemia in Childhood. New England Journal of Medicine 324, 808–815. https://doi.org/10.1056/NEJM199103213241205
194.Lipshultz, S.E., Lipsitz, S.R., Mone, S.M., Goorin, A.M., Sallan, S.E., Sanders, S.P., Orav, E.J., Gelber, R.D., Colan, S.D., 1995. Female Sex and Higher Drug Dose as

Risk Factors for Late Cardiotoxic Effects of Doxorubicin Therapy for Childhood Cancer. New England Journal of Medicine 332, 1738–1744. https://doi.org/10.1056/NEJM199506293322602
195. Lipshultz, S.E., Rifai, N., Dalton, V.M., Levy, D.E., Silverman, L.B., Lipsitz, S.R., Colan, S.D., Asselin, B.L., Barr, R.D., Clavell, L.A., Hurwitz, C.A., Moghrabi, A., Samson, Y., Schorin, M.A., Gelber, R.D., Sallan, S.E., 2004. The effect of dexrazoxane on myocardial injury in doxorubicin-treated children with acute lymphoblastic leukemia. N Engl J Med 351, 145–153. https://doi.org/10.1056/NEJMoa035153
196. Liu, J., Kong, X., Zhang, M., Yang, X., Xu, X., 2019. RNA binding protein 24 deletion disrupts global alternative splicing and causes dilated cardiomyopathy. Protein Cell 10, 405–416. https://doi.org/10.1007/s13238-018-0578-8
197. Liu, Y., Duan, C., Liu, W., Chen, X., Wang, Y., Liu, X., Yue, J., Yang, J., Zhou, X., 2019. Upregulation of let-7f-2-3p by long noncoding RNA NEAT1 inhibits XPO1-mediated HAX-1 nuclear export in both in vitro and in vivo rodent models of doxorubicin-induced cardiotoxicity. Arch Toxicol 93, 3261–3276. https://doi.org/10.1007/s00204-019-02586-4
198. Love, M.I., Huber, W., Anders, S., 2014. Moderated estimation of fold change and dispersion for RNA-seq data with DESeq2. Genome Biol 15, 550. https://doi.org/10.1186/s13059-014-0550-8
199. Lu, J., Shu, R., Zhu, Y., 2018. Dysregulation and Dislocation of SFPQ Disturbed DNA Organization in Alzheimer's Disease and Frontotemporal Dementia. J Alzheimers Dis 61, 1311–1321. https://doi.org/10.3233/JAD-170659
200. Lu, S.H.-A., Lee, K.-Z., Hsu, P.W.-C., Su, L.-Y., Yeh, Y.-C., Pan, C.-Y., Tsai, S.-Y., 2022. Alternative Splicing Mediated by RNA-Binding Protein RBM24 Facilitates Cardiac Myofibrillogenesis in a Differentiation Stage-Specific Manner. Circulation Research 130, 112–129. https://doi.org/10.1161/CIRCRESAHA.121.320080
201. Lyu, Y.L., Kerrigan, J.E., Lin, C.-P., Azarova, A.M., Tsai, Y.-C., Ban, Y., Liu, L.F., 2007b. Topoisomerase IIβ–Mediated DNA Double-Strand Breaks: Implications in Doxorubicin Cardiotoxicity and Prevention by Dexrazoxane. Cancer Research 67, 8839–8846. https://doi.org/10.1158/0008-5472.CAN-07-1649
202. Maatz, H., Jens, M., Liss, M., Schafer, S., Heinig, M., Kirchner, M., Adami, E., Rintisch, C., Dauksaite, V., Radke, M.H., Selbach, M., Barton, P.J.R., Cook, S.A., Rajewsky, N., Gotthardt, M., Landthaler, M., Hubner, N., 2014. RNA-binding protein RBM20 represses splicing to orchestrate cardiac pre-mRNA processing. J Clin Invest 124, 3419–3430. https://doi.org/10.1172/JCI74523
203. Ma, W., Wei, S., Zhang, B., Li, W., 2020. Molecular Mechanisms of Cardiomyocyte Death in Drug-Induced Cardiotoxicity. Front Cell Dev Biol 8, 434. https://doi.org/10.3389/fcell.2020.00434
204. Mahboubi, H., Stochaj, U., 2017. Cytoplasmic stress granules: Dynamic modulators of cell signaling and disease. Biochimica et Biophysica Acta (BBA) - Molecular Basis of Disease 1863, 884–895. https://doi.org/10.1016/j.bbadis.2016.12.022
205. Mair, A., Xu, S.-L., Branon, T.C., Ting, A.Y., Bergmann, D.C., 2019. Proximity labeling of protein complexes and cell-type-specific organellar proteomes in Arabidopsis enabled by TurboID. eLife 8, e47864. https://doi.org/10.7554/eLife.47864
206. Mao, C., Wang, X., Liu, Y., Wang, M., Yan, B., Jiang, Y., Shi, Y., Shen, Y., Liu, X., Lai, W., Yang, R., Xiao, D., Cheng, Y., Liu, S., Zhou, H., Cao, Y., Yu, W., Muegge, K., Yu, H., Tao, Y., 2018. A G3BP1-Interacting lncRNA Promotes Ferroptosis and Apoptosis in Cancer via Nuclear Sequestration of p53. Cancer Res 78, 3484–3496. https://doi.org/10.1158/0008-5472.CAN-17-3454

207. Markmiller, S., Soltanieh, S., Server, K.L., Mak, R., Jin, W., Fang, M.Y., Luo, E.-C., Krach, F., Yang, D., Sen, A., Fulzele, A., Wozniak, J.M., Gonzalez, D.J., Kankel, M.W., Gao, F.-B., Bennett, E.J., Lécuyer, E., Yeo, G.W., 2018b. Context-Dependent and Disease-Specific Diversity in Protein Interactions within Stress Granules. Cell 172, 590-604.e13. https://doi.org/10.1016/j.cell.2017.12.032
208. Maron, B.J., Towbin, J.A., Thiene, G., Antzelevitch, C., Corrado, D., Arnett, D., Moss, A.J., Seidman, C.E., Young, J.B., American Heart Association, Council on Clinical Cardiology, Heart Failure and Transplantation Committee, Quality of Care and Outcomes Research and Functional Genomics and Translational Biology Interdisciplinary Working Groups, Council on Epidemiology and Prevention, 2006. Contemporary definitions and classification of the cardiomyopathies: an American Heart Association Scientific Statement from the Council on Clinical Cardiology, Heart Failure and Transplantation Committee; Quality of Care and Outcomes Research and Functional Genomics and Translational Biology Interdisciplinary Working Groups; and Council on Epidemiology and Prevention. Circulation 113, 1807–1816. https://doi.org/10.1161/CIRCULATIONAHA.106.174287
209. Marshall, A.C., Cummins, J., Kobelke, S., Zhu, T., Widagdo, J., Anggono, V., Hyman, A., Fox, A.H., Bond, C.S., Lee, M., 2023. Different Low-complexity Regions of SFPQ Play Distinct Roles in the Formation of Biomolecular Condensates. Journal of Molecular Biology 435, 168364. https://doi.org/10.1016/j.jmb.2023.168364
210. Martell, J.D., Deerinck, T.J., Sancak, Y., Poulos, T.L., Mootha, V.K., Sosinsky, G.E., Ellisman, M.H., Ting, A.Y., 2012. Engineered ascorbate peroxidase as a genetically-encoded reporter for electron microscopy. Nat Biotechnol 30, 1143–1148. https://doi.org/10.1038/nbt.2375
211. Martin, E.W., Holehouse, A.S., 2020. Intrinsically disordered protein regions and phase separation: sequence determinants of assembly or lack thereof. Emerging Topics in Life Sciences 4, 307–329. https://doi.org/10.1042/ETLS20190164
212. Martin, E.W., Holehouse, A.S., Grace, C.R., Hughes, A., Pappu, R.V., Mittag, T., 2016. Sequence determinants of the conformational properties of an intrinsically disordered protein prior to and upon multisite phosphorylation. Journal of the American Chemical Society 138, 15323. https://doi.org/10.1021/jacs.6b10272
213. McCluggage, F., Fox, A.H., 2021. Paraspeckle nuclear condensates: Global sensors of cell stress? BioEssays 43, 2000245. https://doi.org/10.1002/bies.202000245
214. McNally, E.M., Mestroni, L., 2017. Dilated Cardiomyopathy: Genetic Determinants and Mechanisms. Circ Res 121, 731–748. https://doi.org/10.1161/CIRCRESAHA.116.309396
215. Mehta, M., Raguraman, R., Ramesh, R., Munshi, A., 2022. RNA Binding Proteins (RBPs) and their role in DNA Damage and radiation response in cancer. Adv Drug Deliv Rev 191, 114569. https://doi.org/10.1016/j.addr.2022.114569
216. Melkonian, K., Stolze, S.C., Harzen, A., Nakagami, H., 2022. miniTurbo-based interactomics of two plasma membrane-localized SNARE proteins in *Marchantia polymorpha*. New Phytologist 235, 786–800. https://doi.org/10.1111/nph.18151
217. Mello, S.S., Sinow, C., Raj, N., Mazur, P.K., Bieging-Rolett, K., Broz, D.K., Imam, J.F.C., Vogel, H., Wood, L.D., Sage, J., Hirose, T., Nakagawa, S., Rinn, J., Attardi, L.D., 2017. *Neat1* is a p53-inducible lincRNA essential for transformation suppression. Genes Dev. 31, 1095–1108. https://doi.org/10.1101/gad.284661.116
218. Memon, D., Dawson, K., Smowton, C.S., Xing, W., Dive, C., Miller, C.J., 2016. Hypoxia-driven splicing into noncoding isoforms regulates the DNA damage response. npj Genomic Med 1, 1–7. https://doi.org/10.1038/npjgenmed.2016.20
219. Miyamoto, Y., Saiwaki, T., Yamashita, J., Yasuda, Y., Kotera, I., Shibata, S., Shigeta, M., Hiraoka, Y., Haraguchi, T., Yoneda, Y., 2004. Cellular stresses induce the nuclear

accumulation of importin α and cause a conventional nuclear import block. Journal of Cell Biology 165, 617–623. https://doi.org/10.1083/jcb.200312008
220.More, D.A., Kumar, A., 2020. SRSF3: Newly discovered functions and roles in human health and diseases. Eur J Cell Biol 99, 151099. https://doi.org/10.1016/j.ejcb.2020.151099
221.Mori, F., Tada, M., Kon, T., Miki, Y., Tanji, K., Kurotaki, H., Tomiyama, M., Ishihara, T., Onodera, O., Kakita, A., Wakabayashi, K., 2019b. Phosphorylated TDP-43 aggregates in skeletal and cardiac muscle are a marker of myogenic degeneration in amyotrophic lateral sclerosis and various conditions. Acta Neuropathol Commun 7, 165. https://doi.org/10.1186/s40478-019-0824-1
222.Morimoto, R.I., 2011b. The Heat Shock Response: Systems Biology of Proteotoxic Stress in Aging and Disease. Cold Spring Harb Symp Quant Biol 76, 91–99. https://doi.org/10.1101/sqb.2012.76.010637
223.Morita, T., Satoh, R., Umeda, N., Kita, A., Sugiura, R., 2012. The stress granule protein Vgl1 and poly(A)-binding protein Pab1 are required for doxorubicin resistance in the fission yeast *Schizosaccharomyces pombe*. Biochemical and Biophysical Research Communications 417, 399–403. https://doi.org/10.1016/j.bbrc.2011.11.127
224.Mullard, A., 2019. Biomolecular condensates pique drug discovery curiosity. Nature Reviews Drug Discovery 18, 324–326. https://doi.org/10.1038/d41573-019-00069-w
225.Müller-McNicoll, M., Rossbach, O., Hui, J., Medenbach, J., 2019c. Auto-regulatory feedback by RNA-binding proteins. J Mol Cell Biol 11, 930–939. https://doi.org/10.1093/jmcb/mjz043
226.Muñoz, M.J., Pérez Santangelo, M.S., Paronetto, M.P., de la Mata, M., Pelisch, F., Boireau, S., Glover-Cutter, K., Ben-Dov, C., Blaustein, M., Lozano, J.J., Bird, G., Bentley, D., Bertrand, E., Kornblihtt, A.R., 2009a. DNA damage regulates alternative splicing through inhibition of RNA polymerase II elongation. Cell 137, 708–720. https://doi.org/10.1016/j.cell.2009.03.010
227.Murray-Nerger, L.A., Lozano, C., Burton, E.M., Liao, Y., Ungerleider, N.A., Guo, R., Gewurz, B.E., 2024. The nucleic acid binding protein SFPQ represses EBV lytic reactivation by promoting histone H1 expression. Nat Commun 15, 4156. https://doi.org/10.1038/s41467-024-48333-x
228.Nakagaki-Silva, E.E., Gooding, C., Llorian, M., Jacob, A.G., Richards, F., Buckroyd, A., Sinha, S., Smith, C.W., n.d. Identification of RBPMS as a mammalian smooth muscle master splicing regulator via proximity of its gene with super-enhancers. eLife 8, e46327. https://doi.org/10.7554/eLife.46327
229.Namkoong, S., Ho, A., Woo, Y.M., Kwak, H., Lee, J.H., 2018. Systematic Characterization of Stress-Induced RNA Granulation. Molecular Cell 70, 175-187.e8. https://doi.org/10.1016/j.molcel.2018.02.025
230.Neumann, M., Sampathu, D.M., Kwong, L.K., Truax, A.C., Micsenyi, M.C., Chou, T.T., Bruce, J., Schuck, T., Grossman, M., Clark, C.M., McCluskey, L.F., Miller, B.L., Masliah, E., Mackenzie, I.R., Feldman, H., Feiden, W., Kretzschmar, H.A., Trojanowski, J.Q., Lee, V.M.-Y., 2006. Ubiquitinated TDP-43 in frontotemporal lobar degeneration and amyotrophic lateral sclerosis. Science 314, 130–133. https://doi.org/10.1126/science.1134108
231.Ninomiya, K., Adachi, S., Natsume, T., Iwakiri, J., Terai, G., Asai, K., Hirose, T., 2020. LncRNA-dependent nuclear stress bodies promote intron retention through SR protein phosphorylation. EMBO J 39, e102729. https://doi.org/10.15252/embj.2019102729
232.Nishio, K., Qiao, S., Chang, K.S., 2019. Differential effects of Doxorubicin and Actinomycin D on the stability of RNA binding proteins, RBM10 and RBM5:

Actinomycin D promotes the nuclear speckles targeting of RBM10 and RBM5 through the novel structural elements. https://doi.org/10.1101/627927
233.Nover, L., Scharf, K.D., Neumann, D., 1983. Formation of cytoplasmic heat shock granules in tomato cell cultures and leaves. Mol Cell Biol 3, 1648–1655. https://doi.org/10.1128/mcb.3.9.1648-1655.1983
234.Nsengimana, B., Khan, F.A., Awan, U.A., Wang, D., Fang, N., Wei, W., Zhang, W., Ji, S., 2022. Pseudogenes and Liquid Phase Separation in Epigenetic Expression. Front Oncol 12, 912282. https://doi.org/10.3389/fonc.2022.912282
235.Nunes, C., Mestre, I., Marcelo, A., Koppenol, R., Matos, C.A., Nóbrega, C., 2019. MSGP: the first database of the protein components of the mammalian stress granules. Database (Oxford) 2019, baz031. https://doi.org/10.1093/database/baz031
236.O'Connell, T.D., Rodrigo, M.C., Simpson, P.C., 2007. Isolation and culture of adult mouse cardiac myocytes. Methods Mol Biol 357, 271–296. https://doi.org/10.1385/1-59745-214-9:271
237.Octavia, Y., Tocchetti, C.G., Gabrielson, K.L., Janssens, S., Crijns, H.J., Moens, A.L., 2012. Doxorubicin-induced cardiomyopathy: From molecular mechanisms to therapeutic strategies. Journal of Molecular and Cellular Cardiology 52, 1213–1225. https://doi.org/10.1016/j.yjmcc.2012.03.006
238.Okuda, E.K., Kessler, L.F., Arnold, B., Riegger, R.J., Hernández Cañás, M.C., Zebrowska, E., Bakisoglu, C., Rudigier, M., Krost, C., Nagasse, H.Y., Keiten-Schmitz, J., Müller, S., Stanek, D., Dormann, D., Zarnack, K., Heilemann, M., Müller-McNicoll, M., 2025. Rapid depletion and super-resolution microscopy reveal dual roles of SRSF5 in coordinating nuclear speckle–paraspeckle crosstalk during cellular stress. Nucleic Acids Res 53, gkaf713. https://doi.org/10.1093/nar/gkaf713
239.Paradis, A.N., Gay, M.S., Zhang, L., 2014. Binucleation of cardiomyocytes: the transition from a proliferative to a terminally differentiated state. Drug Discov Today 19, 602–609. https://doi.org/10.1016/j.drudis.2013.10.019
240.Padrón, A., Iwasaki, S., Ingolia, N.T., 2019. Proximity RNA labeling by APEX-Seq Reveals the Organization of Translation Initiation Complexes and Repressive RNA Granules. Mol Cell 75, 875-887.e5. https://doi.org/10.1016/j.molcel.2019.07.030
241.Park, C., Choi, S., Kim, Y.-E., Lee, S., Park, S.-H., Adelstein, R.S., Kawamoto, S., Kim, K.K., 2017. Stress Granules Contain Rbfox2 with Cell Cycle-related mRNAs. Sci Rep 7, 11211. https://doi.org/10.1038/s41598-017-11651-w
242.Pederson, T., 2011. The Nucleolus. Cold Spring Harb Perspect Biol 3, a000638. https://doi.org/10.1101/cshperspect.a000638
243.Pietras, P., Aulas, A., Fay, M.M., Leśniczak-Staszak, M., Sowiński, M., Lyons, S.M., Szaflarski, W., Ivanov, P., 2022. Translation inhibition and suppression of stress granules formation by cisplatin. Biomed Pharmacother 145, 112382. https://doi.org/10.1016/j.biopha.2021.112382
244.Piri, N., Kwong, J.M.K., Song, M., Caprioli, J., 2006. Expression of *hermes* gene is restricted to the ganglion cells in the retina. Neuroscience Letters 405, 40–45. https://doi.org/10.1016/j.neulet.2006.06.049
245.Pisani, G., Baron, B., 2020. NEAT1 and Paraspeckles in Cancer Development and Chemoresistance. Non-Coding RNA 6, 43. https://doi.org/10.3390/ncrna6040043
246.Pollack, A., Kontorovich, A.R., Fuster, V., Dec, G.W., 2015. Viral myocarditis—diagnosis, treatment options, and current controversies. Nat Rev Cardiol 12, 670–680. https://doi.org/10.1038/nrcardio.2015.108
247.Popp, M.W., Maquat, L.E., 2015d. Attenuation of nonsense-mediated mRNA decay facilitates the response to chemotherapeutics. Nat Commun 6, 6632. https://doi.org/10.1038/ncomms7632

248.Posey, A.E., Holehouse, A.S., Pappu, R.V., 2018. Chapter One - Phase Separation of Intrinsically Disordered Proteins, in: Rhoades, E. (Ed.), Methods in Enzymology, Intrinsically Disordered Proteins. Academic Press, pp. 1–30. https://doi.org/10.1016/bs.mie.2018.09.035
249.Potts, M.B., Vaughn, A.E., McDonough, H., Patterson, C., Deshmukh, M., 2005. Reduced Apaf-1 levels in cardiomyocytes engage strict regulation of apoptosis by endogenous XIAP. J Cell Biol 171, 925–930. https://doi.org/10.1083/jcb.200504082
250.Prasad, A., Bharathi, V., Sivalingam, V., Girdhar, A., Patel, B.K., 2019. Molecular Mechanisms of TDP-43 Misfolding and Pathology in Amyotrophic Lateral Sclerosis. Front Mol Neurosci 12, 25. https://doi.org/10.3389/fnmol.2019.00025
251.Prokhorova, E.A., Zamaraev, A.V., Kopeina, G.S., Zhivotovsky, B., Lavrik, I.N., 2015. Role of the nucleus in apoptosis: signaling and execution. Cell Mol Life Sci 72, 4593–4612. https://doi.org/10.1007/s00018-015-2031-y
252.Protter, D.S.W., Parker, R., 2016b. Principles and Properties of Stress Granules. Trends in Cell Biology 26, 668–679. https://doi.org/10.1016/j.tcb.2016.05.004
253.Qian, H., Qian, Y., Liu, Y., Cao, J., Wang, Y., Yang, A., Zhao, W., Lu, Y., Liu, H., Zhu, W., 2023. Identification of novel biomarkers involved in doxorubicin-induced acute and chronic cardiotoxicity, respectively, by integrated bioinformatics. Front. Cardiovasc. Med. 9. https://doi.org/10.3389/fcvm.2022.996809
254.Qian, P., Yan, L.-J., Li, Y.-Q., Yang, H.-T., Duan, H.-Y., Wu, J.-T., Fan, X.-W., Wang, S.-L., 2018. Cyanidin ameliorates cisplatin-induced cardiotoxicity via inhibition of ROS-mediated apoptosis. Exp Ther Med 15, 1959–1965. https://doi.org/10.3892/etm.2017.5617
255.Qin, W., Cho, K.F., Cavanagh, P.E., Ting, A.Y., 2021. Deciphering molecular interactions by proximity labeling. Nat Methods 18, 133–143. https://doi.org/10.1038/s41592-020-01010-5
256.Qin, Y., Mergiotti, M., Russo, M., Huseynov, A., Barnett, S., Lee, M., Miranda, A., Toscano Rivalta, R., Chaves, P., Schneider, M., Ghigo, A., Noseda, M., 2023. BS35 Single-nucleus sequencing of doxorubicin-treated mouse hearts reveals disease progression of cardiomyocytes, in: Basic Science. Presented at the British Cardiovascular Society Annual Conference, ‘Future-proofing Cardiology for the next 10 years’, 5–7 June 2023, BMJ Publishing Group Ltd and British Cardiovascular Society, pp. A268–A270. https://doi.org/10.1136/heartjnl-2023-BCS.248
257.Qiu, Z., Sun, Z., Wang, Z., Wu, Y., Li, Z., Fan, Y., Yang, W., Chen, Y., Hua, S., Jin, W., 2024. RBM20 promotes doxorubicin-induced cardiotoxicity by Atp6v0a1 alternative splicing. European Heart Journal 45, ehae666.3749. https://doi.org/10.1093/eurheartj/ehae666.3749
258.Rabelo-Fernández, R.J., Noriega Rivera, R.A., Rivera, Y.S., Tous-Beveraggi, J., Valiyeva, F., Vivas-Mejia, P.E., 2022c. Increased Expression of the RBPMS Splice Variants Inhibits Cell Proliferation in Ovarian Cancer Cells. Int J Mol Sci 23, 14742. https://doi.org/10.3390/ijms232314742
259.Rabouille, C., 2019. Membraneless organelles in cell biology. Traffic 20, 885–886. https://doi.org/10.1111/tra.12686
260.Ramaswami, M., Taylor, J.P., Parker, R., 2013. Altered “Ribostasis”: RNA-protein granule formation or persistence in the development of degenerative disorders. Cell 154, 10.1016/j.cell.2013.07.038. https://doi.org/10.1016/j.cell.2013.07.038
261.Rambout, X., Detiffe, C., Bruyr, J., Mariavelle, E., Cherkaoui, M., Brohée, S., Demoitié, P., Lebrun, M., Soin, R., Lesage, B., Guedri, K., Beullens, M., Bollen, M., Farazi, T.A., Kettmann, R., Struman, I., Hill, D.E., Vidal, M., Kruys, V., Simonis, N., Twizere, J.-C., Dequiedt, F., 2016. The transcription factor ERG recruits CCR4–NOT

to control mRNA decay and mitotic progression. Nat Struct Mol Biol 23, 663–672. https://doi.org/10.1038/nsmb.3243
262.Rawat, P.S., Jaiswal, A., Khurana, A., Bhatti, J.S., Navik, U., 2021a. Doxorubicin-induced cardiotoxicity: An update on the molecular mechanism and novel therapeutic strategies for effective management. Biomedicine & Pharmacotherapy 139, 111708. https://doi.org/10.1016/j.biopha.2021.111708
263.Ray, D., Kazan, H., Cook, K.B., Weirauch, M.T., Najafabadi, H.S., Li, X., Gueroussov, S., Albu, M., Zheng, H., Yang, A., Na, H., Irimia, M., Matzat, L.H., Dale, R.K., Smith, S.A., Yarosh, C.A., Kelly, S.M., Nabet, B., Mecenas, D., Li, W., Laishram, R.S., Qiao, M., Lipshitz, H.D., Piano, F., Corbett, A.H., Carstens, R.P., Frey, B.J., Anderson, R.A., Lynch, K.W., Penalva, L.O.F., Lei, E.P., Fraser, A.G., Blencowe, B.J., Morris, Q.D., Hughes, T.R., 2013. A compendium of RNA-binding motifs for decoding gene regulation. Nature 499, 172–177. https://doi.org/10.1038/nature12311
264.Reviejo, M., Soto, M., Lozano, E., Asensio, M., Martínez-Augustin, O., Sánchez de Medina, F., Marin, J.J.G., 2021. Impact of alternative splicing on mechanisms of resistance to anticancer drugs. Biochemical Pharmacology 193, 114810. https://doi.org/10.1016/j.bcp.2021.114810
265.Rhee, H.-W., Zou, P., Udeshi, N.D., Martell, J.D., Mootha, V.K., Carr, S.A., Ting, A.Y., 2013. Proteomic Mapping of Mitochondria in Living Cells via Spatially-Restricted Enzymatic Tagging. Science 339, 1328–1331. https://doi.org/10.1126/science.1230593
266.Richardson, P., McKenna, W., Bristow, M., Maisch, B., Mautner, B., O'Connell, J., Olsen, E., Thiene, G., Goodwin, J., Gyarfas, I., Martin, I., Nordet, P., 1996. Report of the 1995 World Health Organization/International Society and Federation of Cardiology Task Force on the Definition and Classification of cardiomyopathies. Circulation 93, 841–842. https://doi.org/10.1161/01.cir.93.5.841
267.Riggs, C.L., Kedersha, N., Ivanov, P., Anderson, P., 2020. Mammalian stress granules and P bodies at a glance. Journal of Cell Science 133, jcs242487. https://doi.org/10.1242/jcs.242487
268.Ritchie, M.E., Phipson, B., Wu, D., Hu, Y., Law, C.W., Shi, W., Smyth, G.K., 2015. limma powers differential expression analyses for RNA-sequencing and microarray studies. Nucleic Acids Res 43, e47. https://doi.org/10.1093/nar/gkv007
269.Rochette, L., Guenancia, C., Gudjoncik, A., Hachet, O., Zeller, M., Cottin, Y., Vergely, C., 2015. Anthracyclines/trastuzumab: new aspects of cardiotoxicity and molecular mechanisms. Trends in Pharmacological Sciences 36, 326–348. https://doi.org/10.1016/j.tips.2015.03.005
270.Rossbach, O., Hung, L.-H., Schreiner, S., Grishina, I., Heiner, M., Hui, J., Bindereif, A., 2009. Auto- and Cross-Regulation of the hnRNP L Proteins by Alternative Splicing. Mol Cell Biol 29, 1442–1451. https://doi.org/10.1128/MCB.01689-08
271.Roux, K.J., Kim, D.I., Raida, M., Burke, B., 2012. A promiscuous biotin ligase fusion protein identifies proximal and interacting proteins in mammalian cells. J Cell Biol 196, 801–810. https://doi.org/10.1083/jcb.201112098
272.Ru, Y., Chen, X.-J., Guo, W.-Z., Gao, S.-G., Qi, Y.-J., Chen, P., Feng, X.-S., Zhang, S.-J., 2018. NEAT1_2–SFPQ axis mediates cisplatin resistance in liver cancer cells in vitro. Onco Targets Ther 11, 5695–5702. https://doi.org/10.2147/OTT.S163774
273.Sahoo, P.K., Lee, S.J., Jaiswal, P.B., Alber, S., Kar, A.N., Miller-Randolph, S., Taylor, E.E., Smith, T., Singh, B., Ho, T.S.-Y., Urisman, A., Chand, S., Pena, E.A., Burlingame, A.L., Woolf, C.J., Fainzilber, M., English, A.W., Twiss, J.L., 2018b. Axonal G3BP1 stress granule protein limits axonal mRNA translation and nerve regeneration. Nat Commun 9, 3358. https://doi.org/10.1038/s41467-018-05647-x

274.Saks, V., Dzeja, P., Schlattner, U., Vendelin, M., Terzic, A., Wallimann, T., 2006. Cardiac system bioenergetics: metabolic basis of the Frank-Starling law. J Physiol 571, 253–273. https://doi.org/10.1113/jphysiol.2005.101444
275.Schneider, J.W., Oommen, S., Qureshi, M.Y., Goetsch, S.C., Pease, D.R., Sundsbak, R.S., Guo, W., Sun, M., Sun, H., Kuroyanagi, H., Webster, D.A., Coutts, A.W., Holst, K.A., Edwards, B.S., Newville, N., Hathcock, M.A., Melkamu, T., Briganti, F., Wei, W., Romanelli, M.G., Fahrenkrug, S.C., Frantz, D.E., Olson, T.M., Steinmetz, L.M., Carlson, D.F., Nelson, T.J., Pipeline, W.P.P., 2020. Dysregulated ribonucleoprotein granules promote cardiomyopathy in RBM20 gene-edited pigs. Nature medicine 26, 1788. https://doi.org/10.1038/s41591-020-1087-x
276.Sears, R.M., May, D.G., Roux, K.J., 2019. BioID as a Tool for Protein-Proximity Labeling in Living Cells. Methods in molecular biology (Clifton, N.J.) 2012, 299. https://doi.org/10.1007/978-1-4939-9546-2_15
277.Shalgi, R., Hurt, J.A., Lindquist, S., Burge, C.B., 2014. Widespread Inhibition of Posttranscriptional Splicing Shapes the Cellular Transcriptome following Heat Shock. Cell Reports 7, 1362–1370. https://doi.org/10.1016/j.celrep.2014.04.044
278.Shapiro, D.M., Ney, M., Eghtesadi, S.A., Chilkoti, A., 2021. Protein Phase Separation Arising from Intrinsic Disorder: First-Principles to Bespoke Applications. J. Phys. Chem. B 125, 6740–6759. https://doi.org/10.1021/acs.jpcb.1c01146
279.Shelkovnikova, T.A., Kukharsky, M.S., An, H., Dimasi, P., Alexeeva, S., Shabir, O., Heath, P.R., Buchman, V.L., 2018b. Protective paraspeckle hyper-assembly downstream of TDP-43 loss of function in amyotrophic lateral sclerosis. Mol Neurodegener 13, 30. https://doi.org/10.1186/s13024-018-0263-7
280.Shen, Q., Yao, Q., Sun, J., Feng, L., Lu, H., Ma, Y., Liu, L., Wang, F., Li, J., Yue, Y., Jin, H., Wang, X., 2014. Downregulation of histone deacetylase 1 by microRNA-520h contributes to the chemotherapeutic effect of doxorubicin. FEBS Letters 588, 184–191. https://doi.org/10.1016/j.febslet.2013.11.034
281.Sheth, U., Parker, R., 2003. Decapping and Decay of Messenger RNA Occur in Cytoplasmic Processing Bodies. Science 300, 805–808. https://doi.org/10.1126/science.1082320
282.Shi, J., Zhang, L., Zhang, Y.-W., Surma, M., Mark Payne, R., Wei, L., 2012b. Downregulation of doxorubicin-induced myocardial apoptosis accompanies postnatal heart maturation. Am J Physiol Heart Circ Physiol 302, H1603–H1613. https://doi.org/10.1152/ajpheart.00844.2011
283.Shi, M., Zhang, H., Wang, L., Zhu, C., Sheng, K., Du, Y., Wang, K., Dias, A., Chen, S., Whitman, M., Wang, E., Reed, R., Cheng, H., 2015. Premature termination codons are recognized in the nucleus in a reading-frame-dependent manner. Cell Discov 1, 1–20. https://doi.org/10.1038/celldisc.2015.1
284.Shimamoto, A., Kitao, S., Ichikawa, K., Suzuki, N., Yamabe, Y., Imamura, O., Tokutake, Y., Satoh, M., Matsumoto, T., Kuromitsu, J., Kataoka, H., Sugawara, K., Sugawara, M., Sugimoto, M., Goto, M., Furuichi, Y., 1996. A unique human gene that spans over 230 kb in the human chromosome 8p11-12 and codes multiple family proteins sharing RNA-binding motifs. Proc Natl Acad Sci U S A 93, 10913–10917. https://doi.org/10.1073/pnas.93.20.10913
285.Shirmanova, M.V., Druzhkova, I.N., Lukina, M.M., Dudenkova, V.V., Ignatova, N.I., Snopova, L.B., Shcheslavskiy, V.I., Belousov, V.V., Zagaynova, E.V., 2017. Chemotherapy with cisplatin: insights into intracellular pH and metabolic landscape of cancer cells in vitro and in vivo. Sci Rep 7, 8911. https://doi.org/10.1038/s41598-017-09426-4
286.Shorter, J., 2016. Phasing in and out. Nature Chem 8, 528–530. https://doi.org/10.1038/nchem.2534

287.Singatulina, A.S., Sukhanova, M.V., Desforges, B., Joshi, V., Pastré, D., Lavrik, O.I., 2022. PARP1 Activation Controls Stress Granule Assembly after Oxidative Stress and DNA Damage. Cells 11, 3932. https://doi.org/10.3390/cells11233932
288.Slišković, I., Eich, H., Müller-McNicoll, M., 2021. Exploring the multifunctionality of SR proteins. Biochemical Society Transactions 50, 187–198. https://doi.org/10.1042/BST20210325
289.Smith, N.E., Spencer-Merris, P., Fox, A.H., Petersen, J., Michael, M.Z., 2022. The Long and the Short of It: NEAT1 and Cancer Cell Metabolism. Cancers 14, 4388. https://doi.org/10.3390/cancers14184388
290.Soliman, A.F., Anees, L.M., Ibrahim, D.M., 2018. Cardioprotective effect of zingerone against oxidative stress, inflammation, and apoptosis induced by cisplatin or gamma radiation in rats. Naunyn Schmiedebergs Arch Pharmacol 391, 819–832. https://doi.org/10.1007/s00210-018-1506-4
291.Somasekharan, S.P., Zhang, F., Saxena, N., Huang, J.N., Kuo, I.-C., Low, C., Bell, R., Adomat, H., Stoynov, N., Foster, L., Gleave, M., Sorensen, P.H., 2020. G3BP1-linked mRNA partitioning supports selective protein synthesis in response to oxidative stress. Nucleic Acids Research 48, 6855–6873. https://doi.org/10.1093/nar/gkaa376
292.Soufari, H., Mackereth, C.D., 2017. Conserved binding of GCAC motifs by MEC-8, couch potato, and the RBPMS protein family. RNA 23, 308–316. https://doi.org/10.1261/rna.059733.116
293.Spallarossa, P., Altieri, P., Aloi, C., Garibaldi, S., Barisione, C., Ghigliotti, G., Fugazza, G., Barsotti, A., Brunelli, C., 2009. Doxorubicin induces senescence or apoptosis in rat neonatal cardiomyocytes by regulating the expression levels of the telomere binding factors 1 and 2. American Journal of Physiology-Heart and Circulatory Physiology 297, H2169–H2181. https://doi.org/10.1152/ajpheart.00068.2009
294.Spannl, S., Tereshchenko, M., Mastromarco, G.J., Ihn, S.J., Lee, H.O., 2019. Biomolecular condensates in neurodegeneration and cancer. Traffic 20, 890–911. https://doi.org/10.1111/tra.12704
295.Speyer, J.L., Green, M.D., Kramer, E., Rey, M., Sanger, J., Ward, C., Dubin, N., Ferrans, V., Stecy, P., Zeleniuch-Jacquotte, A., 1988. Protective effect of the bispiperazinedione ICRF-187 against doxorubicin-induced cardiac toxicity in women with advanced breast cancer. N Engl J Med 319, 745–752. https://doi.org/10.1056/NEJM198809223191203
296.Srinivas, S., Watanabe, T., Lin, C.-S., William, C.M., Tanabe, Y., Jessell, T.M., Costantini, F., 2001. Cre reporter strains produced by targeted insertion of EYFP and ECFP into the ROSA26 locus. BMC Developmental Biology 1, 4. https://doi.org/10.1186/1471-213X-1-4
297.Stamm, P., Kirmes, I., Palmer, A., Molitor, M., Kvandova, M., Kalinovic, S., Mihalikova, D., Reid, G., Wenzel, P., Münzel, T., Daiber, A., Jansen, T., 2021. Doxorubicin induces wide-spread transcriptional changes in the myocardium of hearts distinguishing between mice with preserved and impaired cardiac function. Life Sciences 284, 119879. https://doi.org/10.1016/j.lfs.2021.119879
298.Steffens Reinhardt, L., Groen, K., Newton, C., Avery-Kiejda, K.A., 2023. The role of truncated p53 isoforms in the DNA damage response. Biochimica et Biophysica Acta (BBA) - Reviews on Cancer 1878, 188882. https://doi.org/10.1016/j.bbcan.2023.188882
299.Strigun, A., Wahrheit, J., Niklas, J., Heinzle, E., Noor, F., 2012b. Doxorubicin Increases Oxidative Metabolism in HL-1 Cardiomyocytes as Shown by 13C Metabolic Flux Analysis. Toxicological Sciences 125, 595–606. https://doi.org/10.1093/toxsci/kfr298

300.Sun, W., Xu, J., Wang, L., Jiang, Y., Cui, J., Su, X., Yang, F., Tian, L., Si, Z., Xing, Y., 2022. Non-coding RNAs in cancer therapy-induced cardiotoxicity: Mechanisms, biomarkers, and treatments. Front Cardiovasc Med 9, 946137. https://doi.org/10.3389/fcvm.2022.946137
301.Sun, Y., Ding, L., Zhang, H., Han, J., Yang, X., Yan, J., Zhu, Y., Li, J., Song, H., Ye, Q., 2006. Potentiation of Smad-mediated transcriptional activation by the RNA-binding protein RBPMS. Nucleic Acids Res 34, 6314–6326. https://doi.org/10.1093/nar/gkl914
302.Sung, H.-M., Schott, J., Boss, P., Lehmann, J.A., Hardt, M.R., Lindner, D., Messens, J., Bogeski, I., Ohler, U., Stoecklin, G., 2023. Stress-induced nuclear speckle reorganization is linked to activation of immediate early gene splicing. Journal of Cell Biology 222, e202111151. https://doi.org/10.1083/jcb.202111151
303.Swain, S.M., Whaley, F.S., Gerber, M.C., Ewer, M.S., Bianchine, J.R., Gams, R.A., 1997. Delayed administration of dexrazoxane provides cardioprotection for patients with advanced breast cancer treated with doxorubicin-containing therapy. J Clin Oncol 15, 1333–1340. https://doi.org/10.1200/JCO.1997.15.4.1333
304.Tacyildiz, N., Turker, N., Ucar, T., Incesoy Ozdemir, S., Dincaslan, H., Yaman Ortakoylu, M., Ramoglu, M.G., Yavuz, G., Unal, E.C., 2023. Protective effect of the dexrazoxane against cardiotoxicity of the anthracycline in the treatment of the childhood cancers. JCO 41, e22001–e22001. https://doi.org/10.1200/JCO.2023.41.16_suppl.e22001
305.Takahashi, M., Higuchi, M., Matsuki, H., Yoshita, M., Ohsawa, T., Oie, M., Fujii, M., 2013. Stress Granules Inhibit Apoptosis by Reducing Reactive Oxygen Species Production. Mol Cell Biol 33, 815–829. https://doi.org/10.1128/MCB.00763-12
306.Tan, B., Peng, S., Yatim, S.M.J.M., Gunaratne, J., Hunziker, W., Ludwig, A., 2020. An Optimized Protocol for Proximity Biotinylation in Confluent Epithelial Cell Cultures Using the Peroxidase APEX2. STAR Protocols 1, 100074. https://doi.org/10.1016/j.xpro.2020.100074
307.Tao, Y., Zhang, Q., Wang, H., Yang, X., Mu, H., 2024b. Alternative splicing and related RNA binding proteins in human health and disease. Sig Transduct Target Ther 9, 1–33. https://doi.org/10.1038/s41392-024-01734-2
308.Taqueti, V.R., Mitchell, R.N., Lichtman, A.H., 2006. Protecting the pump: controlling myocardial inflammatory responses. Annu Rev Physiol 68, 67–95. https://doi.org/10.1146/annurev.physiol.68.040104.124611
309.Taylor, R., Hamid, F., Fielding, T., Gordon, P.M., Maloney, M., Makeyev, E.V., Houart, C., 2022. Prematurely terminated intron-retaining mRNAs invade axons in SFPQ null-driven neurodegeneration and are a hallmark of ALS. Nat Commun 13, 6994. https://doi.org/10.1038/s41467-022-34331-4
310.Teixeira, D., Sheth, U., Valencia-Sanchez, M.A., Brengues, M., Parker, R., 2005. Processing bodies require RNA for assembly and contain nontranslating mRNAs. RNA 11, 371–382. https://doi.org/10.1261/rna.7258505
311.Teplova, M., Farazi, T.A., Tuschl, T., Patel, D.J., 2016. Structural basis underlying CAC RNA recognition by the RRM domain of dimeric RNA-binding protein RBPMS. Quarterly Reviews of Biophysics 49, e1. https://doi.org/10.1017/S0033583515000207
312.The UniProt Consortium, 2007. The Universal Protein Resource (UniProt). Nucleic Acids Research 35, D193–D197. https://doi.org/10.1093/nar/gkl929
313.Thomas, J.D., Polaski, J.T., Feng, Q., De Neef, E.J., Hoppe, E.R., McSharry, M.V., Pangallo, J., Gabel, A.M., Belleville, A.E., Watson, J., Nkinsi, N.T., Berger, A.H., Bradley, R.K., 2020. RNA isoform screens uncover the essentiality and tumor-suppressor activity of ultraconserved poison exons. Nat Genet 52, 84–94. https://doi.org/10.1038/s41588-019-0555-z

314.Tourrière, H., Chebli, K., Zekri, L., Courselaud, B., Blanchard, J.M., Bertrand, E., Tazi, J., 2003. The RasGAP-associated endoribonuclease G3BP assembles stress granules. J Cell Biol 160, 823–831. https://doi.org/10.1083/jcb.200212128
315.Tschöpe, C., Ammirati, E., Bozkurt, B., Caforio, A.L.P., Cooper, L.T., Felix, S.B., Hare, J.M., Heidecker, B., Heymans, S., Hübner, N., Kelle, S., Klingel, K., Maatz, H., Parwani, A.S., Spillmann, F., Starling, R.C., Tsutsui, H., Seferovic, P., Van Linthout, S., 2021. Myocarditis and inflammatory cardiomyopathy: current evidence and future directions. Nat Rev Cardiol 18, 169–193. https://doi.org/10.1038/s41569-020-00435-x
316.Tucker, H.O., Huang, C.-J., Tucker, H.O., 2023. Evolving Roles of NonO and SFPQ in DNA Damage Repair and Cell Cycle. https://doi.org/10.20944/preprints202310.0619.v1
317.Twyffels, L., Gueydan, C., Kruys, V., 2011a. Shuttling SR proteins: more than splicing factors. The FEBS Journal 278, 3246–3255. https://doi.org/10.1111/j.1742-4658.2011.08274.x
318.Van den Hoogenhof, M.M.G., Beqqali, A., Amin, A.S., van der Made, I., Aufiero, S., Khan, M.A.F., Schumacher, C.A., Jansweijer, J.A., van Spaendonck-Zwarts, K.Y., Remme, C.A., Backs, J., Verkerk, A.O., Baartscheer, A., Pinto, Y.M., Creemers, E.E., 2018. RBM20 Mutations Induce an Arrhythmogenic Dilated Cardiomyopathy Related to Disturbed Calcium Handling. Circulation 138, 1330–1342. https://doi.org/10.1161/CIRCULATIONAHA.117.031947
319.Van der Zanden, S.Y., Qiao, X., Neefjes, J., 2021. New insights into the activities and toxicities of the old anticancer drug doxorubicin. FEBS J 288, 6095–6111. https://doi.org/10.1111/febs.15583
320.Van Leeuwen, W., Rabouille, C., 2019. Cellular stress leads to the formation of membraneless stress assemblies in eukaryotic cells. Traffic 20, 623–638. https://doi.org/10.1111/tra.12669
321.Van Treeck, B., Parker, R., 2019. Principles of Stress Granules Revealed by Imaging Approaches. Cold Spring Harb Perspect Biol 11, a033068. https://doi.org/10.1101/cshperspect.a033068
322.Vitale, R., Marzocco, S., Popolo, A., 2024. Role of Oxidative Stress and Inflammation in Doxorubicin-Induced Cardiotoxicity: A Brief Account. International Journal of Molecular Sciences 25, 7477. https://doi.org/10.3390/ijms25137477
323.Vogler, T.O., Wheeler, J.R., Nguyen, E.D., Hughes, M.P., Britson, K.A., Lester, E., Rao, B., Betta, N.D., Whitney, O.N., Ewachiw, T.E., Gomes, E., Shorter, J., Lloyd, T.E., Eisenberg, D.S., Taylor, J.P., Johnson, A.M., Olwin, B.B., Parker, R., 2018. TDP-43 and RNA form amyloid-like myo-granules in regenerating muscle. Nature 563, 508–513. https://doi.org/10.1038/s41586-018-0665-2
324.Wallace, K.B., Sardão, V.A., Oliveira, P.J., 2020. Mitochondrial Determinants of Doxorubicin-Induced Cardiomyopathy. Circulation Research 126, 926–941. https://doi.org/10.1161/CIRCRESAHA.119.314681
325.Wang, H., Chen, Y., Li, X., Chen, Guojun, Zhong, L., Chen, Gangbing, Liao, Y., Liao, W., Bin, J., 2016b. Genome-wide analysis of alternative splicing during human heart development. Sci Rep 6, 35520. https://doi.org/10.1038/srep35520
326.Wang, J., Choi, J.-M., Holehouse, A.S., Lee, H.O., Zhang, X., Jahnel, M., Maharana, S., Lemaitre, R., Pozniakovsky, A., Drechsel, D., Poser, I., Pappu, R.V., Alberti, S., Hyman, A.A., 2018. A molecular grammar governing the driving forces for phase separation of prion-like RNA binding proteins. Cell 174, 688-699.e16. https://doi.org/10.1016/j.cell.2018.06.006
327.Wang, J., Gan, Y., Cao, J., Dong, X., Ouyang, W., 2022c. Pathophysiology of stress granules: An emerging link to diseases (Review). Int J Mol Med 49, 44. https://doi.org/10.3892/ijmm.2022.5099

328.Wang, T., Shi, S., Shi, Y., Jiang, P., Hu, G., Ye, Q., Shi, Z., Yu, K., Wang, C., Fan, G., Zhao, S., Ma, H., Chang, A.C.Y., Li, Z., Bian, Q., Lin, C.-P., 2023a. Chemical-induced phase transition and global conformational reorganization of chromatin. Nat Commun 14, 5556. https://doi.org/10.1038/s41467-023-41340-4
329.Wang, Y., Chen, L.-L., 2020. Organization and function of paraspeckles. Essays in Biochemistry 64, 875–882. https://doi.org/10.1042/EBC20200010
330.Wang, Y.-L., Zhao, W.-W., Bai, S.-M., Ma, Y., Yin, X.-K., Feng, L.-L., Zeng, G.-D., Wang, F., Feng, W.-X., Zheng, J., Wang, Y.-N., Zeng, B., Liu, Q., Hung, M.-C., Wan, X.-B., 2022a. DNA damage-induced paraspeckle formation enhances DNA repair and tumor radioresistance by recruiting ribosomal protein P0. Cell Death Dis 13, 1–13. https://doi.org/10.1038/s41419-022-05092-1
331.Weeland, C.J., van den Hoogenhof, M.M., Beqqali, A., Creemers, E.E., 2015. Insights into alternative splicing of sarcomeric genes in the heart. Journal of Molecular and Cellular Cardiology 81, 107–113. https://doi.org/10.1016/j.yjmcc.2015.02.008
332.Wei, C., Qiu, J., Zhou, Y., Xue, Y., Hu, J., Ouyang, K., Banerjee, I., Zhang, C., Chen, B., Li, H., Chen, J., Song, L.-S., Fu, X.-D., 2015. Repression of the Central Splicing Regulator RBFox2 is Functionally Linked to Pressure Overload-induced Heart Failure. Cell Rep 10, 1521–1533. https://doi.org/10.1016/j.celrep.2015.02.013
333.Weins, A., Schwarz, K., Faul, C., Barisoni, L., Linke, W.A., Mundel, P., 2001. Differentiation- and stress-dependent nuclear cytoplasmic redistribution of myopodin, a novel actin-bundling protein. J Cell Biol 155, 393–404. https://doi.org/10.1083/jcb.200012039
334.Weintraub, R.G., Semsarian, C., Macdonald, P., 2017. Dilated cardiomyopathy. Lancet 390, 400–414. https://doi.org/10.1016/S0140-6736(16)31713-5
335.Wexler, L.H., Andrich, M.P., Venzon, D., Berg, S.L., Weaver-McClure, L., Chen, C.C., Dilsizian, V., Avila, N., Jarosinski, P., Balis, F.M., Poplack, D.G., Horowitz, M.E., 1996. Randomized trial of the cardioprotective agent ICRF-187 in pediatric sarcoma patients treated with doxorubicin. J Clin Oncol 14, 362–372. https://doi.org/10.1200/JCO.1996.14.2.362
336.Wheeler, J.R., Matheny, T., Jain, S., Abrisch, R., Parker, R., n.d. Distinct stages in stress granule assembly and disassembly. eLife 5, e18413. https://doi.org/10.7554/eLife.18413
337.Widagdo, J., Udagedara, S., Bhembre, N., Tan, J.Z.A., Neureiter, L., Huang, J., Anggono, V., Lee, M., n.d. Familial ALS-associated SFPQ variants promote the formation of SFPQ cytoplasmic aggregates in primary neurons. Open Biol 12, 220187. https://doi.org/10.1098/rsob.220187
338.Willis, M.S., Parry, T.L., Brown, D.I., Mota, R.I., Huang, W., Beak, J.Y., Sola, M., Zhou, C., Hicks, S.T., Caughey, M.C., Ralph B D'agostino, J., Jordan, J., Hundley, W.G., Jensen, B.C., 2019. Doxorubicin exposure causes subacute cardiac atrophy dependent upon the striated muscle-specific ubiquitin ligase Muscle Ring Finger-1. Circulation. Heart failure 12, e005234. https://doi.org/10.1161/CIRCHEARTFAILURE.118.005234
339.Wolozin, B., Ivanov, P., 2019. Stress granules and neurodegeneration. Nat Rev Neurosci 20, 649–666. https://doi.org/10.1038/s41583-019-0222-5
340.Wu, T., Chen, Z., Zhang, Z., Zhou, X., Gu, Y., Dinenno, F.A., Chen, J., 2024. RBPMS and RBPMS2 Cooperate to Safeguard Cardiac Splicing. https://doi.org/10.1101/2024.11.07.622565
341.Xu, X., Yang, D., Ding, J.-H., Wang, W., Chu, P.-H., Dalton, N.D., Wang, H.-Y., Bermingham, J.R., Ye, Z., Liu, F., Rosenfeld, M.G., Manley, J.L., Ross, J., Chen, J., Xiao, R.-P., Cheng, H., Fu, X.-D., 2005. ASF/SF2-regulated CaMKIIdelta alternative

splicing temporally reprograms excitation-contraction coupling in cardiac muscle. Cell 120, 59–72. https://doi.org/10.1016/j.cell.2004.11.036
342.Yang, C., Wang, Z., Kang, Y., Yi, Q., Wang, T., Bai, Y., Liu, Y., n.d. Stress granule homeostasis is modulated by TRIM21-mediated ubiquitination of G3BP1 and autophagy-dependent elimination of stress granules. Autophagy 19, 1934–1951. https://doi.org/10.1080/15548627.2022.2164427
343.Yang, J., Hung, L.-H., Licht, T., Kostin, S., Looso, M., Khrameeva, E., Bindereif, A., Schneider, A., Braun, T., 2014. RBM24 Is a Major Regulator of Muscle-Specific Alternative Splicing. Developmental Cell 31, 87–99. https://doi.org/10.1016/j.devcel.2014.08.025
344.Yang, K., Yang, J., Yi, J., 2018a. Nucleolar Stress: hallmarks, sensing mechanism and diseases. Cell Stress 2, 125–140. https://doi.org/10.15698/cst2018.06.139
345.Yang, L., Gilbertsen, A., Jacobson, B., Pham, J., Fujioka, N., Henke, C.A., Kratzke, R.A., 2023. SFPQ and Its Isoform as Potential Biomarker for Non-Small-Cell Lung Cancer. International Journal of Molecular Sciences 24, 12500. https://doi.org/10.3390/ijms241512500
346.Yang, Y., Lee, G.C., Nakagaki-Silva, E., Huang, Y., Peacey, M., Partridge, R., Gooding, C., Smith, C.W.J., 2023a. Cell-type specific regulator RBPMS switches alternative splicing via higher-order oligomerization and heterotypic interactions with other splicing regulators. Nucleic Acids Res 51, 9961–9982. https://doi.org/10.1093/nar/gkad652
347.Yap, K., Mukhina, S., Zhang, G., Tan, J.S.C., Ong, H.S., Makeyev, E.V., 2018. A Short Tandem Repeat-Enriched RNA Assembles a Nuclear Compartment to Control Alternative Splicing and Promote Cell Survival. Molecular Cell 72, 525-540.e13. https://doi.org/10.1016/j.molcel.2018.08.041
348.Yasuhara, T., Xing, Y.-H., Bauer, N.C., Lee, L., Dong, R., Yadav, T., Soberman, R.J., Rivera, M.N., Zou, L., 2022. Condensates induced by transcription inhibition localize active chromatin to nucleoli. Molecular Cell 82, 2738-2753.e6. https://doi.org/10.1016/j.molcel.2022.05.010
349.Ye, L., Gu, L., Caprioli, J., Piri, N., 2018. RNA-binding protein Rbpms is represented in human retinas by isoforms A and C and its transcriptional regulation involves Sp1-binding site. Mol Genet Genomics 293, 819–830. https://doi.org/10.1007/s00438-018-1423-8
350.Zbinden, A., Pérez-Berlanga, M., De Rossi, P., Polymenidou, M., 2020. Phase Separation and Neurodegenerative Diseases: A Disturbance in the Force. Developmental Cell 55, 45–68. https://doi.org/10.1016/j.devcel.2020.09.014
351.Zearfoss, N.R., Chan, A.P., Wu, C.F., Kloc, M., Etkin, L.D., 2004. Hermes is a localized factor regulating cleavage of vegetal blastomeres in *Xenopus laevis*. Developmental Biology 267, 60–71. https://doi.org/10.1016/j.ydbio.2003.10.032
352.Zhang, H., Shao, S., Zeng, Y., Wang, X., Qin, Y., Ren, Q., Xiang, S., Wang, Y., Xiao, J., Sun, Y., 2022. Reversible phase separation of HSF1 is required for an acute transcriptional response during heat shock. Nat Cell Biol 24, 340–352. https://doi.org/10.1038/s41556-022-00846-7
353.Zhang, L., Xu, J., Li, M., Chen, X., 2023. The role of long noncoding RNAs in liquid–liquid phase separation. Cellular Signalling 111, 110848. https://doi.org/10.1016/j.cellsig.2023.110848
354.Zhang, S., Liu, X., Bawa-Khalfe, T., Lu, L.-S., Lyu, Y.L., Liu, L.F., Yeh, E.T.H., 2012a. Identification of the molecular basis of doxorubicin-induced cardiotoxicity. Nat Med 18, 1639–1642. https://doi.org/10.1038/nm.2919
355.Zhang, X., Vigers, M., McCarty, J., Rauch, J.N., Fredrickson, G.H., Wilson, M.Z., Shea, J.-E., Han, S., Kosik, K.S., 2020. The proline-rich domain promotes Tau liquid–

liquid phase separation in cells. Journal of Cell Biology 219, e202006054. https://doi.org/10.1083/jcb.202006054
356. Zhang, X., Wang, Z., Xu, Q., Chen, Y., Liu, W., Zhong, T., Li, H., Quan, C., Zhang, L., Cui, C.-P., 2021. Splicing factor Srsf5 deletion disrupts alternative splicing and causes noncompaction of ventricular myocardium. iScience 24. https://doi.org/10.1016/j.isci.2021.103097
357. Zhao, L., Zhang, B., 2017. Doxorubicin induces cardiotoxicity through upregulation of death receptors mediated apoptosis in cardiomyocytes. Scientific Reports 7, 44735. https://doi.org/10.1038/srep44735
358. Zhao, M., Liu, S., Wang, Y., Lv, K., Lou, P., Zhou, P., Zhu, J., Li, L., Cheng, J., Lu, Y., Liu, J., 2024. The mitochondria–paraspeckle axis regulates the survival of transplanted stem cells under oxidative stress conditions. Theranostics 14, 1517–1533. https://doi.org/10.7150/thno.88764
359. Zhou, Y., Wang, G., Wang, P., Li, Z., Yue, T., Wang, J., Zou, P., 2019a. Expanding APEX2 Substrates for Proximity-Dependent Labeling of Nucleic Acids and Proteins in Living Cells. Angewandte Chemie International Edition 58, 11763–11767. https://doi.org/10.1002/anie.201905949

Abbreviations

2DE	Two-dimensional gel electrophoresis
aa	Amino acids
AD	Alzheimer's disease
ALS	Amyotrophic lateral sclerosis
APEX	Engineered ascorbate peroxidase
APS	Ammoniumperoxodisulfat
AS	Alternative splicing
bp	Base pairs
BP	Biotin-phenol
BSA	Bovine serum albumin
BW	Body weight
C57bl/6	C57 black 6 mice
Ca^{2+}	Calcium ions
cDNA	Complementary deoxyribonucleic acid
CMV	Cytomegalovirus
CNOT2	CCR4-NOT Transcription Complex Subunit 2
CNS	Central nervous system
CO_2	Carbon dioxide
Cre	Tyrosine recombinase enzyme derived from the P1 Bacteriophage
DAPI	4',6-diamidino-2-phenylindole
DBHS	Drosophila behavior/human splicing
DCM	Dilated cardiomyopathy
DCP1A	Decapping mRNA 1A
ddH_2O	Double distilled water
DDR	DNA damage repair
DEG	Differentially expressed gene
DMEM	Dulbecco Modified Eagle Medium
DMSO	Dimethyl sulfoxide
DNA	Deoxyribonucleic acid
DNMT3B	DNA (cytosine-5-)-methyltransferase 3 beta
DOX	Doxorubicin
DSB	Double strand break
DTT	1,4-Dithiothreit
E13.5	Embryonic day 13.5

EDC4	Enhancer of mRNA decapping 4
EDTA	Ethylenediaminetetraacetic acid
EIF	Eukaryotic initiation factor
ES cell	Embryonic stem cell
EtOH	Ethanol
EWS	Ewing Sarcoma protein
FBS	Fetal bovine serum
FC	Fold change
FCS	Fetal calf serum
FDR	False discovery rate
For	Forward
FTLD	Frontotemporal lobar dementia
G3BP	Ras-GTPase-activating protein SH3-domain-binding protein
GAPDH	Glyceraldehyde 3-phosphate dehydrogenase
GFP	Green fluorescent protein
GO	Gene ontology
GOI	Gene of interest
h	Hours
H_2O_2	Hydrogen peroxide
HCL	Hydrochloric acid
H&E	Hematoxylin & eosin
HEK293	Human embryonic kidney cells 293
hNRNP	Heterogeneous nuclear ribonucleoproteins
HP1	heterochromatin protein 1
HW	Heart weight
iCLIP	Individual-nucleotide resolution CLIP
IDP	Intrinsically disordered protein
IDR	Intrinsically disordered region
IF	Immunofluorescent / Immunoflourescence staining
IGV	Integrative genomics viewer
IR	Intron retention
kDa	Kilo Dalton
KO	Knockout
LC-MS/MS	Liquid chromatography–mass spectrometry
LIF	Leukemia inhibitory factor
LLPS	Liquid-liquid phase separation
LncRNA	Long non-coding RNA
loxP	Locus of X-over P1
Mass spec	Mass spectrometry
MBNL1	Muscleblind like splicing regulator 1
MEFs	Mouse embryonic fibroblasts
MgCl2	Magnesium chloride

min	Minutes
miRNA	MicroRNA
ml	Millilitre
MLO	Membraneless organelle
mM	Millimolar
mRNA	Messenger ribonucleic acid
NaCl	Sodium chloride
NCBI	National Center for Biotechnology Information
NES	Nuclear export signal
Neo	Neomycin
NHEJ	Non-homologous end joining
nm	Nanometers
NMD	Nonsense-mediated mRNA decay
NONO	Non-POU domain containing octamer binding
OE	Overexpression
ORF	Open reading frame
P0, P1	Postnatal day 0, 1
PAA	Polyacrylamide
PABPC1	Poly(A) binding protein cytoplasmic 1
P-bodies	Processing bodies
PBS	Phosphate-buffered saline
PCE	Poison cassette exon
PCR	Polymerase chain reaction
PFA	Paraformaldehyde
PLD	Prion-like domains
PMSF	Phenylmethylsulfonyl fluoride
PSs	Paraspeckles
PSG	L-Glutamine-penicillin-streptomycin solution
PTBP1	Polypyrimidine tract-binding protein 1
PTC	Premature termination codon
qRT-PCR	Quantitative reverse transcription PCR
RBD	RNA-binding domain
RBFOX1	RNA binding protein, fox-1 homolog
RBM	RNA-binding motif protein
RBPMS	RNA binding protein with multiple splicing
RBPs	RNA-binding proteins

Rev	Reverse
RGC	Retinal ganglion cell
RNA	Ribonucleic acid
RNA-seq	RNA sequencing
RNP	Ribonucleoprotein
ROS	Reactive oxygen species
rpm	Revolutions per minute
RRM	RNA recognition motif
RT	Room temperature
RT-PCR	Reverse transcription PCR
SD	Standard deviation
SDS	Sodium dodecyl sulfate
SFPQ	Splicing factor proline and glutamine rich
SG	Stress granule
SMARCC2	SWI/SNF Related BAF Chromatin Remodeling Complex Subunit C2
SMC	Smooth muscle cell
smFISH	Single-molecule fluorescence in situ hybridization
SRSF	Serine/arginine protein kinase
SWI/SNF	Switch/sucrose nonfermentable
TAE	Tris-acetate-EDTA
TAF15	TATA-box binding protein associated factor 15
TBS	Tris-buffered saline
TBS-T	Tris-buffered saline / Tween-20
TCA	Tricarboxylic acid
TDP-43	TAR DNA-binding protein 43
TE	Tris-EDTA
TEMED	Tetramethylethylenediamine
TIA-1	Cytotoxic granule associated RNA binding protein
TL	Tibia length
Top2	DNA topoisomerase II
U	Unit
UV	Ultraviolet
WT	Wildtype
XMLC2	Xenopus laevis light chain 2
γ-H2AX	Gamma H2A.X variant histone
µl	Microliter
µm	Micrometer

Appendix

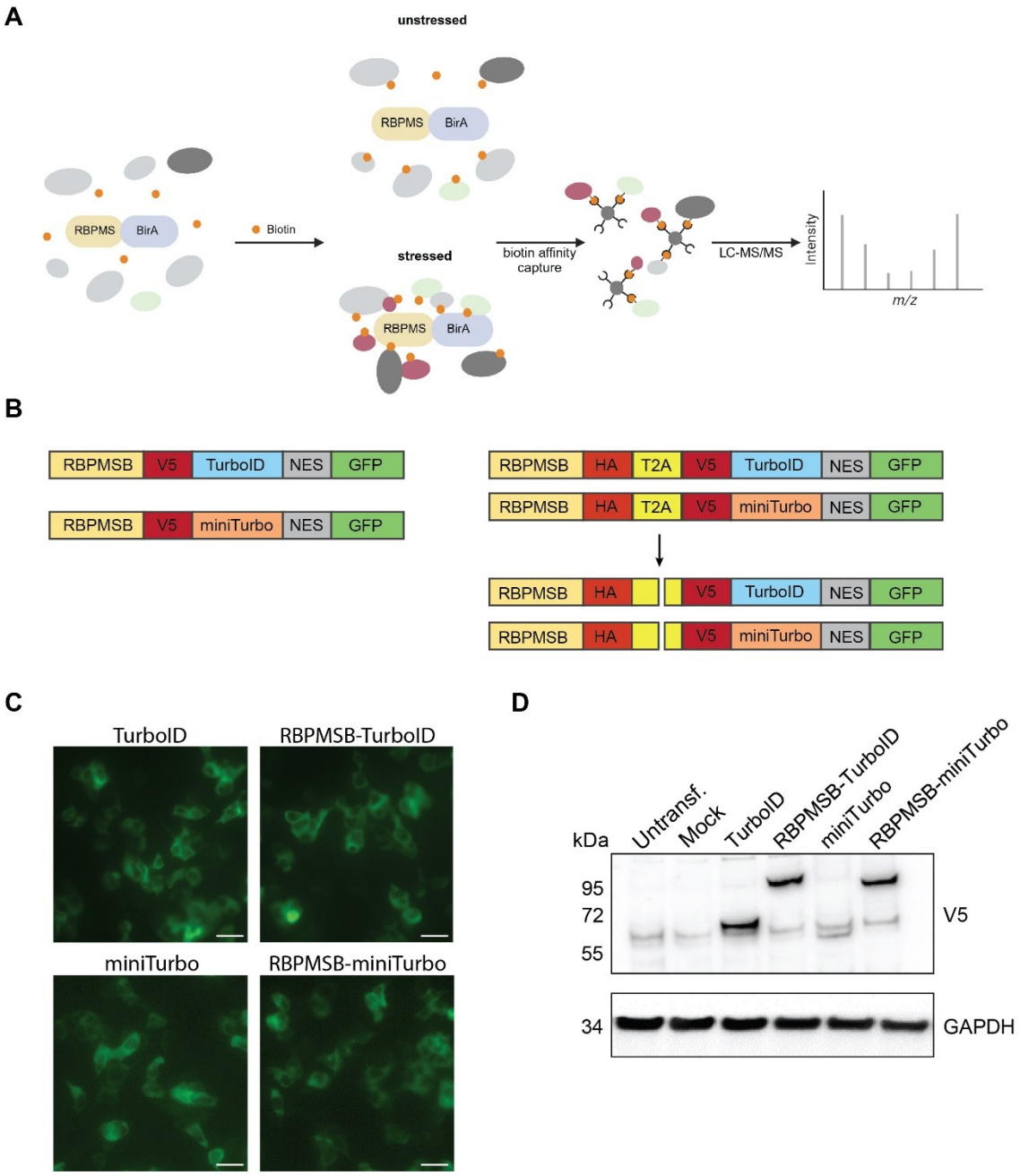

Figure 43 Characterization of promiscuous biotinylation activity in HEK293T cells. **A** Scheme of TurboID and miniTurbo analysis in HEK293T cells transfected with either RBPMSB-TurboID or RBPMSB-miniTurbo and respective TurboID and miniTurbo control expression vectors. Biotinylated proteins in close proximity to the fusion protein were isolated by affinity capture on streptavidin-coated beads and identified by LC-MS/MS. **B** Schematic representation of RBPMSB-V5-TurboID-NES-copGFP (RBPMSB-TurboID)/ miniTurbo-NES-copGFP (RBPMS-miniTurbo) and RBPMSB-T2A-V5-TurboID-NES-copGFP (TurboID)/ RBPMSB-T2A-V5-miniTurbo-NES-copGFP

(miniTurbo). **C** The ligases were stably expressed in HEK293T cells and targeted to the cytosol. The subcellular localization of the fusion-proteins was analyzed by GFP imaging. Scale bar, 20 µm. **D** The protein levels and precise cleavage of the fusion proteins were confirmed by immunoblotting analysis probed with anti-V5 antibody. GAPDH was used as a loading control. Mock= empty vector, non-transf.= non-transfected control cells.

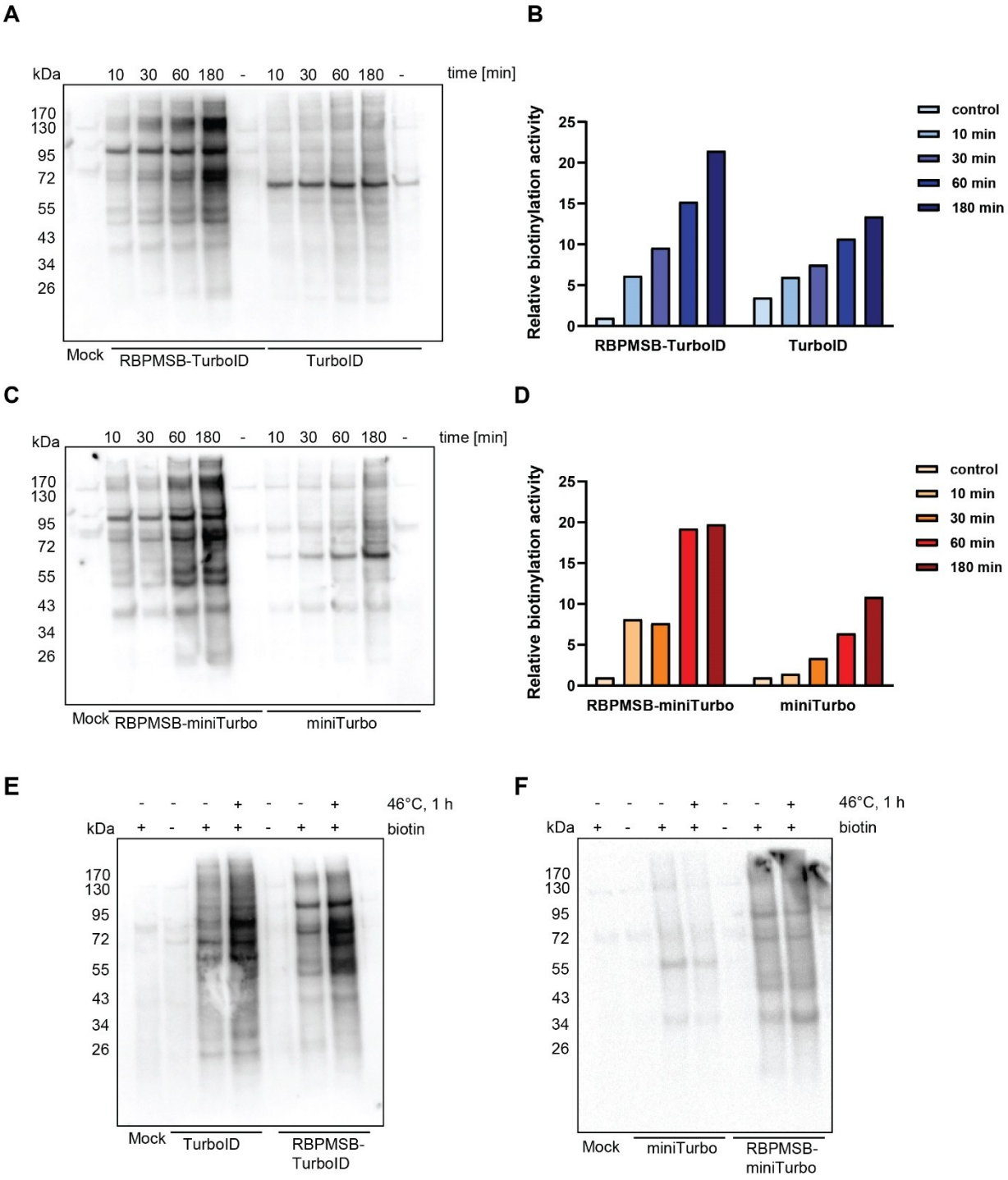

Figure 44 Comparison of the RBPMSB-TurboID and miniTurbo biotin ligases in HEK293T cells.

A-D HEK293T cells were transfected with expression constructs encoding either RBPMSB-TurboID or TurboID (control) and RBPMSB-miniTurbo or miniTurbo (control). Labeling was performed by incubation with 500 µM exogenous biotin for the indicated time points and promiscuously biotinylated proteins were detected by streptavidin-HRP blotting and relative biotinylation activity was quantified. **E, F** Non-transfected cells (mock) served as control.

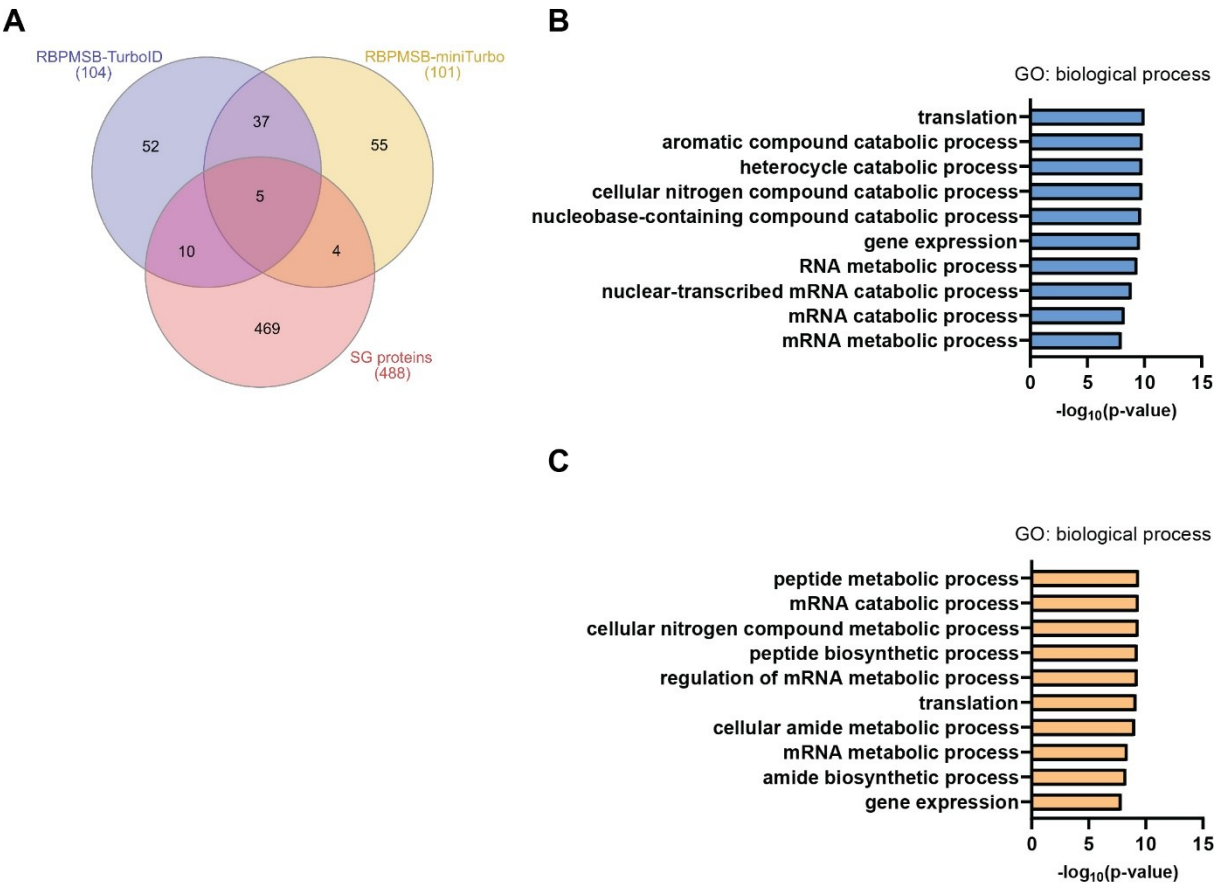

Figure 45 Enrichment analysis of RBPMSB-TurboID and RBPMSB-miniTurbo interactome upon heat stress.

A Venn diagram merging stress-dependent proteins biotinylated by RBPMSB-TurboID or RBPMSB-miniTurbo with known stress granule (SG) proteins. **B, C** Box plots showing GO term enrichment for proteins preferentially labeled in RBPMSB-TurboID (A) or RBPMSB-miniTurbo (B) expressing HEK293T cells. GO terms refer to biological process. Only the top 10 GO Terms are presented. Significance was calculated based on the $-\log_{10}$ p-value.

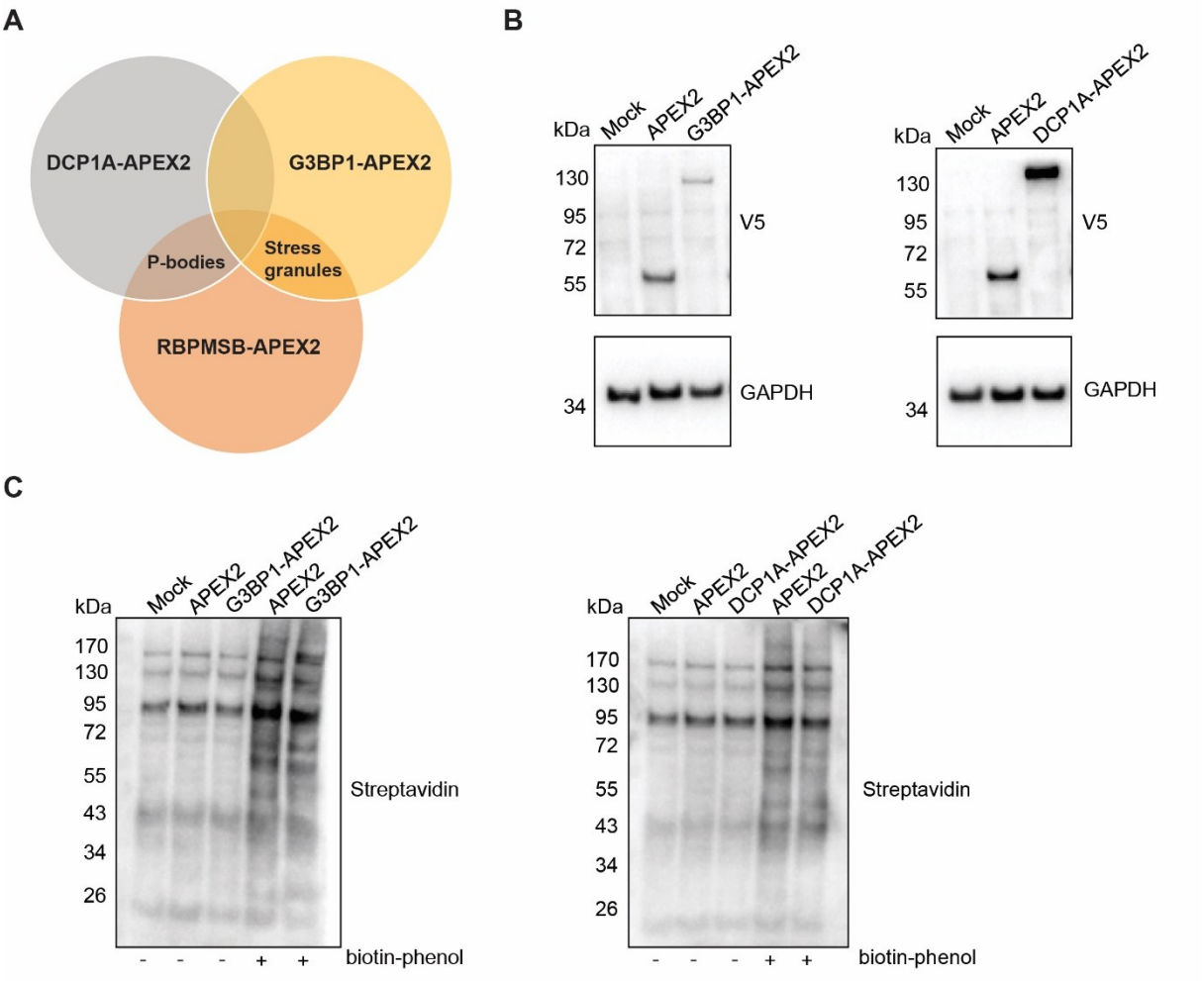

Figure 46 Expanding the knowledge of stress granules and processing bodies composition in the heart by using APEX2 proximity labeling.

A Venn diagram showing the potential overlap of identified proteins by APEX2 proximity labeling of RBPMSB with stress granule (SG) and processing bodies (P-body) proteins. **B** HEK293T cells were stably transfected with fusion plasmids encoding for G3BP1-APEX2 or APEX2/ DCP1A-APEX2 or APEX2. Whole cell lysates were used to confirm the expression levels and successful cleavage of the control APEX2 plasmid by immunoblotting analysis probed with anti-V5 antibody. GAPDH was used as a loading control. **C** HEK293T cells expressing G3BP1-APEX2 or APEX2/ DCP1A-APEX2 or APEX2 were preincubated with the indicated concentrations of biotin-phenol for 30 min, followed by the addition of H_2O_2 at the indicated concentrations for 1 min. Whole cell lysates were probed with streptavidin-HRP. Mock= empty vector, untransf. = untransfected control cells.

RNA recognition motif

RBPMSA
197aa
MNGGGKAEKENTPSEANLQEEEVRTLFVSGLPLDIKPRELYLLFRPFKGYEGSLIKLTSKQPVGFVSFDSRSEAEAAKNALNGIRFDPEIPQTLRLEFAKA
NTKMAKNKLVGTPNPSTPLPNTVPQFIAREPYELTVPALYPSSPEVWAPYPLYPAELAPALPPPAAFTYPASLHAQMRWIPPSEATSQGWKSRQFC

RBPMSB
220aa
MNGGGKAEKENTPSEANLQEEEVRTLFVSGLPLDIKPRELYLLFRPFKGYEGSLIKLTSKQPVGFVSFDSRSEAEAAKNALNGIRFDPEIPQTLRLEFAKA
NTKMAKNKLVGTPNPSTPLPNTVPQFIAREPYELTVPALYPSSPEVWAPYPLYPAELAPALPPPAAFTYPASLHAQCFSPEAKPNTPVFCPLLQQIRFVSG
NVFVTYQPTADQQRELPC

RBPMSC
191aa
MNGGGKAEKENTPSEANLQEEEVRTLFVSGLPLDIKPRELYLLFRPFKGYEGSLIKLTSKQPVGFVSFDSRSEAEAAKNALNGIRFDPEIPQTLRLEFAKA
NTKMAKNKLVGTPNPSTPLPNTVPQFIAREPYALDPSLRGHFPGLEVPAVLLRLCLGCVMAAAICLVGINAVFTGGDCHPAVLQNWSLLA

RBPMS2
206aa
MSNLKPDVEHCTGAGTGSPLEEEVRTLFVSGLPVDIKPRELYLLFRPFKGYEGSLIKLTSRQPVGFVIFDSRAGAEAAKNALNGIRFDPENPQTLRLEFAKA
NTKMAKSKLIATPNPTSVHPALGAHLIARDPYDLMGTALIPASPEAWAPYPLYTTELTPAISHTTFTYPAATAAAAAAATLHAQVRWYPSSDTTQQGWKYR
QFC

Figure 47 Peptide sequences of murine RBPMS variants.

The conserved RNA recognition motif (RRM) domain of the RBPMS family is highlighted in red.

Rbpmsd
627bp
ATGAACGGCGGCGGCAAAGCCGAGAAGGAGAACACCCCGAGCGAGGCCAACCTTCAGGAGGAGGAGGTCCGGACCCTATTTGTCAGCGGTCTG
CCTCTGGACATCAAGCCCCGAGAGCTGTACCTGCTCTTCAGACCATTCAAGGGCTATGAAGGTTCTCTCATAAAGCTCACATCTAAACAGCCCGTA
GGCTTTGTCAGTTTTGACAGTCGCTCAGAAGCAGAGGCCGCAAAGAACGCTTTGAACGGCATCCGCTTCGATCCTGAAATCCCGCAAACGCTACG
ACTAGAGTTTGCTAAGGCAAACACGAAGATGGCCAAGAACAAACTCGTAGGGACTCCAAACCCCAGTACTCCTCTGCCCAACACTGTACCTCAGT
TCATTGCCAGGGAGCCATATGAGCTCACAGTACCTGTACTTTACCCCAGTAGCCCTGAAGTTTGGGCCCCGTACCCTCTGTACCCAGCGGAGTTA
GCGCCTGCTCTTCCTCCTCCTGCCGCTTTCACCTACCCCGCTTCACTGCATGCCCAGGTTCCCAGCATCCCTGGCCTGAGGGCTCTGGCCCCGA
GGCTGCCCTTTCCCAGCTGTCTCAGGAAGGCAGCCCCAGCTCTGCTCTCTGCTTAGTGA

RNA recognition motif

RBPMSD
207aa
MNGGGKAEKENTPSEANLQEEEVRTLFVSGLPLDIKPRELYLLFRPFKGYEGSLIKLTSKQPVGFVSFDSRSEAEAAKNALNGIRFDPEIPQTLRLEFAKA
NTKMAKNKLVGTPNPSTPLPNTVPQFIAREPYELTVPVLYPSSPEVWAPYPLYPAELAPALPPPAAFTYPASLHAQVPSIPGLRALAPRLPFPSCLRKAAP
ALLSA

Figure 48 Open reading frame and peptide sequence of novel murine *Rbpmsd* isoform.

The conserved RNA recognition motif (RRM) domain of the RBPMS family is highlighted in red.

Acknowledgements

First, I would like to express my sincere gratitude to my supervisor, Prof. Dr. Dr. Thomas Braun, for giving me the great opportunity to perform my research in his department at the Max Planck Institute in Bad Nauheim. His support, guidance and continuous encouragement throughout my dissertation have been instrumental in shaping this work. His profound expertise and constructive feedback have greatly enriched my scientific development.

Many thanks also to my PI Dr. André Schneider for his constant help, insightful suggestions at every stage of my projects, and for the constructive discussions and critical feedback that have significantly contributed to the progress of my research.

I would also like to thank my group members for providing a stimulating and supportive academic environment, as well as for their helpful discussions and suggestions. Special thanks go to Selina, Silke, Max and Dong for all the engaging scientific discussions and the enjoyable moments we shared both in the laboratory and during our free time over the years.

I am also deeply thankful to the staff of the animal facility for their dedicated work, and to all my colleagues from the Department of Cardiac Development and Remodeling, especially Sonja, Katja and Marion for their invaluable technical support.

A heartful thank you goes to my family and friends for your constant encouragement and for always being there. This journey would not have been the same without you. Thank you for being part of this important chapter in my life.

To my partner Mirko-thank you for your endless love, understanding, and belief in me, especially during the most challenging moments. Your belief in me has been a constant source of strength.

A special thank you goes to my two bunnies, who have brought comfort, joy, and a much-needed sense of calm into my daily life. Their quiet companionship made even the most stressful days a little brighter.